UNDERSTANDING THE SPATIAL DISTRIBUTION OF SNOW WATER EQUIVALENT IN PAIRED BASINS IN SOUTHWEST MONTANA

by

Jason Paul Welz

A thesis in partial fulfillment
of the requirements for the degree

of

Master of Science

in

Earth Sciences

MONTANA STATE UNIVERSITY
Bozeman, MT

April 2015

ACKNOWLEDGEMENTS

This research would not have been possible without the guidance and support of many people and organizations. First, I would like to thank my advisor, Dr. Jordy Hendrikx, for presenting the initial vision for this project, suggesting an appropriate study site, and mentoring me in countless ways throughout the process. I would also like to thank my committee members, Stuart Challender and Dr. Paul Stoy for imparting their different fields of expertise that were crucial to the overall goal and outcome of this research.

Obtaining a robust field dataset from the Cedar Mountain study site would have been completely unfeasible without the receptiveness of the Yellowstone Club and their head of snow safety, Tom Leonard. Their support of this research provided lift, road and property access allowing for numerous visits to the study site throughout the ten month field campaign. I would also like to thank the many members of the Yellowstone Club ski patrol for their interest and hard work in assisting me with field data collection. I am also grateful to the Montana Institute on Ecosystems for considering my research valuable and funding the primary costs of fieldwork.

I would like to thank my fellow colleagues from the Snow and Avalanche Laboratory at MSU: Karl Wetlaufer, Tom Matthews, Ian Hoyer, and Robyn Wooldridge not only for their continual help in the office, but for assisting me with the fieldwork during peak SWE to provide the most valuable dataset of the study. And finally, to my family and friends who have kept me inspired along this long road and encouraged me to stay on track, thank you.

TABLE OF CONTENTS

TABLE OF CONTENTS - CONTINUED

LIST OF FIGURES

Figure Page

LIST OF FIGURES CONTINUED

Figure Page

LIST OF TABLES

Table Page

ABSTRACT

The goal of this research has been to build upon previous studies focused on what processes control the distribution of snow water equivalent (SWE) in alpine environments. This involved taking a comprehensive look at the widely accepted physiographic variables of: elevation, slope, aspect, solar radiation, and wind exposure, but also avalanche activity, which has been given limited explicit inclusion. The paired basin comparison adopted in this study, between a hypothesized avalanche prone basin and avalanche free basin, has been previously used to correlate avalanche activity with snowmelt runoff. However, it has not been used in an attempt to parse out which variables have the dominant influence on SWE distribution between adjacent areas of very similar physiographic character. While most previous studies have focused on the period of peak SWE to study this distribution, this current research looked at the evolution of the controlling variables throughout snowpack development. A robust dataset of snow depth and SWE measurements were collected during a January 31 - July 10, 2013 field campaign on Cedar Mountain near Big Sky, MT. Physiographic variable values were extracted from a 10 m resolution digital elevation model (DEM) at snow sample points and input as predictors of observed SWE in multiple linear regression (MLR) and binary regression tree (BRT) models to estimate SWE across the study area. Optimal models were selected by various measures of goodness of fit and cross-validation criteria. Calculated R^2 values for MLR models (0.17-0.57) and BRT models (0.33-0.66) were comparable to previous studies indicating a relative level of success in predictive performance. Subsequent analysis of each optimal model's variable selection and predicted SWE distributions revealed differences in the spatial and temporal patterns of this metric between the paired basins, confirming some well-understood processes as well as offering new insights.

1. INTRODUCTION

1.1 Overview

The combined hydroclimatology and topography of the U.S. Intermountain West lead to snowmelt runoff supplying approximately 67-75% of the annual stream discharge in this region (*Cayan*, 1996; *Serreze et al.*, 1999; *Wise*, 2012). The temporal pattern of snowmelt is vital to the functioning of the semi-arid ecosystems in this region, and to the utilitarian needs of the human infrastructure. Operational streamflow forecasting must consider the factors that influence the magnitude and timing of snowmelt runoff in order to harness and allocate water resources appropriately. Consequently, research in snow hydrology has long focused on how to accurately determine the distribution of snow water equivalent (SWE) over landscapes of different scales and degrees of spatial heterogeneity to use as an input for subsequent snowmelt runoff models. In alpine watersheds, depending on the scale and climate, the majority of previous investigations have concluded that some combination of the physiographic variables of: elevation, slope, aspect, solar radiation, landcover, and wind shelter/exposure, are dominant in predicting the spatial pattern of SWE (e.g. *Elder et al.*, 1991, 1998; *Luce et al.*, 1998; *Balk and Elder*, 2000; *Winstral et al.*, 2002; *Anderton et al.*, 2004; *Erickson et al.*, 2005; *Harshburger et al.*, 2010; *Clark et al.*, 2011, *Anderson et al.*, 2014). Some of these studies have mentioned avalanche activity as contributing to the distribution of SWE and subsequent snowmelt runoff, but others have given it explicit consideration as a major predictor (e.g. *Iveronova*, 1966; *Sosedov and Seversky*, 1965; *Martinec and de Quervain*, 1975; *Zalikhanov*, 1975; *de Scally and Gardner*, 1988; *de Scally*, 1996).

The goal of this current study is to build on the previous research by giving equal consideration to all of the aforementioned physiographic variables (i.e. elevation, slope, aspect, solar radiation, and wind exposure) and explicitly consider avalanche activity, in an attempt to parse out which have the dominant influence on the spatial distribution of SWE, through snowpack development, in a paired basin study area in southwest Montana. Analysis was conducted on a dataset consisting of point measurements of snow depth and SWE acquired during a field campaign in the winter of 2013. To accomplish field measurement of snow metrics, a stratified sampling design was adopted, with some modification, from field campaigns with a similar scale and/or goal (*Elder et al.*, 1991; *Elder et al.*, 1998; *Winstral et al.*, 2002; *Erickson et al.*, 2005; *Clark et al.*, 2011). This sampling technique was applied to paired basins (Basin A and Basin B) with many similar physiographic characteristics, but with enough variation to create substantial differences in snowpack distribution worth comparing. In selecting which modeling methodologies were most appropriate for this study, attributes considered were: 1) simplicity, 2) interpretability, 3) appropriateness to data sampling, and 4) performance in similar study designs and scales. Consideration was also given to comparing two modeling techniques with fundamentally different methodologies; hence a comparison of the performance between multiple linear regression (linear) and binary regression tree (nonlinear) analysis was chosen. Through this investigation it is hoped that some of the conclusions drawn by this research can be extrapolated to understand snow distribution processes in similar alpine basins in the greater U.S. Intermountain West.

1.2 Research Questions

This research seeks to further understand the influence of physiographic variables on the snowpack in an alpine setting with an intermountain snow climate in southwest Montana and how this regime evolves during the different periods of snowpack development. Thus, this investigation addresses the main question:

> *What are the dominant physiographic variables that can be used for predicting the spatial distribution of SWE in the selected paired basins (A: 1.38 km^2, B: 1.63 km^2) during the periods of accumulation, peak SWE, and ablation?*

Using a paired basin study design also provided the opportunity to investigate how small differences in the physiographic properties of adjacent basins may lead to larger differences in the spatial distribution of SWE across these landscapes. This lead to the sub-question:

> *How are the dominant processes predicting the spatial distribution of SWE in Basin A and Basin B different and why?*

The paired basins were selected under the hypothesis that Basin A was relatively avalanche prone and Basin B was not. Thus, this study site design provided a potential treatment (naturally through avalanching) and control (non-avalanche) group. Through this setup, an attempt was made to answer the final sub-question:

> *Is there a difference in the spatial distribution of SWE between Basin A and Basin B due to avalanche activity?*

2. LITERATURE REVIEW

2.1 SWE over the Landscape

Elevation is the variable that has traditionally been given primary consideration when modeling snow accumulation in mountainous terrain (*Elder et al.*, 1991, 1998), since long-term averages worldwide indicate a positive relationship between elevation and precipitation (*Dingman*, 2002). This is mainly driven by the orographic effect and other associated atmospheric processes over mountainous landscapes (*Dingman*, 2002). Adiabatic cooling of air occurs at a lapse rate controlled by increasing elevation and the amount of moisture in an air parcel. In turn, this determines the degree of water vapor saturation in rising clouds, as well as the rain-snow transition level, thereby typically leading to higher precipitation and snow accumulation with increasing elevation. Conversely, the lapse rate has a direct effect on ablation due to typically higher ambient temperatures at lower elevation providing more sensible heat input into the snowpack. However, the standard atmospheric lapse rate for change in elevation of -6.5°C km^{-1} can fluctuate on various temporal and spatial scales, driven by the multitude of processes that occur over topographically complex terrain (*Lundquist and Cayan*, 2007). Thus, depending on the physiographic characteristics of the watershed of focus, elevation only offers part of the prediction of snow distribution and is increasingly limited in basins with a relatively small elevation range (*Clark et al.*, 2011). *Elder et al.* (1991) investigated the distribution of SWE in a 1.2 km^2 basin with 636 m of vertical relief in the central Sierra, and found that, while the addition of elevation did improve the performance of models with slope and solar radiation, elevation by itself was not important, as it was outweighed by these other variables.

Since the variables that this work will consider as predictors of SWE are all physiographically based, they are inherently tied to one another, leading to a complexity of multiple interactions. While the orographic effect on snowfall is based on elevation, it has also been shown to be affected by slope and wind speed (*Jones et al.*, 2001). Slope is also important with regard to solar radiation, in combining with aspect to determine the solar angle of incidence. Thus, slope and aspect are important in determining the intensity of solar radiation input, as well as wind exposure. Wind speed, and the subsequent wind redistribution of snow, is controlled by the slope angle and orientation (aspect) of the topographical barrier with which it is interacting. Some studies have demonstrated that wind is the primary parameter controlling the pattern of snow distribution in an alpine landscape (*Clark et al.*, 2011). In the continental snow climate of the Green Lakes Valley watershed in Colorado, *Winstral et al.* (2002) found regression tree models including a wind redistribution parameter to explain 8-23% more of the variance in the observed snow distribution than models without this parameter. In the same study area, *Erickson et al.* (2005) found an index of wind sheltering to be the most important parameter for predicting snow depth. While ambient air temperature, again related to elevation and topography, has traditionally been used as the parameter by which many hydrological models (degree-day) predict the transition of SWE into snowmelt, research (e.g. *Marks and Dozier*, 1992; *Balk and Elder*, 2000; Painter *et al.*, 2007; *Bryant et al.*, 2013) has indicated that it is the snow surface energy budget dominated by net solar radiation that is truly driving this process.

Avalanche activity can potentially play an important role in this complex system by increasing or decreasing the melt rate that occurs from the redistribution and metamorphosis of the undisturbed snow cover. The direction in which this balance swings is a factor of two key changes that occur during avalanching: 1) the snow is transported to a lower elevation with generally warmer temperatures and hence, melt regime, and 2) the areal extent of the snow is either concentrated or expanded (*Martinec and de Quervain*, 1975; *de Scally and Gardner*, 1988; *de Scally*, 1996). In most cases, the first factor introduces the avalanched snow to higher ambient temperatures causing an increase in snowmelt. However, in some cases, this can be outweighed by the second factor as avalanches transport snow covering a larger area with a shallower depth to a smaller area with a greater depth. In decreasing the surface area of the snowpack, it becomes less exposed to solar radiation and the turbulent energy fluxes, thereby slowing the rate of melt. A metamorphosis of the snow structure also occurs during its transport in an avalanche, increasing its density by an average of one third, and retarding melt (*McClung and Schaerer*, 2006). On the other hand, the transformed snow crystals tend to have a lower albedo than the original, allowing for more shortwave radiation to be absorbed and thereby increasing snowmelt. This is compounded by dark debris that may have been picked up during transport, which further decreases the albedo of the snowpack in an avalanche runout zone (*de Scally*, 1996). In all, the complex interplay of these factors determines whether there is an eventual increase or decrease in the rate of snowmelt runoff for the catchment as a whole, as a result of the avalanche activity

(*Martinec and de Quervain*, 1975; *de Scally and Gardner*, 1988; *deScally*, 1996; *McClung and Schaerer*, 2006). While research investigating this process has shown evidence in both directions, the majority of the literature points towards avalanche activity not only increasing the hillslope scale spatial variability of SWE (*Clark et al.*, 2011), but concentrating snow in temporally persistent deposits with a smaller areal extent, thereby having the hydrologic role of extending the period of snowmelt (e.g. *Iveronova*, 1966; *Zalikhanov*, 1975; *de Scally and Gardner*, 1988; *de Scally*, 1996). This is often supported by qualitative evidence such as observations of avalanche debris remaining long into the melt season, when surrounding snowpacks, at the same elevation and aspect, have already melted. The primary terrain attribute for determining avalanche activity and its spatial components is slope angle (*McClung and Shaerer*, 2006). The avalanche variable is further influenced by snow accumulation and aspect related factors, such as the wind redistribution/loading of snow, windslab development, solar input, and snowpack crystal type/layer structure. Clearly avalanche activity is highly related to the other physiographic variables already discussed.

The hydrologic role of avalanche activity was explored by de Scally (1996) in the Cascade Range of British Columbia by comparing the resultant runoff of paired basins: one avalanche-prone (treatment) and one relatively avalanche-free (control). Paired basin studies have been utilized for over 100 years, traditionally to compare the hydrologic impact of land use management (deforestation/reforestation, fire disturbance, human development) between watersheds with very similar pre-treatment physiographic characteristics (*Brown et al.*, 2005). In applying this methodology with natural avalanche activity as a treatment, de Scally's results for the data collected during three consecutive spring/summer runoff periods showed that 16-35% of the difference in unit area discharge between the basins was accounted for by the presence of snow in the avalanche-prone basin after all snow had disappeared in the control basin. While this was attributed to the persistence of large avalanche deposits in the avalanche basin, it was also stated that the majority of this difference was possibly due to far greater losses in evapotranspiration that occur in the heavily forested control basin, bringing into the question the importance of landcover to the distribution of SWE in some watersheds. Other topographic differences between the basins were mentioned as possibilities for the difference in snowmelt attenuation. These concerns highlighted the difference in the two basins with respect to physiographic features. An additional consideration was the amount that each basin's snowmelt and subsequent distribution of SWE could be affected by heavy rain during the late spring/early summer period in a maritime climate. So while the work of *de Scally* (1996) provided a great deal of insight into the hydrologic role of avalanches, due to the aforementioned issues, there remain a number of questions to investigate in order to accurately parse out the true effect of this variable.

2.2 Methods for Estimating the Spatial Distribution of SWE

In the process of gaining an understanding of how these variables influence the distribution of SWE in the selected two basins, a spatial modeling method needed to be used to estimate or predict SWE at locations where no observations have been made. A wide range of spatial interpolation and other statistical techniques have been explored in the field of snow hydrology to estimate SWE from measured points and distribute it over heterogeneous landscapes at many spatial scales. The hierarchy of scales can be generally defined as 1) point, less than 5 m, 2) hillslope, 1-100 m, 3) watershed, 100-10,000 m, and 4) regional, 10 -1000 km (*Clark et al.*, 2011). When selecting methods for a given study or application, one must consider the different types of scale of the (natural) process, measurement, and model, as the ratios between these levels are the leading cause of biases in variances and correlation lengths of field measurements and snow modeling (*Bloschl*, 1999). These issues often arise due to a difference in the measurement scale at which data is collected and the model scale at which prediction or explanation of a variable is needed. Consequently, proper selection of the scale triplet components of measurement scale: 1) spacing, 2) extent, and 3) support, is vital to accurately sampling the spatial variability of the natural process and representing it in subsequent modeling (Figure 1). The underlying platform for determining these scale effects is the semivariogram (or variogram, γ), which provides a mathematical function of how the observed data is correlated with distance (correlation length, λ). This tool is the basis for many of the methodologies used to understand the spatial distribution of environmental metrics such as SWE.

One of the simpler interpolation methods utilized, inverse distance weighting (IDW), does not rely on the structure of a variogram, but works by developing a weighted average of known locations by giving more weight to the nearest points and less with increasing distance. This method can be useful in watershed to regional scale applications where anisotropy of SWE becomes more important due to the orientation of mountain

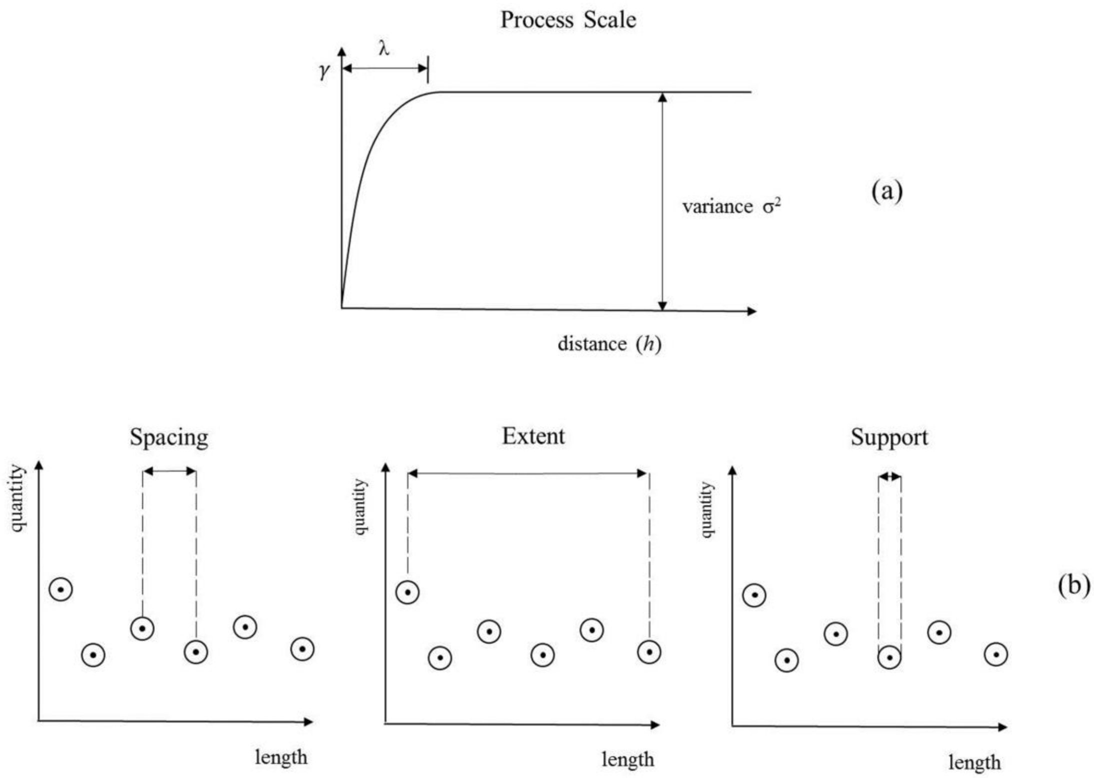

Figure 1. Representation of a variogram (γ) for (a) process scale (correlation length = λ) and how the scale triplet [1) spacing: e.g. distance between SWE sampling points; 2) extent: e.g. length of transect; 3) support: e.g. area of federal SWE sampler tube] of (b) measurement scale are defined [adapted from *Bloschl* (1999)].

ranges (*Fassnacht et al.*, 2003). While IDW offers favorable simplicity, its accuracy can suffer in complex mountain terrain where a variable like SWE does not always vary smoothly in space (*Longley et al.*, 2011). In a study of SWE distribution over the entire Colorado River Basin (approximately 1,040,000 km^2), *Fassnacht et al.* (2003) compared IDW to regression methods and regression detrended IDW methods. Results illustrated that at this regional scale, the IDW method alone was the least accurate (highest RMSE) since it does not account for variations in SWE due to topography. However, hypsometric and multivariate regression (MVR) detrended IDW models yielded substantially lower

RMSE values and realistic results of SWE distribution.

Other interpolation methods include various forms of geostatisitics such as: ordinary kriging, modified kriging, and cokriging (*Phillips et al.*, 1992; *Carroll and Cressie*, 1996; *Erxleben et al.*, 2002). These techniques start by modeling the spatial correlation of the variable of interest (SWE) with a semivariogram (γ), which represents one-half of the average squared difference between binned pairs of sampling points:

$$\gamma\ (h) = \frac{1}{2n} \sum \{[Z(x) - Z(x+h)]^2\} \quad (1)$$

where *Z*, in this study for example, are the SWE depths at *x* and *x* + *h* locations, and *h* is the distance between the points. A mathematical model is then fit to the semivariogram to determine the weights used in one of the various forms of kriging. In ordinary kriging, a variable is estimated by multiplying the value at a sample location by a weight factor for each of the nearest neighbors. Modified kriging first takes into account the hillslope to watershed scale variability trend an independent variable may cause in the surface (trend surface model) of the dependent variable before kriged weighting occurs. Increasing in complexity, cokriging allows for multiple secondary variables to be factored into the estimated values of unsampled points. By this method, a weighted linear combination of the primary and secondary variables is used to determine estimates of the dependent variable (e.g. SWE), and kriged residuals are added to the trend surface model to account for point to hillslope scale variability in the response (*Erxleben et al.*, 2002).

The National Resource Conservation Service (NRCS) uses modified kriging in an elevation-detrended kriging method to spatially interpolate SWE (*Garen et al.*, 1994) over various scales between the 858 automated, remote SNOwpack TELemetry monitoring stations (SNOTELs) and 1185 manual snow courses it maintains in the western US. SWE values from the sites are used in linear regression with elevation as the predictor variable to account for nonstationarity due to the orographic effect. The linear SWE-elevation trend is subtracted from the observed to get the residuals which are then described by a linear variogram to determine the weighted sum of nearby measurements used in the kriging process. The interpolated SWE values within the watershed of each site, along with its historical record, are then used as an index in regression analysis with 18 independent variables to predict nearby seasonal stream discharge. While this system offers a long record of relatively accurate SWE estimation and streamflow prediction over a broad area for average conditions, the regression analysis component of this methodology is limited by the fundamental assumption of a linear relationship between the predictor variables, especially elevation, and SWE (*De Walle and Rango*, 2008).

To investigate how this most widely used and available ground-based SWE dataset could be utilized to generate more accurate distributed SWE estimates; *Harshburger et al.* (2010) applied an alternative linear regression methodology in a 1625 km^2 section the Big Wood River watershed of south-central Idaho. Simple linear regression (elevation vs SWE) was first used with binary (snow-covered; non snow-covered) remote sensed snow covered area data (MODIS). This step ensured that modeled SWE approached 0 cm at a determined snowline and subsequent SWE estimation was restricted to the snow covered area above it. Multiple linear regression (MLR) was then used with elevation, slope, aspect (northness and eastness), terrain ruggedness (relative local vertical relief), latitude, longitude, clear-sky solar radiation, and vegetation cover type as the predictor variables for the response variable of SWE in models. They found the best models with various combinations of these physiographic variables to explain a mean of 82% of the variance in the SWE distribution.

Regression tree analysis was introduced by *Breiman et al.* (1984) to offer a nonlinear alternative to the traditional linear methodologies. Through research in the field of snow hydrology, binary regression tree (BRT) modeling was soon recognized to work well with the often nonlinear distribution of snow properties, yielding more accurate results in modeling this phenomenon than other attempts (e.g. *Elder et al.,* 1998; *Balk and Elder,* 2000; *Erxleben et al.,* 2002; *Winstral et al.,* 2002; *Anderton et al.*, 2004; *Molotch et al.,* 2005). While this methodology was given consideration by *Harshburger et al.* (2010), their study highlights the primary disadvantage of using BRT analysis, that being the requirement of a large and spatially dense sampling dataset. Thus, the large areal extent of their study area and relatively sparse distribution of SNOTEL and snow course data eliminated BRTs as a modeling option. However, *Elder et al.* (1998) applied this methodology with a combination of field measurements for SWE and remotely sensed snow cover data in the 92.8 km^2 Blackcap Basin of the Sierra Nevada, CA and found BRT models, with elevation, slope, and net solar radiation as independent variables, to explain 60-70% of the variance in SWE with 13 to 25 terminal nodes, respectively.

Balk and Elder (2000) added kriging to the BRT methodology to develop a deterministic-stochastic model tested in 6.9 km^2 Loch Vale watershed in the Front Range, Colorado. They conducted intensive snow surveys in April of 1997 and 1998 to obtain snow depth and snow density point measurements and general linear regression analysis was used to distribute snow density across the basin, allowing for a subsequent calculation of distributed SWE. Snow depth was used as the dependent variable input for BRT models with various combinations of the physically based independent variables: elevation, slope, net solar radiation and vegetation to model hillslope to watershed scale variability. BRT estimated snow depths were subtracted from measured snow depths and these residuals were modeled by kriging interpolation to account for point to hillslope scale variability. After multiplying modeled snow depth by modeled snow density, BRTs with 18 terminal nodes explained 54-65% of the variance in SWE across the basin. *Balk and Elder* (2000) noted that an advantage of the BRT to strictly an MLR model was the ability to model the often non-linear relationships of SWE to physiographic variables through multiple splits on the same variable. Furthermore, unlike the MLR, the BRT is easy to interpret by seeing the individual splits on variables and being able to decide if they intuitively make sense. For these reasons, BRTs have been found to be more accurate in most studies involving the goal of distributing SWE over complex terrain (*Balk and Elder*, 2000).

Similar conclusions were made by *Anderton et al.* (2004) in their evaluation of the spatial variability of SWE in a 0.32 km^2 alpine cirque in the Pyrenees Mountains. Their study utilized MLR and BRT analyses with elevation, slope, solar radiation and wind exposure indices (various directions and filter lengths) as predictor variables. While their initial MLR analysis was partially successful in modeling snow distribution, a large degree of the spatial variability could not be predicted by the linear combinations of the physiographic variables. After employing BRT analysis with the same variables, they found pruned trees with 7 to 9 terminal nodes to explain 70-78% of the variance in the snow depth and date of disappearance of the snowpack.

Molotch et al. (2005) applied the BRT methodology along with geostatistical techniques to examine the effect of DEM source and independent variable selection on the modeled distribution of SWE in the 19.1 km^2 Tokopah Basin in the Sierra Nevada. The independent variables of: elevation, slope, aspect, northness, solar radiation, and maximum upwind slope were modeled with a Shuttle Radar Topography Mission (SRTM) 27 m DEM, a National Elevation Dataset (NED) 30 m DEM, and a level 1 standard 7.5 minute 30 m USGS DEM. Modeled independent variable values were input with snow depth and density measurements taken in May, June, and July to subsequently model SWE. Results showed optimally pruned trees of 5, 7, and 8 terminal nodes to explain 31, 39, and 34% of the variance, respectively. It was importantly noted that R^2 values of BRTs cannot be directly compared between studies due to the different characteristics of watersheds, water years, and therefore climatology. However, when these limitations are considered in a comparison, the R^2 values do still offer a value on which to weigh the effectiveness of models between studies.

Erxleben et al. (2002) conducted a comparison of IDW, ordinary kriging, MLR trend surface, modified residual kriging, BRT, and BRT with kriging methods to model to the distribution of snow depth in three 1 km^2 study areas in north central Colorado. Stepwise MLR with the independent variables: x (easting), y (northing), $x * y$, x^2, y^2, elevation, slope, aspect, radiation, and vegetation was used to generate the trend surface that independently modeled snow depth for each site, but these were also integrated with modified residual kriging to improve trend surface model performance. BRTs were grown with elevation, slope, aspect, and net solar radiation as independent variables to model the hillslope to watershed scale variance in data. The residuals from observed and BRT modeled data were then kriged to account for point to hillslope scale variability. The results showed that BRTs with kriging explained the most variance (29.2 and 31.0 %) in snow depth at two of the sites. However, an unkriged BRT performed slightly better in one site (17.5 % compared to 17.2 % of variance) and it was questioned whether the unsubstantial BRT performance improvement by kriging at the other sites was worth the extra computational effort (*Erxleben et al.*, 2002). Following in performance of the BRTs were the modified residual kriging models for all three sites. While the trend surface model performed the next best at two of the sites, it performed particularly poor at one site. The performance of IDW and ordinary kriging was mixed between the sites, but generally, ordinary kriging did not offer any improvement over IDW. While the explained variance in snow data by BRT models was considerably lower than in previous studies, it was concluded that this method was still superior in modeling the nonlinear relationships between physiographic variables and snow distribution metrics (*Erxleben et al.*, 2002). A summary of previous research is presented in Table 1.

The research of this thesis continues to explore the previous investigations of the dominant variables influencing the spatial distribution of snow depth and SWE, but as they relate to mountainous regions of the U.S. Intermountain West. A paired basin research design was adopted from previous studies (e.g. *deScally*, 1996; *Brown et al.*,

2005) that utilized this methodology for a side-by-side comparison of the variables controlling natural phenomena in these study areas with attributes such as area, elevation, and climatic conditions being virtually equal. The design of *de Scally* (1996) was specifically targeted for a comparison of the effect of avalanche activity on the distribution of SWE. However, an attempt was made to select a study area that would eliminate some of the variables in the original design that caused uncertainty in his final results. While the study area of de Scally (1996) involved avalanche-prone and control basins of 5.0 and 11.8 km^2 respectively, the current research looked at two basins much closer in extent, with areas of 1.38 and 1.63 km^2. The substantially smaller area of these basins allowed for a higher density of points for recording the snowpack metrics, thereby leading to a relatively robust sample. In addition, the ease of access to the current study area enabled frequent visits throughout the water year, allowing for a comparison of the difference in dominant variables during the periods of snow accumulation, peak SWE, and ablation. The study area is representative of high alpine basins in this part of southwest Montana and the paired basins were chosen to be as similar as possible with respect to area, elevation range, and to a lesser extent, aspect, with the assumption that total, basin wide snow water equivalent accumulation would be roughly the same in the absence of wind transport. A particular effort was made to select sites with very similar tree and vegetation coverage to possibly avoid the variable that created the most uncertainty in the *de Scally* (1996) design. This research was performed in an intermountain snow climate with substantially different weather patterns, snow accumulation, and avalanche dynamics than the study site of *de Scally* (1996). Unlike at

Table 1. Summary of selected previous field research investigating snow distribution integral to the current study.

References	Region	Study Area (km^2)	Dependent Variable(s)	Independent Variables Considered	Dominant Independent Variable(s)	Significance to current study
Anderson et al. (2014)	Dry Creek Experimental Watershed, SW ID	27	Snow depth Snow density SWE	Elevation Slope Aspect Northness Canopy density WEI	Elevation Slope Aspect Northness Canopy density WEI	Study sampled accumulation, peak SWE, and ablation periods at low, mid, and high elevations and on watershed and hillslope scales. Results indicate different variables being dominant during different time periods at different scales and elevation ranges. The WEI is directly adapted by current study
Anderton et al. (2004)	Pyrenees Mtns Spain	0.32	Max snow depth Snow density Date of snow disappearance Avg melt rate	Elevation Slope Solar radiation Wind exposure indices (direction distance filters)	Wind exposure (Avg direction, 37 m filter)	More of observed variability modeled by nonlinear BRT than linear combinations of independent variables in MLR WEI of current study adapted from wind exposure indices Accumulation through ablation analysis
Balk and Elder (2000)	Loch Vale basin, Front Range, CO	6.9	Snow depth Snow density SCA SWE	Elevation Slope Solar radiation Vegetation	Solar radiation	Successful results using BRT with with cokriging
Clark et al. (2011)	Upper Jollie Catchment, S Alps, NZ	30	Snow depth Snow density SWE	Elevation Solar radiation Drifting (Wind) Preferential deposition Avalanching/ sloughing Vegetation	Elevation Solar radiation Drifting (wind) Preferential deposition	Explicit and implicit analysis of multiscale variability and which variables control snow distribution at different scales Field sampling strategy

Table 1 continued.

References	Region	Study Area (km^2)	Dependent Variable(s)	Independent Variables Considered	Dominant Independent Variable(s)	Significance to current study
de Scally (1996)	Cascade Mtns, SW BC, CAN	5.0/11.8	SWE Avalanche deposit SWE Discharge	Elevation Avalanching/ sloughing Temperature Vegetation Rainfall	Avalanching/ sloughing Vegetation Rainfall	Paired-basin study design for explicit analysis of avalanche activity controlling distribution of SWE
Elder et al. (1991)	Emerald Lake, Sierra Nevada, CA	1.2	Snow depth Snow density SCA SWE	Elevation Slope Solar radiation	Solar radiation	Field sampling strategy in similar size study area Implicit accounting for avalanche/ sloughing variable through modeling with slope Importance of solar radiation at smaller basin scale
Elder et al. (1995)	Emerald Lake, Sierra Nevada, CA	1.2	Snow depth Snow density SCA SWE	Elevation Slope Solar radiation Vegetation Substrate	Solar radiation Substrate Elevation	Improved prediction of distributed SWE with BRT modeling using previous dataset from *Elder et al.* (1991) Method of BRT pruning to provide data usable for distributed snowmelt models
Elder et al. (1998)	Black Cap Basin, Sierra Nevada, CA	92.8	Snow depth Snow density SCA SWE	Elevation Slope Solar radiation	Elevation Solar radiation	Successful results using BRT Importance of elevation at relatively large basin scale
Erickson et al. (2005)	Green Lakes Valley, Front Range, CO	2.3	Snow depth	Elevation Slope Potential radiation Wind shelter Wind drift	Potential radiation Wind shelter	Importance of wind sheltering in comparison to other phyiographic variables in similar scale basin Accuracy of nonlinear trend modeling for abrupt spatial variability of snow depth

Table 1 continued.

References	Region	Study Area (km^2)	Dependent Variable(s)	Independent Variables Considered	Dominant Independent Variable(s)	Significance to current study
Erxleben et al. (2002)	north central CO	1.0 (3)	Snow depth Snow density SWE (total volume)	Elevation Slope Aspect Solar Radiation Vegetation	Elevation Aspect	Comparison of IDW, MLR, geostatisitical methods and BRTs in study basins on same scale as current study Demonstrated superior results provided by nonlinear method of BRTs
Fassnacht et al. (2003)	Colorado River Basin	1.04 x 10^6	SWE	Longitude Latitude Elevation Slope Eastness Northness Distance to ocean Barrier ht (wind) Barrier dist (wind) Shield ht (wind) Forest density	Latitude Elevation Slope (regional) Barrier ht (wind)	Use of hypsometric regression and MLR combined with IDW demonstrated superior modeling technique to just IDW for interpolating SNOTEL data on the regional scale
Harshburger et al. (2010)	Big Wood River Basin, south central, ID	1625	SWE SCA	Elevation Slope Northness Eastness Terrain ruggedness Latitude Longitude Solar radiation Vegetation cover type	Elevation Terrain ruggedness Solar radiation	Use of a simple methodology (MLR) with very successful results predicting the distribution of SWE Example of elevation being primary physiographic variable at the watershed to regional scale

Table 1 continued.

References	Region	Study Area (km^2)	Dependent Variable(s)	Independent Variables Considered	Dominant Independent Variable(s)	Significance to current study
Molotch et al. (2005)	Tokopah Basin, Sierra Nevada, CA	19.1	Snow depth Snow density SWE	Elevation Slope Aspect Northness Solar radiation Maximum upwind slope	Northness Solar radiation	Use of BRT models with different combinations of the physiographic variables used in the current study to successfully distribute snow depth and SWE
Welz et al. (2015) (this study)	Cedar Mtn, Madison Range, MT	1.38 1.63	SWE	Elevation Slope Northness Eastness Solar radiation Wind shelter/ exposure (WEI) Avalanche activity	Wind shelter/ exposure (WEI) Eastness Solar radiation Northness Slope/Avalanche activity	Paired basin comparison of dominant physiographic variables controlling SWE distribution during three phases of snowpack development Comparison of linear (MLR) and non-linear modeling (BRT) predictive performance Explicit consideration of the effect avalanche activity on SWE distribution
Winstral et al. (2002)	Green Lakes Valley, Front Range, CO	2.25	Snow depth SWE	Elevation Solar radiation Slope Redistribution parameters (wind shelter/ exposure)	Max upwind slope parameter (100m)	Used BRTs with physiographic variables to successfully model snow depth and SWE distribution Demonstrated importance of the inclusion of wind redistribution parameter to increase performance of model in predicting distribution of snow depth and SWE in alpine basin similar in size to current study Redistribution parameters are foundation for the simplified WEI used in current study

that maritime site, precipitation at the site of this study came mainly in the form of snow through much of the ablation period. Consequently, this eliminated some of the uncertainty regarding how the late spring distribution of SWE may have been influenced by heavy rain, as in *de Scally* (1996). Furthermore, this study situated in an intermountain snow climate expands the information in the snow hydrology community as to how the avalanche dynamics of this particular region may augment the other physiographic variables influencing the spatial distribution of SWE in alpine basins.

Most of the previous work investigating the distribution of SWE focuses only on the period of peak SWE, as this is the target for operational streamflow forecasting in terms of the total volume of water available for input into stream networks. However, when attempting to understand how the distribution of SWE is influenced by the complexity of interacting physiographic variables, it is important to consider the temporal evolution of these processes. The study conducted by *Anderton et al.* (2004) investigated the topographic controls on both snow accumulation and melt in order to correlate these with the timing of snowpack disappearance. They found there to be no significant evidence that physiographic variables control the spatial variation in melt rates during this season rather that it is mainly predetermined by the distribution of snow at maximum accumulation. *Anderson et al.* (2014) further explored this phenomenon by conducting repeat surveys of snow depth and SWE at physiographically representative transect and grid based sampling points at various scales (point, hillslope, watershed) and times throughout the accumulation, peak SWE, and ablation periods. Research was conducted in the well-established 27 km^2 Dry Creek Experimental Watershed in the foothills near

Boise, Idaho. *Anderson et al.* (2014), through Pearson's correlation coefficient and variogram analysis, were able to determine which independent variables [elevation, slope, aspect, northness, canopy density, and a wind exposure index (WEI)] were most influential in determining snow depth and SWE, as well as their subsequent correlation lengths. They found that elevation was the most dominant variable in determining snow depth on a watershed scale through much of the accumulation period, but was not sufficient in predicting the distribution of SWE into the ablation period when variability on the hillslope scale becomes more apparent, controlled by aspect (and hence solar radiation input) and canopy density. It was also noted that snow redistribution by wind (reflected in the WEI) was an important player through the accumulation period but becomes less influential as the ablation season progresses and warmer temperatures inhibit this process. The study of *Anderson et al.* (2014) provided a valuable framework for the analysis and expected results of the current study. Because it was conducted in a transitional snow climate at lower elevation (950 - 2130 m) and generally at the watershed scale, it leaves room for new developments on this research in an intermountain, high alpine setting where variables like canopy density and precipitation as rainfall are assumed to be negligible. Furthermore, a paired basin study of the temporal evolution of SWE distribution addresses the point expressed by *Elder et al.* (1995) that correlations of snowpack metrics with physiographic variables are not necessarily similar between small adjacent watersheds because the processes driven by these variables tend to vary over must shorter distances.

When conducting research such as this, it is important to make an attempt at keeping a clear distinction between a primary goal of explanation or prediction (*Shmueli*, 2010). In many disciplines, including the environmental sciences, the focus of modeling is almost exclusively for causal explanation. However, this type of modeling is related to the theory of "basic science" aimed at explaining natural phenomena on a conceptual level. While this is certainly an important component of snow hydrology, the concept of prediction is perhaps more reflective of this discipline's ultimate goal. This is related to "applied science", which is concerned with the underlying mathematical relationships connecting sets of variables so that predictions can be made at a measureable level from known values to unknown values (*Shmueli*, 2010). This is the underlying premise of measuring, modeling and spatially distributing snow metrics such as SWE across the landscape. Previous research in snow hydrology has often fused the somewhat ambiguous division between explanation and prediction, sometimes not giving a clear indication whether the modeling of a study has offered explanatory power or predictive power (*Shmueli*, 2010). This distinction is increasingly muddled by the simultaneous use of modeling terminology such as "predictor" variables (e.g. elevation, aspect, etc.) that "explain" a certain amount of variance in the response variable (e.g. SWE). Nevertheless, the distinction between these two ideas has a definite influence on the progression of a methodology and its outcome. This is evident in the large degree of variability in how previous studies have tailored modeling methodologies to suit the specific goals of the research. Despite the ambiguity presented by terminology in the previously discussed investigations into snow distribution, it is clear that the primary goal of most is prediction.

While the distinction between explanation and prediction has been long debated in the philosophy of science and is not even clearly stated in the statistical literature, it is understood among statisticians to be intuitively applied (*Shmueli*, 2010). The intent of this current study is not to delve into the depths of this concept, but to verify that this important distinction was recognized, as it did indeed have a profound impact on how modeling was fit to match the intent. The initial aim and first step of this current methodology was to determine which sets and hierarchical structures of physiographic variables created models with the most power in explaining the variance of observed SWE values. Thus, MLR models were allowed to use all of the explanatory variables and BRT models to grow to full size, thereby offering the most explanatory power. However, predictive power was maximized by scaling back the MLR complexity and pruning the BRTs to find the "true" models that reflect the real underlying processes at work, instead of offering overoptimistic estimations (*Shmueli*, 2010). Then, the ultimate modeling goal of predicting the entire distributions of SWE across the study basins was achieved through estimation with these optimal models. Therefore, the subsequent modeling methodologies utilized and results will be presented and discussed in this context of explanation and prediction.

3. STUDY AREA

The area selected for this research comprises paired alpine basins on the east slopes of Cedar Mountain (approximate center: N 45° 14' 3" W 111° 29' 42") in the Madison Range near Big Sky, in southwest Montana (Figure 2). The hypothesized more avalanche-prone basin (Basin A) has an area of 1.38 km^2 rising from 2721 to 3251 m (530 m), with predominantly east to northeast facing terrain forming the headwaters of the South Fork of the West Fork of the Gallatin River. Directly south, the control basin (Basin B) has an area of 1.63 km^2 ranging from 2645 to 3253 m (608 m). The generally

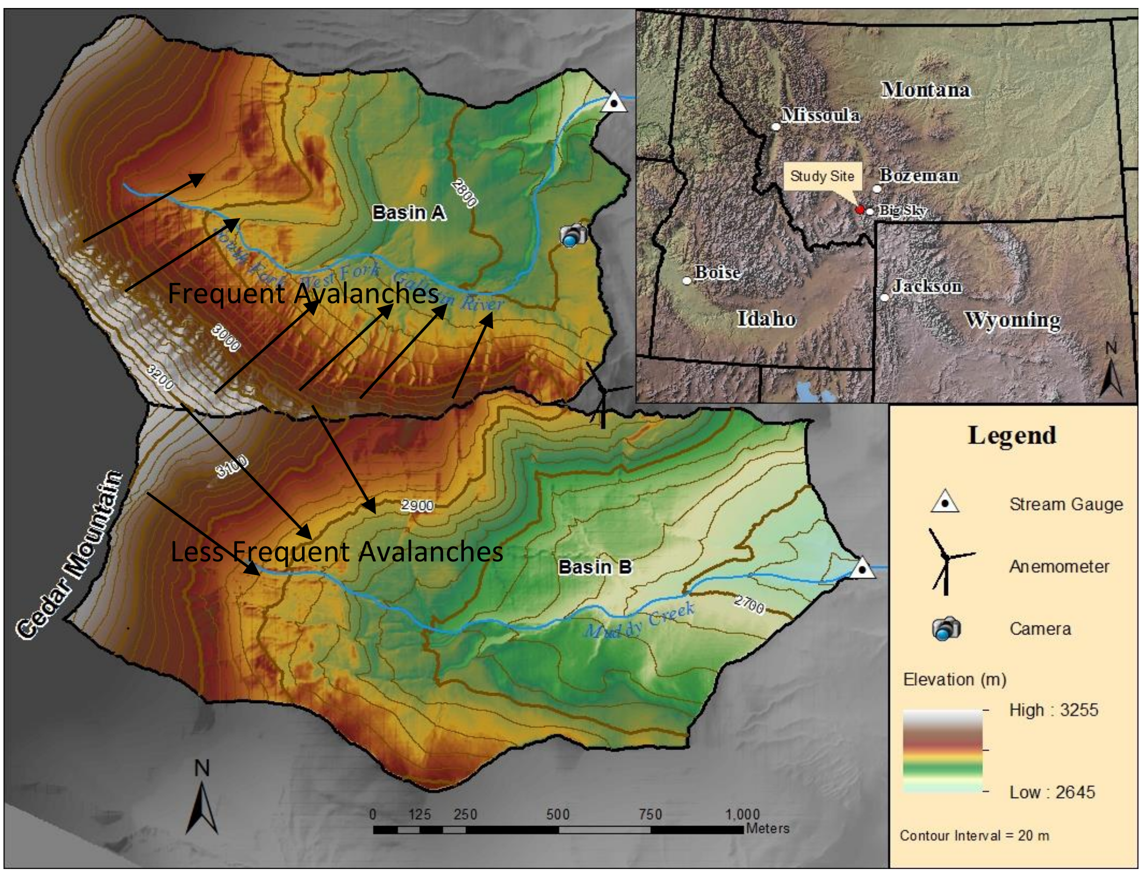

Figure 2. Map of the study site showing the distribution of elevation, aspect, and topographic features associated with suspected frequency of avalanche activity.

east to southeast facing terrain of this basin drains into Muddy Creek which flows around the south side of Pioneer Mountain before joining the South Fork of the West Fork of the Gallatin River approximately 7 km below Basin A. Average slopes are 24.2° and 22.5° in Basin A and B, respectively, with 26.0% and 31.4% of the area in each basin considered avalanche terrain (slope 30-50°). Both basins are undeveloped and exhibit land cover typical of an alpine environment in this region, with sparse ground cover vegetation covering the majority of the area and riparian shrubs limited to stream channels. Conservative estimation of tree cover utilizing satellite imagery in a GIS, is approximately 7% for Basin A and 19% for Basin B. Tree cover consists entirely of evergreen species.

This area of southwest Montana has been generally classified as having an intermountain snow climate (*Mock and Birkeland,* 2000). However, lying on the northern end of the intermountain zone at high elevation, cold average temperatures result in the snowpack of the Big Sky area to trend more towards a continental regime (*Mock and Birkeland*, 2000). The 20-year (1991-2010), October 1 - May 10 averages for precipitation (538 mm) and snow water equivalent (480 mm) from the NRCS Lone Mountain SNOTEL (*NRCS*, 2014) at 2707 m (approximately 6.5 km from the study site), also indicate this area receives substantially less snow than some intermountain ranges to the south, such as the Tetons (Phillips Bench SNOTEL at 2500 m; precipitation: 729 mm, SWE: 660 mm) and Wasatch (Snowbird SNOTEL at 2942 m; precipitation: 1072 mm, SWE: 1087 mm). This cold and relatively drier climatic pattern has an important influence on the magnitude of snow redistributed by wind, as well as potential avalanche activity that can occur due to persistent weaknesses in the typical stratigraphy of this snowpack.

The primary attributes assumed to separate Basin A and B into avalanche-prone and control are their dominant topographic features and distribution of aspect. This applies to the steep, north/northeast facing headwall of Basin A, for which approximately 73% of the slope is 30-50°. This combination of slope and aspect creates more potential for wind loading of snow, causing frequent sloughing and the occasional release of slab avalanches. In comparison, the east/southeast facing headwall of Basin B has approximately 54% of its slope between 30 and 50°. It is thought to have less potential for avalanche activity due to more wind scour than deposition and a less expansive and contiguous avalanche start zone. Consideration of these variables is further addressed in the methods section.

4. METHODS

4.1 Classification of Strata by Physiographic Variables

Snowpack data collection employed a stratified sampling strategy based on the goal of capturing a representative sample from each basin's distribution of physiographic variables (i.e. elevation, slope, aspect, solar radiation, wind exposure/shelter, and avalanche activity). Elevation, slope, aspect, solar radiation, and avalanche zone components were directly modeled from a 1/3 arc second (approximately 10 m cell size and subsequently referred to as such) National Elevation Dataset (NED) (*USGS*, 2013) DEM using Spatial Analyst Tools in ESRI ArcGIS. Wind exposure/shelter was also modeled from this 10 m DEM, but required more processing with ArcMap tools (see section 4.6). Elevation was reclassified into 10 equal interval (approximately 61 m) strata to span the full range of the study area, 2645-3255 m. In reclassifying slope, its relationship to solar radiation intensity, wind shelter/exposure, and avalanche activity was considered. Hence, lower angle areas, where solar intensity and wind redistribution are less influential, were lumped into a 0-15° strata. Conversely, very steep areas that tend to be largely snow-free due to the more profound effect of these variables, along with the constant sloughing of snow, were categorized into 60-90°. For avalanche activity, the second lowest strata, 15-25°, was considered to span the upper limit of runout zones and lower limit of avalanche tracks. Seven 5° strata, spanning 25-60°, were used to classify the remaining terrain, not only to represent the range of over which approximately 98% of all dry-slab avalanches occur (*McClung and Schaerer*, 2006), but to capture the point to hillslope scale topographic features affecting solar intensity/shading and wind redistribution. Aspect was modeled with the Aspect tool in ArcGIS and reclassified into eight, 22.5° degree strata beginning at 0° (north) and running clockwise through 360°. Due to the circular data issue of aspect, it was transformed into a variable of northness and eastness (*Harshburger et al.*, 2010), by taking the cosine and sine of degrees from north, respectively. This yielded surrogate values for aspect between -1 (due south) and +1 (due north) for northness and between -1 (due west) and +1 (due east) for eastness that were used in analysis. The Area Solar Radiation calculation tool in ArcMap was used to model the daily cumulative solar radiation in watt hours per square meter (WH/m^2) from November 1, 2012 to May 1, 2013. These values, ranging 115,374-561,342 WH/m^2, were reclassified by natural breaks (Jenks) into ten strata ranging 1-10. While the previously described slope strata indirectly incorporated avalanche activity, a set of slope strata were created to directly sample of the distribution of SWE in the avalanche zone components. This involved reclassifying slope into strata of the typical angle ranges of the avalanche zone components (*McClung and Schaerer,* 2006): (1) runout (<15°), (2) track (15-30°), and (3) start zone (30-50°).

4.2 Field Campaign Sampling Strategy

Once the physiographic strata were determined, a field sampling strategy was adopted to gain a representative sample by incorporating aspects of similar studies aimed at sampling SWE (e.g. *Elder et al.*, 1998; *Clark et al.*, 2011) and modifying them to match the scale triplet [spacing, extent, support, after *Bloschl* (1999)] considerations particular to the study area. This strategy evolved while testing and adapting the field sampling methods, gaining familiarity with the study site, and considering how to travel safely given the terrain limitations and avalanche danger during the accumulation period (seven visits: January 31-April 11) of data collection. Hence, the overall sampling techniques and strategy were solidified by the start of the peak SWE sampling period (six visits: April 30-May 10), and continued during the ablation period (eight visits: June 1-July 10). Because the primary goal of sampling for this study was to capture the spatial distribution of the snowpack metrics during peak SWE, the general location of the transects/points aggregated during the accumulation period was continued during peak SWE sampling period, but modified slightly and supplemented with additional ones to achieve a sample more representative of the basins' physiographic strata. In order to get a relative idea of the pattern of the declining snowpack, but limited by the infeasibility of getting more than one sample at all peak SWE transects in the allotted timeframe, the visits made during the ablation period involved taking actual measurements at a representative subset of the peak SWE transects. Each transect in this subset was visited at least once and repeated for those where the snowpack was persistent. Transects where melt out occurred prior to the end of this survey period were able to be determined snow-free from vantage points within the study site. In this fashion, snowpack data was recorded for every peak SWE transect/point by the end of the ablation period. Despite this distinction between sampling periods, the same general methods, and scale triplet were maintained during the entire 2013 field campaign.

4.3 Snow Depth and SWE Sampling

Snowpack sampling involved the collection of snow depth and SWE measurements at points along transects following elevation contours. Transects were assigned an identifier, e.g. A1, signifying which basin and the relative level (lowest to highest) of elevation. Some transects sampled in the accumulation period were given an additional a or b (e.g. A1a, A1b) to indicate it had two parts that became one in later surveys or that which had a location that was not close enough to later surveys to be considered the same transect in analysis. However, the general location of these transects/points was continued in the subsequent periods of sampling. Starting point coordinates for transects were predetermined in ArcGIS and located in the field using a handheld Trimble Geo XH GPS, but spacing between points was paced (after calibration with actual distances) to introduce a small degree of randomness to their location. Transects ranged 150-450 m in length with points spaced 15-50 m apart (Figure 3). Snow depth was measured with a 320 cm avalanche probe at the center of every point, as well as 1 m from the center in each cardinal direction (N, E, S, and W). The average of the five depths was considered the snow depth value for that point. Points with snow depths exceeding the probe length were measured with a 150 inch Federal snow sampler (sometimes in two tiers for very deep points) and only one depth value was used due to time constraints. SWE was measured with a Federal snow sampler at a minimum of two, randomly, pre-chosen points along each transect. SWE values were used to calculate average snow density within each transect, which was then used to interpolate SWE across the entire transect from the depths.

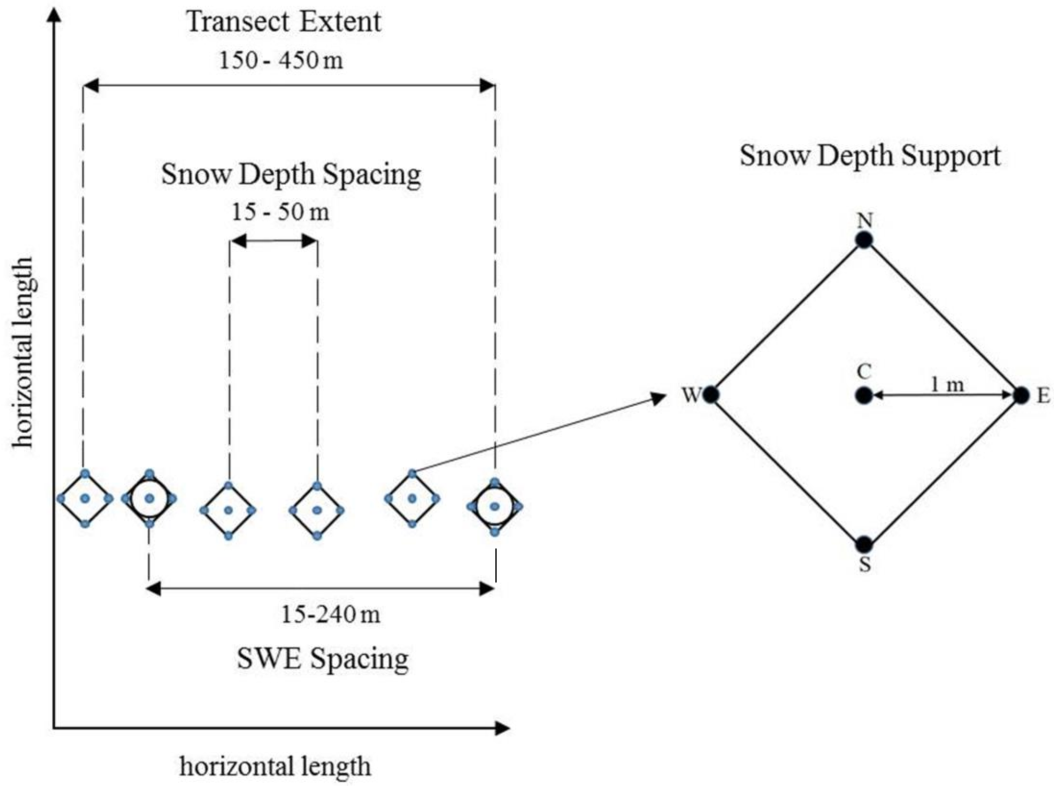

Figure 3. A diagram showing the snow depth and SWE sampling design with respect to the scale triplet.

4.4 Snow Depth and SWE Data Processing

All field data was recorded in a database in a handheld Trimble Geo XH GPS that assigned the snow depth and SWE measurements to the sample points during data collection. This data was downloaded for each survey date as a single shapefile in ArcGIS with the snowpack metrics attached as attributes. Downloading of this field data with GPS Pathfinder® Office to an office database involved differentially correcting it against the Montana State University Continuously Operating Reference Station to provide sub-meter location accuracy of the sample points. This was an important step to ensuring the highest degree of accuracy in the placement of sample points on the 10 m

NED DEM dataset used to model all the physiographic variables. In this way, a database was developed by extracting 10 m DEM cell values for elevation, slope, northness, eastness, solar radiation, and a wind exposure/sheltering variable, to the sample points in ArcGIS. This data was imported from ArcGIS and managed for analysis in an Excel workbook (Appendix A).

4.5 Automated Instrumentation

In order to supplement snowpack measurements with respect to avalanche activity and wind, automated instrumentation was also installed prior to sampling (Figure 2). As a qualitative documentation of avalanche occurrences, a digital SLR camera was installed facing the northeast headwall of Basin A, as it was expected to experience the most frequent activity. The camera collected photos hourly (08:30-16:30) from December 17 to August 19, 2013.

A site specific record of wind was required to enhance the analysis of this variable; hence, an anemometer (Windlog, RainWise Inc.) was installed at 2808 m on the ridge separating Basins A and B (Figure 2). It recorded average scalar wind speed (m/s) and direction (resolution: 22.5 degrees) at 15 minute intervals from December 17 to March 9, 2013.

Water level loggers (pressure transducers: HOBO model U20, 0 to 9 m) were installed at the hydrologic pour point of each basin’s outlet stream (Figure 2) and recorded stage at hourly intervals November 1 to August 21, 2013. Use of this data is discussed in the future work section at the end of this thesis.

4.6 Wind Exposure/Sheltering Variable

A wind exposure index (WEI), E_b^x, (*Lapen and Martz*, 1993; *Anderton et al.*, 2004; *Anderson et al.*, 2014) was derived after field sampling in order to quantify the effect of the wind redistribution of snow. This was modeled utilizing directional elevation data to determine the degree of wind exposure or sheltering at sampling points from the equation:

$$E_b^x = z_i - \bar{z}_b^x \quad (2)$$

where z_i is the DEM derived elevation of a given sample point, and $\bar{z}_b^x$ is the average elevation a given filter distance x (m) and bearing b (°) from the DEM pixel (or sample point) of interest.

In order to model the WEI at a resolution most appropriate to the spatial scale at which this process occurs in the study site, a statistical analysis was performed to compare the WEI modeled with the available 1 m LiDAR and 10 m NED DEM datasets. This involved a basic analysis of the measures of relative standing to get an idea of how the datasets differ (Figure 4). These results showed the major difference in the datasets to be the 1 m LiDAR having a variance that is approximately 30% greater than that of the 10 m NED. The practical interpretation of this is that the higher resolution of the 1 m LiDAR picks up many of the fine details in topography that the lower resolution of the 10 m NED smooths out. In reality, this smoothing effect of the 10 m DEM could represent the way in which the small topographical features of the study site become masked by the snowcover once it reaches a critical depth. Therefore, what may be perceived as greater

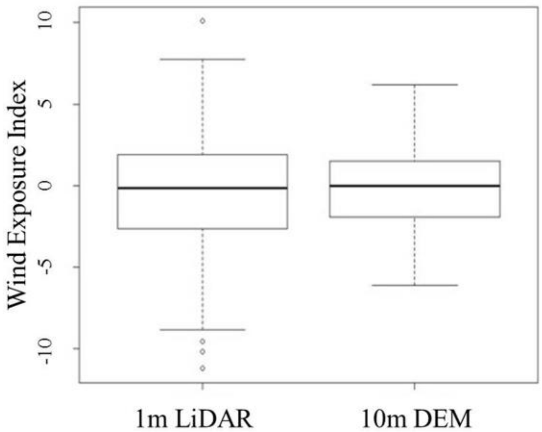

	1 m LiDAR	10 m NED
Minimum	-11.207	-6.108
Q1	-2.634	-1.925
Median	-0.160	0.008
Q3	1.890	1.519
Maximum	10.089	6.184
Mean	-0.266	-0.067
Stand. Dev.	3.189	2.582
n	307	307

Figure 4. A boxplot comparison and table summarizing the measures of relative standing for modeling the WEI with 1 m LiDAR and 10 m NED DEMs.

detail in modeling the wind driven distribution of snow by the 1m LiDAR is possibly just "noise" created by a resolution that is beyond that in which the phenomenon occurs. Consequently, the 10 m NED was chosen as the optimal modeling dataset for the WEI, strictly from a data analysis standpoint. On the more pragmatic side, it was also considered ideal in that it is readily available to the public on the USGS website, whereas the 1 m LiDAR can be difficult and expensive to acquire if not granted through agencies such as NCALM.

With the 10 m NED as the selected input, a series of steps were conducted in ArcMap Tools of ArcGIS to model the WEI (Figure 5). The $\bar{z}_b^x$ variable was derived by first determining the correlation length of snow depth sampling point data to provide the filter distance (*x*), and then the dominant wind direction during the majority of the accumulation season to provide the bearing (*b*). Correlation length was identified by plotting the snow depth data in a semivariogram in the Geostatistical Analyst tool with a lag size set at 27.78 m (as determined through Spatial Statistics/Average Nearest

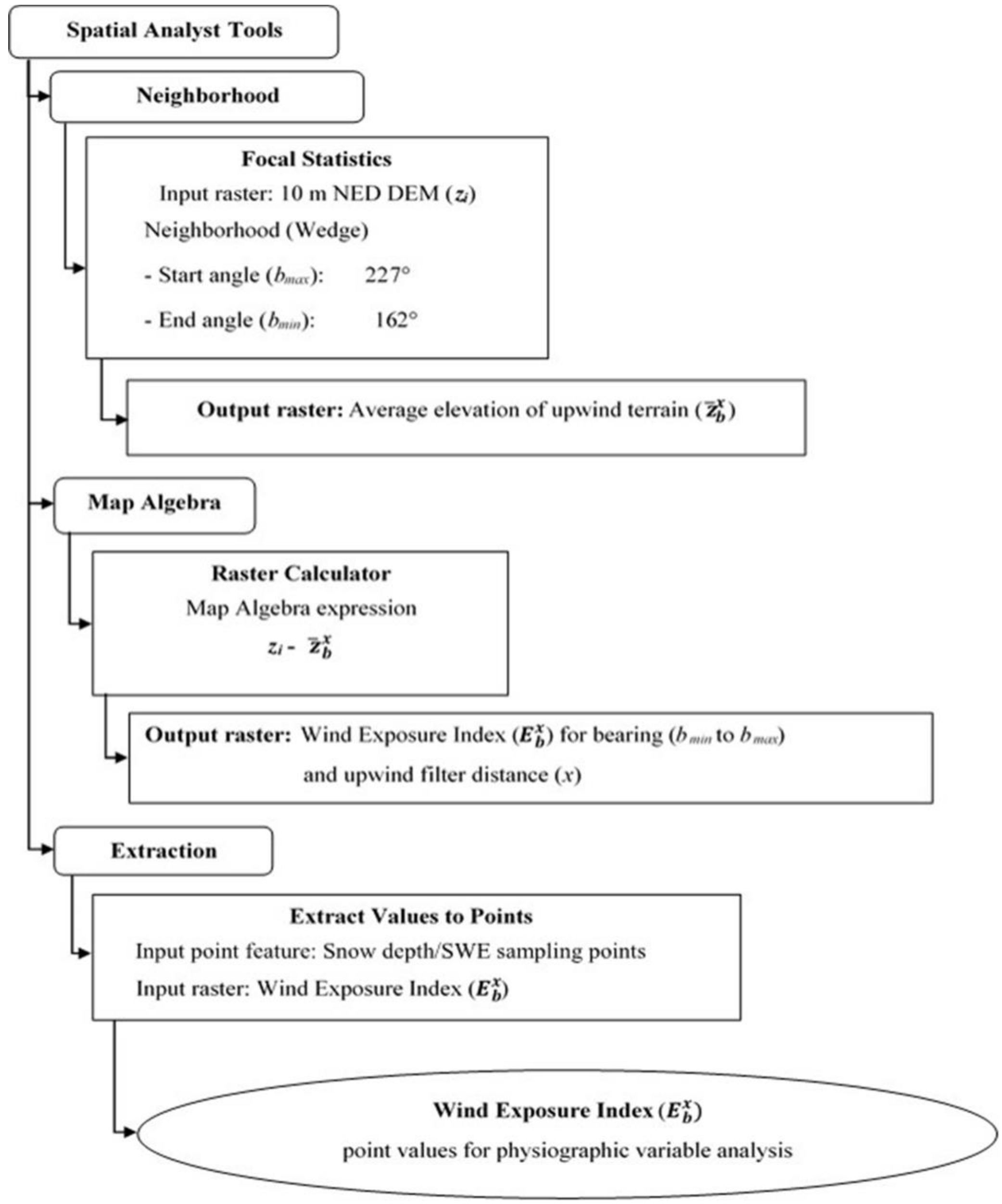

Figure 5. Steps to modeling the wind exposure index ($E_b^x = z_i - \bar{z}_b^x$) in ArcToolbox.

Neighbor). This yielded a range (where the binned data points level off) of 55.47 m (Figure 6), corresponding to the correlation length (filter distance), which was rounded down to a final input of 50 m. To establish the dominant upwind bearing direction (*b*), onsite anemometer data (see section 4.5) was utilized. The average direction of records for sustained wind speeds ≥ 5 m/s, reflecting the average threshold for transport of dry snow (*McClung and Schaerer,* 2006), was calculated and one standard deviation was added/subtracted to this value, yielding a bearing wedge of 162-227°. The filter distance (x) and bearing wedge (b) values were used as input, along with the 10 m NED (z), in the Focal Statistics/Spatial Analyst tool to yield a raster of the average elevation of upwind terrain ($\bar{z}_b^x$). This raster was then subtracted from the original 10 m NED raster (z_i) to yield a raster of E_b^x (WEI), with negative values representing terrain with higher elevation upwind, hence, wind sheltered and leading to snow deposition, and positive values indicating terrain with lower elevation upwind, thus wind exposed and leading to snow scouring. The E_b^x raster values were extracted to the snow depth/SWE sampling points as

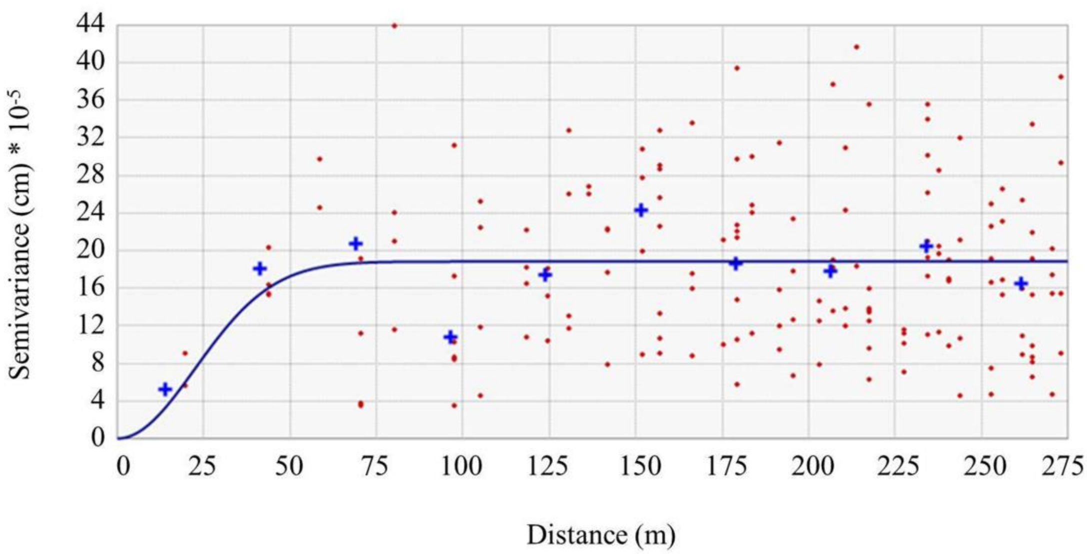

Figure 6. Semivariogram (γ) plot of the half the average squared difference of snow depth (cm) sampling points (red dots), binned by square cells one lag wide (27.78 m) versus the horizontal distance (m) between sampling points. The average of points are shown with blue crosses. The blue line indicates the model fit to the distribution and the range (distance) where the distribution levels off is the correlation length (λ).

input for the wind exposure index (WEI) variable in subsequent analysis.

4.7 Data Analysis

4.7.1 Multiple Linear Regression

Stepwise multiple linear regression (MLR) was used for a preliminary determination of the predictive significance of the six independent variables: elevation, slope, northness, eastness, cumulative solar radiation, and the WEI on the dependent variable: SWE, to thereby obtain the most parsimonious models. This analysis was performed with the statistical software *R*, using the *lm* (linear model) function and adding variables in a stepwise fashion guided by variable significance (p-value) and testing mixed effects with different variable combinations, until the highest adjusted R-squared (further referred to as R^2 and explained in the upcoming analysis section) value was achieved with the fewest number of independent variables. The code for *R* analysis is in Appendix E.

A parallel analysis was simultaneously performed in the ArcMap 10.2 Spatial Analyst/Explanatory Regression tool to provide a guide for mixed effect variable combinations, as it has a function that automatically performs this process given threshold criteria that can be manually set for several statistical metrics. Threshold search criteria were set as follows: (1) Minimum Acceptable Adjusted R-squared: 0.30, (2) Maximum Coefficient p-value Cutoff: 0.05, (3) Maximum Verification Inflation Factor (MaxVIF) Value Cutoff: 4.0, Minimum Acceptable Jarque Bera p-value: 0.1, Minimum Acceptable Spatial Autocorrelation p-value: 0.1. The MaxVIF was particularly helpful as it provided a measure of multicollinearity, thereby determining if any variables were redundant and indicating if one or more should be removed to create a more balanced or stable model. In the end, only the MLR results from *R* were used in analysis, with the explanatory regression of ArcGIS merely used as guide for the stepwise MLR. These results provided an initial indication of which independent variables may be the most dominant in each basin, thus providing a direction for subsequent analyses.

4.7.2 MLR Modeling in a GIS

The best (selected) models from the mixed effects multiple linear regression results were used as input equations in the ArcMap 10.2 Raster Calculator tool, thus providing estimation between observed SWE. This process involved multiplying rasters, derived from the aforementioned 10 m DEM for each of the physiographic variables, by their MLR coefficients and adding them in the regression equation to yield a modeled spatial distribution of SWE.

4.7.3. Binary Regression Trees

Previous investigations into the spatial distribution of SWE in montane catchments (e.g. *Elder et al.,* 1995, 1998; *Balk and Elder,* 2000; *Erxleben et al.,* 2002; *Winstral et al.,* 2002; *Molotch et al.,* 2005) have employed binary regression tree (BRT) methods to distribute this snowpack metric across the landscape. These studies note that this method requires large amounts of data and is therefore more accurate for small catchments, so it was considered appropriate for this current study. The general BRT method developed by Breiman et al. (1984) works by “growing” a tree through recursive partitioning (splitting) of dependent (response) variable samples (values), based on independent (predictor) variable values that maximize the decrease in the misclassification rate. This process creates increasingly smaller, more homogenous subsets of the parent subset eventually ending with modeled dependent variable values (terminal nodes) with the lowest misclassification probability. This is achieved by an algorithm that performs an optimization decision based on a binary splitting criterion that minimizes the residual sum of squares (RSS) of values within a subset and maximizes this measure between subsets. The sum of the RSS for all terminal nodes equals the total deviance of the model; subtracting this value from the model deviance at the root node yields the model's coefficient of determination (R^2). The analysis for the current study was accomplished in *R* using the *rpart* function involving splits for the dependent variable of SWE based on the data for the multiple physiographic independent variables (elevation, slope, northness, eastness, solar radiation, and wind shelter/exposure). The *R* code for this analysis is in Appendix F.

Overfitting, where too complex of a tree is grown (i.e. involves too many splits) is a common problem with the BRT method, thereby increasing its true probability of misclassification of cases placed in subsequent nodes. Like with the addition of predictor variables in MLR, additional splits in a BRT will result in an apparent increase in R^2 (Figure 7), but there is a point when additional splits no longer have any predictive power because the data does not actually have the information to support the increasing tree size. This is indicated by the cross validation relative R^2 (X Relative). To reduce this misclassification probability and optimize model parsimony, a method of pruning is

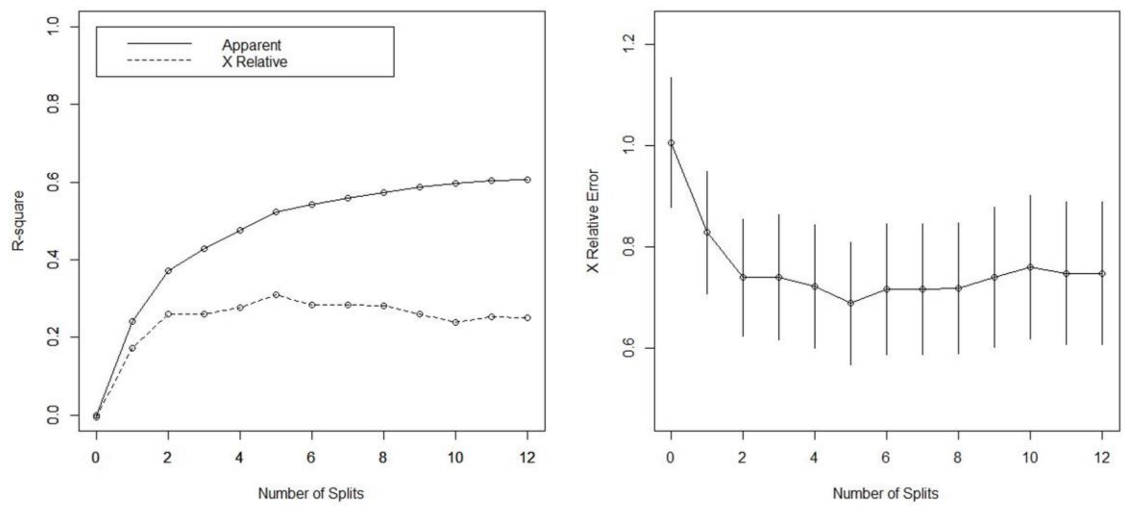

Figure 7. Plots of the apparent and 10-fold cross validation relative (X Relative) R^2 (left) alongside the corresponding 10-fold cross validation error (X Relative Error; right) for each split of the BRT for Basin B during the peak SWE sampling period. The plots indicate that despite an apparent increase in the R^2 beyond 5 splits, the true explanatory value of the tree is reached at this point as further splits go beyond the information of the observed data and introduce more relative error.

employed by *R* (*rpart*) based on a complexity parameter (cp) which determines the decrease in relative error (of the overall model) necessary to justify the complexity cost of an additional split in the tree (Figure 8). This works by the process of 10-fold cross validation, in which the original sample is divided into 10 subsets of auxiliary trees by random selection and an algorithm seeks to minimize the misclassification error while holding a different, training subset out for each of 10 possible runs. Because the 10-fold cross validation involves a randomized process for the initial split on the training subset, each run can produce different estimates of misclassification cost or relative error for the sequence of subsequent splits. To determine a robust estimate of relative error associated with splits, 100 iterations of the cross validation were run (*Winstral et al.*, 2002; *Molotch et al.*, 2005). Optimal tree size was selected with the aid of the *prune* function in *R*, which sets the default cp equal to 0.01, indicating a necessary 1 % decrease in relative error for an additional split. In order to allow a full tree to grow, the cp was manually set to 0. To ensure the pruning decisions made in *R* had allowed a tree to grow to optimal size, the '1 SE rule' was manually employed by analyzing plots of the cp and tree size versus the x-val relative error and targeting the smallest tree size where the x-val relative error reaches a minimum that is ± 1 standard error (Figure 8) (*Brieman et al.*, 1984).

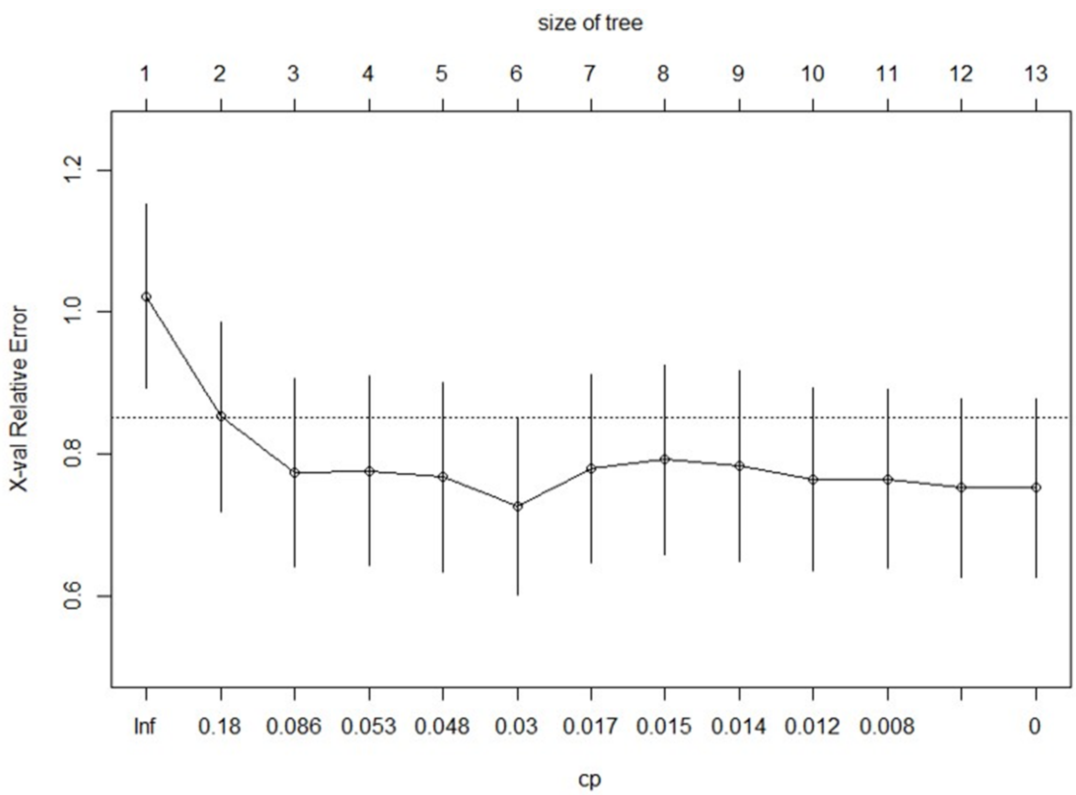

Figure 8. Plot of the complexity parameter (cp) and tree size versus the 10-fold cross validation error (X-val Relative Error) for each split of the full BRT for Basin B for the peak SWE sampling period. The dashed line indicates the upper limit of 1 standard deviation, hence the optimal tree size is 6 nodes where X-val Relative Error is minimized and the tree still meets the 1 SE rule.

5. RESULTS

5.1 Representative Sampling of the Physiographic Variables

The distribution of points sampled in each basin for snow depth and SWE was compared to the distribution of elevation, slope, aspect, solar radiation, and avalanche zone components in each basin in order to assess the representativeness of the sampling design during each data collection period: (1) accumulation, (2) peak SWE, and (3) ablation (Figures 9-14, Table 2). Root mean squared error (RMSE) was used as the measure of fit of the sampling distributions, and RMSE values represent the difference between the distributions of the physiographic variables bins and sampling distributions in percent (%). This was calculated by comparing the percent of raster cells (of total) that fell in each physiographic variable bin to the percent of sampling points that fell into that respective bin. It should be noted that the binning of the physiographic variables substantially reduced the overall variance of their values, thus giving the appearance of more representative sampling than would be realistically possible if each individual raster cell value was considered. The variable of wind exposure/sheltering was not directly analyzed, as it was assumed to be indirectly represented through the sampling of elevation, slope, and aspect.

Of the three periods, the smallest sample was acquired during accumulation with the 1.38 km^2 area of Basin A having 106 snow depth points (76.8 points per km^2) including 14 SWE depths, and the 1.63 km^2 area of Basin B having 63 snow depth points (38.9 points per km^2) including 8 SWE depths (Figure 9). With nearly twice the number

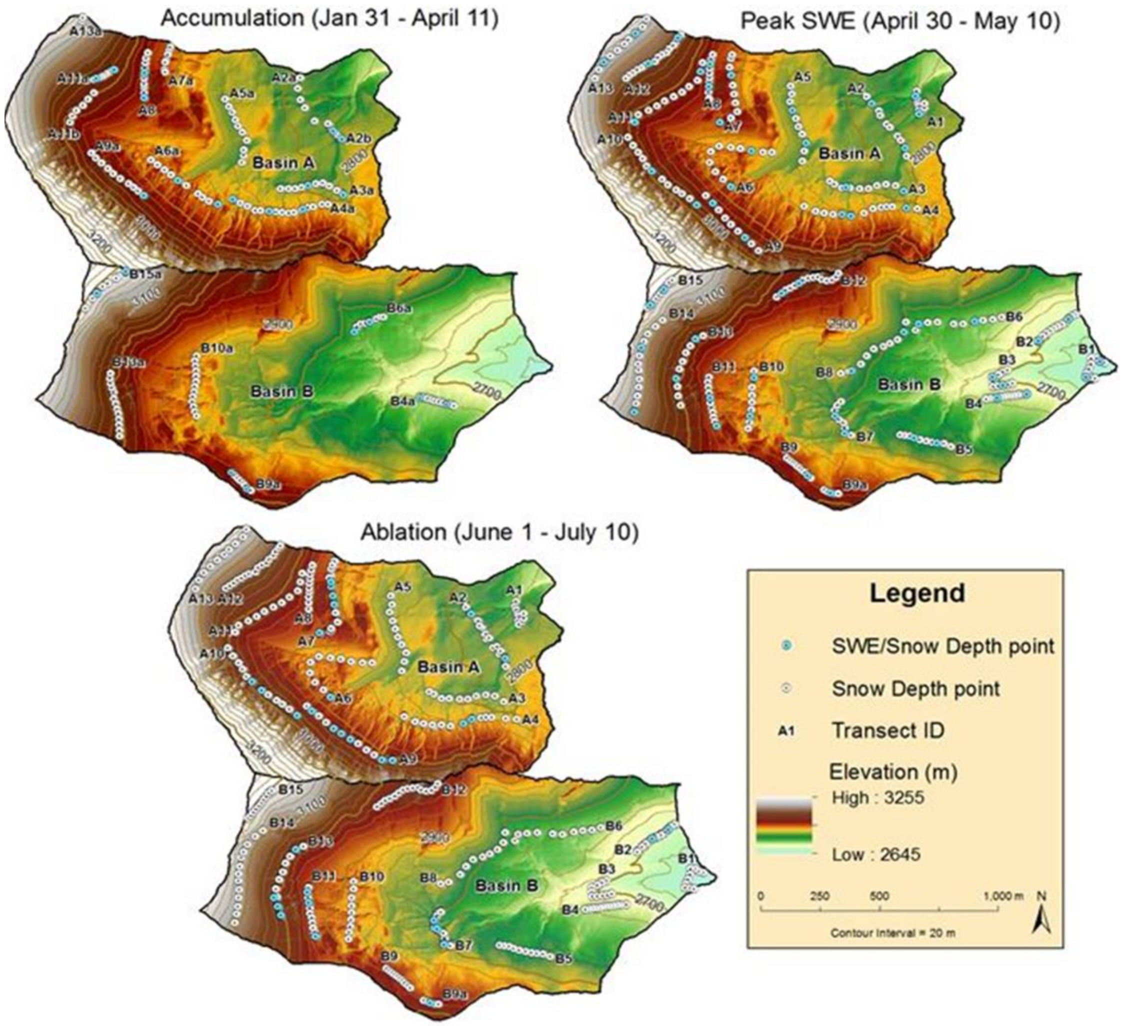

Figure 9. Maps of the study site basins showing the distribution of the points sampled during each sampling period: (1) accumulation, (2) peak SWE, and (3) ablation.

of samples in Basin A than in Basin B, there was inherently greater spatial coverage; however, the points in both basins were relatively evenly distributed among elevation zones (Figure 10). In Basin A, two of the mid-elevation zones between approximately 2767-2950 m were oversampled while the zones greater than approximately 3072 m were undersampled. The sampling imbalance was greater in Basin B, and was somewhat inconsistent leading to a degree of under and oversampling throughout the elevation zones. The poorer elevation sampling in Basin B than in Basin A is reflected in RMSE values of 8.12 and 6.63, respectively.

During peak SWE, sampling was quite proportional to each basin area with 142 snow depths points (102.9 points per km^2) including 27 SWE depths in Basin A and 165 snow depth points (101.9 points per km^2) including 30 SWE depths in Basin B. Unlike during the accumulation season, high elevations were sampled well in Basin A except for an undersampling in the zone of 3072-3133 m. The same was true in Basin B except that the zone of 3011-3072 m was neglected. Aside from these issues and a little oversampling in each basin at the lowest two elevation zones, the sampling distribution matched the distribution of elevation in each basin quite well, as reflected in the lower RMSE values of 4.58 and 5.82 in Basin A and B.

The representativeness of sampling during ablation declined once again, mainly due to repeated surveys at several transects, while others only received a single visit. In Basin A, 298 (142 unique points) snow depths including 44 SWE depths were measured and in Basin B, 329 (165 unique points) snow depths including 30 SWE depths were measured. This lead to a mix of under and oversampling that was more pronounced in Basin B with an RMSE of 7.43 than in Basin A with an RMSE of 5.54.

The issues seen gaining a representative sample of elevation during the accumulation period were also realized in sampling slope angle and the components of avalanche zones (runout, track, start zone). Lower angle slopes (lower avalanche tracks and runouts), generally below 25°, were oversampled at the expense of slopes greater than 30° (start zones) (Figures 9 and 12). Relatively balanced samples were acquired

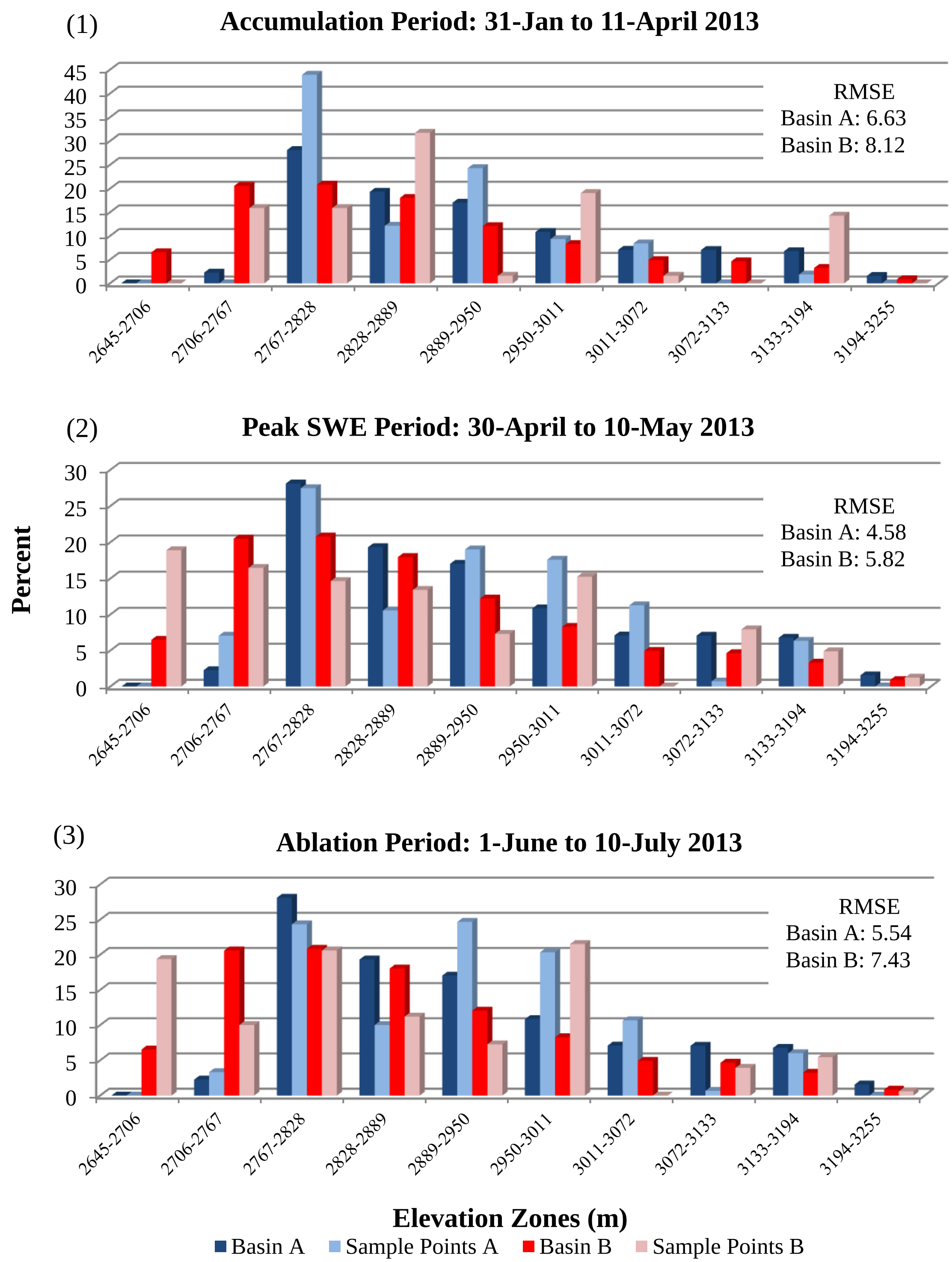

Figure 10. Histograms showing the distribution of elevation in each basin versus the sampling distribution during each sampling period: (1) accumulation, (2) peak SWE, and (3) ablation.

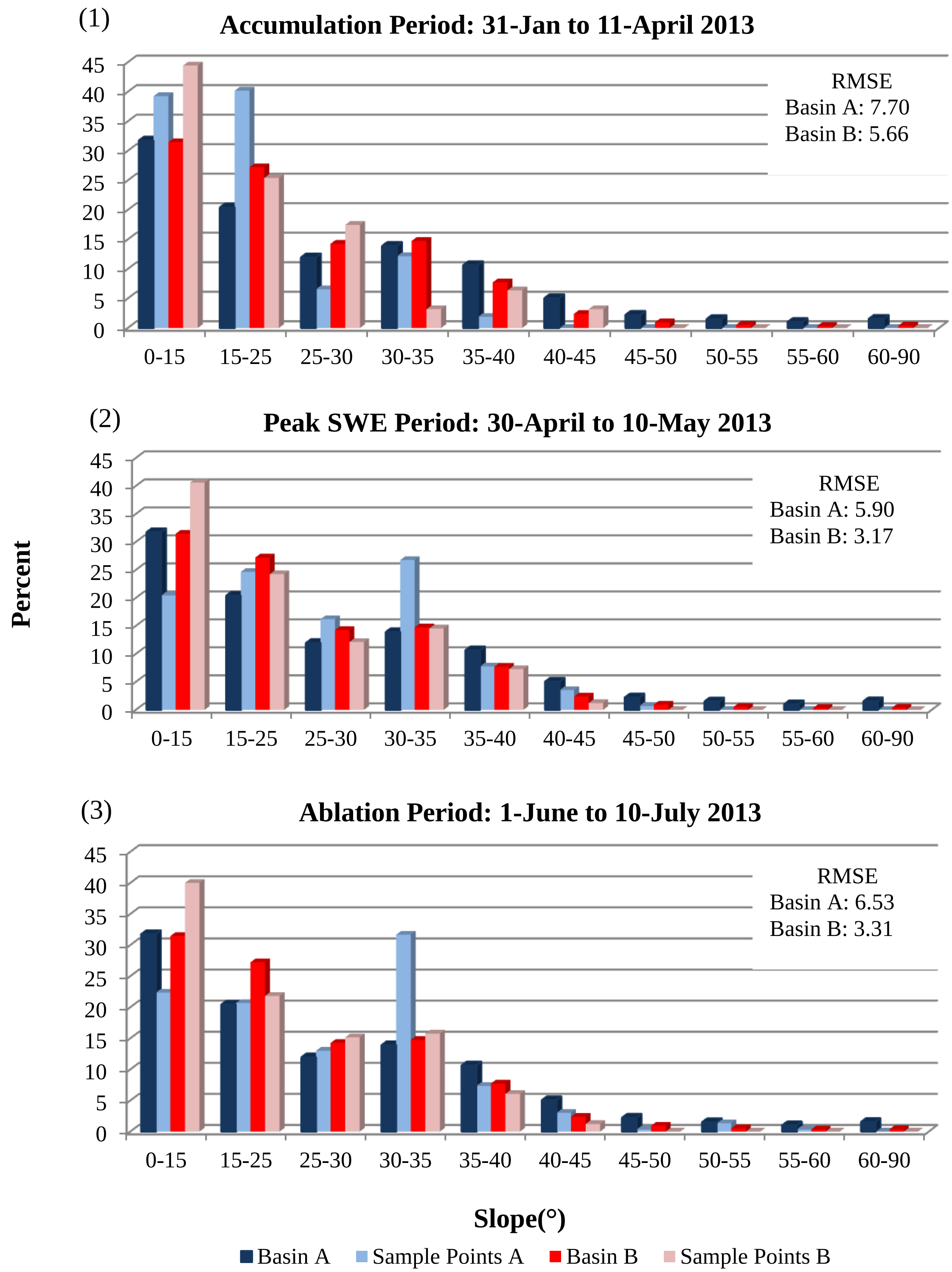

Figure11. Histograms showing the distribution of slope in each basin versus the sampling distribution during each sampling period: (1) accumulation, (2) peak SWE, and (3) ablation.

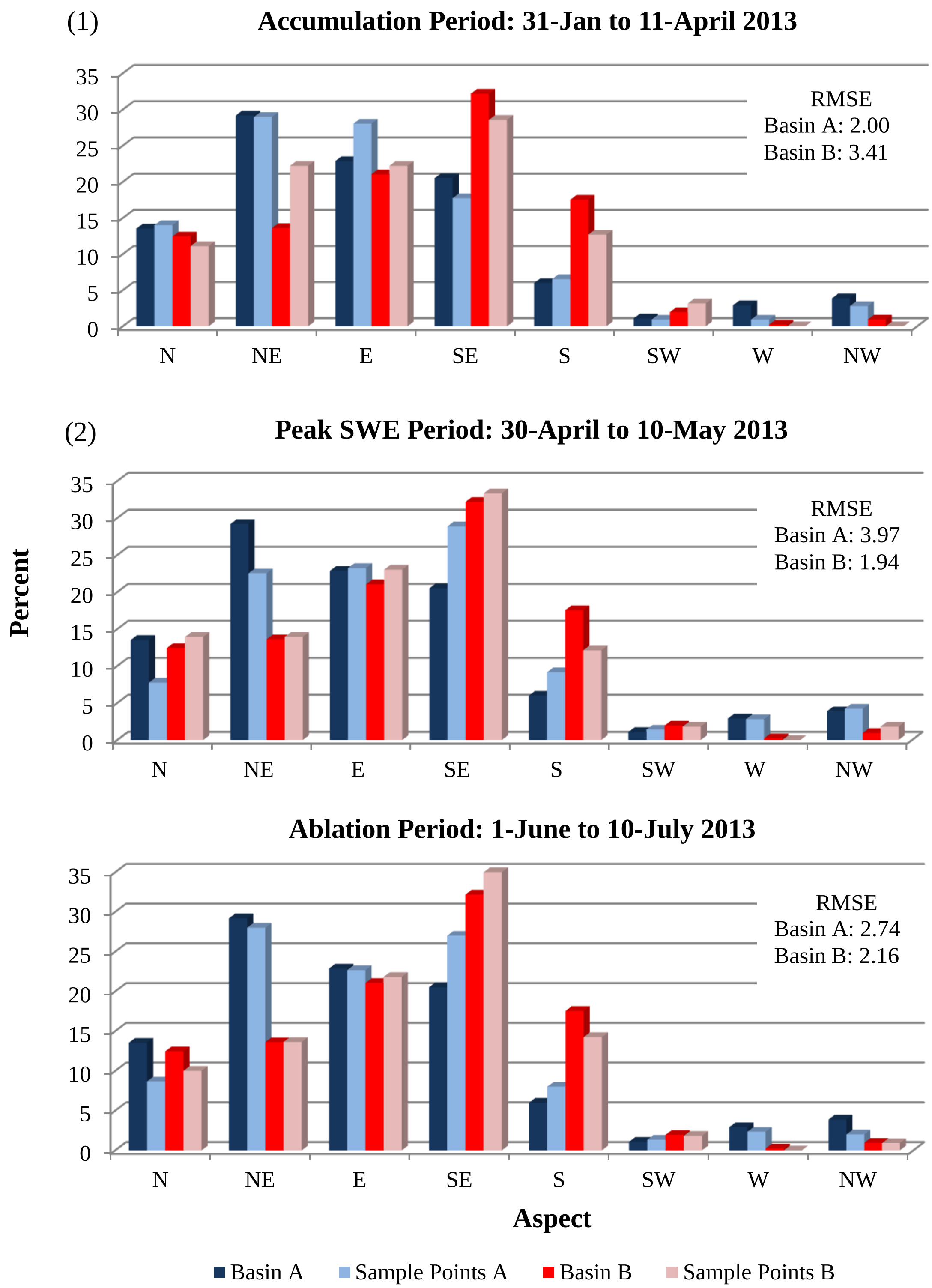

Figure 12. Histograms showing the distribution of aspect in each basin versus the sampling distribution during each sampling period: (1) accumulation, (2) peak SWE, and (3) ablation.

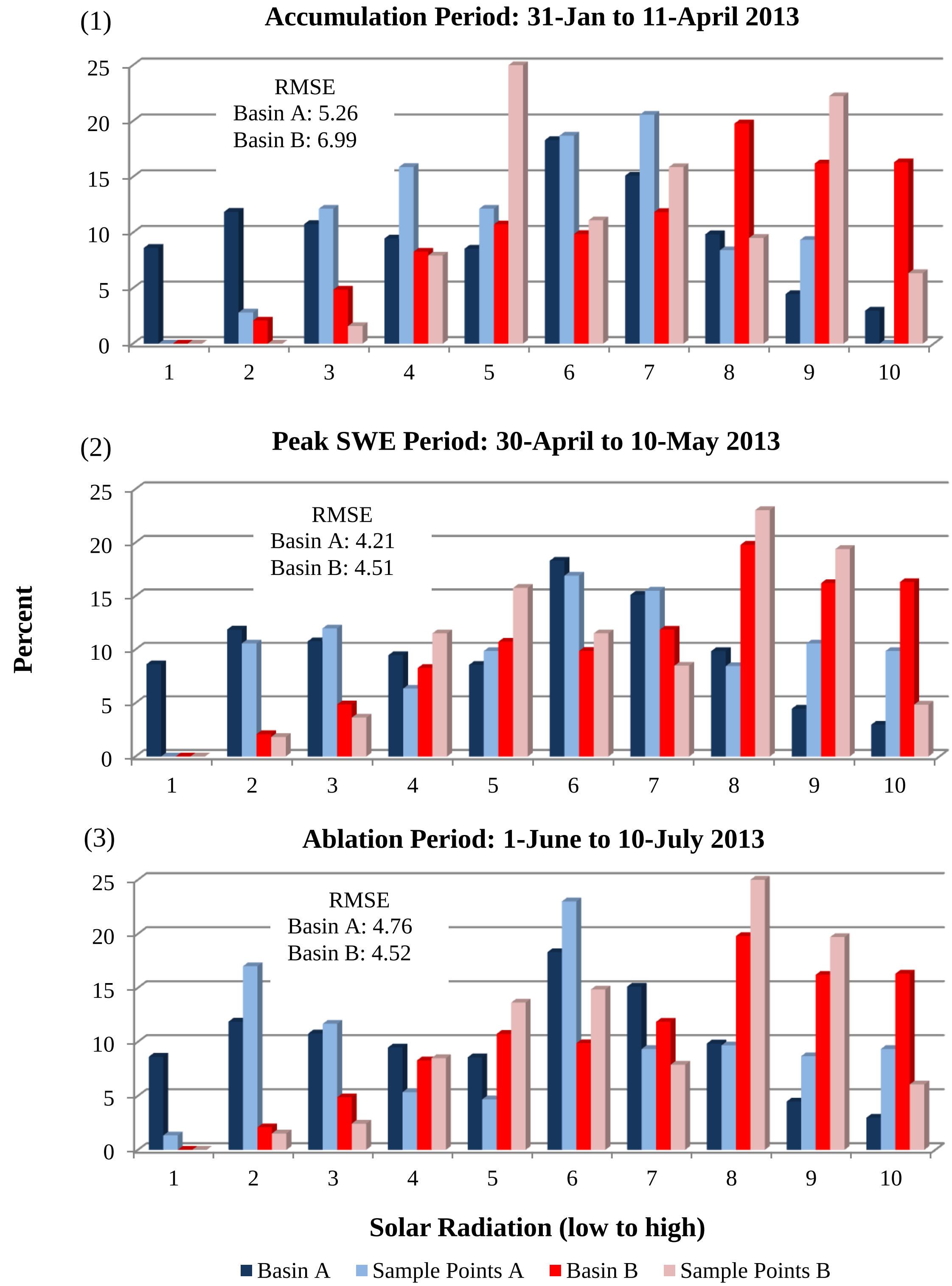

Figure 13. Histograms showing the distribution of cumulative solar radiation class in each basin versus the sampling distribution during each sampling period: (1) accumulation, (2) peak SWE, and (3) ablation.

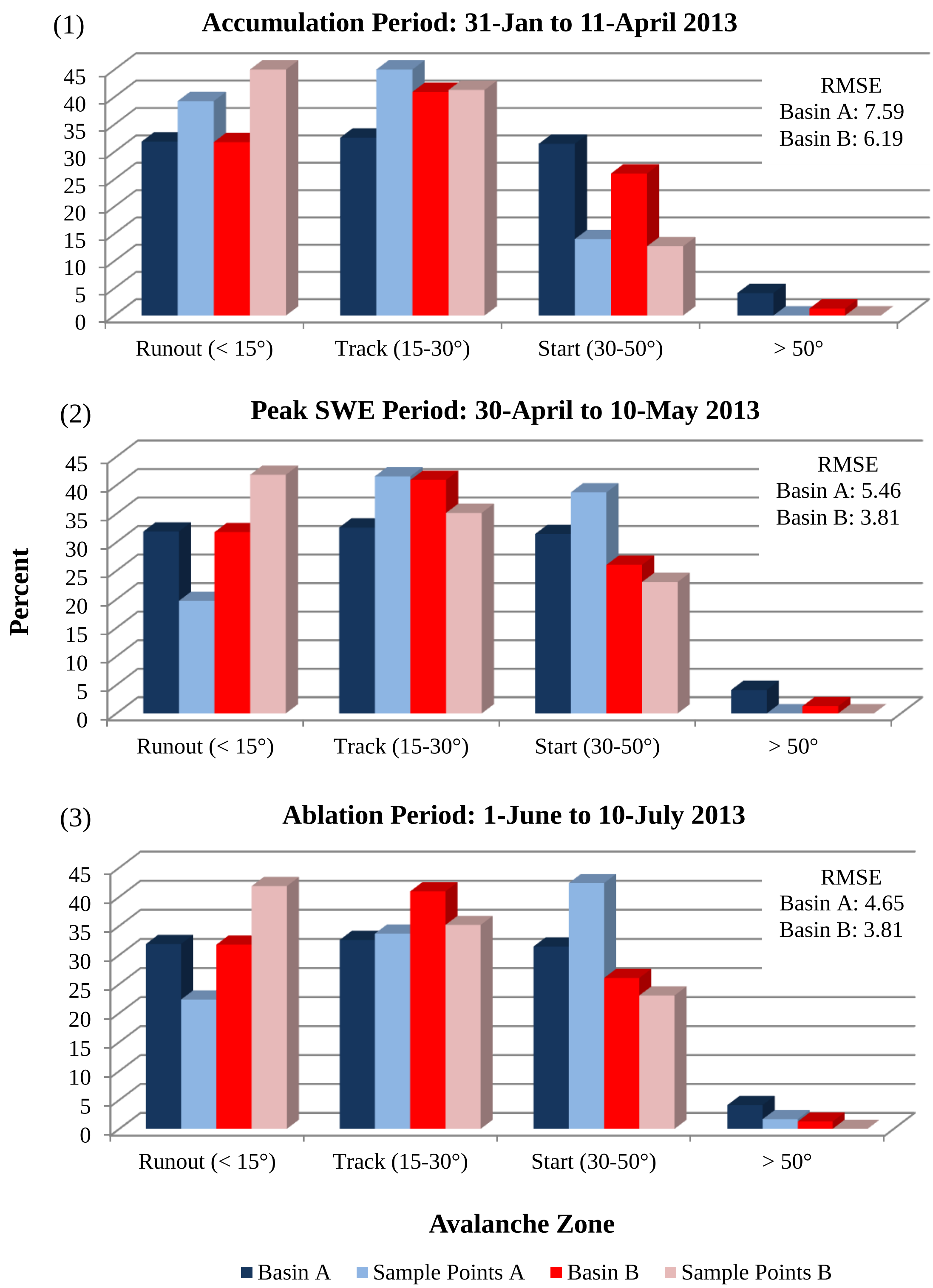

Figure 14. Histograms showing the distribution of avalanche zones in each basin versus the sampling distribution during each sampling period: (1) accumulation, (2) peak SWE, and (3) ablation.

during the corresponding peak SWE and ablation periods as indicated by substantially lower RMSE values in each basin. A notable exception during these periods is seen in Basin A where the sampling in the slope zone 30-35° was approximately twice that of the basin distribution, perhaps due to the multiple transects located under the northeast headwall of this basin.

The sampling design worked best at representing the variable of aspect during all three periods (Figure 12), with RMSE values less than 4.00 (Table 2). This supports the previous observation that, while the sampling distribution was unbalanced between Basin A and B during the accumulation period, it produced a representative sample overall. This also corresponds well to the sampling representativeness of solar radiation during the peak SWE period and ablation periods with RMSE values less than 5.00 (Figure 13 and Table 2). A less representative sample of solar radiation was acquired during the accumulation period. In Basin A, this was primarily limited to areas of low solar input being undersampled leading to a slightly higher RMSE of 5.26 than later periods. However, in Basin B, several zones of mid to high level solar radiation were both under and oversampled leading to a noticeably higher RMSE of 6.99.

Table 2. RMSE values for the distribution of the physiographic variables in each basin versus the sampling distribution. RMSE is the difference in percent (%).

	Accumulation		Peak SWE		Ablation	
	Basin A	Basin B	Basin A	Basin B	Basin A	Basin B
Elevation	6.63	8.12	4.58	5.82	5.54	7.43
Slope	7.70	5.66	5.90	3.17	6.53	3.31
Aspect	2.00	3.41	3.97	1.94	2.74	2.16
Solar Radiation	5.26	6.99	4.21	4.51	4.76	4.52
Avalanche Zone	7.59	6.19	5.46	3.81	4.65	3.81

5.2 Simple and Multiple Linear Regression

Linear regression modeling was used to analyze the effect of the physiographic (independent/predictor) variables of: elevation, slope, northness, eastness, solar radiation, and the WEI on the distribution of SWE (dependent/response) in each basin during each sampling period. Initially, simple linear regression (SLR) offered a quantification of the effect of each individual variable, as well as the direction of the relationship with SWE. Subsequent, stepwise multiple linear regression (MLR) then indicated how much the distribution of SWE could be explained by the mixed effects of combinations of these variables. The maximization of adjusted R^2, relative to model parsimony, was used as the primary measure of model goodness of fit. The R^2 metric was chosen because it provides an intuitive interpretation of model performance by indicating a proportion of the dependent variable variance explained by the independent variable(s) and thus, has been widely used to evaluate modeling in snow hydrology. The adjusted R^2 was specifically chosen for the added penalty for model complexity. The minimization of residual squared error (RSE) was included as an additional check on the trend of model fit. While these measures are more appropriate for explanatory modeling, the Akaike Information Criterion (AIC) is recognized to be a good indicator of predictive accuracy (*Shmueli*, 2010), as well as a measure of complexity cost. Thus, targeting a minimum in the AIC with the fewest predictor variables provided an additional strategy for optimizing both model parsimony and predictive power. Finally, the maximum verification inflation factor (VIF) was used to eliminate models with multicollinearity issues between variables, with a value of 4.0 set as the upper limit of acceptability, as this corresponds to an R^2 of 0.75, indicating a questionable degree of correlation between the variables.

The MLR model assumptions of (1) independent observations, (2) randomization (3) linearity, (4) constant variance, (5) normality, and (6) influential outliers were considered in the sampling design and through diagnostic plots to ensure all were reasonably met (Appendix B). Diagnostic review showed linearity in the scatterplots for the WEI and solar radiation and a correlation matrix (Appendix C) showed correlation coefficients greater than 0.75 for the pairing of these variables, as well as for northness and solar radiation. The strong correlation between the WEI and solar radiation is likely due to the prevailing winds in the study area blowing predominantly from the south. Therefore, the terrain with the highest positive WEI will also have the highest levels of solar radiation. This relationship is more intuitive for northness and solar radiation, as the degree of northness inherently determines the level of solar input. The aforementioned analyses verified this issue through a violation of the linearity assumption, thus models with these variable combinations were not included in the results despite having some of the highest R^2 values. Since actual point raster values of each variable were used in analysis, avalanche zone was not included as it was merely a binned classification of slope. Inclusion created a high degree of multicollinearity between slope and avalanche zone, shown in MLR VIF values, indicating that one of these variables had to be removed to avoid redundancy and inaccurate model results.

5.2.1 Linear Regression Modeling for the Accumulation Period

For Basin A, SLR results showed the top three dominant variables: the WEI, solar radiation, and northness to explain a reasonable proportion of the variance with an R^2 of 0.27, 0.21, and 0.17, respectively (Table 3). Considering multiple variable interactions, MLR results for Basin A showed the combination of the WEI and eastness to be the best performing model, but with only a minimal increase in adjusted R^2 to 0.28. This was also the most parsimonious model since the inclusion of additional variables showed no increase in R^2 values and increased RSE, AIC, and VIF. It was surprising that the addition of elevation, instead of eastness to the WEI, did not produce the best model given that elevation, not eastness, was shown to be significant ($\alpha = 0.001$) in the SLR analysis.

For Basin B, eastness was shown by SLR to be dominant followed by the WEI then slope, but the variance explained by the top variables was far less than in Basin A, with R^2 values of 0.15, 0.08, and 0.00. Unlike in Basin A, model performance increased substantially for Basin B with the addition of independent variables, the best being that with eastness, the WEI, and northness, to yield an R^2 of 0.32. While models in Basin B with four and five variables showed slightly increasing R^2 and decreasing RSE and AIC values, increasing VIF values eliminated them from being considered optimal.

Calculating SWE values from the top MLR model for Basin A with rasters of the WEI and eastness in ArcGIS provided a spatial distribution with a range of 0-1265 mm. The same method applied to the model for Basin B with eastness, the WEI, and northness resulted in a SWE range of 0-1045 mm (Figure 15). The total modeled volume of SWE was 680,436.2 m^3 in Basin A and 524,251.1 m^3 in Basin B (Table 6).

Table 3. SLR and MLR results for the accumulation sampling period. The best (selected) models are highlighted.

BASIN A				
Model: SWE ~ **independent variable** (sign of coefficient)	**AdjR^2**	**RSE**	**AIC**	**VIF**
WEI(-)	0.27	213.8	1442.2	1.0
Solar(-)	0.21	222.3	1450.4	1.0
Northness(+)	0.17	227.9	1455.7	1.0
Elevation(-)	0.10	237.2	1464.2	1.0
Slope(-)	0.00	250.0	1475.3	1.0
Eastness(-)	0.00	251.4	1476.5	1.0
WEI(-) + **Eastness**(+)	0.28	212.3	1441.7	1.1
WEI(-) + **Northness**(+)	0.26	214.7	1444.0	2.4
WEI(-) + **Elevation**(+)	0.26	214.9	1444.2	1.7
WEI(-) + **Northness**(+) + **Eastness**(+)	0.28	212.4	1442.7	2.6
WEI(-) + **Slope**(+) + **Eastness**(+)	0.27	213.2	1443.5	1.2
WEI(-) + **Elevation**(-) + **Eastness**(+)	0.27	213.3	1443.6	3.9
WEI(-) + **Northness**(+) + **Slope**(+) + **Eastness**(+)	0.27	213.2	1444.5	2.6
Solar(-)+ **Elevation**(-) + **Slope**(+) + **Eastness**(+)	0.27	213.6	1444.9	4.7
WEI(-) + **Northness**(+) + **Elevation**(-) + **Slope**(+)	0.25	216.6	1447.8	4.8
WEI(-) + **Northness**(+) + **Elevation**(-) + **Slope**(+) + **Eastness**(+)	0.27	214.0	1446.2	5.0
BASIN B				
Model: SWE ~ **independent variable** (sign of coefficient)	**AdjR^2**	**RSE**	**AIC**	**VIF**
Eastness(+)	0.15	251.2	879.1	1.0
WEI(-)	0.08	260.6	883.7	1.0
Slope(+)	0.00	271.1	888.7	1.0
Solar(-)	0.00	272.9	889.5	1.0
Elevation(-)	0.00	273.8	889.9	1.0
Northness(+)	0.00	273.9	889.9	1.0
Eastness(+) + **WEI**(-)	0.27	232.2	870.1	1.0
Eastness(+) + **Elevation**(-)	0.25	235.7	872.0	1.5
Eastness(+) + **Solar**(-)	0.15	251.2	880.0	1.0
Eastness(+) + **WEI**(-) + **Northness**(-)	0.32	225.0	867.1	1.6
Eastness(+) + **Slope**(+) + **Elevation**(-)	0.29	229.8	869.7	2.1
Eastness(+) + **WEI**(-) + **Slope**(+)	0.26	234	872.0	1.1
Eastness(+) + **WEI**(-) + **Northness**(-) + **Elevation**(-)	0.32	223.9	867.4	2.4
Eastness(+) + **WEI**(-) + **Slope**(+) + **Northness**(-)	0.30	226.9	869.1	1.6
Eastness(+) + **WEI**(-) + **Slope**(+) + **Elevation**(-)	0.29	228.7	870.0	3.9
Eastness(+) + **WEI**(-) + **Slope**(+) + **Northness**(-) +**Elevation**(-)	0.33	223.3	867.9	4.0

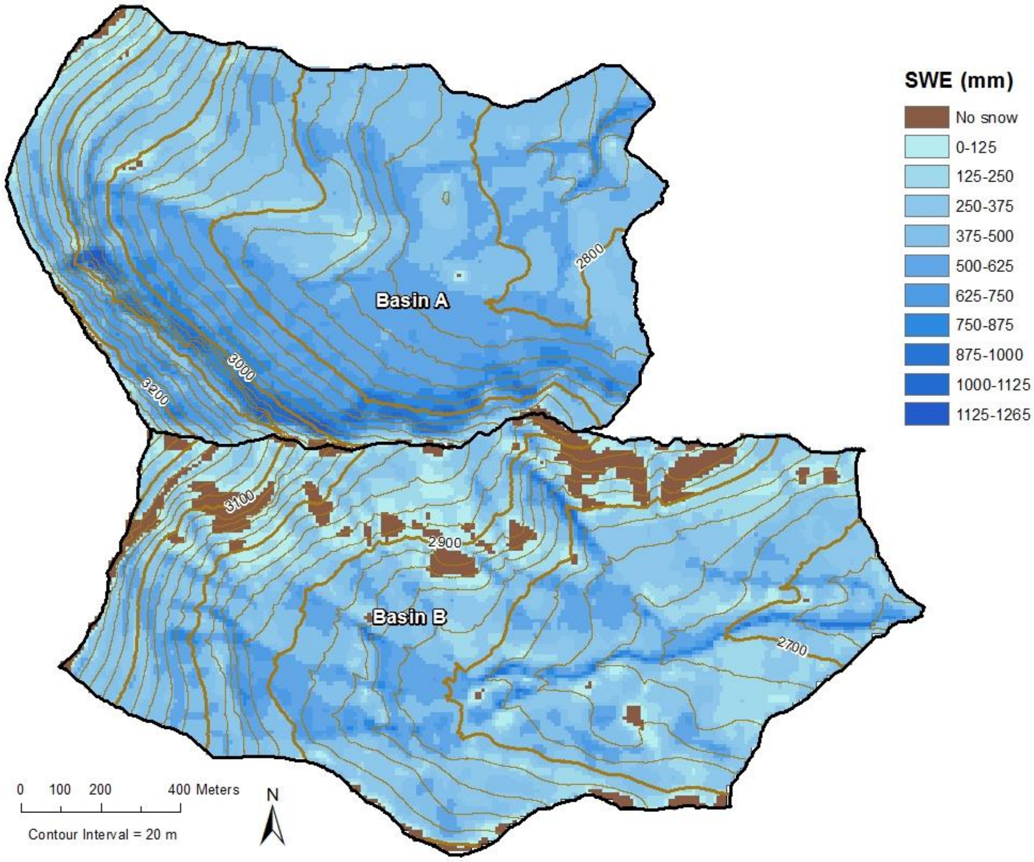

Figure 15. The modeled distribution of SWE for the accumulation period using MLR models: Basin A: *SWE ~ 415.91 + (-59.29)*WEI + (89.93)*Eastness*
Basin B: *SWE ~ 219.91 + (341.42)*Eastness + (-76.38)*WEI + (-105.09)*Northness*

5.2.2 Linear Regression
<u>Modeling for the Peak SWE Period</u>

During the peak SWE sampling period, the dominant independent variable in Basin A was shown to be solar radiation with an R^2 of 0.53, followed by the WEI and northness with R^2 values of 0.48 and 0.40, respectively (Table 4). Model performance for the peak SWE period showed a modest improvement in Basin A, when combining the WEI with slope and eastness, increasing R^2 to 0.57. This pointed to how mixed effects occurred between the two variables shown to have the least significance in SLR results and the most dominant variable to outperform models that would intuitively seem better. This also possibly hinted at the multicollinearity of the WEI to both slope and eastness, but a low VIF of 1.1 indicated there was no violation. The relative simplicity of this model was considered optimal over that with the WEI, northness, slope, and eastness. Despite this four variable model having the lowest RSE and AIC, it showed increasing potential for multicollinearity issues and uncertainty about the true effect of the interaction between the variables, as indicated by an increased VIF of 2.9.

Somewhat opposite results were found in Basin B, with the WEI being the dominant control shown by an R^2 of 0.23, and with solar radiation and northness not showing nearly as much of the variance explained with R^2 values of 0.12 and 0.09, respectively. The addition of slope with the WEI provided over a 32% increase, for an R^2 of 0.31, indicating the best, two variable model. Once again, this is perhaps due to a correlation between slope and the WEI, as each is inherently tied to elevation and terrain features, but since the correlation coefficient for these variables was only 0.07 (Appendix C), it was not considered an issue. Despite the favorable parsimony and relative ease of interpretation of this model, the further addition of eastness and elevation did provide a substantial increase and peak in the R^2 at 0.33. A lowest AIC of 2336.8 and an acceptable VIF of 2.5 also make this model difficult to dismiss despite its four variable complexity.

The distribution of SWE for Basin A with the model using the WEI, eastness and slope had a range of 0-2067 mm, while the model for Basin B with the WEI, slope, eastness, and elevation resulted in a SWE range of 0-1243 mm (Figure 16). Modeled total SWE volume was 834,958.5 m^3 in Basin A and 663,421.1 m^3 in Basin B (Table 6).

Table 4. SLR and MLR results for the peak SWE sampling period. The best (selected) models are highlighted.

BASIN A Model**:** SWE ~ **Independent variable** (sign of coefficient)	**AdjR²**	**RSE**	**AIC**	**VIF**
Solar(-)	0.53	245.2	1969.5	1.0
WEI(-)	0.48	259.2	1985.3	1.0
Northness(+)	0.40	276.8	2003.9	1.0
Elevation(-)	0.10	339.2	2061.7	1.0
Slope(+)	0.00	357.9	2076.9	1.0
Eastness(+)	0.00	359.0	2077.8	1.0
Solar(-) + **Eastness**(+)	0.55	240.7	1965.3	1.0
WEI(-) + **Slope**(+)	0.54	243.3	1968.4	1.1
Solar(-) + **Slope**(+)	0.53	244.6	1969.8	1.0
WEI(-) + **Slope**(+) + **Eastness**(+)	0.57	236.4	1961.2	1.1
WEI(-) + **Northness**(+) + **Slope**(+)	0.55	240.7	1966.3	2.8
Solar(-) + **Elevation**(-) + **Eastness**(+)	0.55	241.3	1967.0	1.3
WEI(-) + **Northness**(+) + **Slope**(+) + **Eastness**(+)	0.57	234.7	1960.1	2.9
Solar(-) + **Elevation**(-) + **Slope**(+) + + **Eastness**(+)	0.56	238.0	1964.0	3.1
WEI(-) + **Northness**(+) + **Elevation**(-) + **Slope**(+)	0.55	241.6	1968.2	3.6
WEI(-) + **Northness**(+) + **Elevation**(-) + **Slope**(+) + **Eastness**(+)	0.57	235.2	1961.6	3.6

BASIN B Model**:** SWE ~ **Independent variable** (sign of coefficient)	**AdjR²**	**RSE**	**AIC**	**VIF**
WEI(-)	0.23	302.1	2356.8	1.0
Solar(-)	0.12	322.2	2378.0	1.0
Northness(+)	0.09	328.8	2384.7	1.0
Slope(+)	0.03	339.4	2395.2	1.0
Eastness(+)	0.02	341.4	2397.1	1.0
Elevation(-)	0.00	344.6	2400.2	1.0
WEI(-) + **Slope**(+)	0.31	287.0	2340.9	1.0
WEI(-) + **Eastness**(+)	0.29	290.3	2344.6	1.0
WEI(-) + **Elevation**(+)	0.24	299.3	2354.7	1.2
WEI(-) + **Slope**(+) + **Eastness**(+)	0.32	284.0	2338.3	1.3
WEI(-) + **Slope**(+) + **Elevation**(-)	0.31	285.9	2340.6	2.5
WEI(-) + **Northness**(-) + **Slope**(+)	0.30	287.2	2342.1	2.1
WEI(-) + **Slope**(+) + **Eastness**(+) + **Elevation**(-)	0.33	281.9	2336.8	2.5
WEI(-) + **Northness**(-) + **Slope**(+) + **Eastness**(+)	0.32	284.3	2339.7	2.1
Solar(-) + **Slope**(+) + **Eastness**(+) + **Elevation**(-)	0.23	302.8	2360.5	2.5
WEI(-) + **Northness**(-) + **Slope**(+) + **Eastness**(+) +**Elevation**(-)	0.33	282.4	2338.4	2.5

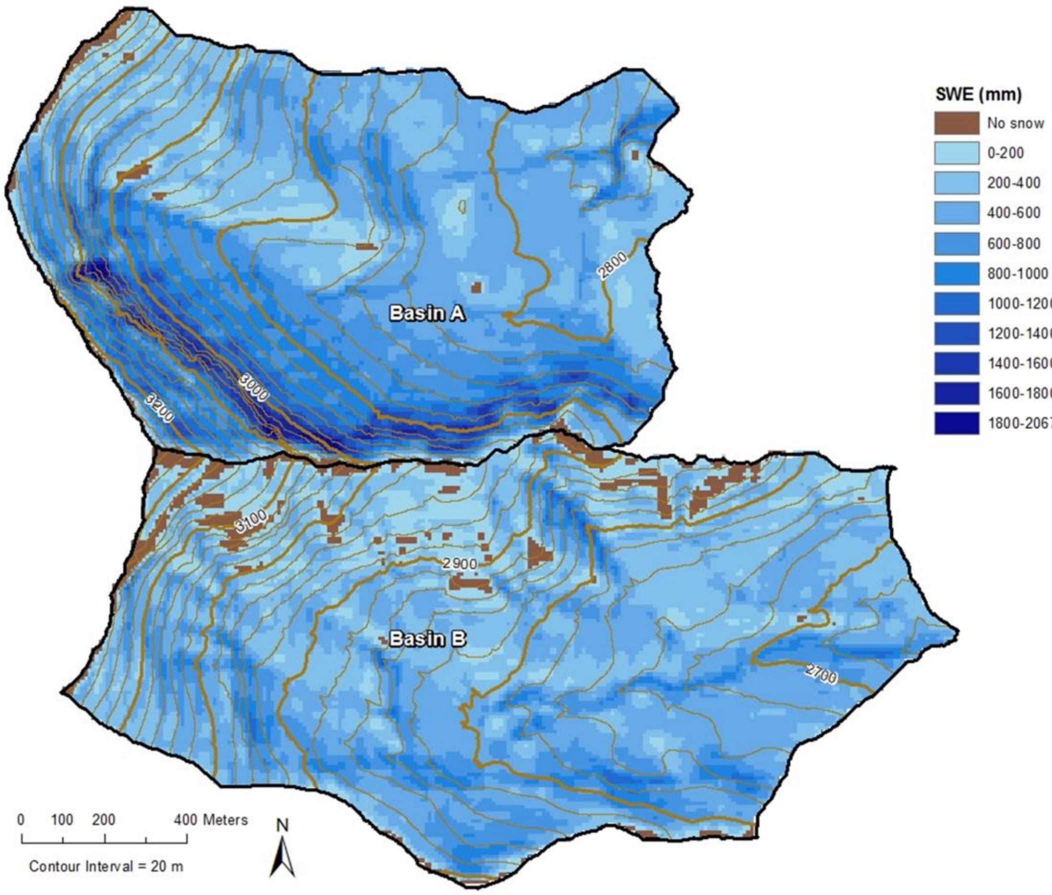

Figure 16. The modeled distribution of SWE for the peak SWE period using MLR models: Basin A: *SWE ~ 296.78 + (-93.02)*WEI + (148.85)*Eastness + (7.99)* Slope* Basin B: *SWE ~ 1410.72 + (-83.05)*WEI + (11.52)*Slope + (180.03)*Eastness + (-0.43)*Elevation.*

5.2.3 Linear Regression
<u>Modeling for the Ablation Period</u>

Continuing with the pattern of peak SWE, solar radiation, followed by the WEI and northness, once again proved to be the principal variables controlling SWE in Basin A during ablation with SLR R^2 of 0.17, 0.17, and 0.11, respectively (Table 5). Despite its low R^2 of 0.00, slope, and eastness, not shown to be significant ($\alpha = 0.05$) in SLR, proved to have the best mixed effect in MLR with the WEI, producing an R^2 of 0.22.

Table 5. SLR and MLR results for the ablation sampling period. The best (selected) models are highlighted.

Model**:** SWE ~ **Independent variable** (sign of coefficient)	**AdjR^2**	**RSE**	**AIC**	**VIF**
BASIN A				
Solar(-)	0.17	314.0	4276.3	1.0
WEI(-)	0.17	314.6	4277.4	1.0
Northness(+)	0.11	326.1	4298.8	1.0
Slope(+)	0.01	336.4	4317.3	1.0
Elevation(-)	0.00	345.4	4333.1	1.0
Eastness(+)	0.00	345.4	4333.1	1.0
WEI(-) + **Slope**(+)	0.22	305.0	4259.9	1.0
WEI(-) + **Elevation**(+)	0.22	305.3	4260.6	1.4
Solar(-) + **Slope**(+)	0.18	311.6	4272.7	1.1
WEI(-) + **Slope**(+) + **Eastness**(+)	0.22	304.4	4259.8	1.1
WEI(-) + **Slope**(+) + **Elevation**(+)	0.22	304.5	4260.0	3.9
WEI(-) + **Elevation**(-) + **Eastness**(+)	0.22	304.9	4260.8	3.9
WEI(-) + **Elevation**(+) + **Slope**(+) + + **Eastness**(+)	0.22	304.1	4260.3	3.9
WEI(-) + **Northness**(-) + **Slope**(+) + **Eastness**(+)	0.22	304.8	4261.5	2.7
WEI(-) + **Northness**(+) + **Elevation**(+) + **Slope**(+)	0.22	305.0	4262.0	4.0
WEI(-) + **Northness**(-) + **Elevation**(+) + **Slope**(+) + **Eastness**(+)	0.22	304.6	4262.2	4.1
BASIN B				
Model**:** SWE ~ **Independent variable** (sign of coefficient)	**AdjR^2**	**RSE**	**AIC**	**VIF**
Eastness(+)	0.10	361.8	4813.0	1.0
Slope(+)	0.06	368.2	4825.6	1.0
Elevation(+)	0.04	372.9	4833.8	1.0
WEI(-)	0.03	374.7	4837.1	1.0
Solar(-)	0.01	378.4	4843.5	1.0
Northness(+)	0.01	378.5	4843.8	1.0
Eastness(+) + **WEI**(-)	0.14	353.3	4799.3	1.0
Eastness(+) + **Slope**(+)	0.12	358.0	4808.0	1.2
Eastness(+) + **Solar**(-)	0.11	358.7	4809.3	1.0
Eastness(+) + **Slope**(+) + **WEI**(-)	0.17	347.5	4789.5	1.2
Eastness(+) + **Elevation**(+) + **WEI**(-)	0.17	347.8	4790.1	1.2
Eastness(+) + **Elevation**(+) + **Solar**(-)	0.13	354.5	4802.5	1.3
Eastness(+) + **Slope**(+) + **Elevation**(+) + **WEI**(-)	0.17	347.1	4789.6	2.3
Eastness(+) + **Slope**(+) + **WEI**(-) + **Northness**(-)	0.17	347.4	4790.2	2.1
Eastness(+) + **Elevation**(+) + **WEI**(-) + **Northness**(-)	0.17	347.5	4790.4	2.2
Eastness(+) + **Slope**(+) + **Elevation**(+) + **WEI**(-) + **Northness**(-)	0.17	346.8	4790.0	2.3

The SLR models for Basin B actually reversed compared to the previous sampling periods to show eastness, slope, and elevation as the most influential with R^2 values of only 0.10, 0.06, and 0.04. The best performing and most parsimonious MLR model combined eastness, slope, and the WEI for an R^2 of 0.17. Directly adding elevation to this model did not increase the R^2 but showed the best predictive accuracy with a minimum in the AIC at 4802.5. However, this improvement was considered unjustified for the cost of complexity and potential for misinterpreting a four variable model.

The distribution of SWE (Figure 17) provided by the top MLR model for Basin A

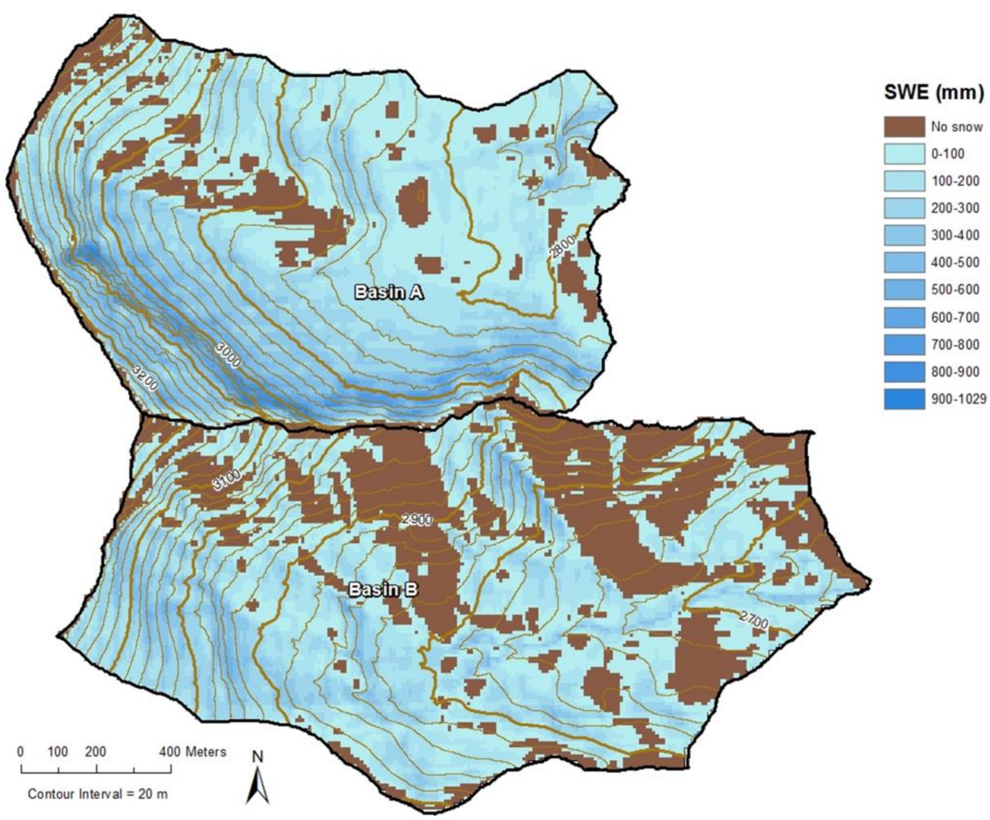

Figure 17. The modeled distribution of SWE for the ablation period using MLR models: Basin A: *SWE ~ -12.14 + (-48.57)*WEI + (6.30)*Slope + (63.91)*Eastness*
Basin B: *SWE ~ 185.78 + (317.81)*Eastness + (7.51)*Slope + (-43.77)*WEI*

with the WEI, slope, and eastness yielded a range of 0-1029 mm, while the model for Basin B with eastness, slope, and the WEI resulted in a SWE range of 0-631 mm. The total modeled volume of SWE was 263,716.8 m^3 in Basin A and 124,007.6 m^3 in Basin B (Table 6).

5.3 Binary Regression Trees

BRT analysis was not bound by the MLR assumptions of (1) linearity, (2) constant variance, (3) normality, and (4) influential outliers. The issue of multicollinearity between independent variables also limited MLR analysis by not allowing consideration of some of the most influential physiographic variables together in a model, i.e. 1) the WEI and solar radiation, and 2) northness and solar radiation. On the other hand, BRT analysis allowed all six physiographic variables to be simultaneously analyzed to predict SWE, thereby possibly including influential processes that MLR lacked the capability of interpreting.

5.3.1 Binary Regression Tree Modeling for the Accumulation Period

The root node of the binary regression tree (BRT), or variable that was most influential in predicting SWE in Basin A during the accumulation period, was solar radiation (Figure 18). The initial split from the root node suggests that locations with the lowest SWE depths (terminal node = 191 mm) were solely controlled by solar radiation if incoming levels exceeded the splitting criterion of 453,300 W/m^2. Below this level, wind became an important factor, and areas with less negative WEI values (more wind exposed) were limited to a moderate level of SWE (terminal node =454 mm), while those with more strongly negative WEI values (more wind sheltered) held the deepest SWE (terminal node = 612 mm). This model resulted in an R^2 of 0.38, and while further splits did increase the “apparent” R^2, this measure only reflects the relative error of the observations used to estimate the model, which generally leads to an overoptimistic estimate of accuracy (*Shmueli*, 2010). On the other hand, the 10-fold cross validation relative error (xerror) provides a more robust measure of the trend in R^2, indicating that the realistic R^2 maximum and optimal tree size coincide at 3 nodes. This tree partitioned 15.1% of the sample points (n = 16) to the lowest SWE, 26.4% (n = 28) to midlevel SWE, and 58.5% (n = 62) to the highest SWE. The Map Algebra/Raster Calculator tool in ArcGIS was utilized to gain a spatial distribution of SWE and a total SWE volume of 695,570.9 m^3 (Figure 19, Table 6).

The BRT for Basin B pruned down to a very simple tree with one split on the root node of eastness with a criterion value of 0.879 leading to modeled values of 259 and 645 mm of SWE in the terminal nodes (Figure 18). As in the modeling for Basin A, a similar trend in “apparent” versus cross-validated relative error, verified that the data limited this tree to an optimal size of 2 nodes. This partitioned 69.8% of the sample points (n = 44) to the 259 mm of modeled SWE, 30.2% (n = 19) to 645 mm. The spatial distribution of SWE (Figure 19) totaled a volume of 531,489.2 m^3 (Table 6), 23.5% less than in Basin A despite Basin B being 15.2% larger in area.

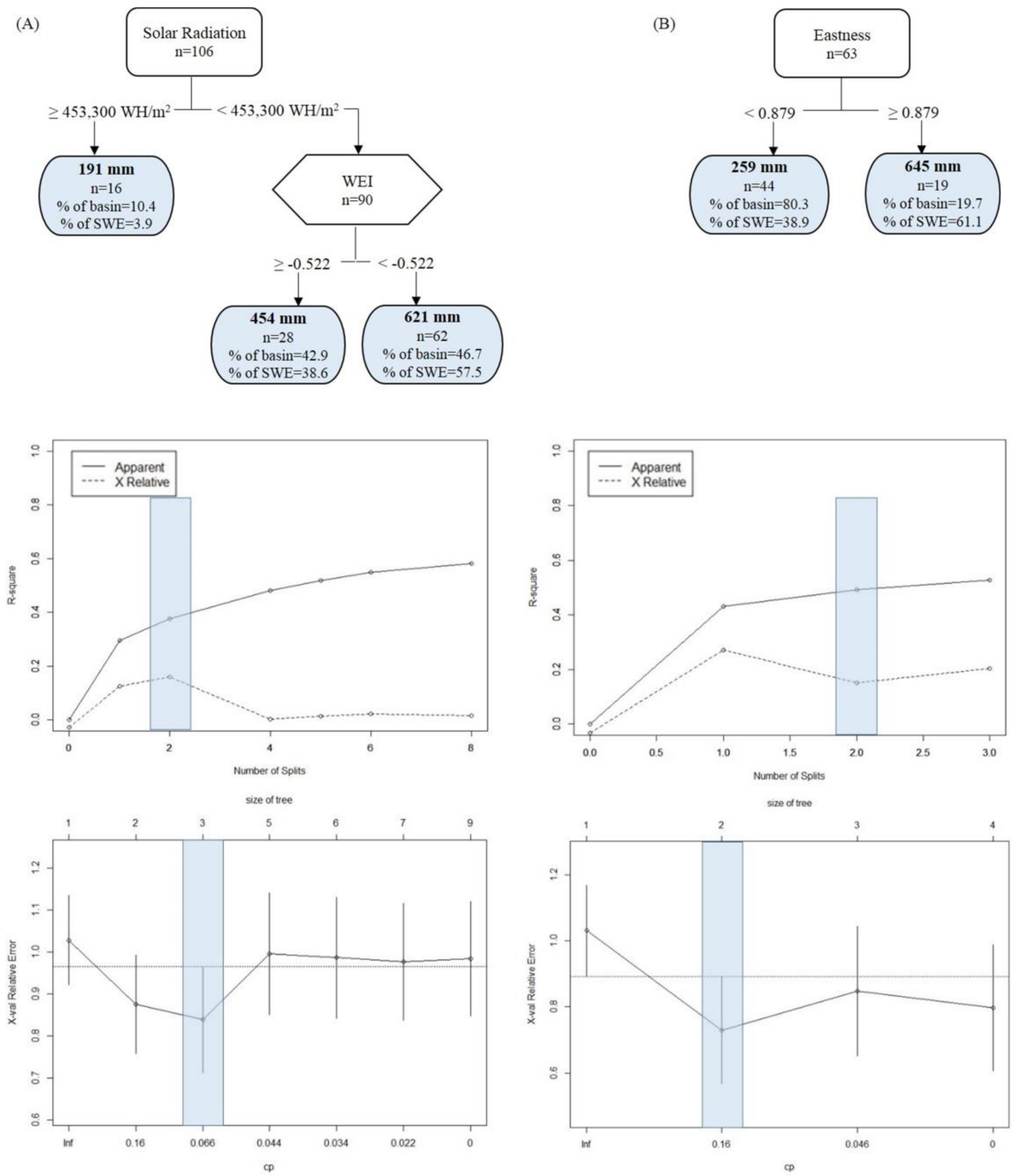

Figure 18. Pruned binary regression trees for Basin A (A) and Basin B (B) during the accumulation sampling period with corresponding plots of R square (apparent and relative to cross validation error) versus number of splits and X-val Relative Error (mean deviance) versus the size of tree (terminal nodes) and complexity parameter (cp), to verify optimal tree size (highlighted in blue).

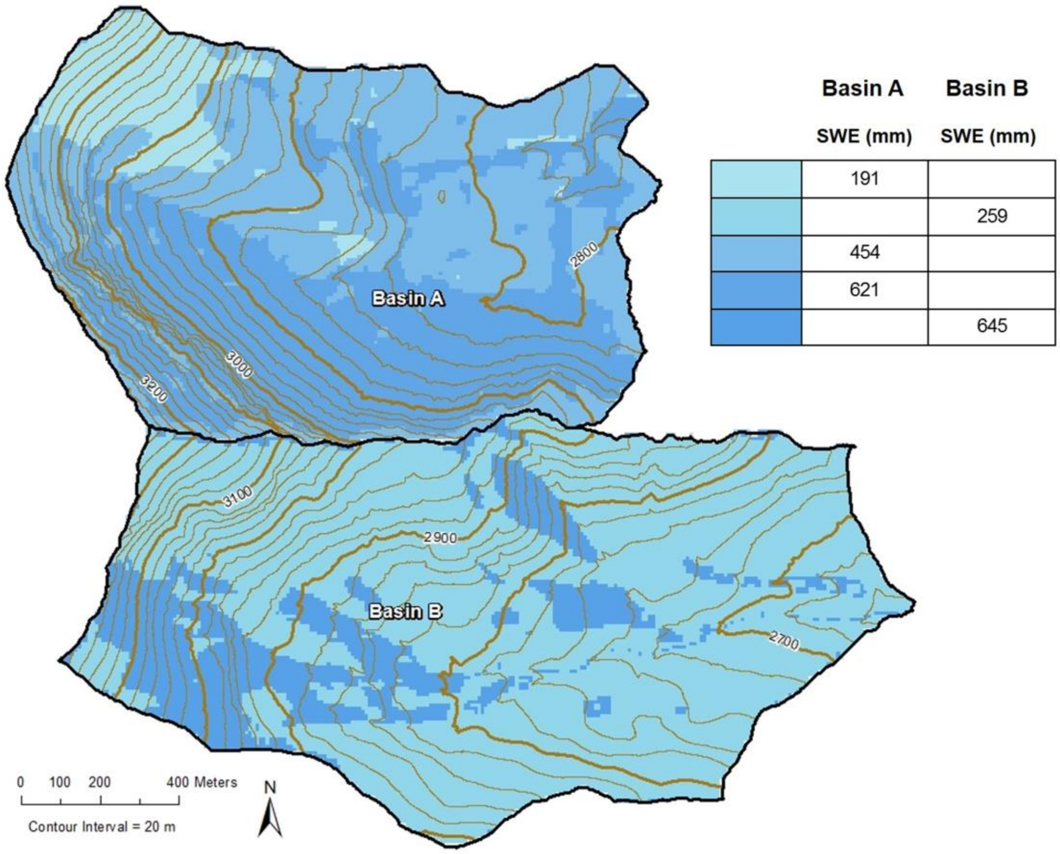

Figure 19. The BRT modeled spatial distribution of SWE for the accumulation period.

5.3.2 Binary Regression Tree
<u>Modeling for the Peak SWE Period</u>

The BRT for Basin A (Figure 20) grew from a root node (n=142) of solar radiation, with the WEI and slope offering further predictive value by splitting into two different tiers of daughter nodes. These subsequently grew a total of 6 terminal nodes for modeled SWE with a range of 204-1199 mm, explaining 66% of the variance. The spatial distribution displayed a fairly distinct dichotomy in the basin with the southern half (northeast facing zone) harboring more than 60% of the 916,334.2 m^3 (Table 6) of modeled SWE (Figure 21).

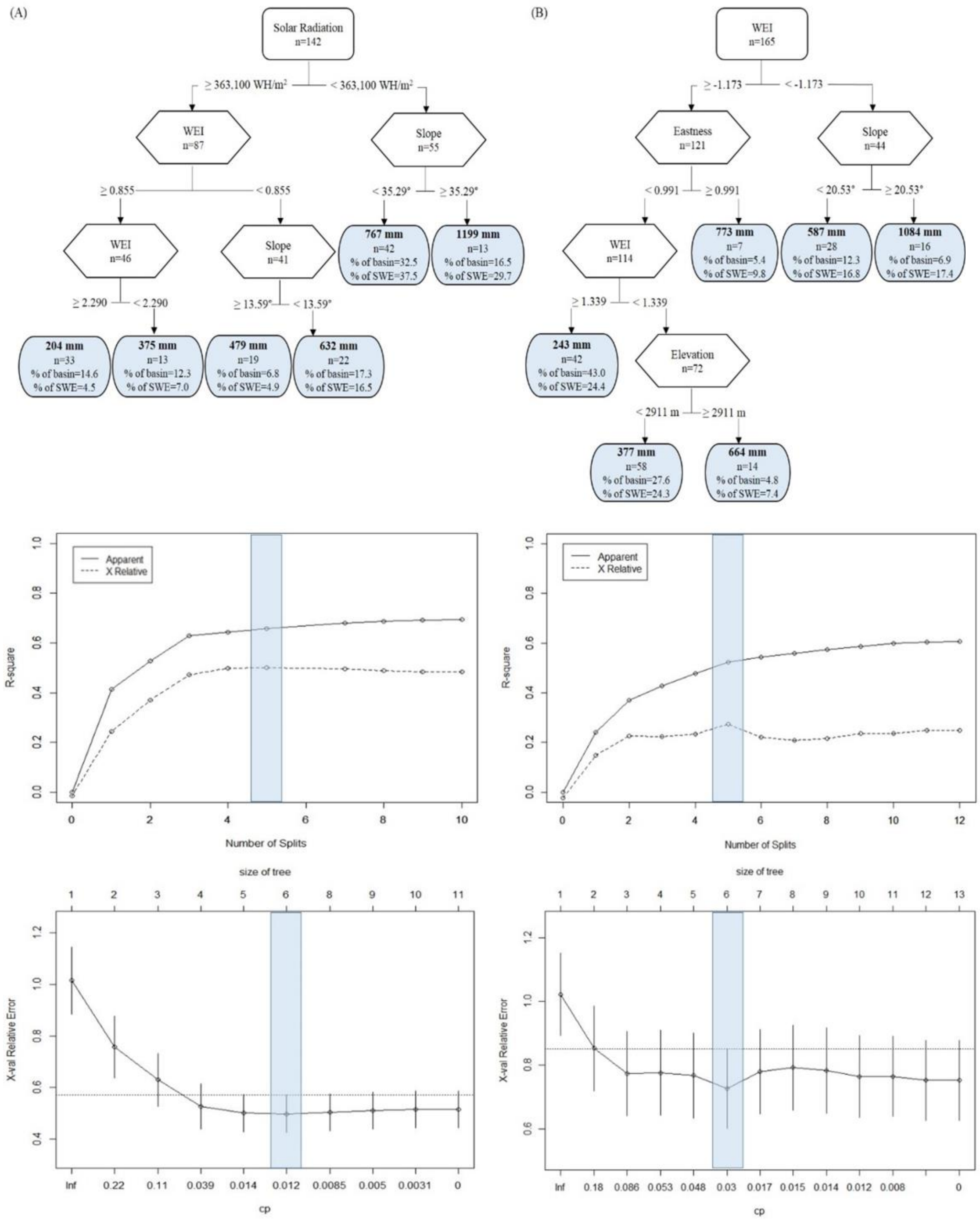

Figure 20. Pruned binary regression trees for Basin A (A) and Basin B (B) during the peak SWE sampling period with corresponding plots of R square (apparent and relative to cross validation error) versus number of splits and X-val Relative Error (mean deviance) versus the size of tree (terminal nodes) and complexity parameter (cp), to verify optimal tree size (highlighted in blue).

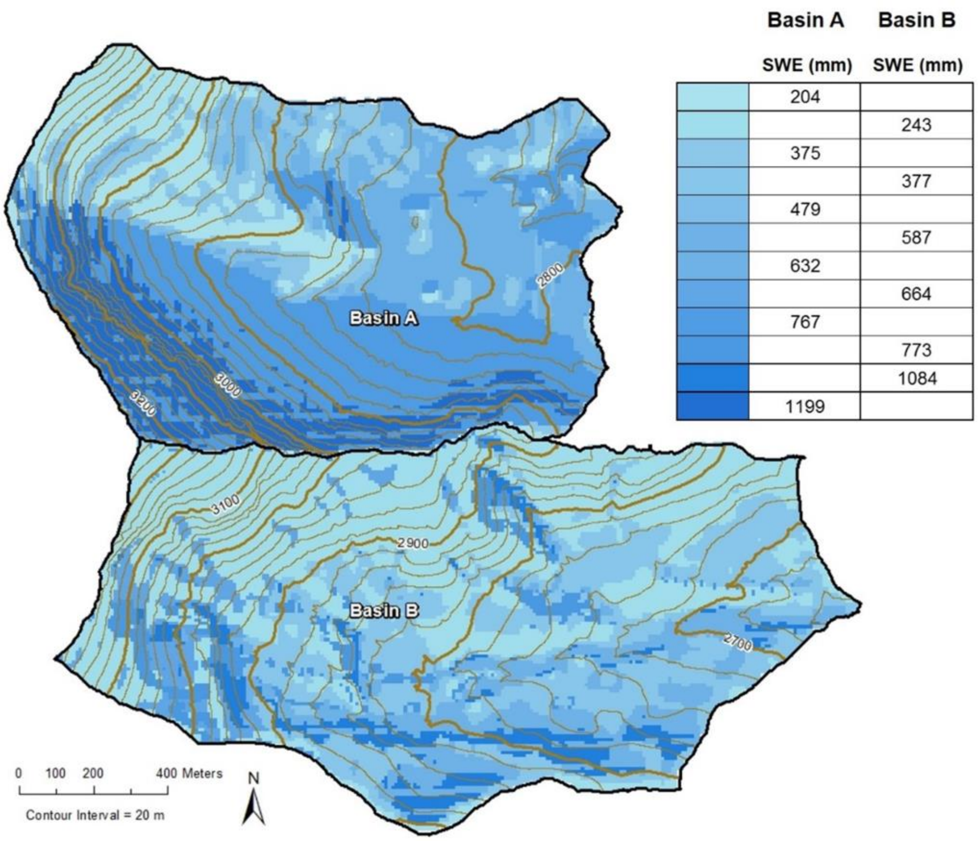

Figure 21. The BRT modeled spatial distribution of SWE for the peak SWE period.

The WEI was shown to be the dominant variable in Basin B, with a root node growing into recursive splits on eastness and slope and then the WEI and elevation. The final 6 node tree explained 52% of the variance in SWE with a range of 243-1084 mm. The spatial distribution of SWE was a bit more of a mosaic than that in Basin A. This did, however, reveal a pattern of the deepest deposits being predominantly in the southern half of the basin, particularly in north and east aspects at mid to high elevation (Figure 21). These zones of deep SWE only covered less than 20% of the basin, reflecting a total modeled basin SWE of 697,387.6 m^3 (Table 6) that was 24% less than in Basin A.

5.3.3 Binary Regression Tree
Modeling for the Ablation Period

Transitioning from peak SWE into the ablation period, the BRT model for Basin A shifted from one based on a root node of solar radiation to the WEI (Figure 22). The WEI was solely responsible for modeling the zones of highest SWE, while further splits on northness and slope determined low to midlevel SWE values in explaining 33% of the variance. With this sampling period spanning into early July, 80.9% of the basin was modeled with the lower values (48 and 173 mm) of SWE; however, the two higher values of SWE (466 and 804 mm) that covered only 19.1 % of the basin, accounted for 66.3 % of the remaining 292,504.5 m^3 (Table 6) of SWE (Figure 23).

The BRT for Basin B grew from a root node of eastness with recursive splits on solar radiation, elevation, and the WEI resulting in a tree of 5 terminal nodes that explained 62% of the variance in SWE. The initial split on eastness determined that, at this point, 80.8% of the basin area that is only slightly off of this aspect was close to melt-out with only 35 mm of modeled SWE. This accounted for 34.9 % of the total volume of 131,780.4 m^3 (Table 6). On the other end of the spectrum, 1.3 % of the basin area with an aspect very close to due east and low solar input was modeled with 1606 mm of SWE, maintaining 26.2% of the total volume. Further splits occurred first, on a value (2926 m) very close to the midpoint of the elevation range and finally on the WEI which divided zones of 65, 239 and 1117 mm, overall leading to a spatial distribution marked by abrupt changes in SWE depths (Figure 23).

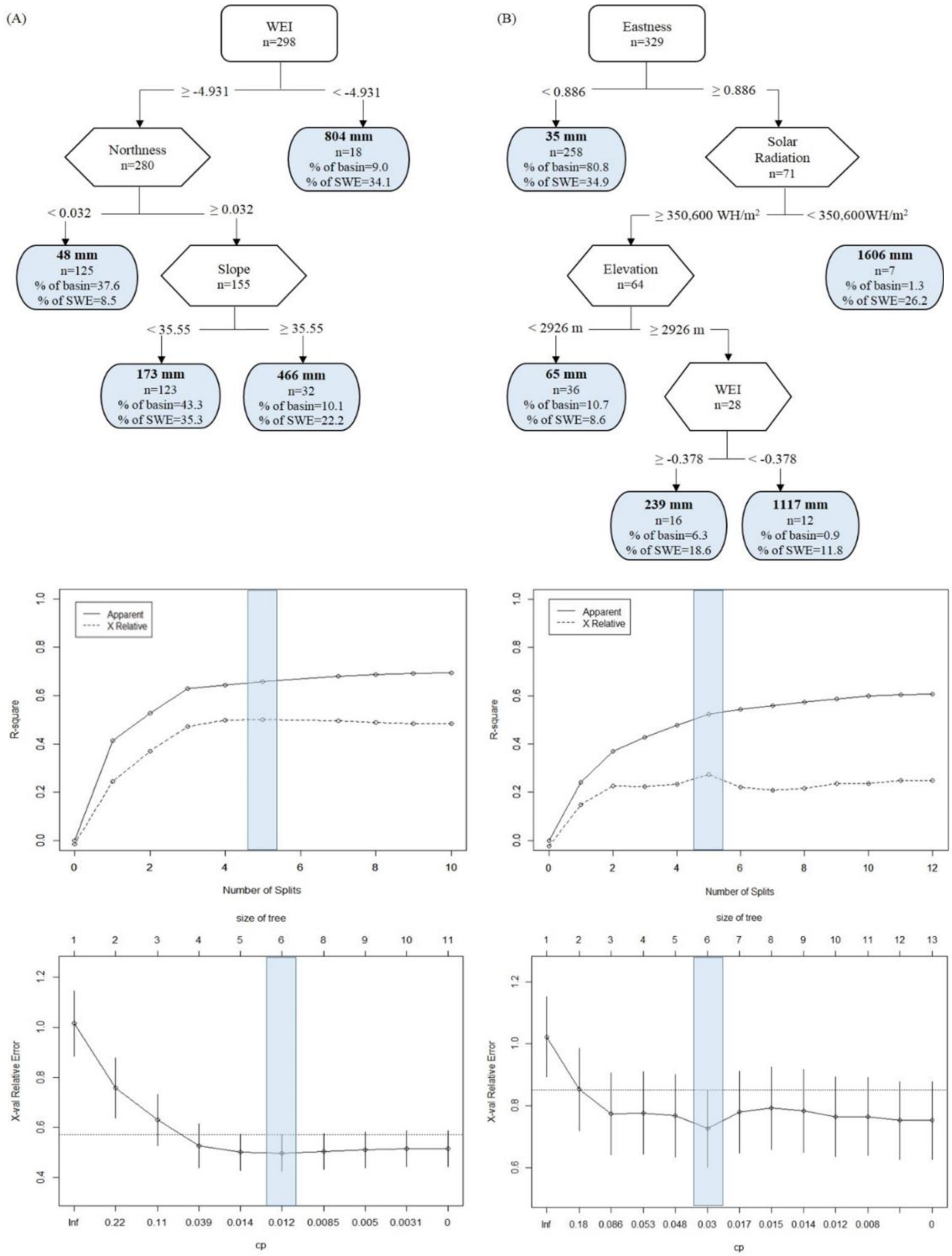

Figure 22. Pruned binary regression trees for Basin A (A) and Basin B (B) during the ablation sampling period with corresponding plots of R square (apparent and relative to cross validation error) versus number of splits and X-val Relative Error (mean deviance) versus the size of tree (terminal nodes) and complexity parameter (cp), to verify optimal tree size (highlighted in blue).

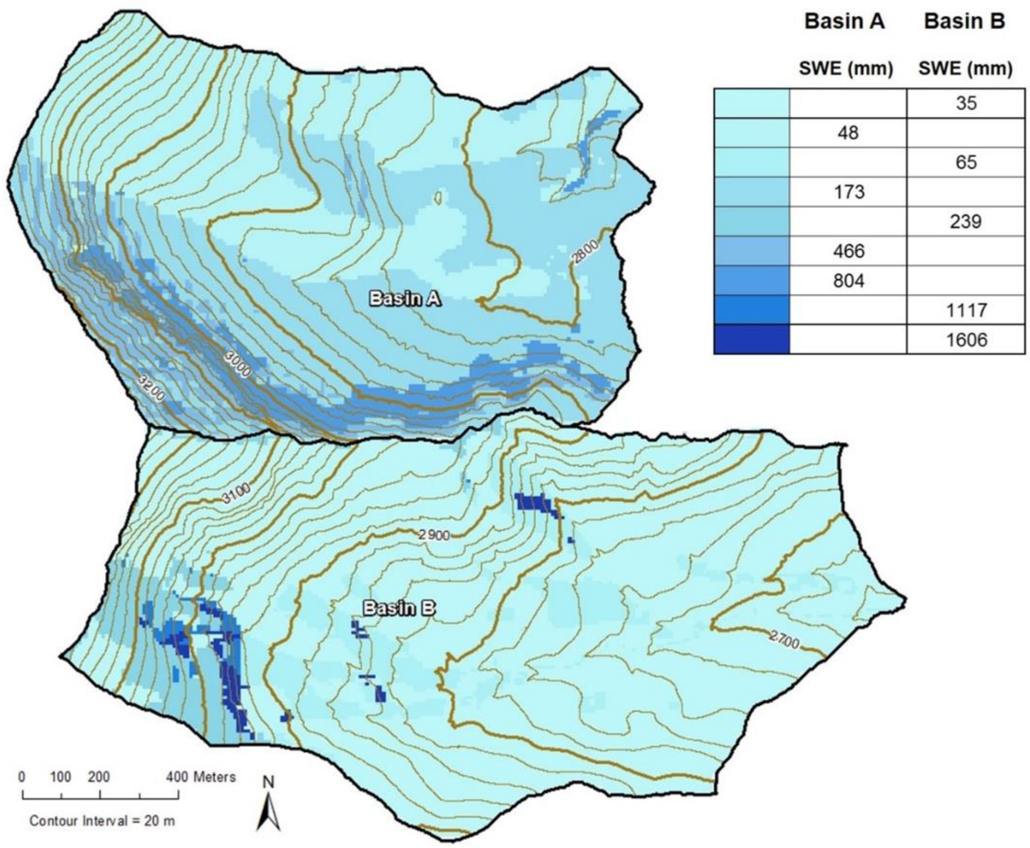

Figure 23. The BRT modeled spatial distribution of SWE for the ablation period.

5.4 Comparison of Linear Regression and Binary Regression Tree Modeling

Goodness of model fit evaluated by R^2 values in MLR was also produced for BRT models (Table 6) through the *rsq.rpart* function in *R*, which derived R^2 values by calculating: 1 - Relative Error (Therneau and Atkinson, 2014). Each model's measures of relative standing were also compared to that of the observed values for the sample points for each survey period. These are displayed in boxplots and analyzed through t-test results in the following subsections.

Table 6. R^2 values, dominant independent variables in order of significance (decreasing p-value) for MLR and in hierarchical order for BRT models, and total modeled SWE volume in each basin during the different sampling periods of snowpack development.

	MLR			BRT		
	R^2	Independent Variables	Total SWE (m^3)	R^2	Independent Variables	Total SWE (m^3)
Basin A						
Accumulation	0.28	WEI Eastness	680436.2	0.38	Solar Radiation WEI	695570.9
Peak SWE	0.57	WEI, Slope Eastness	834958.5	0.66	Solar Radiation WEI Slope	916334.2
Ablation	0.22	WEI Slope Eastness	263716.8	0.33	WEI Northness Slope	292504.5
Basin B						
Accumulation	0.32	Eastness WEI Northness	524251.1	0.48	Eastness	531489.2
Peak SWE	0.33	WEI Slope Eastness Elevation	663421.1	0.53	WEI Slope Eastness Elevation	697387.6
Ablation	0.17	Eastness Slope WEI	124007.6	0.62	Eastness Solar Radiation Elevation WEI	131780.4

5.4.1 Accumulation Period

The best performing MLR model for Basin A explained 28% of the variance in

SWE with the WEI and eastness, while the pruned BRT was able to explain 38% of the variance through splits on solar radiation and the WEI (Table 6). An analysis of the measures of relative standing showed that these values were quite different between the two models, and that the MLR was closer to the observed values for nearly all measures (Figure 24). In particular, the MLR was much better at matching the large range (0-878 mm) of observed values than the BRT. The observed sampling distribution also displayed a large standard deviation (SD) of 250.22 mm from the mean of 511.84. The BRT

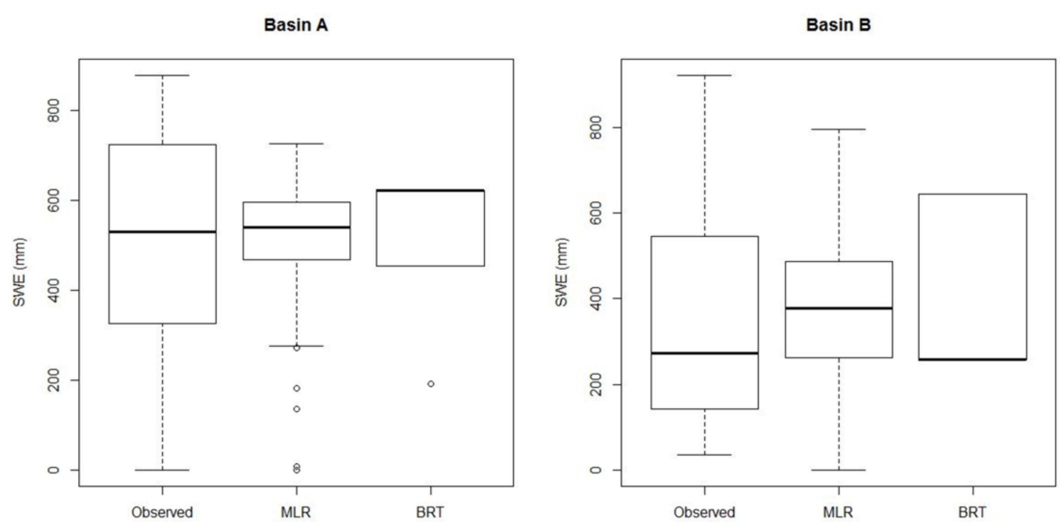

	Obs	MLR	BRT
Min	0.00	0.00	191.00
Q1	326.75	469.00	454.00
Med	529.50	539.00	621.00
Q3	721.25	595.00	621.00
Max	878.00	726.00	621.00
Mean	511.84	512.01	511.98
SD	250.22	134.78	153.67
n	106	106	106

	Obs	MLR	BRT
Min	36.00	0.00	259.00
Q1	142.50	262.50	259.00
Med	273.00	377.00	259.00
Q3	545.50	487.00	645.00
Max	922.00	795.00	645.00
Mean	375.46	376.10	375.41
SD	271.74	158.73	178.58
n	63	63	63

Figure 24. Boxplots comparing the observed SWE values for the accumulation sampling period to the SWE values modeled by MLR and BRT analysis.

displayed a higher SD of 153.67 mm from its mean of 511.98 mm than the MLR model SD of 134.78 mm from its mean of 512.01 mm. However, a two sample t-test between the MLR and BRT models yielded a p-value of 0.999 indicating that there was not a significant ($\alpha = 0.5$) difference between the mean of each model (Table 7).

In Basin B, the MLR model explained 32% of the variance with eastness, the WEI, and northness, while the BRT model managed to explain 48% of the variance based solely on eastness (Table 6). As in Basin A, the measures of relative standing illustrated that the MLR provided a better estimation of the large observed range (36-922 mm); however, the BRT excelled in modeling a median much closer to the observed (Figure 24). The observed sampling distribution had a large SD of 271.74 mm from the mean of 375.46. The BRT displayed a higher SD of 178.58 mm from its mean of 375.41 mm than MLR did with a modeled SD of 158.73 mm from its mean of 376.10 mm. Once again, t-test results (p-value = 0.997) showed these models to have means that were not significantly different (Table 7).

Table 7. Two sample t-test p-values for a comparison of the sample means ($\bar{x}$) between observed, MLR modeled, and BRT modeled SWE in each basin during the accumulation sampling period.

	p-value ($\alpha = 0.05$)	
	Basin A	Basin B
Observed SWE vs MLR SWE	0.995	0.987
Observed SWE vs BRT SWE	0.996	0.999
MLR SWE vs BRT SWE	0.999	0.997

5.4.2 Peak SWE Period

The MLR model for Basin A managed to explain 57% of the variance through the mixed effects between the WEI, slope and eastness, while the BRT found recursive splits on solar radiation, the WEI and slope to explain 66% of the variance (Table 6). The measures of relative standing revealed a substantial difference between the range and median of each model, both of which were more accurately captured by the MLR in comparison to the observed SWE (Figure 25). While the MLR did a good job of closely modeling the minimum observed SWE of 0 mm, both models greatly underestimated the

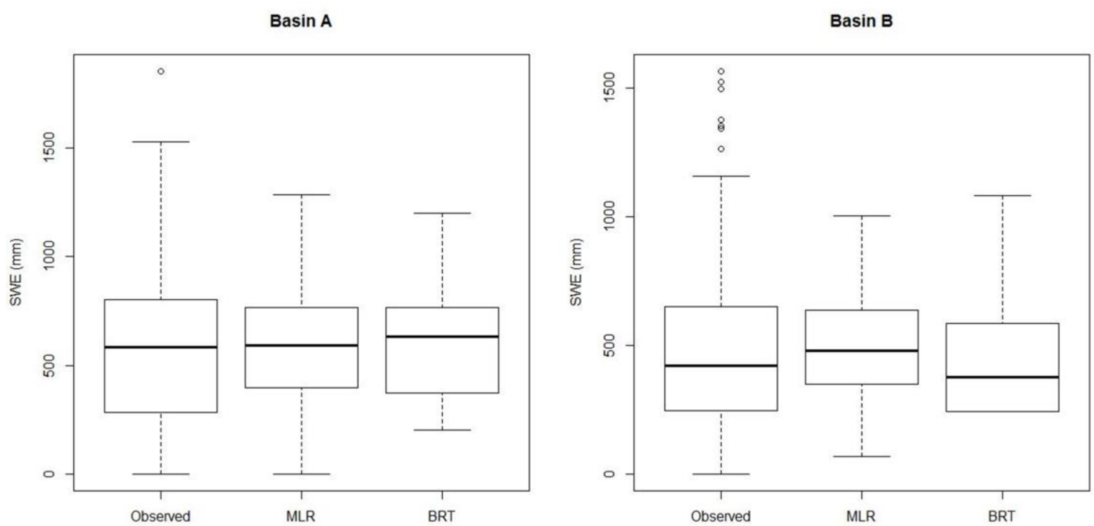

	Obs	MLR	BRT
Min	0.00	1.00	204.00
Q1	285.00	396.50	375.00
Med	584.00	590.50	632.00
Q3	802.00	764.50	767.00
Max	1852.00	1284.00	1199.00
Mean	580.54	580.45	580.37
SD	358.31	271.42	290.69
n	142	142	142

	Obs	MLR	BRT
Min	0.00	70.00	243.00
Q1	248.00	351.00	243.00
Med	421.00	481.00	377.00
Q3	653.00	639.00	587.00
Max	1568.00	1006.00	1084.00
Mean	488.44	489.03	488.24
SD	344.18	202.40	209.42
n	165	165	165

Figure 25. Boxplots comparing the observed SWE values for the peak SWE sampling period to the SWE values modeled by MLR and BRT analysis.

maximum of 1852 mm. This very large range of the observed sampling distribution was reflected in a large SD of 358.31 mm from the mean of 580.54. The BRT displayed only a slightly higher SD of 290.69 mm from its mean of 580.37 mm than the MLR did with a modeled SD of 271.42 mm from its mean of 580.45 mm. A t-test p-value of 0.998 (Table 8) revealed there was no significant difference in the mean SWE values of these models despite the difference in variables involved and explained variance.

For Basin B, both the MLR and BRT models found the WEI, slope, eastness, and elevation to be optimal in explaining 33 and 53% percent of the variance in SWE, respectively. The MLR once again more closely matched the observed range of SWE (0-1568 mm), but both were far away from capturing the maximum (Figure 25). The median of the BRT was within 10% of the observed while the MLR was nearly 15% higher. This very large range of the observed sampling distribution was reflected in a proportionally large SD of 344.18 mm from the mean of 488.44. The BRT displayed only a slightly higher SD of 209.42 mm from its mean of 488.24 mm than the MLR did with a modeled SD of 202.40 mm from its mean of 489.03 mm. There was not shown to be a significant difference in the means of these models, with t-test p-value of 0.982 (Table 8).

Table 8. Two sample t-test p-values for a comparison of the sample means ($\bar{x}$) between observed, MLR modeled, and BRT modeled SWE in each basin during the peak SWE sampling period.

	p-value (α = 0.05)	
	Basin A	Basin B
Observed SWE vs MLR SWE	0.998	0.985
Observed SWE vs BRT SWE	0.997	0.998
MLR SWE vs BRT SWE	0.998	0.982

5.4.3 Ablation Period

The best MLR model found the WEI to be most important when combined with the mixed effects of eastness and slope, thereby explaining 22% of the variance in the distribution of SWE (Table 6). The optimal BRT also stemmed from a root node of the WEI, but found splits on northness and slope to explain 33% of the variance. There was a large degree of variability between the measures of relative standing for the observed, MLR, and BRT modeled SWE (Figure 26). The MLR greatly underestimated the

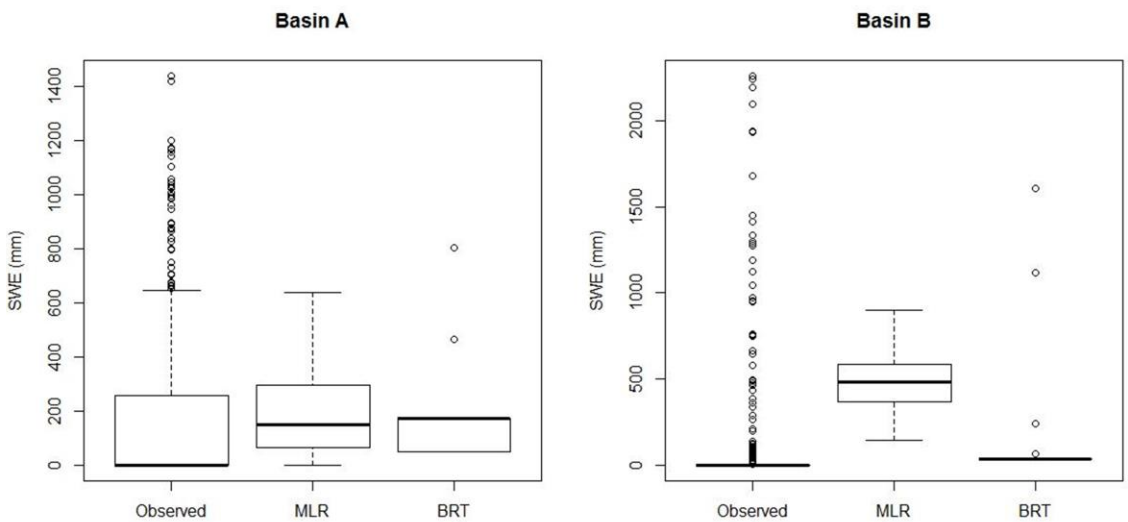

	Obs	MLR	BRT
Min	0.00	0.00	48.00
Q1	0.00	63.00	48.00
Med	0.00	147.50	173.00
Q3	258.00	297.00	173.00
Max	1439.00	640.00	804.00
Mean	190.13	193.56	190.14
SD	344.91	160.13	199.15
n	298	298	298

	Obs	MLR	BRT
Min	0.00	146.00	35.00
Q1	0.00	366.00	35.00
Med	0.00	485.00	35.00
Q3	0.00	588.00	35.00
Max	2260.80	901.00	1606.00
Mean	120.74	492.29	121.09
SD	380.69	158.88	300.33
n	329	329	329

Figure 26. Boxplots comparing the observed SWE values to those modeled by MLR and BRT analysis for the ablation sampling period.

minimum observed SWE of 0 mm, with a modeled minimum of -123 mm, and the BRT did not accurately capture snow free areas, modeling a minimum SWE of 48 mm. Both models also failed to capture the observed maximum SWE of 1439 mm, with the MLR modeling 640 mm and the BRT, 804 mm. MLR and BRT median SWE values of 147.5 and 173 mm were also far from the observed 0 mm. The very large range of the observed sampling distribution was reflected in a disproportionally large SD of 344.91 mm from the mean of 190.13. This pattern carried over to the modeling distributions, with the MLR showing an SD of 160.13 mm from its mean of 193.56 mm and the BRT displaying an even greater disproportion with an SD of 199.15 mm from its mean of 190.14 mm. A t-test p-value of 0.818 indicated there was not a significant difference between the mean SWE values for these models (Table 9).

The best MLR model for Basin B combined eastness, slope, and the WEI to explain 17% of the variance, while the BRT, also stemming from eastness, used recursive splits on solar radiation, elevation and the WEI to explain 62% of the variance in the SWE. The measures of relative standing were once again substantially different between the two models with the MLR greatly overestimating the minimum, Q1, median, Q3, and mean compared to the observed, whereas the BRT values for these measures were relatively close to observed. Both the MLR and BRT models did not manage to capture the observed maximum of 2260.8 mm, but the BRT was much closer with a value of 1606 mm compared to the 901 mm modeled by the MLR. The extremely large range of the observed sampling distribution was once again reflected in a disproportionally large SD of 380.69 mm from the mean of 120.74. This pattern carried over to the modeling distributions of the BRT, with an SD of 300.33 mm from its mean of 121.09 mm. On the hand, the MLR model displayed a modest SD of 158.88 mm from its mean of 492.29 mm. The disparity between the MLR and BRT distributions was confirmed in t-test results that showed the mean SWE ($\bar{x}$) of the MLR versus observed and MLR versus the BRT model to be significantly different with p-values of $2.2*10^{-16}$ for both (Table 9 and Figure 26).

Table 9. Two sample t-test p-values for a comparison of the means ($\bar{x}$) between observed, MLR modeled, and BRT modeled SWE in each basin during the ablation sampling period.

	p-value ($\alpha = 0.05$)	
	Basin A	Basin B
Observed SWE vs MLR SWE	0.877	$2.2*10^{-16}$
Observed SWE vs BRT SWE	1.000	0.989
MLR SWE vs BRT SWE	0.818	$2.2*10^{-16}$

6. DISCUSSION

Two statistical methodologies were utilized in this study to analyze and model the spatial distribution of SWE. These methods were applied to field measurements of snow depth and SWE acquired during the snowpack phases of accumulation, peak SWE, and ablation that were aimed at gaining a representative sample of the physiographic variables believed to be most influential in determining the distribution of snowpack metrics in the paired basin study area. Multiple linear regression (MLR) and binary regression tree (BRT) modeling were chosen because they are two fundamentally different methods, one linear and one nonlinear, that have been successfully used by previous studies to predict the distribution of snow from observations in mountain landscapes similar to the current study. BRT modeling has been more widely used with successful results in this discipline (e.g. *Elder et al.*, 1995, 1998; *Balk and Elder*, 2000; *Erxleben et al.*, 2002; *Winstral et al.*, 2002; *Anderton et al*., 2004; *Molotch et al.*, 2005) in the past twenty years than MLR due to the BRT ability to capture the often nonlinear processes that control snow distribution. However, some studies (e.g. *Harshburger et al.*, 2010) have demonstrated the simplistic utility of MLR as a sole modeling tool, while others have integrated linear regression as part of a more complex modeling scheme (*Elder et al.*, 1991; *Garen et al.*, 1994; *Erxleben et al.*, 2002; *Fassnacht et al.*, 2003).

While the simple and multiple linear regression models used in this current study provided a seemingly intuitive quantification of the effect the physiographic variables have on SWE through R^2 values, it quickly became very difficult to interpret the complex interactions occurring when more than one or two of these variables was included in an

MLR model. This points to the limitation of MLR in providing only a single predictive formula to model the entire data space of the study. Further complication is created by the potential nonlinearity of the multiple interactions between the physiographic variables. Binary regression trees provided a method of simplifying this problem by partitioning the data space into smaller sub-units that were more manageable to understand. Through recursive partitioning of these sub-units, it was possible to break the data down into clusters, small enough to be explained by simple models (terminal nodes: SWE constants). Thus, this tool provided fast prediction of SWE values with the dominant physiographic variables clearly laid out in the structure of the tree, unlike the somewhat invisible interactions occurring in the MLR for the output formula.

The results presented in this study are generally in line with previous studies in that BRT models consistently explained more of the variance in SWE than MLR models throughout the three sampling periods. BRT models were able to capture abrupt changes in SWE depth influenced by the nonlinear distribution of physiographic variables that demonstrated hillslope scale variability. However, the optimal BRT models for prediction were also somewhat simplistic, especially during the data limited accumulation period, thereby leaving a substantial amount of the variability in SWE unexplained. The following subsections delve further into the effectiveness and accuracy of the sampling design, and subsequent MLR and BRT analyses.

Before getting into the discussion of this and previous studies, it is necessary to re-clarify the distinction between explanatory and predictive modeling that has been presented so far in this paper. It should not be misconstrued, by using the terminology “explained the variance”, to indicate the performance of a model with regard to R^2, that explanatory power is being quantified or that explanation is the ultimate goal. The use of this terminology is applied to follow the conventional interpretation of the R^2 statistic, as well as the convention of how modeling is evaluated in the previous studies of this discipline to maintain a relative platform of comparability. Nevertheless, as previously stated, the models highlighted as optimal in the results of this study are all geared for the prediction of distributed SWE, by seeking parsimony in MLR and cross validated pruning in BRT analysis. Hence, for consistency, the same is true of the modeling of previous studies which are used for comparison in the following discussion.

6.1 Representative Sampling of the Physiographic Variables

The sampling distributions were markedly different between the accumulation, peak SWE, and ablation periods. Due to time, weather, and avalanche based safety constraints, the accumulation phase of snowpack development was when the smallest number of samples was obtained; however, the points in each basin were relatively evenly distributed among elevation zones (Figure 10). In Basin A, mid-elevation, low angle zones were oversampled, because of the relatively easy access. On the other hand, upper elevation zones were undersampled, not only due to heightened avalanche danger, but significant cliff areas that were mainly inaccessible. Previous studies (e.g. *Elder et al.*, 1991, *Balk and Elder*, 2000, *Winstral et al.*, 2002, *Erickson et al.*, 2005) have noted similar limitations on representative sampling even during the peak SWE period when snowpack conditions are normally more stable. However, *Kerr et al.* (2013) used automated camera photography of inaccessibly steep alpine terrain which was then orthorectified and used in modeling to determine the distribution of SWE, thereby surmounting this obstacle. The same trend of sampling imbalance was seen in Basin B during accumulation, but was somewhat inconsistent due to the small sample size leading to a degree of under and oversampling in nearly all elevation zones. Peak SWE was the snowpack phase of focus and because the study basins were sampled intensively during an 11 day time span, the most consistent and evenly distributed dataset was acquired during this period. With a melt freeze cycle occurring during much of this period, avalanche terrain at nearly all elevations was able to be safely sampled, but some very steep zones, particularly the northeast headwall of Basin A, were still inaccessible. Not being able to sample in the headwall, the largest contiguous avalanche start zone and source of continual sloughing, limited correlation of subsequent snow distributions in this zone and below, to avalanche activity. Despite the large sample size also acquired during the ablation period, its representativeness suffered from acquiring repeat data observations in persistent snowpack areas, as opposed to patchy or snow-free areas, in the interest of possible correlations to increased deposition from avalanche activity and wind redistribution.

As previously mentioned, consideration of the scale triplet, as defined by *Bloschl* (1999), is crucial to sampling and modeling design. The fundamental issue with choosing the appropriate scale triplet when designing a sampling strategy is that the process scale (correlation length) in an unstudied area, such as that of the current study, is unknown (*Skoien and Bloschl*, 2006). In order to sample with an appropriate spacing (sample points) and extent (transects; basins), previous studies investigating the correlation length of snow distribution in similar scale basins with similar, dominant physiographic processes (e.g. *Balk and Elder*, 2000; *Winstral et al.*, 2002; *Erxleben et al.*, 2002; *Erickson et al.*, 2005; *Clark et al.*, 2011) were considered. In their study of sampling scale effects on environmental monitoring, *Skoien and Bloschl* (2006) stated as rules of thumb: 1) extent should be substantially larger than the correlation length, 2) spacing should be smaller than the correlation length, and 3) support depends on the statistic of interest, but variances are significantly biased and underestimated once support is greater than one third of the correlation length. The previous studies with similar spatial variability in snow depth have used spacings of 5-100 m and extents of 1-93 km^2 (*Clark et al.*, 2011). Thus, this study employed a 15-50 m spacing to capture the point to smaller hillslope scale variability, a 150-450 m transect extent to capture the larger hillslope to watershed scale, within transect, variability, and up to a 1.8 km extent between transects to capture the greater watershed scale variability in snow depth. Support (modeling) was provided at a 10 m scale by the DEM utilized to model the physiographic variables. Post field measurement, the correlation length of snow depth from observed values was estimated to be 55 m (Section 4.6). Hence, it is believed that spacing, extent, and support were appropriately chosen for this study given the rules of thumb suggested by *Skoien and Bloschl* (2006). *Erxleben et al.* (2002) expressed that their study with a 5-25 m spacing and 30 m DEM support may have resulted in a mismatch of scales for the dependent and independent variables, thus leading to low explained variance by subsequent modeling. It is believed that this current study limited this scale issue through a better pairing of spacing and support, and R^2 values for models, especially during the peak SWE sampling period, are on par with those of other studies.

6.2 Data Analysis for the Accumulation Period

6.2.1 Linear Regression Modeling

Wind was expected to be a dominant variable during this period as colder air temperatures and hence, lower snow density in the winter allow for maximum snow redistribution. This was shown by SLR analysis to be true in Basin A, with the greatest amount of the variance in SWE explained by the WEI. It was unexpected to see solar radiation not far behind in predictive power, as it seems that the average solar zenith angle and daylight hours at 45° latitude zone during this period would limit the influence of solar radiation, as well as northness. However, *Anderton et al.* (2004) noted that earlier in the season, differences in solar input are more profound between northerly and southerly aspects in complex topography due to the low solar zenith angle, whereas solar radiation becomes more uniformly distributed as the solar zenith angle becomes larger approaching the summer equinox. It is also possible, for the reasons highlighted by the correlation analysis (Appendix C), that solar radiation and northness showed higher predictive power than elevation, slope, and eastness due to their relation to the WEI in a basin with prevailing south/southwesterly winds. Furthermore, considering that sampling occurred at some transects through April 11, it is becomes more logical that solar radiation would have a strong influence on the overall sample and thus, derived models.

Additional variables in Basin A did not offer much improvement over the SLR model with the WEI. It was surprising that the addition of eastness with the WEI, instead of elevation, produced the best MLR model, given that it was not shown to be significant in SLR, whereas elevation was. It is possible that transects A6a and A9a, where the deepest snow in Basin A was measured, influenced this outcome due to being not only enhanced by substantial wind deposition, but also from having enough of an east aspect to incorporate this variable as well.

Overall, the SLR models for Basin B had less than half the predictive power than that for Basin A. This disparity is possibly due to the much smaller sample size collected in Basin B during this period compared to Basin A, leading to greater variability in the data. This may also explain why eastness came out with nearly twice the predictive power than the WEI in Basin B, as the two due east facing transects (B10a and B13a, Figure 9) accounted for 26 of the 63 total points sampled during this period, and they also harbored the deepest snow. Despite having nearly half the predictive power, the addition of the WEI to eastness produced substantially better performance in an MLR model than the two variables individually. It also explained more of the variance in SWE than the same model in Basin A. This is consistent with the exposure of the majority of Basin B to wind with a far less prominent topographic barrier to the south/southwesterly flow than the northeast headwall creates in Basin A. It seems counterintuitive that northness (only significant at $\alpha = 0.05$) would bring further predictive power to the two variable model in Basin B, with a negative relationship to SWE. However, this supports the observations that the dominant influence of the deep snow measurements of east facing transects B10a and B13a, whereas more north facing transects B4a and B9a held shallower snow due to low elevation and wind scouring, respectively.

The best MLR models discussed above generally performed well in distributing SWE compared to measurements and visual observations made during the accumulation period (Figure 15). This applies to deep snow areas such as, below the northeast facing headwall of Basin A, and wind sheltered gullies in both basins. It also captured the typically shallow snowpack on the wind scoured, southeast aspects of each basin. However, the model did not capture the potential for deeper snowpack in the north facing areas of Basin B and perhaps distributed too much SWE to the lower portion of the main stream channel in Basin B.

6.2.2 Binary Regression Tree Modeling

A 3 node tree for Basin A and 2 node tree for Basin B were determined by cross validation procedures to be optimal for prediction during this period. These models had substantially fewer nodes than previous studies (e.g. *Elder et al.*, 1998*; Balk and Elder,* 2000*; Erxleben et al.,* 2002*; Winstral et al.,* 2002*; Anderton et al.,* 2004; *Molotch et al.,* 2005) that found trees with 5 to 25 nodes to be optimal. This is likely due to the rather small number of observations and general lack of representativeness of the sampling that occurred during accumulation. This produced a higher degree of data heterogeneity (than in the peak SWE sampling period), and as noted by *Elder et al.* (1995), outliers of abnormally deep snow deposits and snow free areas decreased the potential for further partitioning into nodes of increasing homogeneity. This is particularly true with respect to the 63 samples of Basin B, where a full tree of 4 nodes with recursive splits on northness and slope, from eastness, seemed counterintuitive as zones with a more southerly direction were modeled with more SWE. This was deemed unlikely given the increased solar input and potential for wind scour in these areas, hence these nodes were pruned.

While the 3 node tree for the 106 observations for Basin A also seems suspiciously small, pruning employed the same technique of minimizing the 10-fold cross validation relative error with tree size (or model deviance versus tree size) for 100 iterations, as in previous studies (e.g. *Winstral et al.*, 2002; *Molotch et al.*, 2005). A full tree of 9 nodes for Basin A did show increasing R^2 (maximum of 0.58) up to this size, and it may have provided an 'apparent' best estimate of the SWE distribution, but previous studies (*e.g. Elder et al.*, 1995; *Anderton et al*., 2004) have noted, the amount of explained variance in an overfit tree is overoptimistic compared to what the dataset actually warrants and the ability of the model to predict the result in nature. Thus, it seems more accurate, given the datasets for Basin A and Basin B, that the optimally pruned BRTs were able to explain 38% and 48% of the variance, respectively.

The BRT's for this period generally reflected the dominant variables in SLR analysis, but there were some clear differences from the MLR models. The most fundamental difference is seen in the BRT model for Basin A that stems from solar radiation and the WEI, while the MLR model, limited by a multicollinearity violation in combining these variables, found the highest R^2 with the WEI plus eastness. Consequently, the BRT was able to explain 38% of the variance while the MLR only explained 28%. However, the BRT was limited to 3 nodes for a range of 191-621 mm of SWE while the MLR was seemingly more accurate in capturing the observed range 0-878 mm with 0-1265 mm. This difference is clearly seen in the mapped distribution of SWE for each model (Figure 15, Figure 19), as the MLR appears to capture far more of the point to hillslope scale variability than the BRT that is basically comprised of three distinct zones of accumulation. However, while the BRT is perhaps overly simplistic and has not managed to explain some of the variance, the MLR is likely overpredicting detail in the distribution of SWE that the data does not support.

These issues seem to correspond to the MLR and BRT models for Basin B as well. Again, the SLR and BRT results generally agreed, with the eastness being the dominant variable. This seems to be an effect of the deepest SWE recorded in the east/northeast facing transect, B13a, which is likely due to topography at the point, hillslope and watershed scales. This transect spanned a shallow concave bowl on the lee of a very broad northwest to southeast trending ridge with no substantial topographic barriers to the Madison Valley to the west. Thus, this transect presumably received much of this snow from wind deposition despite not being perpendicular to prevailing winds. This hypothesis lends more credibility to the SLR and MLR models showing the WEI to be of secondary importance. The optimal MLR and BRT models found a negative relationship with northness, which seems to be a result of a flawed sampling strategy, in that, southeast facing transects (6a and 15a) were sampled in April when SWE was nearing peak, and north/northeast facing transects were sampled in January when SWE was inherently shallower. Hence, the models with this variable are both suspect.

Despite the inaccuracy in the models for both basins due to the non-representative sampling, some of the patterns highlighted by them appear to be realistic. Assuming the BRT is more accurate than the MLR in Basin A given its higher R^2, it seems possible that even with a low average solar zenith angle during the accumulation period, solar radiation may be the dominant variable controlling SWE distribution in Basin A. This would be an effect of deeper snow being maintained in up to half of its area due to decreased solar radiation input on the north/northeast aspects and shading due to the dominant northeast headwall feature. This same feature also partially explains why the WEI was found in MLR to be more influential as it promotes increased snow deposition due to wind sheltering. The other, east/southeast facing half of the basin clearly is affected by wind exposure which may or may not be preempted by solar radiation. These differences in model variables and structure lead to the MLR model yielding nearly twice the range of SWE than the BRT and subsequent differences in the spatial distribution. In general the MLR displayed far more hillslope scale variability. Despite the contrast in models, the difference in estimated total volume of SWE was 2.2% (Table 6).

In Basin B, conclusions are more difficult to make given the smaller dataset, but the dominance of eastness shown by both the MLR and BRT models is a reflection of the strong influence of the WEI. Hence, despite the lower R^2 of the optimal MLR model compared to the BRT, it may have been more accurate in capturing this process. Once again, the variation in the spatial distribution of SWE by these models only translated into a difference of 1.4% between the estimated total volumes of SWE (Table 6).

6.3 Data Analysis for the Peak SWE Period

6.3.1 Linear Regression Modeling

A working hypothesis was that, by the peak SWE period, solar radiation overcomes the influence of wind on the snowpack. This is primarily due to the more direct solar zenith angle and long daylight hours providing increased energy input, as well as the high average snow density limiting wind transport. SLR analysis supported this hypothesis for Basin A. However, the WEI remained closely influential in Basin A and came out as the dominant variable in Basin B in SLR. The potential for the single variable dominance of WEI in Basin B was considered while field sampling and visually observing substantial wind transport of snow to transects B11 and B13 over the broad ridge that makes up the southern boundary of the basin. This was further verified by the highest measured SWE values in Basin B at these transects. In MLR analysis, the WEI was shown to be dominant in both basins. This was not surprising, as wind had been involved in distributing the snow all winter and early spring and had somewhat predetermined the pattern of SWE by early May. Northness was close behind these two in its predictive value, as it is a reflection of both the WEI, given the prevailing southerly winds, and solar radiation as a function of aspect. Unlike during accumulation, this variable was shown to have the logical, positive relationship with SWE, pointing towards the far more representative sample collected during peak SWE. Elevation showed nearly the same R^2 in Basin A as during the accumulation period, suggesting that this variable is somewhat responsible for the distribution of SWE due to orographics and lapse rate, but in reality, this is probably limited by the 600 meters of vertical relief in the study area. The increasing redistribution of snow by wind with elevation, compounded by solar radiation, further limits the explicit effect of elevation and explains why transects A11, A12, and A13, despite their high elevation, are where some of the lowest SWE values were consistently measured. Elevation not being shown in SLR to be significant (α = 0.05) in Basin B is also evidence for this hypothesis.

Slope was once again not shown to be significant in SLR results for Basin A, and just barely significant in Basin B. However, optimal MLR models showed the mixed effects of slope with the WEI and eastness in Basin A, as well as elevation in Basin B, to greatly increase the explained variance. This is possibly a result of the inherent relationship of the WEI to slope. Thus, in both basins, zones with a steeper leeward slope (e.g. transects B11, B13, A9, and A10) were prone to preferential snow deposition from wind sheltering. On the other hand, the deepest measurements of SWE in Basin A were most consistently found in transects A9 and A10 where obvious, direct wind deposition of snow like in transects B11 and B13 was never actually observed. Furthermore, it was assumed to be less of a control due to A9 and A10 being approximately 100-300 vertical meters below the steep ridgeline and headwall, as opposed to those in Basin B where the drop from the ridge is gradual and generally less than 100 meters. Consequently, in Basin A, it is likely that transects A9 and A10 held deep snow not only because of wind deposition and low levels of incoming solar radiation, but that slope was an important contributing factor due to continual sloughing and slab avalanche transport/deposition of wind loaded snow from the steep terrain in the headwall above. The automated camera taking photos every hour during daylight periods did not record any widespread avalanche cycles, but occasional small slab avalanches were captured and the pattern of cumulative slough deposition was evident in the time record of photographs (Figure 27). In the field evidence of sloughing was also clearly visible in the deposition zones below

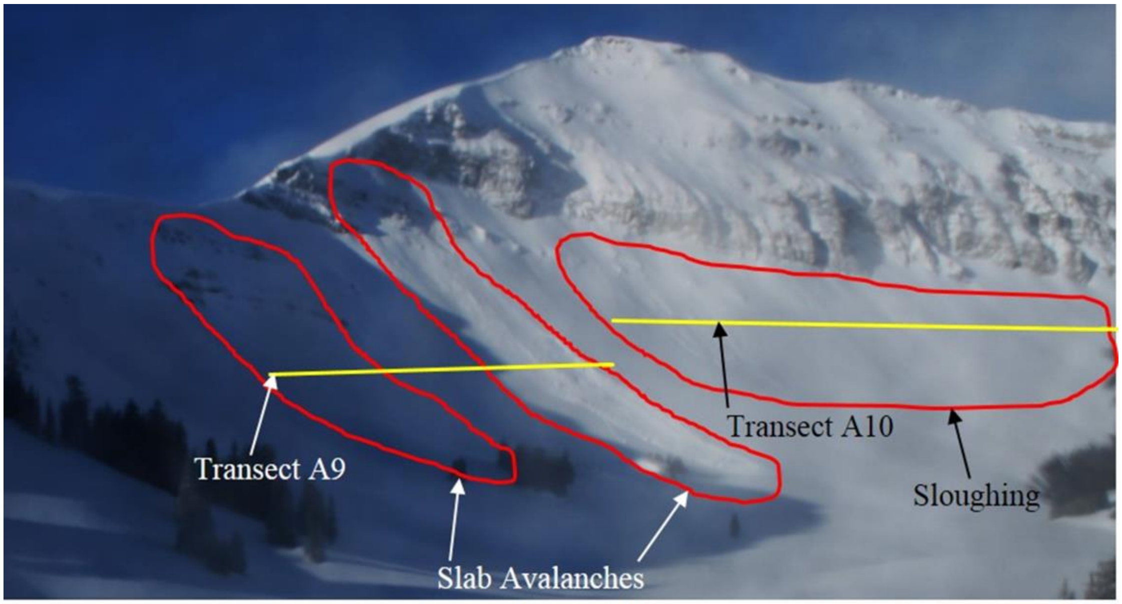

Figure 27. Photo of the northeast headwall of Basin A taken by the automated camera on February 21 at 08:31, showing two slab avalanches into Transect A9 and evidence of the continual sloughing into Transect A10. The cumulative deposition of these processes throughout accumulation was evident in peak SWE sampling.

the northeast headwall and extended ridgeline.

The top models (Basin A and B) for the peak SWE period appeared to capture the spatial distribution of SWE well in many of the same areas of the study basins as during the accumulation season (Figure 16). What really stands out is how the range of SWE (mm) values in Basin A is nearly twice that in Basin B. This reflects the deep snow deposition from wind, and possibly avalanche activity, as well as persistence due to shading below the north/northeast headwall of Basin A. On the other hand, the deepest SWE modeled in Basin B is mainly confined to stream channels and other topographical depressions, and appears to be limited in relative magnitude by a solar component given its overall more southerly aspect. With a maximum measured SWE value of 1852 mm (Appendix A) compared to a modeled value of 2067 mm in Basin A, it seems that the model may overestimate in the lower headwall zone. This is perhaps due to the strong reliance of the WEI as a predictor, when, as described earlier, wind driven snow deposition to this zone up to 300 vertical meters below the ridgeline may not be as substantial as modeled. Conversely, in Basin B, measurements of SWE up to 1568 mm were made in transects B11 and B13 (Appendix A), indicating that the model failed to completely capture the wind deposition in these zones with a maximum modeled SWE of 1267 mm. The relatively low R^2 values of these models indicate that almost 60-70% of the variance in the SWE data is not explained likely due to the inability of MLR to capture the nonlinear processes at work.

6.3.2 Binary Regression Tree Modeling

The timing consistency and relative representativeness of sampling during the peak SWE period produced BRT models that were comparatively successful with regard to previous studies that were conducted during this time period with similarly intensive surveys. The optimally pruned trees for prediction purposes, comprised of 6 nodes for each basin, were relatively small, yet the explained variance (66% in Basin A and 53% in Basin B) was either on par with or greater than previous studies with similar or greater complexity in their models. In one of the most successful applications of this methodology, *Elder et al.* (1998) developed trees of 13 to 25 terminal nodes that explained 60-70% of the variance for a hypothetically more difficult distribution due to the substantially larger study area. It should be noted that these comparatively larger trees were proportional to the larger dataset (709 sample points) acquired for that study. However, in a more similarly sized basin of 6.9 km^2, *Balk and Elder* (2000) explained

54% and 65% of the variance in SWE, nearly equal to the current study, with 18 nodes each for datasets of 197 and 173 snow depth samples, respectively. The similarly sized trees of 5 and 7 nodes (average n = 328) developed by *Molotch et al.* (2005) explained substantially less variance at 31% and 39%, respectively, but in a larger basin (19.1 km^2). In slightly smaller study basins than the current study (three 1 km^2), *Erxleben et al.* (2002) found trees of 7 to 12 nodes to explain 17% to 30% of the variance in snow depth (n = 550). As previously noted, the use of R^2 values as a comparison criterion of model success between studies should include the caveat that these values are not necessarily directly comparable due to the different attributes of the study areas, sampling design, water years, climatology, etc. That being considered, the model performance for the peak SWE period of this current study, in reference to previous studies, is very encouraging. This is especially true considering that within the cross validation process of pruning and associated measures used to select an optimally pruned tree, there is a range in the optimal size (flat area of the minimum in plot of the residual error) in which the model user has the freedom to decide which is most appropriate given an intimate knowledge of the processes at work in the study area. Thus, the models for the current study appear to exhibit a high level of predictive value given their relative parsimony in comparison to previous studies.

Similar to the accumulation period, the MLR model for Basin A predicted maximum SWE (2067 mm) to be nearly twice that of the BRT (1184 mm). The MLR distributed the bulk of maximum values to the apron below the northeast headwall, while the BRT distributed more of these values to the upper face. Spatial distribution of low to medium SWE values between models also displayed contrasts, but were comparable in magnitude. Overall, variation in the modeled SWE distributions only lead to a 9.7% difference in estimated total volume of SWE for Basin A (Table 6). The range and spatial distribution of SWE for the MLR and BRT models was more similar for Basin B, and estimated total volume of SWE only differed by 5.1%.

6.4 Data Analysis for the Ablation Period

6.4.1 Linear Regression Modeling

SLR models for the ablation period continued to show the trend seen in the accumulation and peak SWE models, with regard to the independent variables exhibiting approximately twice the predictive power in Basin A than in Basin B (Table 5). The exact reason(s) for this is uncertain, but it is suspected that the most notable difference between the two basins, the distribution of aspect, could be the root of an explanation. Aspect is a terrain attribute that controls at least two of the variables most consistently shown to be dominant in influencing the distribution of SWE during all three sampling periods: the WEI and eastness. It is considered that a more complex distribution of aspect in Basin B, not as clearly divided between north/northeast and south/southeast (Figure 12), decreased the ability of the models to explain the response through the aforementioned dominant variables.

The SLR results in Basin A continued the pattern from the peak SWE period with solar radiation, followed by the WEI and northness, once again proving to be the principal variables controlling SWE during ablation. This was consistent with our hypothesis, given that solar radiation, and inversely, northness, are assumed to become increasingly important in the energy budget of the snowpack as the melt season progresses (*DeWalle and Rango*, 2008). However, a combination of the WEI with slope and eastness resulted in the best performing MLR model despite the latter two variables having very little predictive value by themselves. The WEI showing dominance and solar radiation being eliminated in the MLR models is once again due to multicollinearity prohibiting these two variables together in a model. Despite this limitation, the best selected model generally reflects the pattern of melt-out observed during this period while sampling in Basin A (Figure 28), in that, the wind sheltered zones (negative WEI values; coefficient = -48.57), particularly below the north/northeast headwall, with greater slope angles (coefficient = 6.304) with a northeast aspect (eastness values closer to 1; coefficient = 63.905) maintained the deepest snow (Transects A9 and A10). On the other hand, those areas with a more southeast aspect had mainly been scoured by wind compounded by increased solar input, and were mainly snow-free (Figure 17). Unfortunately, this model was unable to capture the processes of continual sloughing and occasional slab avalanche activity that are presumed to have been the dominant processes at work to leave the upper elevation, northeast facing portion of the headwall in Basin A snow free by this point. However, that is simply due to the absence of sampling in this zone because of terrain and safety limitations. Nevertheless, it is possible that the persistent snowpack below this headwall is more due to the slope/avalanche activity and solar radiation/northness variables than the combination of the WEI (negative values; wind shelter), slope, and eastness. While sampling and modeling data cannot directly

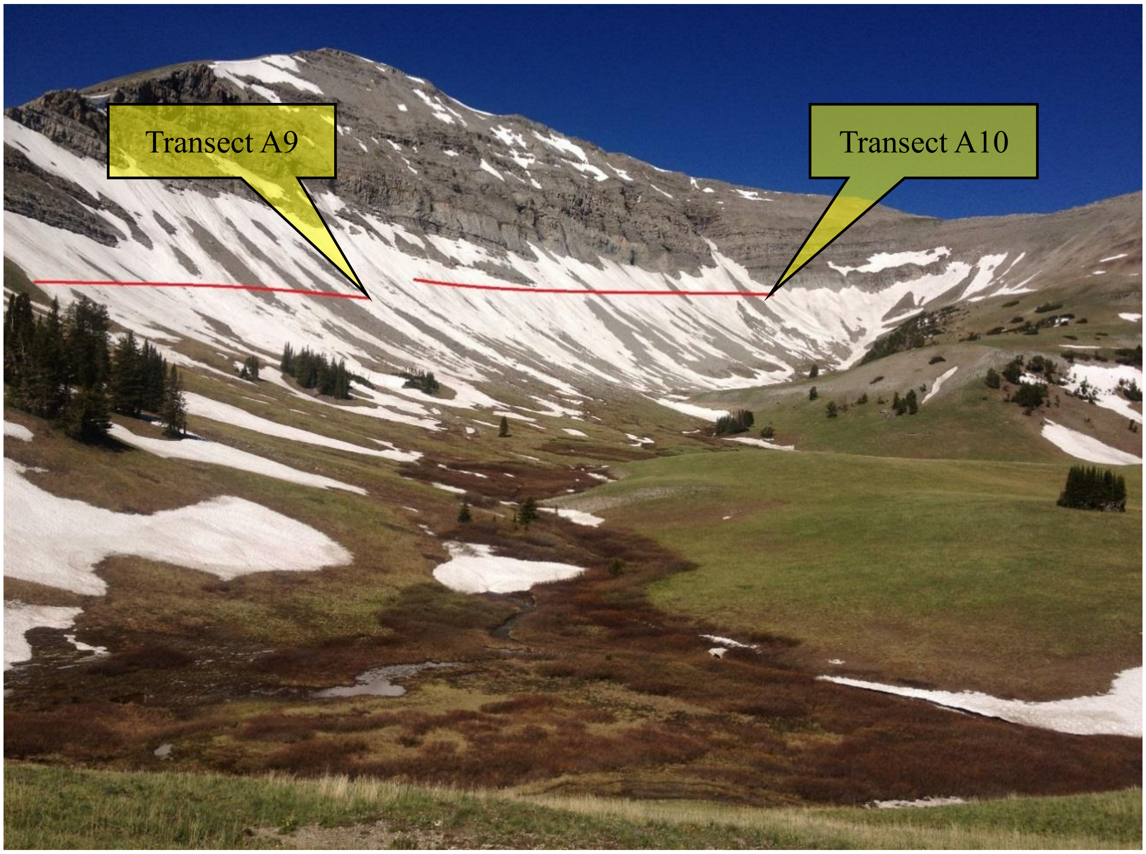

Figure 28. View of Basin A on June 27, 2013 looking west at the headwall (left), northern ridgeline boundary (right), and persistent snowpack on Transects A9 and A10.

substantiate this inference, many wet slides were observed pouring off the headwall during periods of intense solar heating and avalanche debris was photo documented (Figure 29).

For Basin B, the SLR models actually reversed during ablation, compared to the previous sampling periods, to show eastness, slope, and elevation as the most influential. However, it is difficult to ascertain much understanding from variables with R^2 values of only 0.10, 0.06, and 0.04. Similar to the MLR results for the accumulation and peak SWE periods, models with multiple variables showed greater improvement in Basin B than in Basin A for the ablation period (Table 5). MLR results once again showed substantial

Figure 29. View looking southeast at the headwall of Basin A on June 3, 2013 (left) showing multiple point release wet avalanches, and a close-up of one of the debris piles (right) that averaged approximately 1.5 m in depth.

improvement over SLR with the best performing and most parsimonious model combining eastness, slope, and the WEI for an R^2 of 0.17. Despite this low performance, the spatial distribution of SWE predicted by this model did seem to capture the general snowmelt pattern observed in the basin. Eastness coming out as the primary driver during this period can likely be explained once again by the strong influence of anomalously deep and persistent snow deposits, in due east facing transects B11 and B13 (Figure 17), on the regression analysis. As for slope, it seems possible, with a positive coefficient of 7.51, that its direct relationship to SWE is more of a reflection of how the terrain in this basin generally increases in slope with elevation. Hence, towards the latter part of the ablation season, only mid and upper elevation zones maintained snow. It is uncertain why elevation didn't play a role in this top model, but the fact that the next best models integrate elevation is perhaps an indication to this underlying relationship. It is interesting how, despite its lower performance in an SLR model, the WEI once again enhanced the predictive value of the MLR models. However, this seems inherently true since it was the major driver during accumulation and peak SWE, thereby still determining the pattern of SWE during melt out.

The pattern of the declining SWE in Basins A and B during the ablation period was generally captured well by the spatially distributed MLR models (Figure 17). Similar to the peak SWE period, the maximum SWE values for Basin A were nearly twice that for Basin B, likely for the same reasons as explained for the peak SWE period. The models did well in calculating 'no snow' for the broad areas where the snowpack first disappeared, and the deepest SWE values where the snowpack was most persistent. This is especially encouraging given that the models are a single 'snapshot' of the spatial distribution of SWE derived from data that spanned a sampling period of 39 days (June 2 - July 10). A place where the model for Basin B may have been inaccurate is the greater southwest corner of this basin between 3000 and 3200 m. Because of the almost due east aspect of this zone, the emphasis of eastness by this model, that was presumably brought about by anomalously high SWE measurements in transects B11 and B13, caused it to overestimate for the greater area surrounding these transects. In reality, strong prevailing southerly winds allowed only a shallow snowpack to build in this broadly convex area, as observed when travelling through this zone and through measurements in transect B14 (Figure 30). For example, peak SWE measurements in transect B14 had an average SWE of 424 mm compared to 723 mm in transect B13 and 1149 mm in B11 (Appendix A). Furthermore, by the June 27 sampling visit of the ablation period, transect B14 was virtually snow free (Figure 17) while transect B13 had an average SWE of 510 mm and

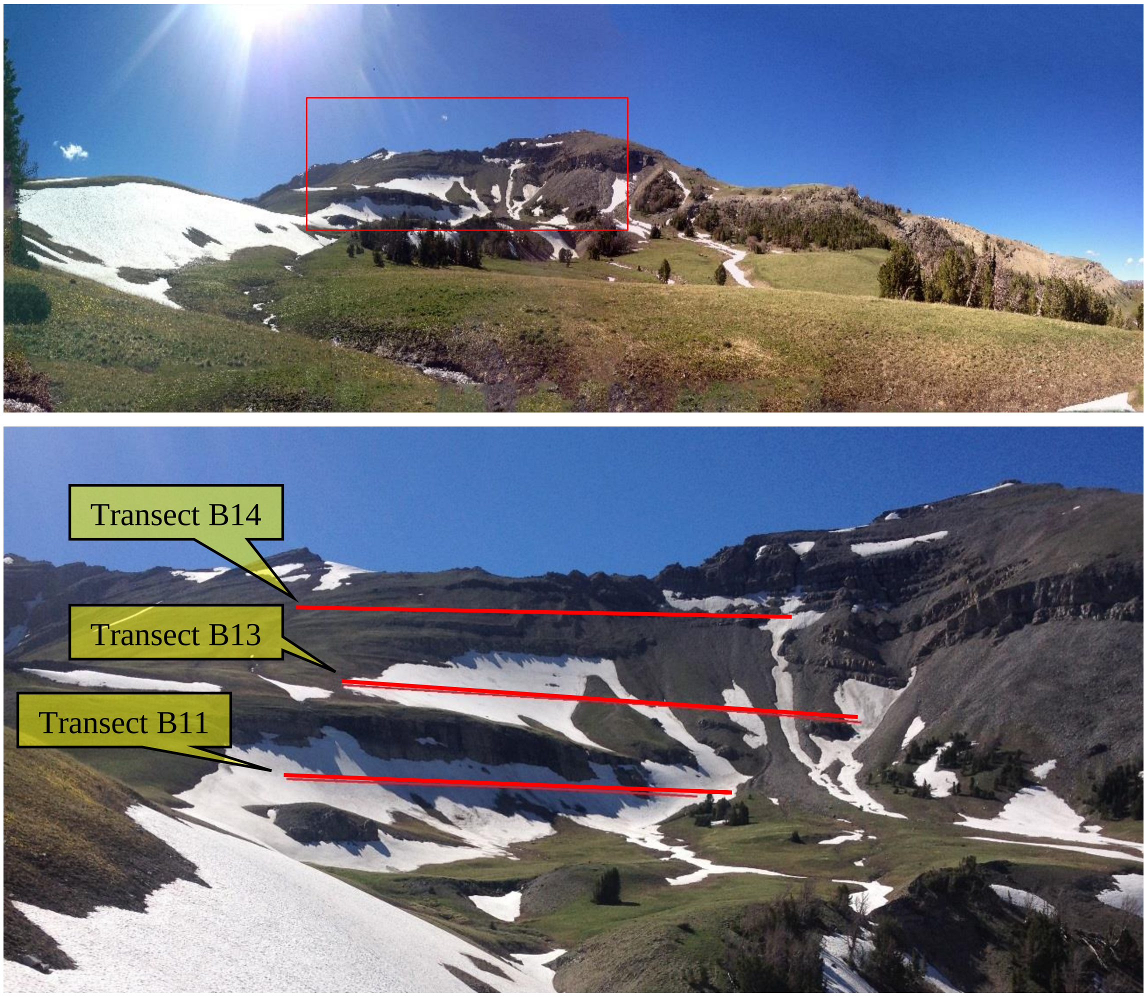

Figure 30. Panoramic view of upper Basin B on June 27, 2013 (upper photo) and a close up (lower; red box in upper photo) showing the persistent snow deposits along transects B11 and B13, and nearly snow-free transect B14.

B11 an average SWE of 514 mm (Appendix A). The eastness variable did not appear to create such an issue with the spatial distribution of SWE in Basin A, likely due to its lower coefficient value than in Basin B (Figure 15).

Overall, the limited predictive power of the independent variables in both basins is perhaps a reflection of a maximum degree of variability in SWE depths during this period, as many transects melted out completely, while a few others (especially A9, A10, B11, and B13) maintained patches of snow with substantial depth into July. Nevertheless, the trends highlighted in the data from the SLR and MLR results do still offer some insight into how the hierarchy of influence on the predictor variables was temporally based. By the ablation period, in Basin B, it stands to reason that WEI is no longer clearly dominant, as wind transport is hampered by the high density of the snow, as well as melt/freeze crusts at this point. It is likely that SLR results in Basin B were heavily influenced by transects B11 and B13 that maintained deep deposits and happen to be due east facing, as well as steep sloped and at mid-high elevation. However, as previously mentioned, the WEI was still most instrumental in predetermining this snowpack pattern throughout the accumulation season.

6.4.2 Binary Regression Tree Modeling

The performance of the optimally pruned BRT model for Basin A declined substantially for the ablation period, while it improved for Basin B. Similar to the accumulation period, this is suspected to be rooted in the inconsistency and lack of representativeness in sampling during ablation. With 298 observations in Basin A and 329 in Basin B, the ablation period was not data limited. This is evidenced by fully grown tree sizes of 21 nodes for Basin A and 23 nodes for Basin, and it shows that maximum tree size throughout the three sampling period was roughly proportional to the number of observations. However, the high degree of heterogeneity within the ablation dataset between snow free areas and those harboring unusually deep snow deposits limited the ability of trees to accurately predict this variability, increasing the probability of misclassification. Thus, optimally pruned trees were limited to 4 nodes in Basin A and 5 nodes in Basin B, which explained 33.3% and 62.3% of the variance in SWE, respectively. It is unclear why model performance for Basin B with only 1 additional node was so much better than for Basin A. In fact, after reaching a plateau near 5 nodes, R^2 only increased from 0.623 to 0.660 for the 23 node tree. A possible explanation is that transect locations in Basin B just happened to be ideal at this point for explaining the distribution of SWE through the tree hierarchy of eastness, solar radiation, elevation, and the WEI. In other words, sampling points either had little or no snow or very deep snow, with few mid-level SWE depths. Thus, the optimal tree could partition this data into fairly homogenous subsets without increasing cross validation relative error (Figure 22). On the other hand, tree size for Basin A showed a steadily increasing R^2 with additional nodes from 0.332 for the optimally pruned 4 node tree to 0.491 for the fully grown 21 node tree. However, this was accompanied by a steep increase in cross validation relative error after the third split. This seems to indicate that the sample points in Basin A displayed a higher degree of heterogeneity between snow free, low, midlevel, and high SWE depths, thereby making it increasingly difficult for trees to partition observations in increasingly homogenous subsets without increasing the probability of misclassification. Due to these potential issues with the sample representativeness of the declining snow pattern, as well as being during a different phase of snowpack development, a direct comparison of the explained variance between BRT models for this and previous studies does not seem appropriate. However, despite these issues, the variance explained by the BRT model for Basin A is still acceptable and the fit for Basin B is actually quite good.

Moving from peak SWE into the ablation period, the BRT model for Basin A made a surprising shift from one based on a root node of solar radiation to one based on the WEI. Furthermore, solar radiation did not factor into the BRT at any point, counterintuitive to the notion that during this period the pattern of snowpack melt is increasingly driven by solar input. The explanation may be the same as that which was offered for the MLR analysis in the ablation period, in that, the WEI was so influential in shaping the distribution of SWE during the accumulation season that this underlying pattern persisted through snowmelt. And as noted by *Anderton et al.* (2004), a more even distribution of solar radiation on all aspects at this time of year actually decreases this variable's influence on melt rates. Hence, the areas of highest SWE (804 mm), once again beneath the northeast headwall (Figure 23), were modeled strictly by the WEI. However, the inclusion of northness as a secondary variable in the tree perhaps functions as a surrogate for solar radiation in modeling the areas with low to midlevel SWE. Thus, the general area of lowest SWE (48 mm) was predicted to be that with greater wind exposure (WEI $\geq$ -4.931) and low northness values (<0.032) indicating an increasing southerly aspect or solar input to compound wind scour. As in the previous sampling periods, this corresponds well to the northern half of the basin, particularly transects A11, A12, and A13. A tertiary split on slope further predicted that terrain with less than a 35.55° slope angle to have less SWE (173 mm) compared to terrain with slopes steeper than this critical angle (modeled with 466 mm of SWE). This is possibly explained by the predominant southerly wind pattern promoting more snow deposition in the lee of steeper rather than gentler northerly slopes, essentially bringing the model back to the root variable. Referring to the map of modeled SWE distribution (Figure 23) this corresponds to 466 mm of SWE being modeled at the top of the northeast headwall where one would intuitively presume there to be heavy wind driven deposition. However, the model does not seem to capture that most of this deposition was likely redistributed, to the band modeled with 804 mm, by continual sloughing due the average slope angle exceeding approximately 50°, which seems to be verified by observation of the snowmelt pattern on June 27 (Figure 12). Consequently, the model seemed to over predict for the top of the headwall at 466 mm of SWE, but appears to be fairly on target for the band of 804 mm according to an average of observations at transect A10 on June 26 (Appendix A), as well as for the zone of 173 mm according an average of transects A4 on June 1 and A6 (points 1-5) on June 27 (Appendix A).

Unlike for the peak SWE BRT rooted with the WEI, the model for the ablation period reverted back to that of the accumulation period with a root node of eastness. A split on this variable alone, with values less than 0.886 (more south to west facing) modeled the lowest SWE at 35 mm, presumably a reflection of maximum wind and solar radiation exposure. This modeled zone contained 78% of the samples (Figure 22) and comprised over 80% of the area of Basin B (Figure 23). While this seems on par with observations for transects B2, B6, B8, B12, and B15, in the northern half of the basin, it clearly missed some of the north facing persistent snowpack in the southeastern third of the basin. Unfortunately, this is likely a result of the sampling distribution for this area, represented by transects B4, B5, B9 and B9a, not accurately capturing the general snow pattern of this zone and B4 and B5 only being sampled on July 10 when they were visually observed with no snow. The dominance of eastness in this basin is once again assumed to be heavily influenced by anomalously deep snow deposits in east facing transects B11 and B13 that still harbored upwards of 1600 mm of SWE by the June 27 sampling visit (Appendix A). Hence, these zones were very accurately modeled by the terminal node of 1606 mm based on an eastness values indicating a nearly due east aspect (greater than 0.886) and low solar input (less than 350,600 W/m^2). While this portion of the model only covered 1.3 % of the basin area, it accounted for 26.2 % of the total volume of SWE indicating the vital importance of these deep deposits on the timing of snowmelt runoff. It is questionable why these zones were not modeled with the WEI as the primary predictor, given the intense windloading observed in this area on the June 14 sampling visit, which presumably occurred during most storms of the season. This may point to how the WEI is limited in capturing micro terrain features such as those along transect B13 where a slight depression in the lee of the broad ridge lead to heavy snow deposition. Instead, the near due eastness of this zone, enhanced by limited solar input, seemed to combine to function as a surrogate for wind deposition. Areas with increased solar radiation were then split between low and high elevation at 2926 m, the low end of which was modeled with a very low SWE of 65 mm. This did however capture the pattern of persistent snow in ephemeral and perennial stream channels that were visually observed but not targeted by sampling. The last split on the WEI provided the largest variance between the terminal nodes of 239 and 1117 mm. Aside from a few anomalies, these zones were once again in the vicinity of transects B11 and B13, adding credence to the question of why the WEI wasn't closer to the root of the tree. It is suspected that if a transect had ended up being placed approximately 20 m downslope of transects B9 and

B9a, the persistent, northeast facing snow deposit seen in the lower left corner of the lower photo in Figure 30 would have been captured and may have tipped the scales towards the dominance of the WEI. Overall, the structure of variables in this model and general dichotomy of SWE values in terminal nodes between low and high seem to realistically capture what was both quantitatively and qualitatively observed in Basin B during the ablation sampling period thus leading to its successful performance.

The range of SWE in Basin A for the BRT was much more similar to the MLR for ablation than in previous periods, but the MLR predicted a substantial amount of snow free area that the BRT did not. However, the zones of low to high SWE were generally similar, and while the greatest discrepancy in estimated total volume of SWE between models was seen here, it was limited to 10.9% (Table 6). Despite the stark contrast in the range and spatial distribution of SWE between MLR and BRT models in Basin B, with the BRT predicting deep deposits around transects B11 and B13 nearly three times that of the MLR, the estimated total volumes of SWE only differed by 6.2% (Table 6).

It is important when modeling the snowpack throughout its evolution to not only consider how the processes influenced by physiographic variables affect the distribution of SWE, but also how the pattern of snow covered area (SCA) affects the energy balance of the snowpack, and hence melt and subsequent streamflow. Early in the ablation season when the snowpack is relatively deep and contiguous in coverage, the magnitude of snowmelt is limited by available energy input rather than SWE and SCA. However, as energy for melt increases through the ablation season, the magnitude of snowmelt becomes increasingly limited by SCA and SWE. The role of SCA becomes progressively important in determining SWE distribution as the snowpack becomes an increasingly heterogeneous pattern of snowfree and snow covered areas. This sets up a positive feedback whereby areas of thin snowcover adjacent to bare ground melt quickly due to advective heat and vapor transfer and enhanced sensible heat input to the snowpack. On the other hand, areas of deep and dense persistent snowcover (i.e. transects A9, A10, B11, and B13) are not affected nearly as much by the enhanced sensible heat of adjacent bare ground. Thus, increasing spatial variability of the snowpack in terms of SCA and SWE leads to early melt-out and runoff input from more homogenously shallow snowpack areas and extended melt and runoff input from deep deposits. This pattern is developing throughout accumulation into peak SWE, but becomes increasingly apparent through ablation, as demonstrated in the study basins.

`

7. CONCLUSIONS

The goal of this study was a comprehensive analysis of the physiographic variables controlling snowpack processes in an alpine environment in order to accurately distribute SWE from point measurements. Previous studies have indicated that correlations of SWE distribution with physiographic variables is very complex and an understanding of these interactions is difficult to develop from a short survey period, such as during the peak SWE snowpack phase, that offers only a small snapshot in time. Hence, this study expanded the investigation of the processes at work through the entire evolution of the snowpack. Since there has also been indications in previous work that the correlations lengths of snow metrics can vary on a number of scales between adjacent basins of similar physiographic character, a paired basin study was employed to parse out these effects. This design also allowed for a comparison of suspected avalanche prone and non avalanche prone basins, as treatment and control groups, to explicitly examine the influence of avlanche activity on the distribution SWE, which has not been completely addressed by previous studies. Finally, a comparison of linear and nonlinear modeling methodologies, both with demonstrated success in different applications of distributing SWE, was conducted to determine which offer more accurate prediction of SWE in the selected scale and environment of the study site.

Field measurement of snow depth and SWE, while employing the same technique, resulted in substantially different samples between the periods of accumulation, peak SWE, and ablation due to weather, safety, and time constraints as well as different considerations on how to gain a representative sample of the evolving snowpack pattern for a given period. This lead to very different models in terms of structure (dominant variables) and performance.

Accumulation:

- Basin A MLR: WEI, Eastness → $R^2 = 0.28$
- Basin A BRT: Solar Radiation, WEI → $R^2 = 0.38$
- Basin B MLR: Eastness, WEI, Northness → $R^2 = 0.32$
- Basin B MLR: Eastness → $R^2 = 0.48$

Peak SWE:

- Basin A MLR: WEI, Slope, Eastness → $R^2 = 0.57$
- Basin A BRT: Solar Radiation, WEI, Slope → $R^2 = 0.66$
- Basin B MLR: WEI, Slope, Eastness, Elevation → $R^2 = 0.33$
- Basin B BRT: WEI, Slope, Eastness, Elevation → $R^2 = 0.53$

Ablation:

- Basin A MLR: WEI, Slope, Eastness → $R^2 = 0.22$
- Basin A BRT: WEI, Northness, Slope → $R^2 = 0.66$
- Basin B MLR: Eastness, Slope, WEI → $R^2 = 0.17$
- Basin B BRT: Eastness, Solar Radiation, Elevation, WEI → $R^2 = 0.62$

The most consistent and representative sample was acquired during the peak SWE period. Sampling during accumulation suffered from limited observations leading to imbalance between basins, while imbalance occurred between in-basin transects during ablation despite having the largest sample size by two fold. These sampling distributions lead to peak SWE models demonstrating the best performance in explaining the most variance in the distribution of SWE. A notable exception is the BRT model for Basin B during ablation, which not only explained an impressive 62% of the variance but very accurately predicted the pattern of melt-out and persistent snow deposits that were observed during field visits. It was clear from snowpack observations, model structures and predicted SWE distributions that the accumulation and peak SWE periods had a profound influence on these elements during ablation. Hence, the pattern of snowpack melt-out was somewhat predetermined, despite a logical shift in dominance of variables controlling this process. Despite the variation between MLR and BRT models with regard to the dominant variables used, the spatial distribution of SWE and relative performance, the estimated total volumes of SWE were very similar between these methodologies (within 1 to 11%). However, the results of this study are consistent with those of previous studies with BRT models offering more accurate prediction of distributed SWE compared with other methodologies when a sufficiently large dataset is available. Nevertheless, MLR as well as BRT models in this study left a substantial amount of the variance unexplained, especially during the accumulation and ablation periods. This can be mainly attributed to sample size and representativeness.

While the sampling strategy and modeling methodologies of this study did not allow for a statistically defensible indication of avalanche activity having a significant effect on the distribution of SWE alongside the other physiographic variables, qualitative evidence of this potential was obvious in correlations between visual observation and modeling distributions for Basin A.

8. LIMITATIONS, IMPROVEMENTS, AND FUTURE WORK

As previously touched upon, the sampling representativeness and scope of this study was very limited by the same issues as experienced in previous studies of this type and environment with regard to: weather, safety, personnel availability, time, and budget. This in turn restricted the accuracy in the modeling prediction of distributed SWE and strength of correlations to the physiographic variables. With a full appraisal of these effects offered by this study, new insight was developed on how this issue could be substantially improved for future work.

The strategy of gaining a representative sample(s) of snow metrics throughout the entire evolution of the seasonal snowpack could be achieved through a well designed plan and effective use of, albeit abundant, resourses. This would ideally involve surveys of the study basins on: January 1, February 15, and March 30 for accumulation; May 1 for peak SWE; and June 1, July 1, and August 1 for ablation. During each visit, all transects/points would be surveyed for a complete dataset for each basin; i.e. accumulation would have three complete datasets, peak SWE one, and ablation three. For proportional consistency in sampling size between basins, sampling point density would be 200 points/km^2 leading to 276 points in 28 transects in Basin A and 326 points in 32 transects in Basin B. In order to achieve the above timeframe for complete surveys, a field crew of eight to sixteen people, two to four groups of two person teams in each basin, is projected to be necessary depending on the difficulty of travel and depth of the snowpack. The sample size of datasets should lead to BRT models justifiably pruned to an optimal size of approximately 10 to 12 terminal nodes given the rough correlation between sample size and tree size. More complex trees, supported by data presumably more closely representative of each basin's physiographic variables, should be effective in explaining the greater majority of variance in SWE throughout snowpack development. MLR modeling could be dropped as it was sufficiently shown in this study to be mainly ineffective in modeling at the scale of the study basins and the nonlinear processes driving SWE distribution in this area.

Returning to basis of this study, the ultimate goal of accurately predicting the distribution of SWE is to correlate this pattern with the subsequent timing and magnitude of snowmelt runoff. This was actually in the original design, but the aforementioned constraints made this fall beyond the scope of the current study. To achieve this, stream gauges (HOBO water level logger model U20: 0 to 9 m depth) were installed at the hydrologic pour point of the outlet stream in each basin (Figure 2) and recorded stage hourly from November 1 to August 21, 2013. Stream velocity was manually measured every two weeks from June 13 to August 21, 2013 with a Marsh-McBirney Model 2000 flowmeter and wading rod along a cross-section (Figure 31) at the water level loggers to generate a rating curve from which to estimate discharge. With a robust sample, as described above, and further work to develop and calibrate models to accurately reflect melt-out patterns at the required scale, it would be feasible to correlate to these analyses with discharge. Thus, it may be then possible parse out which physiographic variables have the overriding influence on predicting the distribution of SWE in each basin when it is most important in contributing to snowmelt runoff. In the big picture, this could lead to more accurate calibration of parameters in spatially distributed snowmelt runoff models.

Figure 31. Photos of each stream discharge measurement site on July 10, 2013, showing the water level loggers in relation to the stream cross section where velocity measurements were taken.

Integrating watershed scale knowledge of the processes driving snowpack evolution in alpine zones is likely to become increasingly important with climate change projections indicating that this is where the vast majority of water will continued to be stored as snow in the future.

REFERENCES CITED

Anderson, B. T., J. P. McNamara, H.-P. Marshall, and A. N. Flores (2014), Insights into the physical processes controlling correlations between snowdistribution and terrain properties, *Water Resour. Res., 50*, 1-19.

Anderton, S. P., S.M. White, and B. Alvera (2004), Evaluation of spatial variability in snow water equivalent for a high mountain catchment, *Hydrol. Processes*, *18*, 435–453.

Balk, B. and K. Elder (2000), Combining binary decision tree and geostatistical methods to estimate snow distribution in a mountain watershed, *Water Resour. Res.*, *36*, 13-26.

Blöschl, G. (1999), Scaling issues in snow hydrology monitoring, *Hydrol. Processes, 13*, 2149-2175.

Breiman, L., J. H. Friedman, R. A. Olshen, and C. J. Stone (1984), *Classification and Regression Trees*, Boca Raton, FL: Chapman and Hall/CRC.

Brown, A.E., L. Zhang, T.A. McMahon, A.W. Western, and R.A. Vertessy (2005), A review of paired catchment studies for determining changes in water yield resulting from alterations in vegetation, *J. Hydrol.*, *310*(1-4), 28-61.

Bryant, A. B., T. H. Painter, J. S. Deems, and S. M. Bender (2013), Impact of dust radiative forcing in snow on accuracy of operational runoff prediction in the Upper Colorado River Basin, *Geophys. Res. Lett.*, *40*, 3945-3949.

Carroll, S. S. and N. Cressie (1996), A comparison of geostatistical methodologies used to estimate snow water equivalent, *Water Resour. Bull.*, *32*, 267–278.

Cayan, D.R. (1996), Interannual climate variability and snowpack in the western United States, *J. of Climate*, *9*, 928-948.

Clark, M.P., J. Hendrikx, A.G. Slater, D. Kavetski, B. Anderson, N.J. Cullen, T. Kerr, E.Ö. Hreinsson, and R.A. Woods (2011), Representing the spatial variability of snow water equivalence and land surface models: a review, *Water Resour. Res.*, *47*, W07539 1-23.

DeWalle, D.R. and A. Rango (2008), *Principles of snow hydrology*, Cambridge, UK: Cambridge University Press.

de Scally, F. A., and J. S. Gardner (1988), The hydrological importance of avalanche snow, Kaghan Valley, Himalaya Mountains, Pakistan, *International Snow Science Workshop, Whistler, B.C., Oct. 11-15, 1988.*

de Scally, F.A. (1996), Avalanche snow melting and summer streamflow differences between high–elevation basins, Cascade Mountains, British Columbia, Canada, *Arctic and Alpine Res.*, *28*(1), 25–34.

Dingman, S.L. (2002). *Physical Hydrology*, Long Grove, IL: Waveland Press, Inc.

Elder, K., J. Dozier, and J. Michaelsen (1991), Snow Accumulation Distribution in an Alpine Watershed, *Water Resour. Res.*, *27*(7), 1541-1552.

Elder, K., J. Michaelsen and J. Dozier (1995), 'Small basin modeling of snow water equivalent using binary regression tree methods' in *Biogeochemistry of Seasonally Snow-Covered Areas*, IAHS-AIHS and IUGG XXI General Assembly, Boulder, Colorado, July, 1995. Internat. Assoc. of Hydrol. Sci., Wallingford, 129-139.

Elder, K., W. Rosenthal, and R.E. Davis. (1998), Estimating the spatial distribution of snow water equivalence in a montane watershed, *Hydrol. Processes*, *12*, 1793 – 1808.

Erickson, T.A., M.W. Williams, and A. Winstral (2005), Persistence of topographic controls on the spatial distribution of snow in rugged mountain terrain, Colorado, United States, *Water Resour. Res.*, *41*, w04014 1-17.

Erxleben, J., K. Elder, and R. Davis (2002), Comparison of spatial interpolation methods for estimating snow distribution in the Colorado Rocky Mountains, *Hydrol. Processes*, *16*, 3627-3649.

Fassnacht, S. R., K. A. Dressler, and R. C. Bales (2003), Snow water equivalent interpolation for the Colorado River Basin from snow telemetry (SNOTEL) data, *Water Resour. Res.*, *39*(8), 1208.

Garen, D.C., G.L. Johnson, and C.L. Hanson (1994), Mean Areal Precipitation for Daily Hydrologic Modeling in Mountainous Regions, *Water Resour. Bull.*, *30*(3), 481-491.

Harshburger, B.J., K.S. Humes, V.P. Walden, T.R. Blandford, B.C. Moore and R.J. Dezzani (2010), Spatial interpolation of snow water equivalency using surface observations and remotely sensed images of snow-covered area, *Hydrol. Processes*, *24*, 1285–1295.

Iveronova, M. I. (1966), The hydrological role of avalanches, in *Proceedings, International Symposium on Scientific Aspects of Snow and Ice Avalanches, Davos, April, 1965*, Internat. Assoc. of Sci. Hydrol. Publication, 69, 73-77.

Jones, H.G., J.W. Pomeroy, D.A. Walker, and R.W. Hoham, (2001), *Snow Ecology: An Interdisciplinary Examination of Snow-Covered Systems*, Cambridge UK: Cambridge University Press.

Kerr, T., M. Clark, J. Hendrikx, and B. Anderson (2013), Snow distribution in a steep mid-latitude alpine catchment, *Adv. Water Resour.*, *55*(0), 17‐24.

Lapen, D.R. and L.W. Martz (1993), The measurement of two simple topographic indices of wind sheltering-exposure from raster digital elevation models. *Comput. Geosci.*, *19*(6): 769–779.

Longley, A.P., M.F. Goodchild, D.J. Maguire, and D.W. Rhind (2011), *Geographic Information Systems and Science*. Hoboken, NJ: John Wiley and Sons, Inc.

Luce, C., D. Tarboton, and K. Cooley (1998), The influence of the spatial distribution of snow on basin-averaged snowmelt, *Hydrol. Processes*, *12*, 1671–1683.

Lundquist, J. D., and D. R. Cayan (2007), Surface temperature patterns in complex terrain: Daily variations and long-term change in the central Sierra Nevada, California, *J. Geophys. Res.*, *112*, 1-15.

Martinec, J. and M. R. de Quervain (1975), The effect of snow displacement by avalanches on snowmelt and runoff, *Proceedings, Snow and Ice Symposium, Moscow, 1971*, Internat. Assoc. of Sci. Hydrol. Publication, 104, 364-377.

Marks, D., J. Dozier, and R. E. Davis (1992), Climate and energy exchange at the snow surface in the Alpine Region of the Sierra Nevada: 1. Meteorological measurements and monitoring, *Water Resour. Res*., *28*(11), 3029–3042.

McClung, D. and P. Schaerer (2006), The Avalanche Handbook. Seattle, WA: The Mountaineers.

Mock, C.J. and K.W. Birkeland (2000), Snow Avalanche Climatology of the Western United States Mountain Ranges, *Bull. Amer. Meteorol. Soc*., *81*, 2367–2392.

Molotch, N.P., M.T. Colee, R.C. Bales, and J. Dozier (2005), Estimating the spatial distribution of snow water equivalent in an alpine basin using binary regression tree models: the impact of digital elevation data and independent variable selection, *Hydrological Processes*, *19*, 1459-1479.

Natural Resource Conservation Service (NRCS) (2013), “Snow Telemetry (SNOTEL) and Snow Course Data and Product”, at http://www.wcc.nrcs.usda.gov/snow/. Site visted April 4, 2013.

Painter, T. H., A. P. Barrett, C. C. Landry, J. C. Neff, M. P. Cassidy, C. R. Lawrence, K. E. McBride, and G. L. Farmer (2007), Impact of disturbed desert soils on duration of mountain snow cover, *Geophys.Res. Lett.*, *34*, 1-6.

Phillips, D.L., J. Dolph and D. Marks (1992), A comparison of geostatistical procedures for spatial analysis of precipitations in mountainous terrain, *Agricul. and Forest Meteorol.*, 58, 119-141.

Shmueli, G (2010), To Explain or to Predict?, *Stat. Sci*., *25*(3), 289-310.

Serreze, M.C., M.P Clark, R.L. Armstrong, D.A. McGinnis, and R.S. Pulwarty (1999), Characteristics of the western United States snowpack from snowpack telemetry (SNOTEL) data, *Water Resour Res.*, *35*, 2145 – 2160.

Sosedov, I. S. and I.V. Seversky (1965), On hydrological role of snow avalanches in the northern slope of the Zailiysky Alatau, *Proceedings, International Symposium on Scientific Aspects of Snow and Ice Avalanches, Davos, April, 1965*, Internat. Assoc. of Sci. Hydrol. Publication, 69, 78-85.

Skoien, J.O. and G. Bloschl (2006), Sampling Scale Effects in Random Fields and Implications of Environmental Monitoring, *Environ. Monit. Assess*., *114*, 521-552.

Therneau, T.M. and E.J. Atkinson (2014), An Introduction to Recursive Partitioning using the RPART Routines, Technical Report, Mayo Foundation, *Section of Statistics*, *61*, 1-62.

United States Geological Survey (USGS) (2013), “NED Spatial Metadata”, http://ned.usgs.gov/downloads.html. Site visited January 16, 2013.

Winstral, A., K. Elder, and R.E. Davis (2002), Spatial snow modeling of wind-redistributed snow using terrain–based parameters, *J. of Hydrometeorol.*, 3:524–538.

Wise, E. K. 2012. Hydroclimatology of the US Intermountain West, *Progresss in Phys. Geog*., 1-22.

Zalikhanov, M. (1975), ‘Hydrological role of avalanches in the Caucasus’ in *Snow and Ice-Symposium, Moscow, 1971*, Internat. Assoc. of Sci. Hydrol. Publication, 104, 390-394.

APPENDICES

APPENDIX A

SNOW SAMPLING DATA

Data Dictionary

Dataset: 10 m DEM
Source: USGS National Elevation Dataset (http://ned.usgs.gov/)
Description: 1/3 arc second (~10 m cell size) raster dataset of elevation used in NAD83 UTM Zone 12N to model all of the following physiographic variables

Accumulation Period: Basin A

GPS_Date	GPS_Time	Northing	Easting	TrnsctID	Pt	SWE	Elev	Slope	Northness	Eastness	Solar	WEI
2/7/2013	10:51:07am	5009651.7	461472.6	A2b	1	283	2783.74	9.15	0.340	-0.941	380309	-2.064
2/7/2013	10:55:28am	5009657.9	461464.1	A2b	2	828	2782.61	5.46	0.488	-0.873	384202	-2.418
2/7/2013	10:59:38am	5009665.2	461457.7	A2b	3	450	2781.62	4.40	0.996	-0.091	379865	-2.193
2/7/2013	11:02:15am	5009672.3	461450.6	A2b	4	856	2781.12	8.90	0.933	0.361	365458	-1.584
2/7/2013	11:05:36am	5009679.6	461443.3	A2b	5	716	2781.51	12.66	0.701	0.713	365255	-1.079
2/7/2013	11:08:44am	5009686.7	461436.3	A2b	6	817	2781.51	12.66	0.701	0.713	365255	-1.079
2/7/2013	11:12:18am	5009695.0	461429.3	A2b	7	325	2781.92	7.88	0.261	0.965	391757	-1.006
2/7/2013	11:22:51am	5009705.5	461425.1	A2b	8	227	2782.98	5.47	-0.193	0.981	406886	-0.146
2/7/2013	11:24:25am	5009714.9	461420.5	A2b	9	342	2782.98	4.59	-0.193	0.981	406886	-0.146
2/7/2013	11:25:51am	5009721.5	461412.9	A2b	10	419	2783.82	5.12	0.137	0.991	398964	-0.104
2/7/2013	12:57:17pm	5009955.0	460514.2	A11a	1	271	3011.85	20.24	-0.684	0.729	467017	2.108
2/7/2013	01:03:09pm	5009950.4	460502.2	A11a	2	70	3016.63	22.25	-0.718	0.696	474692	2.203
2/7/2013	01:04:40pm	5009946.5	460493.2	A11a	3	286	3016.39	26.78	-0.765	0.644	478583	2.322
2/7/2013	01:06:28pm	5009940.0	460484.9	A11a	4	308	3020.98	27.56	-0.812	0.584	486340	2.852
2/7/2013	01:08:00pm	5009933.9	460476.4	A11a	5	225	3019.81	24.28	-0.859	0.512	491403	2.754
2/7/2013	01:09:22pm	5009927.3	460467.4	A11a	6	30	3018.29	24.23	-0.896	0.443	493593	2.530
2/7/2013	01:11:09pm	5009923.0	460459	A11a	7	67	3019.91	24.48	-0.915	0.403	495953	2.437
2/7/2013	01:13:16pm	5009918.3	460448.8	A11a	8	73	3018.04	25.57	-0.886	0.464	488125	2.025
2/7/2013	01:19:03pm	5009915.6	460437.9	A11a	9	283	3021.51	25.15	-0.893	0.451	487108	2.211

2/7/2013	01:26:37pm	5009911.6	460427.2	A11a	10	350	3019.89	13.96	-0.894	0.448	482462	1.971
3/7/2013	12:25:00pm	5009832.1	460639.7	A8	1	536	2942.02	12.75	-0.387	0.922	419844	1.506
3/7/2013	12:28:53pm	5009853.4	460637.9	A8	2	373	2943.13	12.77	-0.182	0.983	410128	0.836
3/7/2013	12:32:31pm	5009879.1	460637.2	A8	3	525	2943.58	13.12	-0.063	0.998	404100	0.229
3/7/2013	12:34:12pm	5009891.9	460637.4	A8	4	264	2943.75	14.00	-0.098	0.995	406385	0.185
3/7/2013	12:36:52pm	5009916.8	460637.3	A8	5	413	2944.45	16.99	-0.195	0.981	414016	0.277
3/7/2013	12:39:01pm	5009932.4	460638.5	A8	6	592	2945.73	20.45	-0.224	0.975	417096	0.615
3/7/2013	12:46:12pm	5009942.3	460639.5	A8	7	332	2946.5	22.44	-0.208	0.978	415930	0.792
3/7/2013	12:48:01pm	5009960.5	460640.7	A8	8	503	2948.09	24.26	-0.188	0.982	413501	1.125
3/7/2013	12:52:06pm	5009982.8	460642.8	A8	9	536	2948.78	25.01	-0.164	0.987	410660	1.068
3/7/2013	12:53:44pm	5010003.8	460646.6	A8	10	518	2946.67	25.52	-0.313	0.950	427164	-0.635
3/7/2013	12:55:27pm	5010028.0	460653.1	A8	11	60	2946.94	25.73	-0.578	0.816	458228	-0.120
3/26/2013	10:02:10am	5009369.2	460950.5	A6a	1	843	2849.96	20.77	0.853	0.522	289443	-1.765
3/26/2013	10:12:51am	5009384.5	460912.4	A6a	2	306	2853.44	20.64	0.835	0.551	292184	-1.784
3/26/2013	10:16:14am	5009400.3	460887	A6a	3	457	2853.84	11.64	0.836	0.548	299025	-2.922
3/26/2013	10:19:37am	5009415.6	460865.8	A6a	4	221	2857.4	20.47	0.675	0.738	302442	-2.626
3/26/2013	10:22:12am	5009450.5	460817	A6a	5	527	2860.96	19.64	0.870	0.492	288559	-2.253
3/26/2013	10:25:00am	5009470.4	460788	A6a	6	618	2861.32	16.49	0.745	0.667	301222	-2.375
3/26/2013	10:35:46am	5009496.3	460753.7	A6a	7	523	2864.75	8.38	0.614	0.789	324120	-2.054
3/26/2013	10:38:09am	5009518.3	460726.8	A6a	8	839	2867.15	6.85	0.785	0.619	315370	-2.458
3/26/2013	10:42:06am	5009540.7	460696.9	A6a	9	752	2868.15	5.51	-0.134	0.991	338567	-1.625
3/26/2013	10:45:42am	5009563.5	460669.1	A6a	10	569	2871.85	5.69	-0.367	0.930	340635	-2.368
3/26/2013	11:30:52am	5009409.6	460636.9	A9a	1	829	2923.34	32.89	0.765	0.644	250674	-3.332
3/26/2013	11:37:01am	5009427.2	460614.1	A9a	2	839	2926.72	31.03	0.721	0.693	250304	-1.978
3/26/2013	11:54:05am	5009444.2	460594.4	A9a	3	580	2928.61	31.34	0.797	0.604	250332	-2.873
3/26/2013	11:56:48am	5009458.6	460574.8	A9a	4	436	2934.51	22.04	0.764	0.645	251401	-3.501
3/26/2013	11:59:14am	5009481.4	460539.6	A9a	5	878	2938.54	31.35	0.886	0.464	230106	-2.061
3/26/2013	12:03:32pm	5009503.2	460509.8	A9a	6	699	2941.44	32.24	0.789	0.615	248334	-4.224
3/26/2013	12:06:42pm	5009525.1	460486.7	A9a	7	710	2943.67	28.08	0.737	0.676	254521	-2.760

3/26/2013	12:08:54pm	5009548.7	460458.9	A9a	8	861	2943.66	26.47	0.769	0.639	254994	-3.962
3/26/2013	12:13:02pm	5009569.7	460434.4	A9a	9	861	2951.13	31.90	0.330	0.944	294219	-2.199
3/26/2013	12:16:29pm	5009592.8	460415.1	A9a	10	664	2957.86	21.74	0.472	0.882	294689	0.114
3/26/2013	12:29:03pm	5009724.4	460327	A11b	1	839	2984.82	28.88	-0.702	0.713	409696	-4.156
3/26/2013	12:31:08pm	5009753.7	460337.9	A11b	2	790	2991.4	43.65	-0.783	0.622	432447	-0.433
3/26/2013	12:34:48pm	5009777.3	460355.1	A11b	3	56	3006.29	30.87	-0.906	0.423	468867	7.524
3/26/2013	12:36:48pm	5009799.1	460380.1	A11b	4	172	3005.22	18.04	-0.911	0.412	474434	8.015
3/26/2013	12:38:39pm	5009824.8	460403.2	A11b	5	292	3006.84	25.94	-0.764	0.645	465653	5.713
3/26/2013	12:40:21pm	5009852.0	460427.8	A11b	6	369	3003.93	26.73	-0.719	0.695	464772	3.438
4/11/2013	09:31:52am	5009389.0	461016.8	A4a	1	726	2834.68	16.15	0.861	0.508	299726	-1.298
4/11/2013	09:36:27am	5009375.2	461046.3	A4a	2	385	2831.66	12.86	0.764	0.645	312423	-1.169
4/11/2013	09:38:49am	5009362.0	461075.3	A4a	3	0	2830.36	10.31	0.868	0.496	296631	-3.451
4/11/2013	09:39:37am	5009345.5	461107	A4a	4	0	2829.55	15.40	0.972	0.234	288917	-2.353
4/11/2013	09:41:20am	5009343.3	461134.4	A4a	5	624	2827.42	16.21	0.967	0.254	287408	-1.711
4/11/2013	09:43:43am	5009340.1	461165.1	A4a	6	682	2823.98	16.00	0.949	0.316	291693	-1.538
4/11/2013	09:48:49am	5009337.6	461194	A4a	7	444	2823.66	16.23	0.941	0.337	285722	-2.064
4/11/2013	09:50:42am	5009336.4	461220.6	A4a	8	0	2821.22	17.71	0.994	0.113	276711	-2.511
4/11/2013	09:52:25am	5009331.4	461248.8	A4a	9	492	2820.26	17.72	0.988	0.153	278317	-2.627
4/11/2013	09:54:14am	5009334.4	461270.4	A4a	10	646	2819.18	20.72	0.989	-0.148	264098	-4.599
4/11/2013	09:56:10am	5009346.5	461307.6	A4a	11	477	2820.73	23.05	0.933	-0.360	270823	-2.466
4/11/2013	10:01:20am	5009357.4	461330.9	A4a	12	759	2815.86	10.82	0.999	0.053	271662	-2.433
4/11/2013	10:03:27am	5009360.4	461349.7	A4a	13	697	2815.25	10.97	0.998	0.064	272500	-3.065
4/11/2013	10:05:29am	5009368.5	461383.1	A4a	14	378	2811.35	11.26	0.996	0.090	271404	-2.578
4/11/2013	10:08:07am	5009369.4	461415	A4a	15	708	2809.94	13.42	0.995	0.095	258580	-3.263
4/11/2013	10:31:58am	5009415.0	461475.7	A3a	1	742	2796.96	16.63	0.971	-0.239	296094	-3.673
4/11/2013	10:33:58am	5009431.0	461448.8	A3a	2	843	2794.67	6.04	0.987	0.159	309554	-3.008
4/11/2013	10:36:22am	5009447.5	461422	A3a	3	557	2791.13	5.42	0.988	0.151	339922	-2.773
4/11/2013	10:39:25am	5009463.6	461392.9	A3a	4	557	2792.65	4.65	-0.927	0.374	380328	-0.436
4/11/2013	10:40:45am	5009459.4	461362.6	A3a	5	631	2793.57	2.75	-0.155	0.988	361518	-2.213

4/11/2013	10:43:25am	5009452.0	461332.5	A3a	6	657	2796.31	7.62	0.931	0.364	333753	-2.205
4/11/2013	10:49:40am	5009442.8	461303.4	A3a	7	872	2798.65	7.55	0.955	0.297	333056	-2.517
4/11/2013	10:52:26am	5009438.3	461274.9	A3a	8	817	2800.05	5.18	0.650	0.760	344322	-2.017
4/11/2013	10:55:06am	5009437.7	461246.3	A3a	9	609	2802.53	5.57	0.818	0.575	342637	-1.402
4/11/2013	10:57:14am	5009439.0	461214.6	A3a	10	653	2805.04	7.18	0.836	0.548	340221	-1.666
4/11/2013	11:19:09am	5009550.9	461049.7	A5a	1	723	2816.7	5.44	-0.555	0.832	390099	-0.528
4/11/2013	11:20:30am	5009580.5	461057.2	A5a	2	759	2817.39	4.06	-0.688	0.725	407053	-0.678
4/11/2013	11:22:45am	5009611.5	461060	A5a	3	345	2819.16	13.28	-0.508	0.861	418406	-0.447
4/11/2013	11:25:25am	5009648.4	461071.3	A5a	4	503	2818.29	6.17	0.349	0.937	384916	-0.516
4/11/2013	11:27:32am	5009682.9	461053.8	A5a	5	532	2817.08	6.28	0.719	0.695	381369	-1.852
4/11/2013	11:29:27am	5009709.8	461034.9	A5a	6	642	2818.01	9.63	0.354	0.935	377923	-3.365
4/11/2013	11:31:19am	5009734.6	461023.2	A5a	7	785	2819.71	15.76	0.261	0.965	373666	-2.751
4/11/2013	11:34:18am	5009769.1	461010.1	A5a	8	734	2820.53	22.05	0.145	0.989	384215	-1.901
4/11/2013	11:35:51am	5009793.5	460995.7	A5a	9	0	2826.68	10.27	0.010	1.000	394941	-0.517
4/11/2013	11:39:09am	5009826.9	460980.5	A5a	10	822	2829.01	8.23	0.211	0.977	387434	-1.541
4/11/2013	12:18:57pm	5010052.6	460749.2	A7a	4	660	2916.64	20.87	-0.369	0.929	429103	1.586
4/11/2013	12:21:06pm	5010032.9	460741.2	A7a	5	341	2916.25	14.28	-0.600	0.800	444504	1.278
4/11/2013	12:22:10pm	5010023.0	460737.9	A7a	6	627	2918.36	14.28	-0.637	0.771	449258	1.376
4/11/2013	12:23:40pm	5009997.6	460730.3	A7a	7	473	2915.88	11.63	-0.255	0.967	416075	-0.473
4/11/2013	12:24:59pm	5009978.5	460726.4	A7a	8	521	2915.7	11.83	-0.119	0.993	408813	-0.334
4/11/2013	12:26:00pm	5009955.0	460725.3	A7a	9	877	2915.8	14.73	0.309	0.951	379642	-0.705
4/11/2013	12:27:26pm	5009942.7	460727.4	A7a	10	767	2916.8	15.52	0.397	0.918	371344	-0.191
4/11/2013	12:59:52pm	5010164.7	460376.2	A13a	1	148	3149.81	33.51	-0.612	0.791	486257	5.142
4/11/2013	01:01:25pm	5010179.7	460380	A13a	2	264	3154.76	30.30	-0.236	0.972	433392	3.902
4/11/2013	01:35:47pm	5009920.1	461297.6	A2a	3	186	2797.57	3.85	-0.267	0.964	408855	0.400
4/11/2013	01:37:06pm	5009873.1	461285.9	A2a	4	278	2796.75	6.47	-0.857	0.515	428678	0.522
4/11/2013	01:38:28pm	5009822.3	461296.2	A2a	5	761	2790.36	9.01	-0.447	0.895	420778	-0.755
4/11/2013	01:40:20pm	5009788.7	461316.1	A2a	6	479	2788.82	11.40	0.888	0.460	356758	-0.919
4/11/2013	01:41:15pm	5009732.6	461358.3	A2a	7	664	2788.47	8.22	0.547	0.837	387320	-0.069

Accumulation Period: Basin B

GPS_Date	GPS_Time	Northing	Easting	TrnsctID	Pt	SWE	Elev	Slope	Northness	Eastness	Solar	WEI
1/31/2013	11:15:14 AM	5008534.6	461802.1	B4a	1	233	2721.88	9.50	0.994	0.109	313589	-0.463
1/31/2013	11:36:50 AM	5008531.2	461817.5	B4a	2	313	2721.63	9.53	0.992	0.124	316166	-0.303
1/31/2013	11:41:23 AM	5008528.6	461833.8	B4a	3	323	2720.03	10.09	0.956	0.293	325165	-0.863
1/31/2013	11:43:44 AM	5008523.9	461850.6	B4a	4	218	2718.90	7.41	0.994	0.110	324811	-1.485
1/31/2013	11:45:55 AM	5008520.1	461866.4	B4a	5	208	2720.94	12.81	1.000	0.031	331761	-1.022
1/31/2013	11:48:44 AM	5008515.2	461882.7	B4a	6	408	2720.92	12.31	1.000	0.014	335013	-0.702
1/31/2013	11:52:41 AM	5008509.4	461900.0	B4a	7	230	2722.41	10.68	0.999	0.045	344848	-0.824
1/31/2013	11:59:52 AM	5008504.5	461916.3	B4a	8	238	2722.35	10.90	0.999	0.048	343916	-0.794
1/31/2013	12:01:55 PM	5008500.9	461931.5	B4a	9	218	2723.64	10.21	0.997	0.083	348178	-0.846
1/31/2013	12:04:35 PM	5008496.5	461946.9	B4a	10	273	2723.33	10.50	0.990	0.139	347111	-0.847
1/31/2013	1:11:06 PM	5008208.3	461008.9	B9a	1	141	2881.94	8.66	0.949	0.316	332244	-0.898
1/31/2013	1:20:30 PM	5008196.7	461021.5	B9a	2	162	2884.10	16.90	0.837	0.547	343867	-0.456
1/31/2013	1:22:18 PM	5008185.6	461031.4	B9a	3	131	2883.16	17.91	0.765	0.644	346428	-0.651
1/31/2013	1:24:02 PM	5008174.2	461042.6	B9a	4	117	2883.38	16.20	0.766	0.643	339959	-0.942
1/31/2013	1:26:36 PM	5008163.0	461054.2	B9a	5	244	2882.28	12.52	0.845	0.534	323702	-1.574
1/31/2013	1:29:23 PM	5008151.5	461064.4	B9a	6	199	2883.50	19.61	0.914	0.407	315220	-1.495
1/31/2013	1:34:19 PM	5008140.1	461075.9	B9a	7	59	2884.17	19.84	0.946	0.324	307641	-1.339
1/31/2013	1:36:19 PM	5008131.0	461088.9	B9a	8	59	2885.17	21.89	0.946	0.323	289740	-1.398
2/19/2013	12:43:49pm	NA	NA	B13a	9	846	3001.84	30.38	0.337	0.942	356213	-1.262
2/19/2013	12:44:49pm	NA	NA	B13a	10	702	3003.15	23.26	0.405	0.914	346478	-1.047
2/19/2013	12:47:10pm	NA	NA	B13a	11	846	3003.64	23.99	0.042	0.999	387067	-3.124
2/19/2013	12:49:01pm	NA	NA	B13a	12	479	3007.24	26.74	-0.692	0.722	472862	-0.123
2/19/2013	12:51:03pm	NA	NA	B13a	13	36	3013.34	23.61	-0.411	0.912	441485	3.908

2/19/2013	01:25:20pm	NA	NA	B10a	1	472	2894.71	9.59	-0.964	0.264	481319	1.873
2/19/2013	01:27:22pm	NA	NA	B10a	2	472	2887.99	9.74	-0.902	0.432	446623	-0.112
2/19/2013	01:28:39pm	NA	NA	B10a	3	846	2886.27	8.08	-0.438	0.899	424486	0.113
2/19/2013	01:30:28pm	5008555.4	460511.4	B10a	4	50	2885.48	11.14	-0.205	0.979	415303	0.531
2/19/2013	01:32:02pm	5008575.1	460503.4	B10a	5	551	2884.65	10.19	-0.246	0.969	417107	0.708
2/19/2013	01:33:47pm	5008595.2	460495.7	B10a	6	313	2883.73	8.87	-0.361	0.933	422104	0.929
2/19/2013	01:35:17pm	5008615.9	460492.9	B10a	7	259	2882.78	10.14	-0.669	0.744	438199	1.288
2/19/2013	01:36:33pm	5008636.9	460495.7	B10a	8	565	2880.14	8.30	-0.790	0.614	448035	0.888
2/19/2013	01:38:15pm	5008712.8	460860.1	B10a	9	191	2878.84	10.61	-0.682	0.731	439837	0.702
2/19/2013	01:39:29pm	5008691.8	460853.8	B10a	9	421	2876.96	8.83	-0.684	0.730	434109	-0.012
2/19/2013	01:40:44pm	5008670.3	460855.5	B10a	10	846	2875.06	8.27	-0.082	0.997	408462	0.623
2/19/2013	01:42:38pm	5008647.9	460856.9	B10a	11	205	2874.76	11.82	-0.253	0.968	418519	1.397
2/19/2013	01:43:59pm	5008626.0	460858.5	B10a	12	65	2871.70	15.14	-0.511	0.860	432037	1.224
2/19/2013	12:36:00pm	5008602.7	460857.1	B13a	8	846	3005.11	29.57	0.452	0.892	340942	-0.629
2/19/2013	12:33:00pm	5008580.0	460853.4	B13a	7	846	3002.12	29.64	0.103	0.995	391097	-0.533
2/19/2013	12:30:00pm	5008559.2	460849.6	B13a	6	846	3000.25	18.23	0.389	0.921	364382	-1.279
2/19/2013	12:27:00pm	5008537.9	460844.9	B13a	5	846	3003.48	19.77	0.426	0.905	359590	0.372
2/19/2013	12:24:00pm	5008515.1	460842.6	B13a	4	684	3003.08	18.17	0.120	0.993	394718	1.986
2/19/2013	12:21:00pm	5008493.5	460847.1	B13a	3	522	3003.26	18.10	-0.086	0.996	414199	2.010
2/19/2013	12:18:00pm	5008470.9	460852.7	B13a	2	648	3001.54	18.45	0.177	0.984	388424	-0.048
2/19/2013	12:15:00pm	5008451.7	460859.3	B13a	1	846	3003.28	16.45	0.130	0.992	397026	1.623
4/4/2013	09:32:43am	5009076.6	460561.6	B15a	1	77	3174.73	18.69	-0.610	0.792	474399	7.756
4/4/2013	09:36:30am	5009058.3	460532.8	B15a	2	141	3174.73	19.67	-0.891	0.454	522691	6.121
4/4/2013	09:37:38am	5009049.5	460519.5	B15a	3	144	3179.64	15.34	-0.906	0.422	523687	3.469
4/4/2013	09:39:51am	5009028.7	460487.0	B15a	4	141	3181.21	30.40	-0.880	0.476	523446	1.897
4/4/2013	09:42:14am	5009014.2	460463.6	B15a	5	141	3178.61	22.43	-0.857	0.515	506441	3.600
4/4/2013	09:44:52am	5008986.9	460439.3	B15a	6	169	3181.98	25.30	-0.719	0.695	496419	2.366
4/4/2013	09:49:24am	5008970.5	460426.7	B15a	7	118	3181.51	24.58	-0.684	0.729	490742	2.227
4/4/2013	09:53:33am	5008961.9	460420.0	B15a	8	118	3179.16	22.07	-0.655	0.756	483306	3.647

4/4/2013	09:56:05am	5008918.7	460391.0	B15a	9	71	3183.69	31.27	-0.502	0.865	469257	2.354
4/4/2013	10:35:35am	5008816.2	461524.4	B6a	1	922	2772.04	24.19	-0.032	0.999	389715	-2.083
4/4/2013	10:37:52am	5008840.5	461535.5	B6a	3	94	2771.09	19.29	-0.984	0.179	475605	-1.326
4/4/2013	10:41:17am	5008840.4	461535.2	B6a	2	778	2771.09	19.29	-0.984	0.179	475605	-1.326
4/4/2013	10:44:32am	5008850.9	461552.7	B6a	4	261	2776.42	9.89	-0.988	0.155	478615	1.615
4/4/2013	10:45:31am	5008854.5	461570.9	B6a	5	340	2775.41	10.04	-0.984	0.178	475674	1.653
4/4/2013	10:47:17am	5008861.1	461586.7	B6a	6	408	2773.82	9.96	-0.979	0.203	476832	1.512
4/4/2013	10:51:35am	5008863.0	461588.4	B6a	7	374	2773.82	9.96	-0.979	0.203	476832	1.512
4/4/2013	10:56:05am	5008875.0	461618.4	B6a	8	378	2775.12	21.31	-0.987	0.164	488175	1.478
4/4/2013	10:57:25am	5008879.3	461630.0	B6a	9	540	2777.01	22.18	-0.992	0.124	492478	1.715
4/4/2013	10:59:03am	5008883.3	461647.9	B6a	10	416	2775.96	23.77	-0.983	0.181	496654	1.786

Peak SWE Period: Basin A

GPS_Date	GPS_Time	Northing	Easting	TrnsctID	Pt	SWE	Elev	Slope	Northness	Eastness	Solar	WEI
4/30/2013	01:18:12pm	5009729.7	460328.9	A11	1	495	2984.82	28.88	-0.702	0.713	409696	-4.156
4/30/2013	01:40:55pm	5009761.5	460343.1	A11	2	728	2994.90	49.86	-0.930	0.367	450931	1.669
4/30/2013	01:47:56pm	5009779.5	460384.9	A11	3	323	2995.11	46.68	-0.931	0.365	474869	5.617
4/30/2013	01:50:55pm	5009798.5	460420.4	A11	4	356	2986.41	24.14	-0.872	0.489	469885	3.167
4/30/2013	01:53:58pm	5009821.1	460453.4	A11	5	285	2985.23	22.23	-0.865	0.502	461838	1.061
4/30/2013	01:56:02pm	5009839.7	460490.9	A11	6	170	2985.22	24.58	-0.945	0.328	481088	2.465
4/30/2013	01:58:40pm	5009859.2	460525.7	A11	7	138	2983.62	18.92	-0.940	0.342	485497	3.328
4/30/2013	02:09:56pm	5009883.7	460557.4	A11	8	72	2982.88	25.56	-0.642	0.766	464209	4.823
4/30/2013	02:19:07pm	5009910.1	460592.1	A11	9	140	2964.33	32.10	-0.378	0.926	432335	1.028
4/30/2013	02:27:28pm	5009947.1	460605.2	A11	10	561	2965.86	28.53	-0.248	0.969	419075	1.255
4/30/2013	02:32:35pm	5009987.0	460613.5	A11	11	740	2965.49	36.66	-0.309	0.951	427475	0.379
4/30/2013	04:26:36pm	5010177.0	460377.2	A13	1	213	3154.76	30.30	-0.236	0.972	433392	3.902
4/30/2013	04:32:13pm	5010142.3	460361.5	A13	2	241	3154.83	45.07	-0.745	0.667	511400	5.760

4/30/2013	04:35:50pm	5010113.6	460331.8	A13	3	43	3150.27	38.81	-0.853	0.521	531851	5.690
4/30/2013	04:41:42pm	5010088.1	460302.5	A13	4	59	3154.46	34.01	-0.868	0.497	529369	5.081
4/30/2013	04:45:18pm	5010068.7	460285.2	A13	5	48	3149.64	23.12	-0.911	0.411	536692	5.825
4/30/2013	04:48:35pm	5010041.8	460255.2	A13	6	196	3143.39	32.29	-0.886	0.463	528456	4.559
4/30/2013	04:50:51pm	5010016.5	460225.2	A13	7	348	3136.80	29.37	-0.859	0.512	525088	4.547
4/30/2013	04:53:29pm	5009988.4	460198.1	A13	8	274	3142.87	28.25	-0.801	0.599	508675	4.886
4/30/2013	05:03:58pm	5009956.0	460176.3	A13	9	61	3135.92	38.31	-0.699	0.715	496923	3.048
4/30/2013	05:06:46pm	5009918.5	460161.2	A13	10	79	3133.87	34.55	-0.545	0.838	471028	2.435
4/30/2013	10:50:10am	5009411.1	460627.3	A9	1	775	2926.41	29.99	0.712	0.702	250836	-3.338
4/30/2013	10:53:35am	5009378.8	460655.9	A9	2	742	2928.08	32.40	0.870	0.494	226854	-3.185
4/30/2013	11:14:03am	5009348.0	460681.6	A9	3	803	2934.46	24.39	0.900	0.437	229316	-2.656
4/30/2013	11:17:06am	5009314.3	460707.5	A9	4	897	2937.69	25.17	0.821	0.570	247379	-2.228
4/30/2013	11:23:01am	5009285.2	460733.9	A9	5	1104	2941.83	29.71	0.929	0.370	220044	-2.418
4/30/2013	11:34:58am	5009257.1	460761.8	A9	6	1292	2948.17	35.30	0.898	0.440	218463	-3.528
4/30/2013	12:11:19pm	5009229.5	460792.6	A9	7	771	2945.11	23.66	0.851	0.525	224378	-3.260
4/30/2013	12:14:18pm	5009201.9	460820.1	A9	8	867	2947.84	33.78	0.858	0.514	216343	-4.529
4/30/2013	12:20:09pm	5009172.5	460850.2	A9	9	590	2955.86	39.47	0.923	0.385	194550	-5.423
5/6/2013	01:02:07pm	5009840.7	461305.0	A4	13	921	2812.31	24.62	0.999	-0.049	253390	-4.456
5/6/2013	01:17:40pm	5009809.3	461326.6	A3	1	843	2793.97	3.95	0.992	-0.127	313823	-4.454
5/6/2013	01:27:42pm	5009778.8	461356.6	A3	2	792	2790.49	1.98	0.747	0.665	358204	-2.153
5/6/2013	01:30:53pm	5009758.8	461362.3	A3	3	671	2792.65	3.38	-0.513	0.858	364364	-1.795
5/6/2013	01:33:34pm	5009721.3	461389.1	A3	4	799	2794.07	5.15	-0.101	0.995	361192	-2.175
5/6/2013	01:36:26pm	5009706.2	461402.3	A3	5	848	2798.32	10.75	0.994	0.112	318341	-2.149
5/6/2013	01:39:43pm	5009667.8	461436.1	A3	6	858	2800.05	5.18	0.650	0.760	344322	-2.017
5/6/2013	01:42:31pm	5009649.4	461450.6	A3	7	874	2803.60	5.67	0.814	0.581	342678	-1.423
5/6/2013	01:54:22pm	5009617.9	461469.4	A3	8	1023	2805.01	3.42	-0.115	0.993	361903	-1.739
5/6/2013	02:01:40pm	5009581.9	461473.8	A3	9	815	2808.20	6.13	-0.958	0.286	384746	-1.552
5/6/2013	02:02:25pm	5009431.0	461463.7	A3	10	510	2809.21	1.70	-0.882	0.471	380460	-1.277
5/6/2013	02:12:00pm	5009453.9	461427.4	A5	1	225	2820.58	15.52	-0.627	0.779	421947	-0.277

5/6/2013	02:31:12pm	5009459.5	461387.3	A5	2	486	2821.37	23.29	-0.544	0.839	427137	0.520
5/6/2013	02:42:37pm	5009454.6	461348.4	A5	3	609	2823.36	25.22	0.425	0.905	356293	0.344
5/6/2013	02:48:57pm	5009441.8	461318.5	A5	4	1289	2824.68	22.25	0.597	0.802	326407	-2.350
5/6/2013	02:53:11pm	5009439.9	461276.0	A5	5	877	2826.38	31.33	0.370	0.929	348149	-1.461
5/6/2013	02:56:13pm	5009442.5	461234.4	A5	6	794	2827.50	27.02	0.391	0.921	355659	-1.075
5/6/2013	03:05:06pm	5009444.3	461201.1	A5	7	1137	2827.48	13.01	0.232	0.973	380437	-0.896
5/6/2013	03:13:31pm	5009461.1	461168.5	A5	8	904	2829.16	9.23	0.193	0.981	385753	-1.893
5/6/2013	03:16:19pm	5009487.9	461143.1	A5	9	248	2827.27	4.79	-0.564	0.826	409125	-0.528
5/6/2013	03:19:00pm	5009365.5	461043.2	A5	10	423	2831.10	13.79	-0.963	0.271	450995	-0.141
5/6/2013	03:28:30pm	5009344.1	461090.7	A2	1	297	2791.29	8.60	-0.952	0.307	437745	0.137
5/6/2013	03:32:14pm	5009334.3	461125.9	A2	2	983	2785.56	6.42	-0.635	0.773	422120	-2.066
5/6/2013	03:38:49pm	5009329.5	461163.7	A2	3	841	2785.65	8.74	0.814	0.581	374801	-0.534
5/6/2013	03:39:57pm	5009328.4	461201.7	A2	4	810	2786.48	7.93	0.735	0.678	378022	-0.380
5/6/2013	03:42:30pm	5009323.3	461239.6	A2	5	647	2787.13	5.58	0.529	0.849	387040	0.036
5/6/2013	03:45:19pm	5009334.2	461293.7	A2	6	583	2784.68	8.47	0.354	0.935	392905	-0.035
5/6/2013	03:47:43pm	5009355.3	461332.3	A2	7	565	2783.38	8.31	0.724	0.690	378980	-0.281
5/6/2013	03:50:24pm	5009359.5	461368.7	A2	8	244	2782.65	6.32	0.659	0.752	385509	-1.483
5/6/2013	03:59:09pm	5009361.8	461388.7	A2	9	291	2784.03	8.90	0.411	-0.911	378043	-2.760
5/6/2013	04:01:42pm	5009362.0	461413.0	A2	10	719	2786.96	13.39	-0.150	-0.989	396826	-2.848
5/6/2013	12:01:57pm	5009356.5	461473.1	A4	1	493	2833.06	13.94	0.735	0.678	308269	-1.726
5/6/2013	12:07:48pm	5009352.8	461519.9	A4	2	883	2830.55	16.61	0.977	0.211	283978	-2.962
5/6/2013	12:10:33pm	5009561.7	461034.2	A4	3	740	2830.45	17.40	0.975	0.223	283591	-1.978
5/6/2013	12:13:04pm	5009567.6	461036.4	A4	4	617	2830.28	17.71	0.949	0.316	283684	-1.873
5/6/2013	12:15:44pm	5009640.1	461050.7	A4	5	346	2825.44	17.12	0.968	0.253	281082	-2.389
5/6/2013	12:30:26pm	5009677.0	461033.5	A4	6	748	2823.41	18.69	0.996	0.093	271219	-2.752
5/6/2013	12:38:29pm	5009710.4	461016.5	A4	7	1059	2821.18	23.60	0.938	-0.348	262398	-3.896
5/6/2013	12:40:59pm	5009744.6	461006.0	A4	8	729	2819.17	22.07	0.999	0.045	264127	-2.644
5/6/2013	12:43:31pm	5009780.4	460994.0	A4	9	875	2814.84	13.53	0.999	0.052	272608	-3.111
5/6/2013	12:46:01pm	5009817.5	460981.9	A4	10	578	2814.67	21.58	1.000	0.028	266797	-2.928

5/6/2013	12:49:12pm	5009850.9	460991.7	A4	11	653	2814.03	25.28	0.998	0.065	251826	-2.935
5/6/2013	12:56:47pm	5009887.3	460986.6	A4	12	890	2814.87	25.69	0.985	0.174	253647	-3.803
5/7/2013	10:40:00am	5010106.8	460521.2	A8	1	431	2942.02	12.75	-0.387	0.922	419844	1.506
5/7/2013	10:44:04am	5010093.9	460510.7	A8	2	522	2943.13	12.77	-0.182	0.983	410128	0.836
5/7/2013	10:47:42am	5010077.2	460499.7	A8	3	528	2943.58	13.12	-0.063	0.998	404100	0.229
5/7/2013	10:50:53am	5010063.0	460490.3	A8	4	283	2943.99	15.31	-0.152	0.988	410360	0.167
5/7/2013	10:51:51am	5010046.1	460472.0	A8	5	381	2944.45	16.99	-0.195	0.981	414016	0.277
5/7/2013	10:53:00am	5010030.7	460461.0	A8	6	676	2942.96	21.28	-0.126	0.992	407983	0.253
5/7/2013	10:54:19am	5010021.1	460442.5	A8	7	454	2944.09	23.59	-0.161	0.987	410546	0.449
5/7/2013	10:55:24am	5010009.5	460425.6	A8	8	655	2944.70	24.54	-0.149	0.989	408886	0.463
5/7/2013	10:59:30am	5009990.6	460413.1	A8	9	537	2945.84	25.12	-0.158	0.987	409294	-0.174
5/7/2013	11:01:05am	5009984.5	460386.7	A8	10	433	2946.94	29.51	-0.578	0.816	458228	-0.120
5/7/2013	11:33:39am	5009975.5	460371.0	A12	1	60	3049.36	20.47	-0.337	0.942	439828	3.783
5/7/2013	11:35:52am	5009965.4	460355.2	A12	2	88	3051.91	28.93	-0.645	0.764	481276	3.769
5/7/2013	11:39:17am	5009955.6	460338.2	A12	3	93	3052.12	28.94	-0.705	0.710	491647	3.402
5/7/2013	11:40:50am	5009944.0	460321.6	A12	4	410	3051.89	37.47	-0.726	0.688	494663	2.906
5/7/2013	11:41:58am	5009933.2	460305.1	A12	5	135	3056.13	27.24	-0.684	0.730	484515	3.566
5/7/2013	11:43:30am	5009919.9	460289.3	A12	6	594	3053.11	25.89	-0.696	0.718	483588	4.146
5/7/2013	11:45:14am	5009832.1	460639.7	A12	7	0	3060.16	24.75	-0.824	0.566	499372	3.421
5/7/2013	11:47:24am	5009859.9	460638.4	A12	8	178	3062.67	19.29	-0.832	0.555	502117	3.522
5/7/2013	11:50:43am	5009883.3	460640.5	A12	9	229	3054.88	30.05	-0.929	0.370	518777	3.731
5/7/2013	11:53:20am	5009936.2	460637.6	A12	10	475	3063.40	32.20	-0.894	0.447	518811	4.260
5/7/2013	11:58:29am	5009921.1	460642.4	A12	11	267	3063.38	33.49	-0.908	0.420	522136	4.544
5/7/2013	12:01:38pm	5009941.4	460642.9	A12	12	235	3061.14	29.81	-0.869	0.495	514896	4.435
5/7/2013	12:02:21pm	5009961.2	460644.4	A12	13	294	3064.15	24.48	-0.850	0.527	511494	4.590
5/7/2013	12:03:10pm	5009979.8	460645.5	A12	14	203	3065.52	33.63	-0.839	0.544	509718	4.806
5/7/2013	12:04:01pm	5010000.1	460649.7	A12	15	527	3070.70	39.57	-0.820	0.573	508159	4.702
5/7/2013	12:05:07pm	5010021.4	460656.6	A12	16	245	3068.45	38.11	-0.748	0.663	496736	4.689
5/9/2013	08:35:23am	5009864.0	461517.1	A10	1	1852	2965.41	39.87	0.737	0.675	218273	-5.398

5/9/2013	08:44:18am	5009841.2	461511.5	A10	2	1213	2966.04	35.92	0.772	0.635	227262	-1.263
5/9/2013	08:50:10am	5009828.5	461517.6	A10	3	736	2972.68	35.27	0.891	0.454	211291	-2.638
5/9/2013	08:51:04am	5009811.0	461520.6	A10	4	1298	2979.24	36.20	0.825	0.565	215795	-4.717
5/9/2013	09:02:15am	5009799.0	461526.4	A10	5	1260	2986.19	39.12	0.821	0.571	200816	-4.799
5/9/2013	09:08:34am	5009780.1	461524.9	A10	6	1152	2980.31	36.61	0.794	0.608	218475	-4.511
5/9/2013	09:19:10am	5009764.2	461526.7	A10	7	1223	2983.92	41.66	0.814	0.581	202321	-4.950
5/9/2013	09:30:37am	5009776.4	461539.8	A10	8	1527	2993.16	49.38	0.627	0.779	226499	-5.128
5/9/2013	09:47:01am	5009790.0	461548.5	A10	9	1076	2994.22	37.86	0.433	0.901	261822	-2.133
5/9/2013	09:50:39am	5009811.4	461549.6	A10	10	803	2997.07	46.82	0.498	0.867	261448	0.286
5/9/2013	09:54:35am	5009370.5	460590.4	A10	11	790	3005.44	35.69	0.620	0.785	258391	-0.708
5/9/2013	09:58:44am	5009397.4	460558.1	A10	12	1516	3006.74	43.56	0.137	0.991	325902	0.859
5/9/2013	12:05:36pm	5009417.9	460527.1	A1	2	649	2756.41	16.81	0.439	0.898	351175	-3.752
5/9/2013	12:09:32pm	5009434.8	460503.3	A1	3	738	2757.06	18.43	0.728	0.685	299767	-3.409
5/9/2013	12:11:28pm	5009458.3	460468.0	A1	4	760	2759.70	25.61	0.663	0.748	299859	-2.285
5/9/2013	12:20:37pm	5009481.4	460441.5	A1	5	464	2760.94	22.25	0.485	0.875	332509	-3.633
5/9/2013	12:22:27pm	5009516.6	460399.9	A1	6	517	2762.83	17.21	0.288	0.958	369695	-4.024
5/9/2013	12:27:18pm	5009538.0	460377.3	A1	7	587	2763.47	8.65	0.734	0.679	364313	-4.912
5/9/2013	12:32:26pm	5009570.3	460360.8	A1	8	823	2764.48	16.38	0.733	-0.681	330705	-4.339
5/9/2013	12:35:45pm	5009597.3	460342.4	A1	9	290	2765.10	16.85	0.412	-0.911	355004	-3.229
5/9/2013	12:38:53pm	5009627.2	460319.6	A1	10	481	2763.41	22.73	0.016	-1.000	375653	-1.039
5/9/2013	12:41:53pm	5009662.6	460298.5	A1	1	653	2758.59	25.74	-0.337	0.942	420422	2.107
5/10/2013	09:45:05am	5009451.7	460731.9	A6	1	724	2877.60	23.07	0.871	0.492	273818	-2.245
5/10/2013	09:56:06am	5009482.0	460701.4	A6	2	653	2876.90	18.83	0.844	0.537	279020	-2.617
5/10/2013	09:58:23am	5009513.4	460667.7	A6	3	501	2879.49	19.61	0.805	0.594	260923	-2.993
5/10/2013	10:01:18am	5009555.3	460643.9	A6	4	776	2874.82	23.47	0.204	0.979	326411	-3.617
5/10/2013	10:04:54am	5009601.9	460647.9	A6	5	451	2880.42	16.74	-0.920	0.393	383822	-0.419
5/10/2013	10:07:55am	5009625.6	460683.8	A6	6	604	2881.89	11.84	-0.993	0.119	419164	0.809
5/10/2013	10:10:40am	5009620.9	460731.7	A6	7	333	2879.94	20.85	-0.999	-0.035	428769	0.092
5/10/2013	10:13:24am	5009613.9	460774.2	A6	8	280	2879.10	17.87	-0.963	-0.268	416988	0.348

5/10/2013	10:16:54am	5009604.2	460818.4	A6	9	237	2877.90	16.05	-0.999	0.042	428803	0.874
5/10/2013	10:19:52am	5009597.8	460867.7	A6	10	51	2875.65	17.05	-1.000	-0.020	436773	1.933
5/10/2013	10:23:09am	5009598.7	460907.2	A6	11	0	2873.24	32.16	-0.962	0.273	478369	4.931
5/10/2013	11:03:02am	5009726.9	460687.4	A7	1	285	2914.34	16.45	-0.966	0.259	441576	1.428
5/10/2013	11:05:19am	5009748.1	460733.8	A7	2	89	2916.64	6.11	-0.966	0.257	434097	2.759
5/10/2013	11:20:10am	5009774.7	460760.7	A7	3	0	2912.94	13.47	0.250	0.968	383787	1.467
5/10/2013	11:31:14am	5009813.8	460752.2	A7	4	0	2913.68	24.48	0.300	0.954	371441	1.533
5/10/2013	11:34:03am	5009850.7	460747.3	A7	5	620	2909.66	30.58	0.145	0.989	378756	0.528
5/10/2013	11:37:50am	5009888.1	460742.0	A7	6	924	2915.90	30.75	0.122	0.992	385539	2.145
5/10/2013	11:41:03am	5009931.3	460734.0	A7	7	639	2915.47	16.47	0.304	0.953	376532	0.438
5/10/2013	11:55:06am	5009968.1	460727.5	A7	8	525	2915.34	12.89	0.091	0.996	395908	-0.807
5/10/2013	11:57:52am	5010006.0	460734.0	A7	9	870	2915.01	12.93	-0.592	0.806	436284	0.061
5/10/2013	11:58:57am	5010021.2	460739.2	A7	10	585	2916.25	13.70	-0.600	0.800	444504	1.278

Peak SWE Period: Basin B

GPS_Date	GPS_Time	Northing	Easting	TrnsctID	Pt	SWE	Elev	Slope	Northness	Eastness	Solar	WEI
4/30/2013	10:00:08am	5008649.8	460829.4	B10	1	464	2890.36	14.47	-0.200	0.980	414266	0.983
4/30/2013	10:03:38am	5008619.4	460830.6	B10	2	421	2888.7	15.09	-0.204	0.979	415040	0.981
4/30/2013	10:17:42am	5008580.4	460822.4	B10	3	375	2886.49	14.79	-0.719	0.695	446014	1.186
4/30/2013	10:25:02am	5008544.9	460821.7	B10	4	444	2882.83	12.93	-0.643	0.765	440160	0.900
4/30/2013	10:28:00am	5008515.7	460821.8	B10	5	425	2878.86	14.34	-0.684	0.730	438335	-0.805
4/30/2013	10:32:20am	5008483.9	460818.8	B10	6	250	2879.59	11.53	0.326	0.945	391407	1.386
4/30/2013	10:36:33am	5008455.7	460815.0	B10	7	352	2880.22	14.63	-0.329	0.944	420011	0.609
4/30/2013	10:47:05am	5008429.7	460810.9	B10	8	290	2878.85	15.01	-0.474	0.880	428057	0.008
4/30/2013	10:49:25am	5008400.5	460806.7	B10	9	429	2879.5	13.26	0.124	0.992	391584	-1.709
4/30/2013	02:20:45pm	5008623.4	460640.6	B11	1	735	2932.35	23.88	-0.636	0.772	448917	0.126
4/30/2013	02:24:17pm	5008602.7	460635.5	B11	2	1526	2931.17	26.95	-0.240	0.971	410274	-3.538

4/30/2013	02:25:48pm	5008581.2	460637.1	B11	3	1039	2926.81	30.64	0.123	0.992	370367	-3.877
4/30/2013	02:31:08pm	5008556.4	460641.7	B11	4	1097	2930.35	35.30	0.127	0.992	369127	-0.809
4/30/2013	02:42:30pm	5008534.9	460644.7	B11	5	1022	2923.2	33.67	0.106	0.994	375612	-0.294
4/30/2013	02:44:59pm	5008513.6	460646.3	B11	6	1048	2923.77	34.28	0.031	1.000	382984	-0.288
4/30/2013	02:50:14pm	5008491.9	460652.7	B11	7	1072	2924.12	35.00	0.086	0.996	374063	-1.454
4/30/2013	02:54:02pm	5008470.9	460655.9	B11	8	1159	2920.81	22.58	0.110	0.994	373361	-1.542
4/30/2013	02:56:49pm	5008450.2	460659.8	B11	9	996	2922.04	24.02	0.262	0.965	353447	-2.955
4/30/2013	02:59:26pm	5008430.3	460666.2	B11	10	1344	2921.79	22.07	0.526	0.851	322037	-3.038
4/30/2013	03:08:08pm	5008411.5	460674.0	B11	11	1499	2923.15	25.15	0.620	0.785	309424	-2.709
4/30/2013	10:14:40am	5008803.2	460617.5	B13	1	869	2994.07	36.35	-0.982	0.191	533258	3.106
4/30/2013	10:24:29am	5008787.8	460584.8	B13	2	696	2989.08	29.39	-0.758	0.653	489003	-1.197
4/30/2013	10:28:19am	5008760.2	460561.3	B13	3	285	2999.67	38.06	-0.824	0.567	506085	3.508
4/30/2013	10:32:54am	5008729.2	460542.6	B13	4	1118	2998.89	26.68	-0.102	0.995	401304	1.712
4/30/2013	10:35:09am	5008691.7	460529.5	B13	5	85	3000.61	34.37	-0.659	0.752	475181	3.073
4/30/2013	10:39:45am	5008658.1	460514.5	B13	6	549	2998.47	31.41	0.148	0.989	379704	1.745
4/30/2013	10:44:55am	5008618.7	460501.6	B13	7	243	3004.17	26.76	-0.717	0.697	476517	0.443
4/30/2013	10:58:00am	5008618.7	460501.6	B13	8	1354	2998.07	32.42	0.314	0.949	357003	-1.995
4/30/2013	11:12:04am	5008541.3	460510.0	B13	9	1568	3005.11	29.51	0.452	0.892	340942	-0.629
4/30/2013	11:15:16am	5008501.6	460522.1	B13	10	1098	3002.4	30.77	0.189	0.982	380235	-1.225
4/30/2013	11:58:47am	5008473.0	460326.3	B14	1	232	3103.89	23.49	-0.508	0.861	463618	2.152
4/30/2013	12:07:14pm	5008509.4	460335.0	B14	2	155	3106.34	31.68	-0.516	0.856	465892	1.991
4/30/2013	12:07:57pm	5008542.9	460340.3	B14	3	139	3105.81	33.06	-0.525	0.851	468239	2.757
4/30/2013	12:13:48pm	5008579.9	460344.1	B14	4	453	3110.9	38.40	-0.178	0.984	421347	1.292
4/30/2013	12:18:16pm	5008614.7	460346.2	B14	5	77	3112.19	40.86	-0.009	1.000	394256	0.360
4/30/2013	12:22:46pm	5008652.7	460344.1	B14	6	66	3112.53	44.54	-0.036	0.999	392603	-0.125
4/30/2013	12:27:02pm	5008682.2	460343.4	B14	7	79	3113.79	46.35	-0.137	0.991	406624	-0.223
4/30/2013	12:32:00pm	5008716.1	460348.6	B14	8	75	3111.55	47.61	-0.255	0.967	422508	0.409
4/30/2013	01:04:26pm	5008752.7	460355.0	B14	9	378	3118.9	46.24	-0.359	0.933	437957	0.543
4/30/2013	01:09:24pm	5008779.0	460366.1	B14	10	799	3113.24	36.86	-0.529	0.848	466242	0.803

4/30/2013	01:25:48pm	5008810.3	460381.7	B14	11	1115	3125.33	30.90	-0.761	0.649	507896	0.242
4/30/2013	01:31:49pm	5008871.9	460445.8	B14	12	987	3117.46	43.26	-0.812	0.584	519241	0.957
4/30/2013	01:38:24pm	5008872.0	460445.7	B14	13	609	3115.07	34.05	-0.761	0.649	511247	4.469
4/30/2013	04:34:04pm	5008528.7	461810.5	B4	1	581	2721.88	9.50	0.994	0.109	313589	-0.463
4/30/2013	04:33:21pm	5008530.7	461825.5	B4	2	493	2721.34	10.19	0.986	0.168	319124	-0.211
4/30/2013	04:32:33pm	5008532.7	461842.3	B4	3	592	2719.29	7.97	0.976	0.217	325718	-1.330
4/30/2013	04:31:12pm	5008534.3	461856.0	B4	4	377	2718.78	7.04	0.999	0.047	323846	-1.406
4/30/2013	04:30:23pm	5008537.6	461871.0	B4	5	473	2716.54	14.11	1.000	0.013	323624	-1.408
4/30/2013	04:29:26pm	5008540.6	461886.0	B4	6	751	2716.56	14.24	1.000	-0.001	323001	-1.227
4/30/2013	04:28:43pm	5008542.1	461900.4	B4	7	428	2716.54	14.06	1.000	0.022	324416	-1.143
4/30/2013	04:27:54pm	5008543.6	461913.5	B4	8	416	2716.47	13.80	0.999	0.032	326280	-1.133
4/30/2013	04:27:00pm	5008545.6	461929.1	B4	9	507	2716.14	13.60	0.996	0.085	327961	-1.046
4/30/2013	04:26:03pm	5008546.9	461944.8	B4	10	462	2713.59	13.29	0.991	0.134	330093	-1.034
4/30/2013	04:25:02pm	5008548.2	461959.9	B4	11	509	2712.47	14.27	0.978	0.209	326869	-0.998
4/30/2013	04:20:00pm	5008547.9	461973.5	B4	12	509	2711.66	14.35	0.985	0.171	324631	-0.884
4/30/2013	02:20:50pm	5008323.8	461660.3	B5	1	627	2767.43	11.01	0.879	-0.477	336051	-4.157
4/30/2013	02:24:25pm	5008335.7	461631.0	B5	2	834	2763.88	16.43	0.973	-0.231	301117	-3.379
4/30/2013	02:27:34pm	5008339.3	461602.5	B5	3	727	2759.44	10.73	0.999	0.041	290468	-3.770
4/30/2013	02:36:01pm	5008342.3	461581.0	B5	4	640	2759.88	10.40	0.992	0.126	289278	-3.578
4/30/2013	02:39:06pm	5008347.0	461558.2	B5	5	675	2762.84	12.06	0.928	0.373	301412	-2.530
4/30/2013	02:42:09pm	5008353.8	461530.4	B5	6	722	2765.63	8.00	0.866	0.499	322043	-2.418
4/30/2013	02:46:54pm	5008360.3	461506.6	B5	7	686	2767.61	10.04	0.849	0.528	335069	-2.882
4/30/2013	02:54:03pm	5008367.9	461486.1	B5	8	627	2767.73	8.53	0.878	0.478	346228	-2.589
4/30/2013	02:57:20pm	5008371.1	461465.5	B5	9	610	2769.8	14.56	0.930	0.369	321806	-3.325
4/30/2013	03:00:15pm	5008375.5	461446.5	B5	10	653	2769.49	12.76	0.909	0.416	332009	-3.042
4/30/2013	11:16:16am	5008273.1	460967.9	B9	1	572	2875.38	11.07	0.893	0.450	325189	-0.640
4/30/2013	11:27:09am	5008262.8	460981.4	B9	2	394	2874.25	12.81	0.905	0.425	323088	-0.767
4/30/2013	11:29:29am	5008255.0	460993.3	B9	3	110	2873.46	16.18	0.923	0.386	325471	-1.048
4/30/2013	11:31:36am	5008247.2	461003.2	B9	4	148	2874.88	16.38	0.946	0.324	322387	-1.136

4/30/2013	11:33:24am	5008238.8	461013.5	B9	5	129	2876.66	16.82	0.957	0.291	319089	-0.740
4/30/2013	11:35:13am	5008230.5	461023.8	B9	6	167	2878.3	17.79	0.911	0.413	329647	-0.258
4/30/2013	11:40:42am	5008220.8	461034.6	B9	7	241	2877.8	14.65	0.820	0.573	336423	-0.233
4/30/2013	11:43:30am	5008211.1	461044.5	B9	8	277	2876.28	12.38	0.784	0.621	336033	-0.270
4/30/2013	11:49:05am	5008199.1	461057.1	B9	9	248	2874.59	17.00	0.698	0.716	341128	-0.713
4/30/2013	11:54:58am	5008188.1	461068.6	B9	10	347	2876.44	20.14	0.760	0.649	338272	-1.550
5/5/2013	04:59:49pm	5008896.1	462188.4	B2	1	363	2703.57	9.96	-0.972	0.236	446644	0.801
5/5/2013	05:02:00pm	5008887.1	462172.0	B2	2	413	2702.98	9.79	-0.938	0.345	442776	0.810
5/5/2013	05:03:57pm	5008875.1	462159.4	B2	3	714	2702.82	8.40	-0.876	0.483	439398	0.861
5/5/2013	05:05:59pm	5008863.2	462146.4	B2	4	295	2703.05	11.55	-0.873	0.487	441526	1.172
5/5/2013	05:07:35pm	5008852.8	462129.5	B2	5	359	2703.04	11.18	-0.905	0.426	446361	1.224
5/5/2013	05:10:46pm	5008843.1	462111.9	B2	6	345	2703	12.53	-0.898	0.440	446168	1.227
5/5/2013	05:12:20pm	5008835.6	462096.3	B2	7	271	2703.87	11.76	-0.884	0.467	447233	1.287
5/5/2013	05:14:07pm	5008824.5	462081.0	B2	8	392	2702.35	7.73	-0.860	0.510	445291	1.007
5/5/2013	05:15:36pm	5008813.3	462064.6	B2	9	407	2703.25	8.47	-0.852	0.524	442535	0.989
5/5/2013	05:19:49pm	5008800.0	462049.8	B2	10	324	2704.63	12.15	-0.791	0.612	436734	0.885
5/5/2013	05:21:39pm	5008779.7	462030.6	B2	11	452	2703.12	10.92	-0.723	0.691	435591	1.002
5/5/2013	02:46:20pm	5008826.5	461512.0	B6	1	1264	2778.29	20.87	0.103	0.995	373645	-1.942
5/5/2013	03:03:05pm	5008853.8	461525.2	B6	2	1009	2778.45	9.33	-0.981	0.196	464080	-0.176
5/5/2013	03:08:12pm	5008859.3	461563.0	B6	3	403	2775.93	9.64	-0.986	0.168	476984	1.686
5/5/2013	03:10:51pm	5008862.4	461605.4	B6	4	355	2772.53	11.03	-0.976	0.220	481215	1.245
5/5/2013	03:13:15pm	5008855.8	461670.9	B6	5	348	2766.99	8.76	-0.970	0.245	462373	0.391
5/5/2013	03:14:04pm	5008855.4	461711.5	B6	6	194	2764.15	16.52	-0.937	0.349	466135	1.490
5/5/2013	03:22:59pm	5008866.3	461761.0	B6	7	608	2760.21	10.64	-0.993	0.119	489024	0.482
5/5/2013	03:27:21pm	5008870.1	461797.3	B6	8	389	2758.54	13.06	-0.972	0.236	476263	1.184
5/5/2013	03:29:51pm	5008874.3	461836.7	B6	9	519	2755.36	9.45	-0.976	0.216	468716	0.877
5/5/2013	03:32:28pm	5008883.5	461875.0	B6	10	431	2754.52	19.45	-0.942	0.335	479567	2.256
5/5/2013	01:31:09pm	5008639.7	461198.0	B8	1	349	2821.51	8.00	-0.977	0.214	441220	1.278
5/5/2013	01:36:45pm	5008648.8	461231.7	B8	2	189	2820.76	9.74	-0.936	0.352	447377	1.495

5/5/2013	01:48:30pm	5008680.6	461280.7	B8	3	458	2815.91	17.00	-0.635	0.772	455311	1.944
5/5/2013	01:51:41pm	5008715.4	461305.2	B8	4	526	2820.32	28.69	-0.548	0.836	448808	2.355
5/5/2013	01:55:40pm	5008744.8	461334.2	B8	5	373	2812.65	14.53	-0.780	0.626	466167	1.391
5/5/2013	01:59:57pm	5008756.0	461375.9	B8	6	454	2807.19	30.00	-0.944	0.331	509145	0.178
5/5/2013	02:03:52pm	5008770.2	461403.8	B8	7	380	2802.94	34.73	-0.894	0.449	506445	3.410
5/5/2013	02:07:10pm	5008788.1	461436.9	B8	8	324	2804.69	28.18	-0.891	0.455	499182	3.977
5/5/2013	02:17:54pm	5008819.5	461462.1	B8	9	549	2806.91	18.26	-0.337	0.942	424617	6.184
5/5/2013	02:30:22pm	5008863.4	461469.7	B8	10	980	2801.67	27.98	0.091	0.996	364865	1.024
5/5/2013	12:33:36pm	5008134.8	461126.4	B9a	11	679	2878.41	25.65	0.932	0.362	265007	-3.022
5/5/2013	12:38:23pm	5008128.6	461140.4	B9a	12	1000	2876.96	26.75	0.936	0.352	257975	-3.274
5/5/2013	12:23:51pm	5008122.9	461154.7	B9a	13	1042	2878.08	29.36	0.957	0.289	244541	-4.757
5/5/2013	12:42:05pm	5008119.0	461170.2	B9a	14	824	2875.98	30.61	0.998	0.065	229856	-5.136
5/5/2013	12:42:55pm	5008118.3	461187.9	B9a	15	563	2880.74	16.38	1.000	-0.007	222042	-5.119
5/6/2013	09:31:29am	5008924.3	460383.7	B15	1	197	3186.02	25.96	-0.591	0.806	482895	1.648
5/6/2013	09:37:04am	5008936.2	460394.4	B15	2	303	3185.56	25.68	-0.673	0.740	495211	1.643
5/6/2013	09:40:19am	5008950.0	460406.1	B15	3	208	3182.31	33.12	-0.691	0.723	493143	2.509
5/6/2013	09:44:47am	5008964.1	460417.9	B15	4	121	3181.51	24.58	-0.684	0.729	490742	2.227
5/6/2013	09:47:28am	5008976.7	460429.8	B15	5	139	3181.66	25.27	-0.743	0.669	499685	2.369
5/6/2013	09:49:50am	5008990.3	460440.8	B15	6	315	3181.98	26.50	-0.719	0.695	496419	2.366
5/6/2013	09:54:40am	5009004.1	460450.5	B15	7	291	3179.69	29.23	-0.775	0.632	497115	2.828
5/6/2013	10:02:58am	5009017.2	460461.0	B15	8	272	3184.16	33.72	-0.867	0.498	530628	1.036
5/6/2013	10:05:08am	5009032.6	460472.7	B15	9	355	3183.29	32.75	-0.874	0.486	530366	1.125
5/6/2013	10:07:31am	5009043.9	460485.1	B15	10	364	3193.92	34.62	-0.912	0.410	548995	4.469
5/9/2013	03:22:06pm	5008687.4	462310.0	B1	1	0	2660.31	11.27	-0.998	0.062	454361	1.640
5/9/2013	03:22:28pm	5008692.9	462290.0	B1	2	217	2660.68	13.59	-0.996	0.091	458382	0.580
5/9/2013	03:29:48pm	5008705.5	462274.6	B1	3	245	2665.7	9.04	-0.981	0.194	465303	1.568
5/9/2013	03:31:30pm	5008704.1	462253.7	B1	4	500	2667.57	6.80	-0.958	0.286	446677	0.816
5/9/2013	03:33:45pm	5008681.8	462252.3	B1	5	538	2662.71	12.54	-0.706	0.708	437251	-0.083
5/9/2013	03:35:45pm	5008658.8	462245.5	B1	6	537	2660.72	7.77	-0.615	0.789	425681	-1.865

5/9/2013	03:38:01pm	5008639.6	462233.1	B1	7	570	2661.12	11.74	-0.425	0.905	410958	-3.164
5/9/2013	03:44:21pm	5008623.7	462230.9	B1	8	760	2663.26	23.50	0.997	0.073	253621	-4.227
5/9/2013	03:46:02pm	5008621.4	462253.1	B1	9	860	2663.42	19.08	0.994	0.106	292276	-2.300
5/9/2013	03:50:33pm	5008617.4	462274.1	B1	10	700	2662.75	7.63	0.933	0.361	349560	-1.099
5/9/2013	03:03:27pm	5008653.7	461899.2	B3	1	31	2704.08	25.18	-0.915	0.404	485288	0.771
5/9/2013	02:35:25pm	5008645.9	461881.4	B3	2	315	2703.87	16.44	-0.901	0.433	475047	0.208
5/9/2013	02:37:49pm	5008634.1	461861.2	B3	3	204	2708.15	10.20	-0.952	0.306	483421	-0.100
5/9/2013	02:42:15pm	5008624.5	461838.3	B3	4	267	2707.2	20.18	-0.900	0.437	459371	-1.553
5/9/2013	02:44:40pm	5008604.0	461837.1	B3	5	469	2705.7	13.62	-0.277	0.961	408265	-1.942
5/9/2013	02:48:40pm	5008584.6	461840.3	B3	6	561	2706.11	6.55	1.000	-0.012	308621	-3.333
5/9/2013	02:50:42pm	5008586.1	461859.3	B3	7	574	2703.56	11.13	1.000	0.029	312870	-3.576
5/9/2013	02:54:22pm	5008588.7	461882.2	B3	8	665	2703.92	11.21	0.998	-0.055	280433	-2.386
5/9/2013	02:58:26pm	5008592.7	461902.3	B3	9	653	2704.42	10.83	0.998	-0.067	281086	-1.792
5/9/2013	02:59:40pm	5008596.5	461921.5	B3	10	487	2704.78	9.98	1.000	0.030	290033	-1.149
5/10/2013	07:57:45am	5008972.4	460926.1	B12	1	407	2969.58	26.98	-0.852	0.524	496349	2.932
5/10/2013	08:16:08am	5008986.8	460947.1	B12	2	1378	2971.32	21.27	-0.882	0.470	493341	1.117
5/10/2013	08:28:52am	5009000.6	460962.7	B12	3	122	2975.94	14.20	-0.953	0.304	503337	2.188
5/10/2013	08:30:50am	5009009.5	460982.4	B12	4	230	2972.84	10.75	-0.946	0.326	490934	2.346
5/10/2013	08:33:36am	5009019.6	461002.6	B12	5	0	2972.45	17.12	-0.899	0.439	478170	2.070
5/10/2013	08:39:30am	5009032.5	461019.8	B12	6	852	2970.99	15.06	-0.885	0.466	471844	1.173
5/10/2013	08:48:17am	5009045.8	461037.9	B12	7	118	2974.03	15.81	-0.968	0.249	484510	1.875
5/10/2013	08:50:20am	5009053.2	461058.8	B12	8	0	2974.69	12.89	-0.944	0.330	469952	2.270
5/10/2013	08:52:58am	5009055.6	461079.8	B12	9	7	2973.33	11.85	-0.987	0.158	470486	2.211
5/10/2013	08:55:06am	5009058.5	461100.6	B12	10	139	2973.14	11.72	-0.990	-0.140	467790	1.807
5/10/2013	08:56:33am	5009046.7	461115.2	B12	11	0	2972.46	13.74	-0.987	-0.160	477715	2.102
5/10/2013	08:57:37am	5009041.2	461136.2	B12	12	0	2970.22	15.68	-0.995	0.097	486261	2.208
5/10/2013	08:58:58am	5009045.2	461157.7	B12	13	0	2970.86	21.05	-0.904	0.427	494646	3.522
5/10/2013	09:00:17am	5009056.6	461174.1	B12	14	9	2969.85	18.30	-0.659	0.753	465939	3.790
5/10/2013	09:01:38am	5009073.9	461184.8	B12	15	6	2967.11	21.05	0.273	0.962	396065	4.315

5/10/2013	02:03:08pm	5008371.1	461239.4	B7	1	468	2798.66	18.59	0.968	0.250	301597	-2.232
5/10/2013	02:08:50pm	5008379.2	461212.3	B7	2	487	2799.31	11.48	0.825	0.565	355874	-1.309
5/10/2013	02:11:02pm	5008403.6	461214.4	B7	3	303	2797.54	9.36	0.405	0.914	386244	-0.936
5/10/2013	02:12:39pm	5008424.9	461208.9	B7	4	94	2796.86	8.91	0.900	0.436	358650	-0.775
5/10/2013	02:14:49pm	5008438.6	461188.6	B7	5	373	2797.41	10.18	0.636	0.772	367280	-1.009
5/10/2013	02:18:34pm	5008456.6	461172.3	B7	6	196	2799.29	11.71	0.367	0.930	384610	-0.439
5/10/2013	02:19:55pm	5008480.5	461170.6	B7	7	234	2798.99	12.12	-0.167	0.986	407552	-0.103
5/10/2013	02:21:19pm	5008502.4	461181.0	B7	8	359	2798.9	9.11	-0.592	0.806	429748	0.009
5/10/2013	02:22:08pm	5008517.8	461197.9	B7	9	0	2797.3	13.43	-0.812	0.583	449778	-0.472

Ablation Period: Basin A

GPS_Date	GPS_Time	Northing	Easting	TrnsctID	Pt	SWE	Elev	Slope	Northness	Eastness	Solar	WEI
6/1/2013	NA	5009449.0	460732.0	A6	1	1159	2877.60	23.07	0.871	0.492	273818	-2.245
6/1/2013	NA	5009482.0	460701.0	A6	2	640	2876.90	18.83	0.844	0.537	279020	-2.617
6/1/2013	NA	5009513.0	460668.0	A6	3	1023	2879.49	20.12	0.805	0.594	260923	-2.993
6/1/2013	NA	5009555.0	460646.0	A6	4	962	2874.82	23.47	0.204	0.979	326411	-3.617
6/1/2013	NA	5009602.0	460648.0	A6	5	425	2880.42	16.74	-0.920	0.393	383822	-0.419
6/1/2013	NA	5009625.6	460683.8	A6	6	0	2881.89	11.84	-0.993	0.119	419164	0.809
6/1/2013	NA	5009620.9	460731.7	A6	7	0	2879.94	20.85	-0.999	-0.035	428769	0.092
6/1/2013	NA	5009613.9	460774.2	A6	8	0	2879.10	17.87	-0.963	-0.268	416988	0.348
6/1/2013	NA	5009604.2	460818.4	A6	9	0	2877.90	16.05	-0.999	0.042	428803	0.874
6/1/2013	NA	5009597.8	460867.7	A6	10	0	2875.65	17.05	-1.000	-0.020	436773	1.933
6/1/2013	NA	5009598.7	460907.2	A6	11	0	2873.24	32.16	-0.962	0.273	478369	4.931
6/2/2013	9:31:54 AM	5009368.8	460590.8	A10	1	1421	2960.51	44.24	0.742	0.670	219560	-6.108
6/2/2013	9:40:54 AM	5009395.6	460558.2	A10	2	828	2966.04	35.92	0.772	0.635	227262	-1.263
6/2/2013	9:48:19 AM	5009416.0	460527.9	A10	3	709	2978.24	33.17	0.884	0.468	216903	-2.469
6/2/2013	9:57:23 AM	5009432.7	460503.6	A10	4	987	2975.68	37.64	0.830	0.558	221220	-4.692
6/2/2013	10:05:57AM	5009456.2	460469.1	A10	5	1047	2977.81	36.41	0.860	0.510	204826	-5.357
6/2/2013	10:13:31AM	5009479.5	460442.0	A10	6	876	2980.31	36.61	0.794	0.608	218475	-4.511
6/2/2013	10:41:39AM	5009516.2	460401.0	A10	7	997	2983.92	41.66	0.814	0.581	202321	-4.950

6/2/2013	10:49:09AM	5009535.7	460379.1	A10	8	1168	2993.16	49.38	0.627	0.779	226499	-5.128
6/2/2013	10:57:25AM	5009571.2	460362.0	A10	9	879	2994.22	37.86	0.433	0.901	261822	-2.133
6/2/2013	11:09:18AM	5009598.1	460342.7	A10	10	515	2997.07	46.82	0.498	0.867	261448	0.286
6/2/2013	11:19:35AM	5009627.4	460312.5	A10	11	1027	3005.44	35.69	0.620	0.785	258391	-0.708
6/2/2013	11:31:30AM	5009661.6	460298.4	A10	12	1143	3006.74	43.56	0.137	0.991	325902	0.859
6/2/2013	12:17:56PM	5009727.0	460687.1	A7	1	176	2914.34	16.45	-0.966	0.259	441576	1.428
6/2/2013	12:28:20PM	5009732.9	460729.1	A7	2	5	2914.89	8.79	-0.998	0.067	441140	2.191
6/2/2013	12:33:41PM	5009774.8	460761.1	A7	3	5	2912.94	13.47	0.250	0.968	383787	1.467
6/2/2013	12:38:17PM	5009814.1	460752.7	A7	4	5	2913.68	24.48	0.300	0.954	371441	1.533
6/2/2013	12:46:23PM	5009850.8	460746.6	A7	5	660	2916.36	29.41	0.094	0.996	386842	0.947
6/2/2013	12:52:19PM	5009887.5	460742.8	A7	6	1008	2916.02	30.14	0.049	0.999	392159	1.933
6/2/2013	12:57:59PM	5009931.4	460734.2	A7	7	652	2915.47	16.47	0.304	0.953	376532	0.438
6/2/2013	1:13:10 PM	5009968.2	460728.0	A7	8	488	2915.34	12.89	0.091	0.996	395908	-0.807
6/2/2013	1:19:16 PM	5010006.5	460733.6	A7	9	962	2915.01	12.93	-0.592	0.806	436284	0.061
6/2/2013	1:33:55 PM	5010039.4	460745.5	A7	10	409	2917.75	16.63	-0.532	0.847	441263	1.643
6/2/2013	1:58:10 PM	5009841.0	461305.0	A2	1	61	2791.29	8.60	-0.952	0.307	437745	0.137
6/2/2013	2:14:23 PM	5009809.3	461326.5	A2	2	874	2785.56	6.42	-0.635	0.773	422120	-2.066
6/2/2013	2:21:40 PM	5009779.1	461356.4	A2	3	751	2787.07	10.02	0.824	0.567	367124	-0.463
6/2/2013	2:24:29 PM	5009759.9	461362.9	A2	4	676	2786.48	7.93	0.735	0.678	378022	-0.380
6/2/2013	2:29:04 PM	5009721.3	461389.6	A2	5	563	2787.13	5.58	0.529	0.849	387040	0.036
6/2/2013	2:32:57 PM	5009706.6	461403.1	A2	6	353	2784.68	8.47	0.354	0.935	392905	-0.035
6/2/2013	2:36:23 PM	5009667.9	461436.0	A2	7	410	2783.38	8.31	0.724	0.690	378980	-0.281
6/2/2013	2:39:00 PM	5009649.5	461450.4	A2	8	1058	2782.65	6.32	0.659	0.752	385509	-1.483
6/2/2013	2:48:10 PM	5009618.5	461469.7	A2	9	1035	2784.03	8.90	0.411	-0.911	378043	-2.760
6/2/2013	3:11:52 PM	5009582.6	461474.7	A2	10	666	2786.96	13.39	-0.150	-0.989	396826	-2.848
6/13/2013	1:52:49 PM	5009841.6	461305.6	A2	1	0	2791.29	8.60	-0.952	0.307	437745	0.137
6/13/2013	1:55:18 PM	5009810.3	461327.3	A2	2	897	2785.56	6.42	-0.635	0.773	422120	-2.066
6/13/2013	1:58:33 PM	5009778.1	461357.9	A2	3	496	2785.65	8.74	0.814	0.581	374801	-0.534
6/13/2013	2:00:41 PM	5009758.6	461363.0	A2	4	396	2786.48	7.93	0.735	0.678	378022	-0.380
6/13/2013	2:03:16 PM	5009722.4	461389.3	A2	5	258	2786.61	6.40	0.550	0.835	386059	-0.046
6/13/2013	2:04:52 PM	5009707.7	461402.6	A2	6	0	2784.68	8.47	0.354	0.935	392905	-0.035
6/13/2013	2:07:32 PM	5009669.1	461436.3	A2	7	68	2783.38	8.31	0.724	0.690	378980	-0.281
6/13/2013	2:09:43 PM	5009649.4	461451.7	A2	8	892	2782.65	6.32	0.659	0.752	385509	-1.483
6/13/2013	2:12:24 PM	5009617.8	461469.7	A2	9	797	2785.74	11.98	0.375	-0.927	371699	-1.994

6/13/2013	2:14:46 PM	5009582.2	461474.2	A2	10	377	2786.96	13.39	-0.150	-0.989	396826	-2.848
6/14/2013	4:20:49 PM	5009368.8	460591.0	A10	1	1439	2960.51	44.24	0.742	0.670	219560	-6.108
6/14/2013	4:40:14 PM	5009394.3	460558.6	A10	2	640	2966.04	35.92	0.772	0.635	227262	-1.263
6/14/2013	4:43:24 PM	5009415.2	460528.6	A10	3	460	2978.24	33.17	0.884	0.468	216903	-2.469
6/14/2013	4:46:19 PM	5009433.0	460504.6	A10	4	705	2975.68	37.64	0.830	0.558	221220	-4.692
6/14/2013	4:49:47 PM	5009457.7	460469.7	A10	5	894	2977.81	36.41	0.860	0.510	204826	-5.357
6/14/2013	4:54:09 PM	5009478.7	460442.3	A10	6	676	2980.31	36.61	0.794	0.608	218475	-4.511
6/14/2013	4:58:01 PM	5009518.0	460401.4	A10	7	947	2983.92	41.66	0.814	0.581	202321	-4.950
6/14/2013	5:15:48 PM	5009539.1	460378.6	A10	8	1105	2993.16	49.38	0.627	0.779	226499	-5.128
6/14/2013	5:19:12 PM	5009571.2	460360.5	A10	9	672	2994.22	37.86	0.433	0.901	261822	-2.133
6/14/2013	5:21:52 PM	5009597.6	460343.7	A10	10	175	2997.07	46.82	0.498	0.867	261448	0.286
6/14/2013	5:24:33 PM	5009627.1	460320.4	A10	11	1201	3005.44	35.69	0.620	0.785	258391	-0.708
6/14/2013	5:28:45 PM	5009662.0	460297.7	A10	12	960	3006.74	43.56	0.137	0.991	325902	0.859
6/14/2013	5:42:15 PM	5009726.9	460687.6	A7	1	37	2914.34	16.45	-0.966	0.259	441576	1.428
6/14/2013	5:45:09 PM	5009744.7	460734.7	A7	2	36	2916.64	6.11	-0.966	0.257	434097	2.759
6/14/2013	5:47:30 PM	5009773.9	460761.2	A7	3	27	2913.44	11.68	0.237	0.972	386712	1.875
6/14/2013	5:49:49 PM	5009812.9	460753.5	A7	4	30	2913.68	24.48	0.300	0.954	371441	1.533
6/14/2013	5:51:48 PM	5009849.8	460748.8	A7	5	530	2909.66	30.58	0.145	0.989	378756	0.528
6/14/2013	6:07:59 PM	5009888.1	460742.8	A7	6	642	2915.90	30.75	0.122	0.992	385539	2.145
6/14/2013	6:10:59 PM	5009929.7	460734.6	A7	7	362	2916.18	16.99	0.291	0.957	376539	0.689
6/14/2013	6:23:24 PM	5009967.6	460728.3	A7	8	238	2915.34	12.89	0.091	0.996	395908	-0.807
6/14/2013	6:27:48 PM	5010004.8	460734.6	A7	9	795	2915.01	12.93	-0.592	0.806	436284	0.061
6/14/2013	6:29:39 PM	5010021.0	460739.3	A7	10	25	2916.25	13.70	-0.600	0.800	444504	1.278
6/26/2013	12:00:00PM	5010106.8	460521.2	A12	1	0	3049.36	20.47	-0.337	0.942	439828	3.783
6/26/2013	12:00:00PM	5010093.9	460510.7	A12	2	0	3051.91	28.93	-0.645	0.764	481276	3.769
6/26/2013	12:00:00PM	5010077.2	460499.7	A12	3	0	3052.12	28.94	-0.705	0.710	491647	3.402
6/26/2013	12:00:00PM	5010063.0	460490.3	A12	4	0	3051.89	37.47	-0.726	0.688	494663	2.906
6/26/2013	12:00:00PM	5010046.1	460472.0	A12	5	0	3056.13	27.24	-0.684	0.730	484515	3.566
6/26/2013	12:00:00PM	5010030.7	460461.0	A12	6	0	3053.11	25.89	-0.696	0.718	483588	4.146
6/26/2013	12:00:00PM	5010021.1	460442.5	A12	7	0	3060.16	24.75	-0.824	0.566	499372	3.421
6/26/2013	12:00:00PM	5010009.5	460425.6	A12	8	0	3062.67	19.29	-0.832	0.555	502117	3.522
6/26/2013	12:00:00PM	5009990.6	460413.1	A12	9	0	3054.88	30.05	-0.929	0.370	518777	3.731
6/26/2013	12:00:00PM	5009984.5	460386.7	A12	10	0	3063.40	32.20	-0.894	0.447	518811	4.260
6/26/2013	12:00:00PM	5009975.5	460371.0	A12	11	0	3063.38	33.49	-0.908	0.420	522136	4.544

6/26/2013	12:00:00PM	5009965.4	460355.2	A12	12	0	3061.14	29.81	-0.869	0.495	514896	4.435
6/26/2013	12:00:00PM	5009955.6	460338.2	A12	13	0	3064.15	24.48	-0.850	0.527	511494	4.590
6/26/2013	12:00:00PM	5009944.0	460321.6	A12	14	0	3065.52	33.63	-0.839	0.544	509718	4.806
6/26/2013	12:00:00PM	5009933.2	460305.1	A12	15	0	3070.70	39.57	-0.820	0.573	508159	4.702
6/26/2013	12:00:00PM	5009919.9	460289.3	A12	16	0	3068.45	38.11	-0.748	0.663	496736	4.689
6/26/2013	12:00:00PM	5010177.0	460377.2	A13	1	0	3154.76	30.30	-0.236	0.972	433392	3.902
6/26/2013	12:00:00PM	5010142.3	460361.5	A13	2	0	3154.83	45.07	-0.745	0.667	511400	5.760
6/26/2013	12:00:00PM	5010113.6	460331.8	A13	3	0	3150.27	38.81	-0.853	0.521	531851	5.690
6/26/2013	12:00:00PM	5010088.1	460302.5	A13	4	0	3154.46	34.01	-0.868	0.497	529369	5.081
6/26/2013	12:00:00PM	5010068.7	460285.2	A13	5	0	3149.64	23.12	-0.911	0.411	536692	5.825
6/26/2013	12:00:00PM	5010041.8	460255.2	A13	6	0	3143.39	32.29	-0.886	0.463	528456	4.559
6/26/2013	12:00:00PM	5010016.5	460225.2	A13	7	0	3136.80	29.37	-0.859	0.512	525088	4.547
6/26/2013	12:00:00PM	5009988.4	460198.1	A13	8	0	3142.87	28.25	-0.801	0.599	508675	4.886
6/26/2013	12:00:00PM	5009956.0	460176.3	A13	9	0	3135.92	38.31	-0.699	0.715	496923	3.048
6/26/2013	12:00:00PM	5009918.5	460161.2	A13	10	0	3133.87	34.55	-0.545	0.838	471028	2.435
6/26/2013	12:58:09PM	5009370.1	460590.4	A10	1	986	2965.41	39.87	0.737	0.675	218273	-5.398
6/26/2013	1:04:43 PM	5009397.8	460558.3	A10	2	330	2966.04	35.92	0.772	0.635	227262	-1.263
6/26/2013	1:08:22 PM	5009419.2	460528.7	A10	3	0	2972.68	35.27	0.891	0.454	211291	-2.638
6/26/2013	1:10:09 PM	5009436.4	460505.1	A10	4	395	2971.51	36.17	0.844	0.536	225998	-3.295
6/26/2013	1:12:22 PM	5009458.2	460468.5	A10	5	452	2986.19	39.12	0.821	0.571	200816	-4.799
6/26/2013	1:16:04 PM	5009482.0	460442.3	A10	6	210	2980.31	36.61	0.794	0.608	218475	-4.511
6/26/2013	1:19:57 PM	5009517.7	460401.7	A10	7	447	2983.92	41.66	0.814	0.581	202321	-4.950
6/26/2013	1:26:22 PM	5009538.8	460378.8	A10	8	729	2993.16	49.38	0.627	0.779	226499	-5.128
6/26/2013	1:28:23 PM	5009570.4	460361.0	A10	9	230	2994.22	37.86	0.433	0.901	261822	-2.133
6/26/2013	1:31:14 PM	5009598.9	460343.5	A10	10	0	2997.07	46.82	0.498	0.867	261448	0.286
6/26/2013	1:32:40 PM	5009628.1	460321.2	A10	11	867	3000.14	41.78	0.660	0.751	231664	-1.344
6/26/2013	1:34:36 PM	5009661.6	460299.3	A10	12	491	3006.74	43.56	0.137	0.991	325902	0.859
6/26/2013	1:46:44 PM	5009725.7	460688.0	A7	1	0	2914.98	17.23	-0.943	0.331	443933	1.489
6/26/2013	1:48:01 PM	5009740.5	460735.0	A7	2	0	2916.64	6.11	-0.966	0.257	434097	2.759
6/26/2013	1:49:16 PM	5009776.0	460760.6	A7	3	0	2912.94	13.47	0.250	0.968	383787	1.467
6/26/2013	1:50:44 PM	5009813.7	460754.0	A7	4	0	2913.68	24.48	0.300	0.954	371441	1.533
6/26/2013	1:53:14 PM	5009853.1	460747.6	A7	5	37	2909.38	31.25	0.068	0.998	385360	0.928
6/26/2013	1:55:09 PM	5009888.1	460743.4	A7	6	323	2915.90	30.75	0.122	0.992	385539	2.145
6/26/2013	2:05:06 PM	5009932.8	460735.9	A7	7	0	2915.47	16.47	0.304	0.953	376532	0.438

6/26/2013	2:12:29 PM	5009976.3	460735.2	A7	8	0	2913.58	12.07	-0.137	0.991	409968	-0.248
6/26/2013	2:13:57 PM	5010018.7	460746.3	A7	9	0	2916.25	13.70	-0.600	0.800	444504	1.278
6/26/2013	2:14:51 PM	5010038.6	460750.4	A7	10	0	2915.68	21.69	-0.488	0.873	436821	1.672
6/26/2013	2:27:59 PM	5009834.5	461303.1	A2	1	0	2791.04	7.69	-0.589	0.808	422497	-0.309
6/26/2013	2:29:41 PM	5009809.5	461326.3	A2	2	297	2785.56	6.42	-0.635	0.773	422120	-2.066
6/26/2013	2:43:50 PM	5009782.3	461351.8	A2	3	0	2787.07	10.02	0.824	0.567	367124	-0.463
6/26/2013	2:45:13 PM	5009737.8	461366.1	A2	4	0	2786.47	6.46	0.668	0.744	382117	-0.244
6/26/2013	2:45:13 PM	5009719.8	461384.5	A2	5	0	2787.13	5.58	0.529	0.849	387040	0.036
6/26/2013	2:46:35 PM	5009702.0	461392.3	A2	6	0	2786.80	9.05	0.456	0.890	388789	0.108
6/26/2013	2:48:39 PM	5009664.1	461418.4	A2	7	0	2784.80	6.80	0.658	0.753	380455	-0.221
6/26/2013	2:50:04 PM	5009636.4	461446.3	A2	8	209	2783.09	6.95	0.545	0.839	388689	-1.580
6/26/2013	2:57:22 PM	5009618.1	461470.3	A2	9	323	2785.74	11.98	0.375	-0.927	371699	-1.994
6/26/2013	3:08:38 PM	5009584.5	461469.7	A2	10	0	2787.18	13.12	0.055	-0.998	385760	-2.054
6/27/2013	10:09:59AM	5009409.8	460630.3	A9	1	258	2926.41	29.99	0.712	0.702	250836	-3.338
6/27/2013	10:13:03AM	5009389.0	460654.9	A9	2	570	2923.53	30.75	0.866	0.500	232697	-3.317
6/27/2013	10:20:05AM	5009366.7	460682.8	A9	3	102	2925.57	30.97	0.916	0.402	232730	-3.001
6/27/2013	10:23:53AM	5009339.1	460712.2	A9	4	98	2930.37	29.57	0.871	0.491	236302	-1.198
6/27/2013	10:26:06AM	5009312.8	460745.6	A9	5	523	2930.15	30.75	0.895	0.447	229262	-2.542
6/27/2013	10:30:50AM	5009290.6	460778.5	A9	6	541	2922.52	24.89	0.874	0.486	232588	-2.295
6/27/2013	10:35:23AM	5009267.8	460815.3	A9	7	644	2923.57	36.55	0.853	0.522	229234	-2.202
6/27/2013	10:40:18AM	5009246.6	460848.9	A9	8	37	2923.19	35.40	0.860	0.510	235646	-1.048
6/27/2013	10:42:06AM	5009221.0	460884.2	A9	9	0	2916.39	31.40	0.879	0.478	228852	-3.525
6/27/2013	10:43:38AM	5009198.6	460916.5	A9	10	0	2917.89	32.77	0.835	0.550	221611	-3.421
6/27/2013	10:46:39AM	5009178.5	460953.1	A9	11	837	2912.42	27.71	1.000	0.027	157693	-8.083
6/27/2013	10:50:04AM	5009176.1	460993.4	A9	12	1174	2906.83	43.45	0.986	0.168	167111	-7.563
6/27/2013	11:08:38AM	5009365.9	461044.6	A4	1	0	2833.06	13.94	0.735	0.678	308269	-1.726
6/27/2013	11:16:00AM	5009343.2	461087.2	A4	2	0	2830.55	16.61	0.977	0.211	283978	-2.962
6/27/2013	11:18:08AM	5009334.2	461126.1	A4	3	10	2830.45	17.40	0.975	0.223	283591	-1.978
6/27/2013	11:20:56AM	5009320.8	461169.2	A4	4	0	2830.76	18.98	0.945	0.328	278058	-2.548
6/27/2013	11:24:25AM	5009328.1	461202.4	A4	5	0	2825.44	17.12	0.968	0.253	281082	-2.389
6/27/2013	11:25:55AM	5009322.5	461239.7	A4	6	0	2823.41	18.69	0.996	0.093	271219	-2.752
6/27/2013	11:31:42AM	5009334.5	461293.7	A4	7	558	2821.18	23.60	0.938	-0.348	262398	-3.896
6/27/2013	11:36:07AM	5009353.6	461331.8	A4	8	309	2819.17	22.07	0.999	0.045	264127	-2.644
7/10/2013	1:55:00 PM	5009370.5	460590.4	A10	1	0	2965.41	39.87	0.737	0.675	218273	-5.398

7/10/2013	1:55:00 PM	5009397.4	460558.1	A10	2	0	2966.04	35.92	0.772	0.635	227262	-1.263
7/10/2013	1:55:00 PM	5009417.9	460527.1	A10	3	0	2972.68	35.27	0.891	0.454	211291	-2.638
7/10/2013	1:55:00 PM	5009434.8	460503.3	A10	4	0	2979.24	36.20	0.825	0.565	215795	-4.717
7/10/2013	1:55:00 PM	5009458.3	460468.0	A10	5	0	2986.19	39.12	0.821	0.571	200816	-4.799
7/10/2013	1:55:00 PM	5009481.4	460441.5	A10	6	0	2980.31	36.61	0.794	0.608	218475	-4.511
7/10/2013	1:55:00 PM	5009516.6	460399.9	A10	7	0	2983.92	41.66	0.814	0.581	202321	-4.950
7/10/2013	1:55:00 PM	5009538.0	460377.3	A10	8	0	2993.16	49.38	0.627	0.779	226499	-5.128
7/10/2013	1:55:00 PM	5009570.3	460360.8	A10	9	0	2994.22	37.86	0.433	0.901	261822	-2.133
7/10/2013	1:55:00 PM	5009597.3	460342.4	A10	10	0	2997.07	46.82	0.498	0.867	261448	0.286
7/10/2013	1:55:00 PM	5009627.2	460319.6	A10	11	0	3005.44	35.69	0.620	0.785	258391	-0.708
7/10/2013	1:55:00 PM	5009662.6	460298.5	A10	12	0	3006.74	43.56	0.137	0.991	325902	0.859
7/10/2013	1:55:00 PM	5009409.8	460630.3	A9	1	0	2926.41	29.99	0.712	0.702	250836	-3.338
7/10/2013	1:55:00 PM	5009389.0	460654.9	A9	2	0	2923.53	30.75	0.866	0.500	232697	-3.317
7/10/2013	1:55:00 PM	5009366.7	460682.8	A9	3	0	2925.57	30.97	0.916	0.402	232730	-3.001
7/10/2013	1:55:00 PM	5009339.1	460712.2	A9	4	0	2930.37	29.57	0.871	0.491	236302	-1.198
7/10/2013	1:55:00 PM	5009312.8	460745.6	A9	5	0	2930.15	30.75	0.895	0.447	229262	-2.542
7/10/2013	1:55:00 PM	5009290.6	460778.5	A9	6	0	2922.52	24.89	0.874	0.486	232588	-2.295
7/10/2013	1:55:00 PM	5009267.8	460815.3	A9	7	0	2923.57	36.55	0.853	0.522	229234	-2.202
7/10/2013	1:55:00 PM	5009246.6	460848.9	A9	8	0	2923.19	35.40	0.860	0.510	235646	-1.048
7/10/2013	1:55:00 PM	5009221.0	460884.2	A9	9	0	2916.39	31.40	0.879	0.478	228852	-3.525
7/10/2013	1:55:00 PM	5009198.6	460916.5	A9	10	0	2917.89	32.77	0.835	0.550	221611	-3.421
7/10/2013	1:58:25 PM	5009173.9	460994.6	A9	11	472	2906.83	43.45	0.986	0.168	167111	-7.563
7/10/2013	2:09:09 PM	5009177.6	460949.2	A9	12	801	2912.42	27.71	1.000	0.027	157693	-8.083
7/10/2013	2:30:00 PM	5009864.0	461517.1	A1	1	0	2758.59	25.74	-0.337	0.942	420422	2.107
7/10/2013	2:30:00 PM	5009841.2	461511.5	A1	2	0	2756.41	16.81	0.439	0.898	351175	-3.752
7/10/2013	2:30:00 PM	5009828.5	461517.6	A1	3	0	2757.06	18.43	0.728	0.685	299767	-3.409
7/10/2013	2:30:00 PM	5009811.0	461520.6	A1	4	0	2759.70	25.61	0.663	0.748	299859	-2.285
7/10/2013	2:30:00 PM	5009799.0	461526.4	A1	5	0	2760.94	22.25	0.485	0.875	332509	-3.633
7/10/2013	2:30:00 PM	5009780.1	461524.9	A1	6	0	2762.83	17.21	0.288	0.958	369695	-4.024
7/10/2013	2:30:00 PM	5009764.2	461526.7	A1	7	0	2763.47	8.65	0.734	0.679	364313	-4.912
7/10/2013	2:30:00 PM	5009776.4	461539.8	A1	8	0	2764.48	16.38	0.733	-0.681	330705	-4.339
7/10/2013	2:30:00 PM	5009790.0	461548.5	A1	9	0	2765.10	16.85	0.412	-0.911	355004	-3.229
7/10/2013	2:30:00 PM	5009811.4	461549.6	A1	10	0	2763.41	22.73	0.016	-1.000	375653	-1.039
7/10/2013	2:30:00 PM	5009729.7	460328.9	A11	1	0	2984.82	28.88	-0.702	0.713	409696	-4.156

7/10/2013	2:30:00 PM	5009761.5	460343.1	A11	2	0	2994.90	49.86	-0.930	0.367	450931	1.669
7/10/2013	2:30:00 PM	5009779.5	460384.9	A11	3	0	2995.11	46.68	-0.931	0.365	474869	5.617
7/10/2013	2:30:00 PM	5009798.5	460420.4	A11	4	0	2986.41	24.14	-0.872	0.489	469885	3.167
7/10/2013	2:30:00 PM	5009821.1	460453.4	A11	5	0	2985.23	22.23	-0.865	0.502	461838	1.061
7/10/2013	2:30:00 PM	5009839.7	460490.9	A11	6	0	2985.22	24.58	-0.945	0.328	481088	2.465
7/10/2013	2:30:00 PM	5009859.2	460525.7	A11	7	0	2983.62	18.92	-0.940	0.342	485497	3.328
7/10/2013	2:30:00 PM	5009883.7	460557.4	A11	8	0	2982.88	25.56	-0.642	0.766	464209	4.823
7/10/2013	2:30:00 PM	5009910.1	460592.1	A11	9	0	2964.33	32.10	-0.378	0.926	432335	1.028
7/10/2013	2:30:00 PM	5009947.1	460605.2	A11	10	0	2965.86	28.53	-0.248	0.969	419075	1.255
7/10/2013	2:30:00 PM	5009987.0	460613.5	A11	11	0	2965.49	36.66	-0.309	0.951	427475	0.379
7/10/2013	2:30:00 PM	5010106.8	460521.2	A12	1	0	3068.45	38.11	-0.748	0.663	496736	4.689
7/10/2013	2:30:00 PM	5010093.9	460510.7	A12	2	0	3070.70	39.57	-0.820	0.573	508159	4.702
7/10/2013	2:30:00 PM	5010077.2	460499.7	A12	3	0	3065.52	33.63	-0.839	0.544	509718	4.806
7/10/2013	2:30:00 PM	5010063.0	460490.3	A12	4	0	3064.15	24.48	-0.850	0.527	511494	4.590
7/10/2013	2:30:00 PM	5010046.1	460472.0	A12	5	0	3061.14	29.81	-0.869	0.495	514896	4.435
7/10/2013	2:30:00 PM	5010030.7	460461.0	A12	6	0	3063.38	33.49	-0.908	0.420	522136	4.544
7/10/2013	2:30:00 PM	5010021.1	460442.5	A12	7	0	3063.40	32.20	-0.894	0.447	518811	4.260
7/10/2013	2:30:00 PM	5010009.5	460425.6	A12	8	0	3054.88	30.05	-0.929	0.370	518777	3.731
7/10/2013	2:30:00 PM	5009990.6	460413.1	A12	9	0	3062.67	19.29	-0.832	0.555	502117	3.522
7/10/2013	2:30:00 PM	5009984.5	460386.7	A12	10	0	3060.16	24.75	-0.824	0.566	499372	3.421
7/10/2013	2:30:00 PM	5009975.5	460371.0	A12	11	0	3053.11	25.89	-0.696	0.718	483588	4.146
7/10/2013	2:30:00 PM	5009965.4	460355.2	A12	12	0	3056.13	27.24	-0.684	0.730	484515	3.566
7/10/2013	2:30:00 PM	5009955.6	460338.2	A12	13	0	3051.89	37.47	-0.726	0.688	494663	2.906
7/10/2013	2:30:00 PM	5009944.0	460321.6	A12	14	0	3052.12	28.94	-0.705	0.710	491647	3.402
7/10/2013	2:30:00 PM	5009933.2	460305.1	A12	15	0	3051.91	28.93	-0.645	0.764	481276	3.769
7/10/2013	2:30:00 PM	5009919.9	460289.3	A12	16	0	3049.36	20.47	-0.337	0.942	439828	3.783
7/10/2013	2:30:00 PM	5010177.0	460377.2	A13	1	0	3133.87	34.55	-0.545	0.838	471028	2.435
7/10/2013	2:30:00 PM	5010142.3	460361.5	A13	2	0	3135.92	38.31	-0.699	0.715	496923	3.048
7/10/2013	2:30:00 PM	5010113.6	460331.8	A13	3	0	3142.87	28.25	-0.801	0.599	508675	4.886
7/10/2013	2:30:00 PM	5010088.1	460302.5	A13	4	0	3136.80	29.37	-0.859	0.512	525088	4.547
7/10/2013	2:30:00 PM	5010068.7	460285.2	A13	5	0	3143.39	32.29	-0.886	0.463	528456	4.559
7/10/2013	2:30:00 PM	5010041.8	460255.2	A13	6	0	3149.64	23.12	-0.911	0.411	536692	5.825
7/10/2013	2:30:00 PM	5010016.5	460225.2	A13	7	0	3154.46	34.01	-0.868	0.497	529369	5.081
7/10/2013	2:30:00 PM	5009988.4	460198.1	A13	8	0	3150.27	38.81	-0.853	0.521	531851	5.690

7/10/2013	2:30:00 PM	5009956.0	460176.3	A13	9	0	3154.83	45.07	-0.745	0.667	511400	5.760
7/10/2013	2:30:00 PM	5009918.5	460161.2	A13	10	0	3154.76	30.30	-0.236	0.972	433392	3.902
7/10/2013	2:30:00 PM	5009840.7	461305.0	A2	1	0	2791.29	8.60	-0.952	0.307	437745	0.137
7/10/2013	2:30:00 PM	5009809.3	461326.6	A2	2	0	2785.93	6.71	0.588	0.809	382892	-1.835
7/10/2013	2:30:00 PM	5009778.8	461356.6	A2	3	0	2787.07	10.02	0.824	0.567	367124	-0.463
7/10/2013	2:30:00 PM	5009758.8	461362.3	A2	4	0	2786.48	7.93	0.735	0.678	378022	-0.380
7/10/2013	2:30:00 PM	5009721.3	461389.1	A2	5	0	2787.13	5.58	0.529	0.849	387040	0.036
7/10/2013	2:30:00 PM	5009706.2	461402.3	A2	6	0	2784.68	8.47	0.354	0.935	392905	-0.035
7/10/2013	2:30:00 PM	5009667.8	461436.1	A2	7	0	2783.38	8.31	0.724	0.690	378980	-0.281
7/10/2013	2:30:00 PM	5009649.4	461450.6	A2	8	0	2782.65	6.32	0.659	0.752	385509	-1.483
7/10/2013	2:30:00 PM	5009617.9	461469.4	A2	9	0	2785.74	11.98	0.375	-0.927	371699	-1.994
7/10/2013	2:30:00 PM	5009581.9	461473.8	A2	10	0	2786.96	13.39	-0.150	-0.989	396826	-2.848
7/10/2013	2:30:00 PM	5009431.0	461463.7	A3	1	0	2793.97	3.95	0.992	-0.127	313823	-4.454
7/10/2013	2:30:00 PM	5009453.9	461427.4	A3	2	0	2790.49	1.98	0.747	0.665	358204	-2.153
7/10/2013	2:30:00 PM	5009459.5	461387.3	A3	3	0	2792.65	3.38	-0.513	0.858	364364	-1.795
7/10/2013	2:30:00 PM	5009454.6	461348.4	A3	4	0	2794.07	5.15	-0.101	0.995	361192	-2.175
7/10/2013	2:30:00 PM	5009441.8	461318.5	A3	5	0	2798.32	10.75	0.994	0.112	318341	-2.149
7/10/2013	2:30:00 PM	5009439.9	461276.0	A3	6	0	2800.05	5.18	0.650	0.760	344322	-2.017
7/10/2013	2:30:00 PM	5009442.5	461234.4	A3	7	0	2803.60	5.67	0.814	0.581	342678	-1.423
7/10/2013	2:30:00 PM	5009444.3	461201.1	A3	8	0	2805.01	3.42	-0.115	0.993	361903	-1.739
7/10/2013	2:30:00 PM	5009461.1	461168.5	A3	9	0	2808.20	6.13	-0.958	0.286	384746	-1.552
7/10/2013	2:30:00 PM	5009487.9	461143.1	A3	10	0	2809.21	1.70	-0.882	0.471	380460	-1.277
7/10/2013	2:30:00 PM	5009365.5	461043.2	A4	1	0	2833.06	13.94	0.735	0.678	308269	-1.726
7/10/2013	2:30:00 PM	5009344.1	461090.7	A4	2	0	2830.55	16.61	0.977	0.211	283978	-2.962
7/10/2013	2:30:00 PM	5009334.3	461125.9	A4	3	0	2830.45	17.40	0.975	0.223	283591	-1.978
7/10/2013	2:30:00 PM	5009329.5	461163.7	A4	4	0	2830.28	17.71	0.949	0.316	283684	-1.873
7/10/2013	2:30:00 PM	5009328.4	461201.7	A4	5	0	2825.44	17.12	0.968	0.253	281082	-2.389
7/10/2013	2:30:00 PM	5009323.3	461239.6	A4	6	0	2823.41	18.69	0.996	0.093	271219	-2.752
7/10/2013	2:30:00 PM	5009334.2	461293.7	A4	7	0	2821.18	23.60	0.938	-0.348	262398	-3.896
7/10/2013	2:30:00 PM	5009355.3	461332.3	A4	8	0	2819.17	22.07	0.999	0.045	264127	-2.644
7/10/2013	2:30:00 PM	5009359.5	461368.7	A4	9	0	2814.84	13.53	0.999	0.052	272608	-3.111
7/10/2013	2:30:00 PM	5009361.8	461388.7	A4	10	0	2814.67	21.58	1.000	0.028	266797	-2.928
7/10/2013	2:30:00 PM	5009362.0	461413.0	A4	11	0	2814.03	25.28	0.998	0.065	251826	-2.935
7/10/2013	2:30:00 PM	5009356.5	461473.1	A4	12	0	2814.87	25.69	0.985	0.174	253647	-3.803

7/10/2013	2:30:00 PM	5009352.8	461519.9	A4	13	0	2812.31	24.62	0.999	-0.049	253390	-4.456
7/10/2013	2:30:00 PM	5009561.7	461034.2	A5	1	0	2820.58	15.52	-0.627	0.779	421947	-0.277
7/10/2013	2:30:00 PM	5009567.6	461036.4	A5	2	0	2821.37	23.29	-0.544	0.839	427137	0.520
7/10/2013	2:30:00 PM	5009640.1	461050.7	A5	3	0	2823.36	25.22	0.425	0.905	356293	0.344
7/10/2013	2:30:00 PM	5009677.0	461033.5	A5	4	0	2824.68	22.25	0.597	0.802	326407	-2.350
7/10/2013	2:30:00 PM	5009710.4	461016.5	A5	5	0	2826.38	31.33	0.370	0.929	348149	-1.461
7/10/2013	2:30:00 PM	5009744.6	461006.0	A5	6	0	2827.50	27.02	0.391	0.921	355659	-1.075
7/10/2013	2:30:00 PM	5009780.4	460994.0	A5	7	0	2827.48	13.01	0.232	0.973	380437	-0.896
7/10/2013	2:30:00 PM	5009817.5	460981.9	A5	8	0	2829.16	9.23	0.193	0.981	385753	-1.893
7/10/2013	2:30:00 PM	5009850.9	460991.7	A5	9	0	2827.27	4.79	-0.564	0.826	409125	-0.528
7/10/2013	2:30:00 PM	5009887.3	460986.6	A5	10	0	2831.10	13.79	-0.963	0.271	450995	-0.141
7/10/2013	2:30:00 PM	5009451.7	460731.9	A6	1	0	2877.60	23.07	0.871	0.492	273818	-2.245
7/10/2013	2:30:00 PM	5009482.0	460701.4	A6	2	0	2876.90	18.83	0.844	0.537	279020	-2.617
7/10/2013	2:30:00 PM	5009513.4	460667.7	A6	3	0	2879.49	19.61	0.805	0.594	260923	-2.993
7/10/2013	2:30:00 PM	5009555.3	460643.9	A6	4	0	2874.82	23.47	0.204	0.979	326411	-3.617
7/10/2013	2:30:00 PM	5009601.9	460647.9	A6	5	0	2880.42	16.74	-0.920	0.393	383822	-0.419
7/10/2013	2:30:00 PM	5009625.6	460683.8	A6	6	0	2881.89	11.84	-0.993	0.119	419164	0.809
7/10/2013	2:30:00 PM	5009620.9	460731.7	A6	7	0	2879.94	20.85	-0.999	-0.035	428769	0.092
7/10/2013	2:30:00 PM	5009613.9	460774.2	A6	8	0	2879.10	17.87	-0.963	-0.268	416988	0.348
7/10/2013	2:30:00 PM	5009604.2	460818.4	A6	9	0	2877.90	16.05	-0.999	0.042	428803	0.874
7/10/2013	2:30:00 PM	5009597.8	460867.7	A6	10	0	2875.65	17.05	-1.000	-0.020	436773	1.933
7/10/2013	2:30:00 PM	5009598.7	460907.2	A6	11	0	2873.24	32.16	-0.962	0.273	478369	4.931
7/10/2013	2:30:00 PM	5009727.0	460687.1	A7	1	0	2914.34	16.45	-0.966	0.259	441576	1.428
7/10/2013	2:30:00 PM	5009732.9	460729.1	A7	2	0	2916.64	6.11	-0.966	0.257	434097	2.759
7/10/2013	2:30:00 PM	5009774.8	460761.1	A7	3	0	2912.94	13.47	0.250	0.968	383787	1.467
7/10/2013	2:30:00 PM	5009814.1	460752.7	A7	4	0	2913.68	24.48	0.300	0.954	371441	1.533
7/10/2013	2:30:00 PM	5009850.8	460746.6	A7	5	0	2909.66	30.58	0.145	0.989	378756	0.528
7/10/2013	2:30:00 PM	5009887.5	460742.8	A7	6	0	2915.90	30.75	0.122	0.992	385539	2.145
7/10/2013	2:30:00 PM	5009931.4	460734.2	A7	7	0	2915.47	16.47	0.304	0.953	376532	0.438
7/10/2013	2:30:00 PM	5009968.2	460728.0	A7	8	0	2915.34	12.89	0.091	0.996	395908	-0.807
7/10/2013	2:30:00 PM	5010006.5	460733.6	A7	9	0	2915.01	12.93	-0.592	0.806	436284	0.061
7/10/2013	2:30:00 PM	5010039.4	460745.5	A7	10	0	2916.25	13.70	-0.600	0.800	444504	1.278
7/10/2013	2:30:00 PM	5009832.1	460639.7	A8	1	0	2942.02	12.75	-0.387	0.922	419844	1.506
7/10/2013	2:30:00 PM	5009859.9	460638.4	A8	2	0	2943.13	12.77	-0.182	0.983	410128	0.836

7/10/2013	2:30:00 PM	5009883.3	460640.5	A8	3	0	2943.58	13.12	-0.063	0.998	404100	0.229
7/10/2013	2:30:00 PM	5009936.2	460637.6	A8	4	0	2943.99	15.31	-0.152	0.988	410360	0.167
7/10/2013	2:30:00 PM	5009921.1	460642.4	A8	5	0	2944.45	16.99	-0.195	0.981	414016	0.277
7/10/2013	2:30:00 PM	5009941.4	460642.9	A8	6	0	2942.96	21.28	-0.126	0.992	407983	0.253
7/10/2013	2:30:00 PM	5009961.2	460644.4	A8	7	0	2944.09	23.59	-0.161	0.987	410546	0.449
7/10/2013	2:30:00 PM	5009979.8	460645.5	A8	8	0	2944.70	24.54	-0.149	0.989	408886	0.463
7/10/2013	2:30:00 PM	5010000.1	460649.7	A8	9	0	2945.84	25.12	-0.158	0.987	409294	-0.174
7/10/2013	2:30:00 PM	5010021.4	460656.6	A8	10	0	2946.94	29.51	-0.578	0.816	458228	-0.120

Ablation Period: Basin B

GPS_Date	GPS_Time	Northing	Easting	TrnsctID	Pt	SWE	Elev	Slope	Northness	Eastness	Solar	WEI
6/3/2013	8:24:32 AM	5008803.1	460617.9	B13	1	946	2994.07	36.347	-0.982	0.191	533258	3.106
6/3/2013	8:30:44 AM	5008787.1	460585.1	B13	2	1286	2989.08	29.394	-0.758	0.653	489003	-1.197
6/3/2013	8:53:42 AM	5008760.2	460561.9	B13	3	120	2999.67	38.062	-0.824	0.567	506085	3.508
6/3/2013	8:58:31 AM	5008728.7	460542.9	B13	4	1277	2998.55	26.626	-0.206	0.979	415991	3.455
6/3/2013	9:04:52 AM	5008691.6	460529.5	B13	5	43	3000.61	34.375	-0.659	0.752	475181	3.073
6/3/2013	9:10:12 AM	5008658.5	460515.4	B13	6	475	2998.47	31.414	0.148	0.989	379704	1.745
6/3/2013	9:16:33 AM	5008618.7	460502.1	B13	7	86	3004.17	26.762	-0.717	0.697	476517	0.443
6/3/2013	9:46:51 AM	5008581.0	460501.0	B13	8	1939	3001.41	22.711	0.401	0.916	347703	-2.061
6/3/2013	10:01:46AM	5008540.7	460510.7	B13	9	2261	3005.11	29.513	0.452	0.892	340942	-0.629
6/3/2013	11:13:16AM	5008502.1	460521.9	B13	10	2246	3002.4	30.768	0.189	0.982	380235	-1.225
6/3/2013	12:46:21PM	5008517.9	461197.8	B7	1	17	2797.3	13.428	-0.812	0.583	449778	-0.472
6/3/2013	12:48:29PM	5008502.5	461181.9	B7	2	262	2798.9	9.1095	-0.592	0.806	429748	0.009
6/3/2013	12:50:59PM	5008480.7	461170.9	B7	3	761	2798.99	12.123	-0.167	0.986	407552	-0.103
6/3/2013	12:59:49PM	5008456.8	461172.6	B7	4	43	2799.29	11.713	0.367	0.930	384610	-0.439
6/3/2013	1:14:58 PM	5008438.8	461188.7	B7	5	211	2797.41	10.178	0.636	0.772	367280	-1.009
6/3/2013	1:21:06 PM	5008425.3	461209.0	B7	6	26	2796.86	8.9135	0.900	0.436	358650	-0.775
6/3/2013	1:24:23 PM	5008404.5	461214.8	B7	7	138	2797.54	9.3551	0.405	0.914	386244	-0.936

6/3/2013	1:27:04 PM	5008379.8	461212.9	B7	8	387	2799.31	11.478	0.825	0.565	355874	-1.309
6/3/2013	1:39:16 PM	5008378.6	461239.8	B7	9	340	2795.71	15.581	0.928	0.372	322721	-3.379
6/3/2013	2:51:57 PM	5008780.3	462031.0	B2	1	69	2703.12	10.916	-0.723	0.691	435591	1.002
6/3/2013	2:55:02 PM	5008800.4	462050.5	B2	2	5	2704.63	12.154	-0.791	0.612	436734	0.885
6/3/2013	2:56:57 PM	5008814.2	462064.6	B2	3	25	2703.25	8.4749	-0.852	0.524	442535	0.989
6/3/2013	2:59:10 PM	5008824.1	462081.3	B2	4	10	2703.91	11.594	-0.884	0.467	446486	1.140
6/3/2013	3:01:23 PM	5008836.1	462097.4	B2	5	5	2703.87	11.763	-0.884	0.467	447233	1.287
6/3/2013	3:03:41 PM	5008843.9	462112.1	B2	6	5	2703	12.531	-0.898	0.440	446168	1.227
6/3/2013	3:05:22 PM	5008853.5	462130.3	B2	7	5	2703.04	11.182	-0.905	0.426	446361	1.224
6/3/2013	3:08:47 PM	5008863.6	462146.7	B2	8	5	2703.05	11.546	-0.873	0.487	441526	1.172
6/3/2013	3:11:12 PM	5008875.3	462159.6	B2	9	495	2702.82	8.396	-0.876	0.483	439398	0.861
6/3/2013	3:15:14 PM	5008887.1	462171.7	B2	10	74	2702.98	9.7867	-0.938	0.345	442776	0.810
6/3/2013	3:17:07 PM	5008896.1	462188.6	B2	11	127	2703.57	9.9584	-0.972	0.236	446644	0.801
6/13/2013	4:39:00 PM	5008826.5	461512.0	B6	1	0	2778.29	20.872	0.103	0.995	373645	-1.942
6/13/2013	4:39:00 PM	5008853.8	461525.2	B6	2	0	2778.45	9.3273	-0.981	0.196	464080	-0.176
6/13/2013	4:39:00 PM	5008859.3	461563.0	B6	3	0	2775.93	9.6377	-0.986	0.168	476984	1.686
6/13/2013	4:39:00 PM	5008862.4	461605.4	B6	4	0	2772.53	11.029	-0.976	0.220	481215	1.245
6/13/2013	4:39:00 PM	5008855.8	461670.9	B6	5	0	2766.99	8.7601	-0.970	0.245	462373	0.391
6/13/2013	4:39:00 PM	5008855.4	461711.5	B6	6	0	2764.15	16.517	-0.937	0.349	466135	1.490
6/13/2013	4:39:00 PM	5008866.3	461761.0	B6	7	0	2760.21	10.637	-0.993	0.119	489024	0.482
6/13/2013	4:39:00 PM	5008870.1	461797.3	B6	8	0	2758.54	13.058	-0.972	0.236	476263	1.184
6/13/2013	4:39:00 PM	5008874.3	461836.7	B6	9	0	2755.36	9.4459	-0.976	0.216	468716	0.877
6/13/2013	4:39:00 PM	5008883.5	461875.0	B6	10	0	2754.52	19.448	-0.942	0.335	479567	2.256
6/13/2013	4:39:00 PM	5008639.7	461198.0	B8	1	0	2821.51	7.9959	-0.977	0.214	441220	1.278
6/13/2013	4:39:00 PM	5008648.8	461231.7	B8	2	0	2820.76	9.7354	-0.936	0.352	447377	1.495
6/13/2013	4:39:00 PM	5008680.6	461280.7	B8	3	0	2815.91	17.003	-0.635	0.772	455311	1.944
6/13/2013	4:39:00 PM	5008715.4	461305.2	B8	4	0	2820.32	28.689	-0.548	0.836	448808	2.355
6/13/2013	4:39:00 PM	5008744.8	461334.2	B8	5	0	2812.65	14.527	-0.780	0.626	466167	1.391
6/13/2013	4:39:00 PM	5008756.0	461375.9	B8	6	0	2807.19	30.004	-0.944	0.331	509145	0.178

6/13/2013	4:39:00 PM	5008770.2	461403.8	B8	7	0	2802.94	34.725	-0.894	0.449	506445	3.410
6/13/2013	4:39:00 PM	5008788.1	461436.9	B8	8	0	2804.69	28.184	-0.891	0.455	499182	3.977
6/13/2013	6:14:00 PM	5008896.1	462188.4	B2	1	0	2703.12	10.916	-0.723	0.691	435591	1.002
6/13/2013	6:14:00 PM	5008887.1	462172.0	B2	2	0	2704.63	12.154	-0.791	0.612	436734	0.885
6/13/2013	6:14:00 PM	5008875.1	462159.4	B2	3	0	2703.25	8.4749	-0.852	0.524	442535	0.989
6/13/2013	6:14:00 PM	5008863.2	462146.4	B2	4	0	2702.35	7.7287	-0.860	0.510	445291	1.007
6/13/2013	6:14:00 PM	5008852.8	462129.5	B2	5	0	2703.87	11.763	-0.884	0.467	447233	1.287
6/13/2013	6:14:00 PM	5008843.1	462111.9	B2	6	0	2703	12.531	-0.898	0.440	446168	1.227
6/13/2013	6:14:00 PM	5008835.6	462096.3	B2	7	0	2703.04	11.182	-0.905	0.426	446361	1.224
6/13/2013	6:14:00 PM	5008824.5	462081.0	B2	8	0	2703.05	11.546	-0.873	0.487	441526	1.172
6/13/2013	6:14:00 PM	5008813.3	462064.6	B2	9	0	2702.82	8.396	-0.876	0.483	439398	0.861
6/13/2013	6:14:00 PM	5008800.0	462049.8	B2	10	0	2702.98	9.7867	-0.938	0.345	442776	0.810
6/13/2013	6:14:00 PM	5008779.7	462030.6	B2	11	0	2703.57	9.9584	-0.972	0.236	446644	0.801
6/13/2013	6:14:00 PM	5008819.5	461462.1	B8	9	0	2806.91	18.256	-0.337	0.942	424617	6.184
6/13/2013	6:14:00 PM	5008863.4	461469.7	B8	10	0	2801.67	27.982	0.091	0.996	364865	1.024
6/14/2013	11:00:50AM	5008518.4	461197.2	B7	1	22	2797.3	13.428	-0.812	0.583	449778	-0.472
6/14/2013	11:07:17AM	5008503.0	461180.0	B7	2	49	2798.9	9.1095	-0.592	0.806	429748	0.009
6/14/2013	11:14:15AM	5008480.8	461169.9	B7	3	578	2798.99	12.123	-0.167	0.986	407552	-0.103
6/14/2013	11:17:12AM	5008456.3	461171.9	B7	4	59	2799.29	11.713	0.367	0.930	384610	-0.439
6/14/2013	11:19:40AM	5008438.5	461188.0	B7	5	65	2797.41	10.178	0.636	0.772	367280	-1.009
6/14/2013	11:22:36AM	5008424.9	461208.1	B7	6	70	2796.86	8.9135	0.900	0.436	358650	-0.775
6/14/2013	11:25:53AM	5008403.5	461213.5	B7	7	59	2797.54	9.3551	0.405	0.914	386244	-0.936
6/14/2013	11:28:46AM	5008378.4	461211.6	B7	8	108	2799.31	11.478	0.825	0.565	355874	-1.309
6/14/2013	11:33:12AM	5008370.4	461237.9	B7	9	54	2798.66	18.588	0.968	0.250	301597	-2.232
6/14/2013	12:28:20PM	5008805.3	460616.8	B13	1	493	2994.07	36.347	-0.982	0.191	533258	3.106
6/14/2013	12:43:41PM	5008789.9	460584.9	B13	2	1126	2993.96	31.616	-0.902	0.431	513663	-0.610
6/14/2013	12:57:46PM	5008762.5	460562.6	B13	3	73	2999.67	38.062	-0.824	0.567	506085	3.508
6/14/2013	1:02:23 PM	5008731.8	460541.9	B13	4	974	2998.89	26.679	-0.102	0.995	401304	1.712
6/14/2013	1:06:49 PM	5008694.6	460528.2	B13	5	11	3002.81	33.282	-0.494	0.869	452653	3.694

6/14/2013	1:17:15 PM	5008661.5	460514.3	B13	6	666	3001.42	31.527	0.084	0.996	384877	-0.065
6/14/2013	1:21:39 PM	5008621.8	460501.3	B13	7	56	3004.17	26.762	-0.717	0.697	476517	0.443
6/14/2013	1:24:20 PM	5008580.4	460492.7	B13	8	2100	3006.45	23.638	0.413	0.911	344141	-1.327
6/14/2013	1:38:52 PM	5008544.0	460510.2	B13	9	1932	3005.11	29.513	0.452	0.892	340942	-0.629
6/14/2013	1:53:29 PM	5008503.0	460521.5	B13	10	2195	3002.12	29.637	0.103	0.995	391097	-0.533
6/27/2013	12:00:00PM	5008972.4	460926.1	B12	1	0	2969.58	26.98	-0.852	0.524	496349	2.932
6/27/2013	12:00:00PM	5008986.8	460947.1	B12	2	0	2971.32	21.272	-0.882	0.470	493341	1.117
6/27/2013	12:00:00PM	5009000.6	460962.7	B12	3	0	2975.94	14.201	-0.953	0.304	503337	2.188
6/27/2013	12:00:00PM	5009009.5	460982.4	B12	4	0	2972.84	10.745	-0.946	0.326	490934	2.346
6/27/2013	12:00:00PM	5009019.6	461002.6	B12	5	0	2972.45	17.123	-0.899	0.439	478170	2.070
6/27/2013	12:00:00PM	5009032.5	461019.8	B12	6	0	2970.99	15.06	-0.885	0.466	471844	1.173
6/27/2013	12:00:00PM	5009045.8	461037.9	B12	7	0	2974.03	15.812	-0.968	0.249	484510	1.875
6/27/2013	12:00:00PM	5009053.2	461058.8	B12	8	0	2974.69	12.893	-0.944	0.330	469952	2.270
6/27/2013	12:00:00PM	5009055.6	461079.8	B12	9	0	2973.33	11.847	-0.987	0.158	470486	2.211
6/27/2013	12:00:00PM	5009058.5	461100.6	B12	10	0	2973.14	11.716	-0.990	-0.140	467790	1.807
6/27/2013	12:00:00PM	5009046.7	461115.2	B12	11	0	2972.46	13.744	-0.987	-0.160	477715	2.102
6/27/2013	12:00:00PM	5009041.2	461136.2	B12	12	0	2970.22	15.679	-0.995	0.097	486261	2.208
6/27/2013	12:00:00PM	5009045.2	461157.7	B12	13	0	2970.86	21.05	-0.904	0.427	494646	3.522
6/27/2013	12:00:00PM	5009056.6	461174.1	B12	14	0	2969.85	18.296	-0.659	0.753	465939	3.790
6/27/2013	12:00:00PM	5009073.9	461184.8	B12	15	0	2967.11	21.054	0.273	0.962	396065	4.315
6/27/2013	12:33:15PM	5008802.3	460617.5	B13	1	0	2994.07	36.347	-0.982	0.191	533258	3.106
6/27/2013	12:41:50PM	5008790.0	460584.8	B13	2	462	2993.96	31.616	-0.902	0.431	513663	-0.610
6/27/2013	12:49:26PM	5008759.0	460561.4	B13	3	0	2999.67	38.062	-0.824	0.567	506085	3.508
6/27/2013	12:52:09PM	5008728.9	460542.1	B13	4	433	2998.89	26.679	-0.102	0.995	401304	1.712
6/27/2013	12:55:17PM	5008690.8	460530.2	B13	5	0	3000.61	34.375	-0.659	0.752	475181	3.073
6/27/2013	12:57:21PM	5008658.6	460514.0	B13	6	0	2998.47	31.414	0.148	0.989	379704	1.745
6/27/2013	12:59:48PM	5008619.5	460501.0	B13	7	0	3004.17	26.762	-0.717	0.697	476517	0.443
6/27/2013	1:04:38 PM	5008579.5	460496.4	B13	8	1334	3003.15	23.257	0.405	0.914	346478	-1.047
6/27/2013	1:08:08 PM	5008540.6	460509.6	B13	9	1191	3005.11	29.513	0.452	0.892	340942	-0.629

6/27/2013	1:34:50 PM	5008503.4	460521.4	B13	10	1682	3002.12	29.637	0.103	0.995	391097	-0.533
6/27/2013	1:53:27 PM	5008603.7	460634.1	B11	2	1414	2931.17	26.951	-0.240	0.971	410274	-3.538
6/27/2013	2:05:19 PM	5008626.4	460640.4	B11	1	0	2933.97	20.335	-0.711	0.703	448530	0.565
6/27/2013	2:17:31 PM	5008583.2	460635.8	B11	3	1452	2926.81	30.643	0.123	0.992	370367	-3.877
6/27/2013	2:24:16 PM	5008557.7	460639.5	B11	4	957	2930.35	35.297	0.127	0.992	369127	-0.809
6/27/2013	2:33:58 PM	5008536.2	460642.7	B11	5	0	2931.15	35.29	0.120	0.993	369722	-0.712
6/27/2013	2:37:16 PM	5008513.6	460646.3	B11	6	0	2923.77	34.275	0.031	1.000	382984	-0.288
6/27/2013	2:40:16 PM	5008492.0	460650.0	B11	7	39	2924.12	34.999	0.086	0.996	374063	-1.454
6/27/2013	2:46:25 PM	5008473.3	460652.8	B11	8	286	2924.5	36.348	0.139	0.990	366346	-2.017
6/27/2013	2:50:05 PM	5008450.3	460655.9	B11	9	0	2922.04	24.015	0.262	0.965	353447	-2.955
6/27/2013	2:54:48 PM	5008430.3	460661.8	B11	10	748	2921.79	22.065	0.526	0.851	322037	-3.038
6/27/2013	3:01:22 PM	5008411.8	460667.9	B11	11	754	2926.57	27.761	0.598	0.801	301990	-2.953
6/27/2013	3:05:00 PM	5008273.1	460967.9	B9	1	0	2875.38	11.071	0.893	0.450	325189	-0.640
6/27/2013	3:05:00 PM	5008262.8	460981.4	B9	2	0	2874.25	12.808	0.905	0.425	323088	-0.767
6/27/2013	3:05:00 PM	5008255.0	460993.3	B9	3	0	2873.46	16.182	0.923	0.386	325471	-1.048
6/27/2013	3:05:00 PM	5008247.2	461003.2	B9	4	0	2874.88	16.38	0.946	0.324	322387	-1.136
6/27/2013	3:05:00 PM	5008238.8	461013.5	B9	5	0	2876.66	16.817	0.957	0.291	319089	-0.740
6/27/2013	3:05:00 PM	5008230.5	461023.8	B9	6	0	2878.3	17.793	0.911	0.413	329647	-0.258
6/27/2013	3:05:00 PM	5008220.8	461034.6	B9	7	0	2877.8	14.647	0.820	0.573	336423	-0.233
6/27/2013	3:05:00 PM	5008211.1	461044.5	B9	8	0	2876.28	12.382	0.784	0.621	336033	-0.270
6/27/2013	3:05:00 PM	5008199.1	461057.1	B9	9	0	2874.59	16.997	0.698	0.716	341128	-0.713
6/27/2013	3:05:00 PM	5008188.1	461068.6	B9	10	0	2876.44	20.135	0.760	0.649	338272	-1.550
6/27/2013	3:05:00 PM	5008134.8	461126.4	B9a	1	0	2878.41	25.65	0.932	0.362	265007	-3.022
6/27/2013	3:23:05 PM	5008127.1	461140.2	B9a	2	95	2881.15	27.574	0.953	0.304	251896	-3.512
6/27/2013	3:30:32 PM	5008124.2	461152.9	B9a	3	196	2878.08	29.355	0.957	0.289	244541	-4.757
6/27/2013	3:35:00 PM	5008924.3	460383.7	B15	1	0	3186.02	25.962	-0.591	0.806	482895	1.648
6/27/2013	3:35:00 PM	5008936.2	460394.4	B15	2	0	3185.56	25.678	-0.673	0.740	495211	1.643
6/27/2013	3:35:00 PM	5008950.0	460406.1	B15	3	0	3182.31	33.118	-0.691	0.723	493143	2.509
6/27/2013	3:35:00 PM	5008964.1	460417.9	B15	4	0	3181.51	24.58	-0.684	0.729	490742	2.227

6/27/2013	3:35:00 PM	5008976.7	460429.8	B15	5	0	3181.66	25.273	-0.743	0.669	499685	2.369
6/27/2013	3:35:00 PM	5008990.3	460440.8	B15	6	0	3181.98	26.505	-0.719	0.695	496419	2.366
6/27/2013	3:35:00 PM	5009004.1	460450.5	B15	7	0	3179.69	29.232	-0.775	0.632	497115	2.828
6/27/2013	3:35:00 PM	5009017.2	460461.0	B15	8	0	3184.16	33.722	-0.867	0.498	530628	1.036
6/27/2013	3:35:00 PM	5009032.6	460472.7	B15	9	0	3183.29	32.746	-0.874	0.486	530366	1.125
6/27/2013	3:35:00 PM	5009043.9	460485.1	B15	10	0	3193.92	34.617	-0.912	0.410	548995	4.469
6/27/2013	3:35:00 PM	5008896.1	462188.4	B2	1	0	2703.12	10.916	-0.723	0.691	435591	1.002
6/27/2013	3:35:00 PM	5008887.1	462172.0	B2	2	0	2704.63	12.154	-0.791	0.612	436734	0.885
6/27/2013	3:35:00 PM	5008875.1	462159.4	B2	3	0	2703.25	8.4749	-0.852	0.524	442535	0.989
6/27/2013	3:35:00 PM	5008863.2	462146.4	B2	4	0	2702.35	7.7287	-0.860	0.510	445291	1.007
6/27/2013	3:35:00 PM	5008852.8	462129.5	B2	5	0	2703.87	11.763	-0.884	0.467	447233	1.287
6/27/2013	3:35:00 PM	5008843.1	462111.9	B2	6	0	2703	12.531	-0.898	0.440	446168	1.227
6/27/2013	3:35:00 PM	5008835.6	462096.3	B2	7	0	2703.04	11.182	-0.905	0.426	446361	1.224
6/27/2013	3:35:00 PM	5008824.5	462081.0	B2	8	0	2703.05	11.546	-0.873	0.487	441526	1.172
6/27/2013	3:35:00 PM	5008813.3	462064.6	B2	9	0	2702.82	8.396	-0.876	0.483	439398	0.861
6/27/2013	3:35:00 PM	5008800.0	462049.8	B2	10	0	2702.98	9.7867	-0.938	0.345	442776	0.810
6/27/2013	3:35:00 PM	5008779.7	462030.6	B2	11	0	2703.57	9.9584	-0.972	0.236	446644	0.801
6/27/2013	3:35:00 PM	5008119.0	461170.2	B9a	4	0	2875.98	30.61	0.998	0.065	229856	-5.136
6/27/2013	3:35:00 PM	5008118.3	461187.9	B9a	5	0	2880.74	16.384	1.000	-0.007	222042	-5.119
6/27/2013	3:44:53 PM	5008372.9	461239.4	B7	1	0	2795.71	15.581	0.928	0.372	322721	-3.379
6/27/2013	3:47:13 PM	5008381.4	461211.6	B7	2	0	2798.15	9.9861	0.634	0.773	371755	-1.274
6/27/2013	3:48:25 PM	5008405.3	461213.1	B7	3	0	2797.54	9.3551	0.405	0.914	386244	-0.936
6/27/2013	3:49:36 PM	5008429.5	461208.7	B7	4	0	2796.86	8.9135	0.900	0.436	358650	-0.775
6/27/2013	3:50:50 PM	5008440.1	461188.3	B7	5	0	2797.41	10.178	0.636	0.772	367280	-1.009
6/27/2013	3:52:03 PM	5008445.1	461182.4	B7	1a	0	2797.97	8.9426	0.354	0.935	384180	-0.754
6/27/2013	3:57:52 PM	5008457.2	461171.7	B7	6	0	2799.29	11.713	0.367	0.930	384610	-0.439
6/27/2013	3:59:43 PM	5008479.9	461170.6	B7	3a	0	2798.99	12.123	-0.167	0.986	407552	-0.103
6/27/2013	4:03:33 PM	5008478.2	461169.3	B7	7	360	2798.99	12.123	-0.167	0.986	407552	-0.103
6/27/2013	4:13:09 PM	5008505.1	461180.0	B7	8	0	2798.9	9.1095	-0.592	0.806	429748	0.009

6/27/2013	4:14:13 PM	5008515.9	461187.4	B7	4a	0	2798.67	12.356	-0.726	0.688	441814	-0.111
6/27/2013	4:18:25 PM	5008520.2	461198.3	B7	9	0	2799.25	13.614	-0.915	0.404	456903	0.266
7/10/2013	4:30:00 PM	5008803.2	460617.5	B13	1	0	2994.07	36.347	-0.982	0.191	533258	3.106
7/10/2013	4:30:00 PM	5008787.8	460584.8	B13	2	0	2993.96	31.616	-0.902	0.431	513663	-0.610
7/10/2013	4:30:00 PM	5008760.2	460561.3	B13	3	0	2999.67	38.062	-0.824	0.567	506085	3.508
7/10/2013	4:30:00 PM	5008729.2	460542.6	B13	4	0	2998.89	26.679	-0.102	0.995	401304	1.712
7/10/2013	4:30:00 PM	5008691.7	460529.5	B13	5	0	3000.61	34.375	-0.659	0.752	475181	3.073
7/10/2013	4:30:00 PM	5008658.1	460514.5	B13	6	0	2998.47	31.414	0.148	0.989	379704	1.745
7/10/2013	4:30:00 PM	5008618.7	460501.6	B13	7	0	3004.17	26.762	-0.717	0.697	476517	0.443
7/10/2013	4:39:52 PM	5008580.8	460496.4	B13	8	464	2998.07	32.423	0.314	0.949	357003	-1.995
7/10/2013	4:46:21 PM	5008541.2	460508.8	B13	9	488	3005.11	29.513	0.452	0.892	340942	-0.629
7/10/2013	4:57:39 PM	5008503.2	460521.5	B13	10	647	3002.4	30.768	0.189	0.982	380235	-1.225
7/10/2013	5:30:00 PM	5008687.4	462310.0	B1	1	0	2660.31	11.266	-0.998	0.062	454361	1.640
7/10/2013	5:30:00 PM	5008692.9	462290.0	B1	2	0	2660.68	13.591	-0.996	0.091	458382	0.580
7/10/2013	5:30:00 PM	5008705.5	462274.6	B1	3	0	2665.7	9.043	-0.981	0.194	465303	1.568
7/10/2013	5:30:00 PM	5008704.1	462253.7	B1	4	0	2667.57	6.798	-0.958	0.286	446677	0.816
7/10/2013	5:30:00 PM	5008681.8	462252.3	B1	5	0	2662.71	12.541	-0.706	0.708	437251	-0.083
7/10/2013	5:30:00 PM	5008658.8	462245.5	B1	6	0	2661.85	10.189	-0.629	0.778	429665	-0.542
7/10/2013	5:30:00 PM	5008639.6	462233.1	B1	7	0	2661.12	11.738	-0.425	0.905	410958	-3.164
7/10/2013	5:30:00 PM	5008623.7	462230.9	B1	8	0	2663.26	23.501	0.997	0.073	253621	-4.227
7/10/2013	5:30:00 PM	5008621.4	462253.1	B1	9	0	2663.42	19.082	0.994	0.106	292276	-2.300
7/10/2013	5:30:00 PM	5008617.4	462274.1	B1	10	0	2662.75	7.6325	0.933	0.361	349560	-1.099
7/10/2013	5:30:00 PM	5008649.8	460829.4	B10	1	0	2890.36	14.467	-0.200	0.980	414266	0.983
7/10/2013	5:30:00 PM	5008619.4	460830.6	B10	2	0	2888.7	15.092	-0.204	0.979	415040	0.981
7/10/2013	5:30:00 PM	5008580.4	460822.4	B10	3	0	2886.49	14.79	-0.719	0.695	446014	1.186
7/10/2013	5:30:00 PM	5008544.9	460821.7	B10	4	0	2882.83	12.932	-0.643	0.765	440160	0.900
7/10/2013	5:30:00 PM	5008515.7	460821.8	B10	5	0	2878.86	14.338	-0.684	0.730	438335	-0.805
7/10/2013	5:30:00 PM	5008483.9	460818.8	B10	6	0	2879.59	11.531	0.326	0.945	391407	1.386
7/10/2013	5:30:00 PM	5008455.7	460815.0	B10	7	0	2880.22	14.627	-0.329	0.944	420011	0.609

7/10/2013	5:30:00 PM	5008429.7	460810.9	B10	8	0	2878.85	15.012	-0.474	0.880	428057	0.008
7/10/2013	5:30:00 PM	5008400.5	460806.7	B10	9	0	2879.5	13.257	0.124	0.992	391584	-1.709
7/10/2013	5:30:00 PM	5008623.4	460640.6	B11	1	0	2932.35	23.882	-0.636	0.772	448917	0.126
7/10/2013	5:30:00 PM	5008534.9	460644.7	B11	4	0	2930.35	35.297	0.127	0.992	369127	-0.809
7/10/2013	5:30:00 PM	5008535.0	460645.8	B11	5	0	2923.2	33.672	0.106	0.994	375612	-0.294
7/10/2013	5:30:00 PM	5008491.9	460652.7	B11	6	0	2923.77	34.275	0.031	1.000	382984	-0.288
7/10/2013	5:30:00 PM	5008470.9	460655.9	B11	7	0	2924.12	34.999	0.086	0.996	374063	-1.454
7/10/2013	5:30:00 PM	5008450.2	460659.8	B11	8	0	2920.81	22.581	0.110	0.994	373361	-1.542
7/10/2013	5:30:00 PM	5008430.3	460666.2	B11	9	0	2922.04	24.015	0.262	0.965	353447	-2.955
7/10/2013	5:30:00 PM	5008411.5	460674.0	B11	10	0	2921.79	22.065	0.526	0.851	322037	-3.038
7/10/2013	5:30:00 PM	5008411.8	460667.9	B11	11	0	2923.15	25.146	0.620	0.785	309424	-2.709
7/10/2013	5:30:00 PM	5008972.4	460926.1	B12	1	0	2969.58	26.98	-0.852	0.524	496349	2.932
7/10/2013	5:30:00 PM	5008986.8	460947.1	B12	2	0	2971.32	21.272	-0.882	0.470	493341	1.117
7/10/2013	5:30:00 PM	5009000.6	460962.7	B12	3	0	2975.94	14.201	-0.953	0.304	503337	2.188
7/10/2013	5:30:00 PM	5009009.5	460982.4	B12	4	0	2972.84	10.745	-0.946	0.326	490934	2.346
7/10/2013	5:30:00 PM	5009019.6	461002.6	B12	5	0	2972.45	17.123	-0.899	0.439	478170	2.070
7/10/2013	5:30:00 PM	5009032.5	461019.8	B12	6	0	2970.99	15.06	-0.885	0.466	471844	1.173
7/10/2013	5:30:00 PM	5009045.8	461037.9	B12	7	0	2974.03	15.812	-0.968	0.249	484510	1.875
7/10/2013	5:30:00 PM	5009053.2	461058.8	B12	8	0	2974.69	12.893	-0.944	0.330	469952	2.270
7/10/2013	5:30:00 PM	5009055.6	461079.8	B12	9	0	2973.33	11.847	-0.987	0.158	470486	2.211
7/10/2013	5:30:00 PM	5009058.5	461100.6	B12	10	0	2973.14	11.716	-0.990	-0.140	467790	1.807
7/10/2013	5:30:00 PM	5009046.7	461115.2	B12	11	0	2972.46	13.744	-0.987	-0.160	477715	2.102
7/10/2013	5:30:00 PM	5009041.2	461136.2	B12	12	0	2970.22	15.679	-0.995	0.097	486261	2.208
7/10/2013	5:30:00 PM	5009045.2	461157.7	B12	13	0	2970.86	21.05	-0.904	0.427	494646	3.522
7/10/2013	5:30:00 PM	5009056.6	461174.1	B12	14	0	2969.85	18.296	-0.659	0.753	465939	3.790
7/10/2013	5:30:00 PM	5009073.9	461184.8	B12	15	0	2967.11	21.054	0.273	0.962	396065	4.315
7/10/2013	5:30:00 PM	5008473.0	460326.3	B14	1	0	3103.89	23.494	-0.508	0.861	463618	2.152
7/10/2013	5:30:00 PM	5008509.4	460335.0	B14	2	0	3106.34	31.678	-0.516	0.856	465892	1.991
7/10/2013	5:30:00 PM	5008542.9	460340.3	B14	3	0	3105.81	33.063	-0.525	0.851	468239	2.757

7/10/2013	5:30:00 PM	5008579.9	460344.1	B14	4	0	3110.9	38.404	-0.178	0.984	421347	1.292
7/10/2013	5:30:00 PM	5008614.7	460346.2	B14	5	0	3112.19	40.86	-0.009	1.000	394256	0.360
7/10/2013	5:30:00 PM	5008652.7	460344.1	B14	6	0	3112.53	44.541	-0.036	0.999	392603	-0.125
7/10/2013	5:30:00 PM	5008682.2	460343.4	B14	7	0	3113.79	46.354	-0.137	0.991	406624	-0.223
7/10/2013	5:30:00 PM	5008716.1	460348.6	B14	8	0	3111.55	47.605	-0.255	0.967	422508	0.409
7/10/2013	5:30:00 PM	5008752.7	460355.0	B14	9	0	3118.9	46.241	-0.359	0.933	437957	0.543
7/10/2013	5:30:00 PM	5008779.0	460366.1	B14	10	0	3113.24	36.86	-0.529	0.848	466242	0.803
7/10/2013	5:30:00 PM	5008810.3	460381.7	B14	11	0	3125.33	30.895	-0.761	0.649	507896	0.242
7/10/2013	5:30:00 PM	5008871.9	460445.8	B14	12	0	3117.46	43.262	-0.812	0.584	519241	0.957
7/10/2013	5:30:00 PM	5008872.0	460445.7	B14	13	0	3115.07	34.055	-0.761	0.649	511247	4.469
7/10/2013	5:30:00 PM	5008924.3	460383.7	B15	1	0	3186.02	25.962	-0.591	0.806	482895	1.648
7/10/2013	5:30:00 PM	5008936.2	460394.4	B15	2	0	3185.56	25.678	-0.673	0.740	495211	1.643
7/10/2013	5:30:00 PM	5008950.0	460406.1	B15	3	0	3182.31	33.118	-0.691	0.723	493143	2.509
7/10/2013	5:30:00 PM	5008964.1	460417.9	B15	4	0	3184.69	27.73	-0.663	0.748	492350	1.738
7/10/2013	5:30:00 PM	5008976.7	460429.8	B15	5	0	3181.66	25.273	-0.743	0.669	499685	2.369
7/10/2013	5:30:00 PM	5008990.3	460440.8	B15	6	0	3181.98	25.296	-0.719	0.695	496419	2.366
7/10/2013	5:30:00 PM	5009004.1	460450.5	B15	7	0	3179.69	29.232	-0.775	0.632	497115	2.828
7/10/2013	5:30:00 PM	5009017.2	460461.0	B15	8	0	3184.16	33.722	-0.867	0.498	530628	1.036
7/10/2013	5:30:00 PM	5009032.6	460472.7	B15	9	0	3183.29	32.746	-0.874	0.486	530366	1.125
7/10/2013	5:30:00 PM	5009043.9	460485.1	B15	10	0	3193.92	34.617	-0.912	0.410	548995	4.469
7/10/2013	5:30:00 PM	5008896.1	462188.4	B2	1	0	2703.57	9.9584	-0.972	0.236	446644	0.801
7/10/2013	5:30:00 PM	5008887.1	462172.0	B2	2	0	2702.98	9.7867	-0.938	0.345	442776	0.810
7/10/2013	5:30:00 PM	5008875.1	462159.4	B2	3	0	2702.82	8.396	-0.876	0.483	439398	0.861
7/10/2013	5:30:00 PM	5008863.2	462146.4	B2	4	0	2703.05	11.546	-0.873	0.487	441526	1.172
7/10/2013	5:30:00 PM	5008852.8	462129.5	B2	5	0	2703.04	11.182	-0.905	0.426	446361	1.224
7/10/2013	5:30:00 PM	5008843.1	462111.9	B2	6	0	2703	12.531	-0.898	0.440	446168	1.227
7/10/2013	5:30:00 PM	5008835.6	462096.3	B2	7	0	2703.87	11.763	-0.884	0.467	447233	1.287
7/10/2013	5:30:00 PM	5008824.5	462081.0	B2	8	0	2702.35	7.7287	-0.860	0.510	445291	1.007
7/10/2013	5:30:00 PM	5008813.3	462064.6	B2	9	0	2704.11	10.256	-0.846	0.533	440062	0.907

7/10/2013	5:30:00 PM	5008800.0	462049.8	B2	10	0	2704.63	12.154	-0.791	0.612	436734	0.885
7/10/2013	5:30:00 PM	5008779.7	462030.6	B2	11	0	2703.12	10.916	-0.723	0.691	435591	1.002
7/10/2013	5:30:00 PM	5008653.7	461899.2	B3	1	0	2704.08	25.184	-0.915	0.404	485288	0.771
7/10/2013	5:30:00 PM	5008645.9	461881.4	B3	2	0	2706.08	15.366	-0.932	0.361	472150	0.206
7/10/2013	5:30:00 PM	5008634.1	461861.2	B3	3	0	2708.15	10.198	-0.952	0.306	483421	-0.100
7/10/2013	5:30:00 PM	5008624.5	461838.3	B3	4	0	2707.2	20.179	-0.900	0.437	459371	-1.553
7/10/2013	5:30:00 PM	5008604.0	461837.1	B3	5	0	2705.7	13.622	-0.277	0.961	408265	-1.942
7/10/2013	5:30:00 PM	5008584.6	461840.3	B3	6	0	2706.11	6.5474	1.000	-0.012	308621	-3.333
7/10/2013	5:30:00 PM	5008586.1	461859.3	B3	7	0	2703.56	11.134	1.000	0.029	312870	-3.576
7/10/2013	5:30:00 PM	5008588.7	461882.2	B3	8	0	2703.92	11.21	0.998	-0.055	280433	-2.386
7/10/2013	5:30:00 PM	5008592.7	461902.3	B3	9	0	2704.42	10.831	0.998	-0.067	281086	-1.792
7/10/2013	5:30:00 PM	5008596.5	461921.5	B3	10	0	2704.78	9.9795	1.000	0.030	290033	-1.149
7/10/2013	5:30:00 PM	5008547.9	461973.5	B4	1	0	2711.66	14.347	0.985	0.171	324631	-0.884
7/10/2013	5:30:00 PM	5008548.2	461959.9	B4	2	0	2713.26	13.732	0.987	0.161	330040	-1.008
7/10/2013	5:30:00 PM	5008546.9	461944.8	B4	3	0	2713.59	13.289	0.991	0.134	330093	-1.034
7/10/2013	5:30:00 PM	5008545.6	461929.1	B4	4	0	2716.14	13.595	0.996	0.085	327961	-1.046
7/10/2013	5:30:00 PM	5008543.6	461913.5	B4	5	0	2716.47	13.797	0.999	0.032	326280	-1.133
7/10/2013	5:30:00 PM	5008542.1	461900.4	B4	6	0	2716.54	14.056	1.000	0.022	324416	-1.143
7/10/2013	5:30:00 PM	5008540.6	461886.0	B4	7	0	2716.56	14.238	1.000	-0.001	323001	-1.227
7/10/2013	5:30:00 PM	5008537.6	461871.0	B4	8	0	2716.54	14.113	1.000	0.013	323624	-1.408
7/10/2013	5:30:00 PM	5008534.3	461856.0	B4	9	0	2718.78	7.0446	0.999	0.047	323846	-1.406
7/10/2013	5:30:00 PM	5008532.7	461842.3	B4	10	0	2719.29	7.9671	0.976	0.217	325718	-1.330
7/10/2013	5:30:00 PM	5008530.7	461825.5	B4	11	0	2721.34	10.194	0.986	0.168	319124	-0.211
7/10/2013	5:30:00 PM	5008528.7	461810.5	B4	12	0	2721.88	9.5018	0.994	0.109	313589	-0.463
7/10/2013	5:30:00 PM	5008323.8	461660.3	B5	1	0	2767.43	11.013	0.879	-0.477	336051	-4.157
7/10/2013	5:30:00 PM	5008335.7	461631.0	B5	2	0	2763.88	16.434	0.973	-0.231	301117	-3.379
7/10/2013	5:30:00 PM	5008339.3	461602.5	B5	3	0	2759.44	10.735	0.999	0.041	290468	-3.770
7/10/2013	5:30:00 PM	5008342.3	461581.0	B5	4	0	2759.88	10.396	0.992	0.126	289278	-3.578
7/10/2013	5:30:00 PM	5008347.0	461558.2	B5	5	0	2762.84	12.064	0.928	0.373	301412	-2.530

7/10/2013	5:30:00 PM	5008353.8	461530.4	B5	6	0	2765.63	7.9951	0.866	0.499	322043	-2.418
7/10/2013	5:30:00 PM	5008360.3	461506.6	B5	7	0	2767.61	10.036	0.849	0.528	335069	-2.882
7/10/2013	5:30:00 PM	5008367.9	461486.1	B5	8	0	2767.73	8.5308	0.878	0.478	346228	-2.589
7/10/2013	5:30:00 PM	5008371.1	461465.5	B5	9	0	2769.8	14.564	0.930	0.369	321806	-3.325
7/10/2013	5:30:00 PM	5008375.5	461446.5	B5	10	0	2769.49	12.757	0.909	0.416	332009	-3.042
7/10/2013	5:30:00 PM	5008826.5	461512.0	B6	1	0	2778.29	20.872	0.103	0.995	373645	-1.942
7/10/2013	5:30:00 PM	5008853.8	461525.2	B6	2	0	2778.45	9.3273	-0.981	0.196	464080	-0.176
7/10/2013	5:30:00 PM	5008859.3	461563.0	B6	3	0	2775.93	9.6377	-0.986	0.168	476984	1.686
7/10/2013	5:30:00 PM	5008862.4	461605.4	B6	4	0	2772.53	11.029	-0.976	0.220	481215	1.245
7/10/2013	5:30:00 PM	5008855.8	461670.9	B6	5	0	2766.99	8.7601	-0.970	0.245	462373	0.391
7/10/2013	5:30:00 PM	5008855.4	461711.5	B6	6	0	2764.15	16.517	-0.937	0.349	466135	1.490
7/10/2013	5:30:00 PM	5008866.3	461761.0	B6	7	0	2760.21	10.637	-0.993	0.119	489024	0.482
7/10/2013	5:30:00 PM	5008870.1	461797.3	B6	8	0	2758.54	13.058	-0.972	0.236	476263	1.184
7/10/2013	5:30:00 PM	5008874.3	461836.7	B6	9	0	2755.36	9.4459	-0.976	0.216	468716	0.877
7/10/2013	5:30:00 PM	5008883.5	461875.0	B6	10	0	2754.52	19.448	-0.942	0.335	479567	2.256
7/10/2013	5:30:00 PM	5008371.1	461239.4	B7	1	0	2798.66	18.588	0.968	0.250	301597	-2.232
7/10/2013	5:30:00 PM	5008379.2	461212.3	B7	2	0	2799.31	11.478	0.825	0.565	355874	-1.309
7/10/2013	5:30:00 PM	5008403.6	461214.4	B7	3	0	2797.54	9.3551	0.405	0.914	386244	-0.936
7/10/2013	5:30:00 PM	5008424.9	461208.9	B7	4	0	2796.86	8.9135	0.900	0.436	358650	-0.775
7/10/2013	5:30:00 PM	5008438.6	461188.6	B7	5	0	2797.41	10.178	0.636	0.772	367280	-1.009
7/10/2013	5:30:00 PM	5008456.6	461172.3	B7	6	0	2799.29	11.713	0.367	0.930	384610	-0.439
7/10/2013	5:30:00 PM	5008480.5	461170.6	B7	7	0	2798.99	12.123	-0.167	0.986	407552	-0.103
7/10/2013	5:30:00 PM	5008502.4	461181.0	B7	8	0	2798.9	9.1095	-0.592	0.806	429748	0.009
7/10/2013	5:30:00 PM	5008517.8	461197.9	B7	9	0	2797.3	13.428	-0.812	0.583	449778	-0.472
7/10/2013	5:30:00 PM	5008639.7	461198.0	B8	1	0	2821.51	7.9959	-0.977	0.214	441220	1.278
7/10/2013	5:30:00 PM	5008648.8	461231.7	B8	2	0	2820.76	9.7354	-0.936	0.352	447377	1.495
7/10/2013	5:30:00 PM	5008680.6	461280.7	B8	3	0	2815.91	17.003	-0.635	0.772	455311	1.944
7/10/2013	5:30:00 PM	5008715.4	461305.2	B8	4	0	2820.32	28.689	-0.548	0.836	448808	2.355
7/10/2013	5:30:00 PM	5008744.8	461334.2	B8	5	0	2812.65	14.527	-0.780	0.626	466167	1.391

7/10/2013	5:30:00 PM	5008756.0	461375.9	B8	6	0	2807.19	30.004	-0.944	0.331	509145	0.178
7/10/2013	5:30:00 PM	5008770.2	461403.8	B8	7	0	2802.94	34.725	-0.894	0.449	506445	3.410
7/10/2013	5:30:00 PM	5008788.1	461436.9	B8	8	0	2804.69	28.184	-0.891	0.455	499182	3.977
7/10/2013	5:30:00 PM	5008819.5	461462.1	B8	9	0	2806.91	18.256	-0.337	0.942	424617	6.184
7/10/2013	5:30:00 PM	5008863.4	461469.7	B8	10	0	2801.67	27.982	0.091	0.996	364865	1.024
7/10/2013	5:30:00 PM	5008273.1	460967.9	B9	1	0	2875.38	11.071	0.893	0.450	325189	-0.640
7/10/2013	5:30:00 PM	5008262.8	460981.4	B9	2	0	2874.25	12.808	0.905	0.425	323088	-0.767
7/10/2013	5:30:00 PM	5008255.0	460993.3	B9	3	0	2873.46	16.182	0.923	0.386	325471	-1.048
7/10/2013	5:30:00 PM	5008247.2	461003.2	B9	4	0	2874.88	16.38	0.946	0.324	322387	-1.136
7/10/2013	5:30:00 PM	5008238.8	461013.5	B9	5	0	2876.66	16.817	0.957	0.291	319089	-0.740
7/10/2013	5:30:00 PM	5008230.5	461023.8	B9	6	0	2878.3	17.793	0.911	0.413	329647	-0.258
7/10/2013	5:30:00 PM	5008220.8	461034.6	B9	7	0	2877.8	14.647	0.820	0.573	336423	-0.233
7/10/2013	5:30:00 PM	5008211.1	461044.5	B9	8	0	2876.28	12.382	0.784	0.621	336033	-0.270
7/10/2013	5:30:00 PM	5008199.1	461057.1	B9	9	0	2874.59	16.997	0.698	0.716	341128	-0.713
7/10/2013	5:30:00 PM	5008188.1	461068.6	B9	10	0	2876.44	20.135	0.760	0.649	338272	-1.550
7/10/2013	5:30:00 PM	5008134.8	461126.4	B9a	1	0	2878.41	25.65	0.932	0.362	265007	-3.022
7/10/2013	5:30:00 PM	5008128.6	461140.4	B9a	2	0	2876.96	26.746	0.936	0.352	257975	-3.274
7/10/2013	5:30:00 PM	5008122.9	461154.7	B9a	3	0	2878.08	29.355	0.957	0.289	244541	-4.757
7/10/2013	5:30:00 PM	5008119.0	461170.2	B9a	4	0	2875.98	30.61	0.998	0.065	229856	-5.136
7/10/2013	5:30:00 PM	5008118.3	461187.9	B9a	5	0	2880.74	16.384	1.000	-0.007	222042	-5.119
7/10/2013	5:34:18 PM	5008603.5	460633.7	B11	2	1302	2931.17	26.951	-0.240	0.971	410274	-3.538
7/10/2013	5:44:02 PM	5008584.7	460637.1	B11	3	1044	2926.81	30.643	0.123	0.992	370367	-3.877

APPENDIX B

DIAGNOSTIC PLOTS FOR THE PHYSIOGRAPHIC VARIABLES

Basin A: Accumulation Period

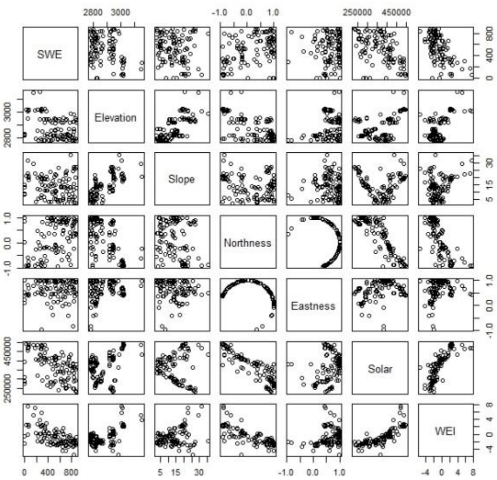

Basin B: Accumulation Period

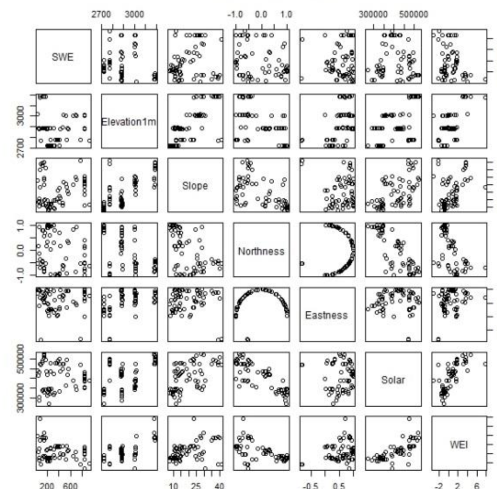

Basin A: Peak SWE Period

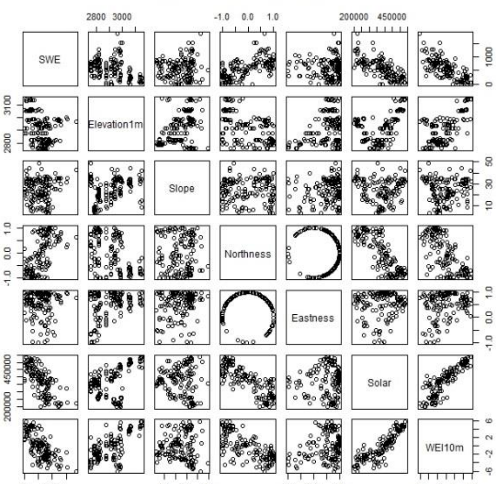

Basin B: Peak SWE Period

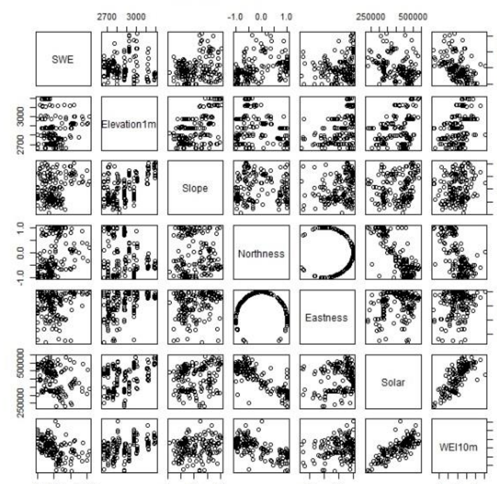

Basin A: Ablation Period

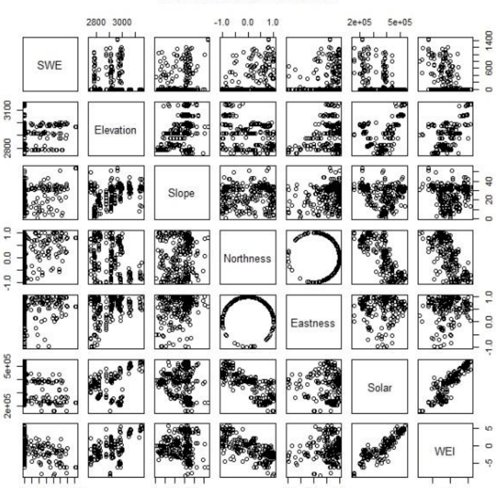

Basin B: Ablation Period

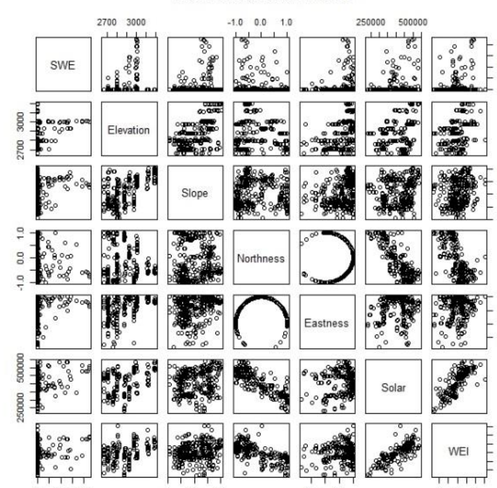

APPENDIX C

CORRELATION MATRICES FOR THE PHYSIOGRAPHIC VARIABLES

Basin A: Accumulation Period

	SWE	Elevation	Slope	Northness	Eastness	Solar	WEI
SWE	1.00000	-0.32513	0.05374	0.38866	-0.00200	0.46455	-0.54828
Elevation	-0.32513	1.00000	0.62806	-0.49241	0.30810	-0.48002	0.62584
Slope	0.05374	0.62806	1.00000	-0.02000	0.29061	-0.08782	0.08818
Northness	0.38866	0.49241	-0.02000	1.00000	-0.17633	-0.75181	-0.64327
Eastness	0.00200	0.30810	0.29061	-0.17633	1.00000	0.20821	0.15481
Solar	-0.48002	0.46455	-0.08782	-0.64327	0.20821	0.78829	1.00000
WEI	-0.54828	0.62584	0.08818	-0.75181	0.15481	1.00000	0.78829

Basin B: Accumulation Period

	SWE	Elevation	Slope	Northness	Eastness	Solar	WEI
SWE	1.00000	-0.03335	0.54344	-0.24250	0.03653	-0.05336	-0.29830
Elevation	-0.03335	1.00000	0.67690	-0.41312	0.43979	0.44082	0.61085
Slope	0.15402	0.67690	1.00000	-0.52313	-0.05833	0.54344	0.35912
Northness	-0.24250	-0.41312	0.52313	1.00000	0.05399	-0.81038	-0.54031
Eastness	0.03653	0.43979	-0.05833	0.05399	1.00000	0.00516	0.24803
Solar	0.05336	0.44082	0.35912	-0.81038	0.00516	1.00000	1.00000
WEI	-0.29830	0.61085	0.15402	-0.54031	0.24803	0.69719	0.69719

Basin A: Peak SWE Period

	SWE	Elevation	Slope	Northness	Eastness	Solar	WEI
SWE	1.00000	-0.33664	0.10084	0.62411	0.00591	-0.73682	-0.70856
Elevation	-0.33664	1.00000	0.42104	-0.43883	0.08138	0.46549	0.65117
Slope	0.10084	0.42104	1.00000	-0.00234	0.18883	-0.06629	0.01541
Northness	0.62411	-0.43883	-0.00234	1.00000	-0.09508	-0.81439	-0.69366
Eastness	-0.73682	0.34968	0.18883	0.81439	1.00000	0.08138	0.22884
Solar	0.00591	0.46549	-0.06629	-0.09508	0.34968	1.00000	0.87437
WEI	-0.70856	0.65117	0.01541	0.69366	0.22884	0.87437	1.00000

Basin B: Peak SWE Period

	SWE	Elevation	Slope	Northness	Eastness	Solar	WEI
SWE	1.00000	-0.14224	0.19547	0.48252	0.07313	-0.55402	-0.58932
Elevation	-0.14224	1.00000	0.50394	-0.29452	0.37952	0.36791	0.47360
Slope	0.19547	0.50394	1.00000	-0.01787	0.22515	0.03260	1.00000
Northness	0.48252	-0.29452	-0.01787	1.00000	0.22169	-0.80466	-0.67153
Eastness	0.07313	0.37952	0.22169	-0.10306	1.00000	0.12503	0.22515
Solar	-0.55402	0.36791	0.03260	-0.80466	0.12503	0.83376	0.83376
WEI	-0.58932	0.47360	0.07221	-0.67153	0.10306	1.00000	0.07221

Basin A: Ablation Period

	SWE	Elevation	Slope	Northness	Eastness	Solar	WEI
SWE	1.00000	-0.02560	0.14079	0.34085	0.10108	-0.42746	-0.42918
Elevation	-0.02560	1.00000	0.49866	-0.37367	0.34675	0.31723	0.51138
Slope	0.14079	0.49866	1.00000	0.06595	0.26250	-0.16535	-0.03349
Northness	0.34085	-0.37367	0.06595	1.00000	-0.01985	-0.81125	-0.71517
Eastness	0.10108	0.34675	0.26250	-0.01985	1.00000	-0.01111	0.16232
Solar	-0.42746	0.31723	-0.16535	-0.81125	-0.01111	1.00000	0.88070
WEI	-0.42918	0.51138	-0.03349	-0.71517	0.16232	0.88070	1.00000

Basin B: Ablation Period

	SWE	Elevation	Slope	Northness	Eastness	Solar	WEI
SWE	1.00000	0.20386	0.23904	-0.04823	0.16507	0.12549	0.11586
Elevation	0.20386	1.00000	0.12222	-0.04987	0.39909	0.29384	0.28743
Slope	0.23904	0.61440	0.61440	0.04262	0.28163	0.13007	0.12222
Northness	-0.04823	-0.04987	0.04262	1.00000	0.06582	-0.82970	-0.66143
Eastness	0.16507	0.39909	0.28163	0.06582	1.00000	0.06088	0.13252
Solar	0.12549	0.29384	0.13007	-0.82970	0.06088	1.00000	0.79068
WEI	0.11586	0.28743	1.00000	-0.66143	0.13252	0.79068	1.00000

APPENDIX D

SIMPLE AND MULTIPLE LINEAR REGRESSION *R* CODE

<u>Basin A</u>

```
model1Aa = lm(SWE ~ Elevation, data=SWEdataA)
summary(model1Aa)
AIC(model1Aa, k=2)

model1Ab = lm(SWE ~ Slope, data=SWEdataA)
summary(model1Ab)
AIC(model1Ab, k=2)

model1Ac = lm(SWE ~ Northness, data=SWEdataA)
summary(model1Ac)
AIC(model1Ac, k=2)

model1Ad = lm(SWE ~ Solar, data=SWEdataA)
summary(model1Ad)
AIC(model1Ad, k=2)


model1Ae = lm(SWE ~ AvyZone, data=SWEdataA)
summary(model1Ae)
AIC(model1Ae, k=2)

model1Af = lm(SWE ~ Eastness, data=SWEdataA)
summary(model1Af)
AIC(model1Af, k=2)

model1Ag = lm(SWE ~ WEI, data=SWEdataA)
summary(model1Ag)
AIC(model1Ag, k=2)
```

2 Variables

```
model2Aa = lm(SWE ~ Slope + Solar, data=SWEdataA)
summary(model2Aa)
AIC(model2Aa, k=2)
vif(model2Aa)

model2Ab = lm(SWE ~ Solar + Eastness, data=SWEdataA)
summary(model2Ab)
AIC(model2Ab, k=2)
vif(model2Ab)
```

```
model2Ac = lm(SWE ~ Slope + Northness, data=SWEdataA)
summary(model2Ac)
AIC(model2Ac)

model2Ad = lm(SWE ~ Slope + Elevation, data=SWEdataA)
summary(model2Ad)

model2Ae = lm(SWE ~ Northness + Elevation1m, data=SWEdataA)
summary(model2Ae)
AIC(model2Ae)
vif(model2Ae)

model2Af = lm(SWE ~ AvyZone + Elevation, data=SWEdataA)
summary(model2Af)
AIC(model2Af)

model2Ag = lm(SWE ~ Solar + Elevation, data=SWEdataA)
summary(model2Ag)
AIC(model2Ag)
vif(model2Ag)

model2Ah = lm(SWE ~ Solar + AvyZone, data=SWEdataA)
summary(model2Ah)
AIC(model2Ah)

model2Ai = lm(SWE ~ WEI + Slope, data=SWEdataA)
summary(model2Ai)
AIC(model2Ai)
vif(model2Ai)

model2Aj = lm(SWE ~ WEI + Northness, data=SWEdataA)
summary(model2Aj)
AIC(model2Aj)
vif(model2Aj)

model2Ak = lm(SWE ~ WEI10m + AvyZone, data=SWEdataA)
summary(model2Ak)
AIC(model2Ak)

model2Al = lm(SWE ~ WEI + Elevation, data=SWEdataA)
summary(model2Al)
AIC(model2Al)
vif(model2Al)
```

```
model2Am = lm(SWE ~ WEI + Eastness, data=SWEdataA)
summary(model2Am)
AIC(model2Am)
vif(model2Am)


model2An = lm(SWE ~ WEI + Slope, data=SWEdataA)
summary(model2An)
AIC(model2An)
vif(model2An)
```

3 Variables

```
model3Aa = lm(SWE ~ Solar + Slope + Northness, data=SWEdataA)
summary(model3Aa)
AIC(model3Aa)

model3Ab = lm(SWE ~ Elevation + Slope + Northness, data=SWEdataA)
summary(model3Ab)

model3Ac = lm(SWE ~ Elevation + Slope + Solar, data=SWEdata)
summary(model3Ac)

model3Ad = lm(SWE ~ Elevation + Slope + Eastness, data=SWEdataA)
summary(model3Ad)

model3Ae = lm(SWE ~ AvyZone + Solar + Elevation, data=SWEdataA)
summary(model3Ae)
AIC(model3Ae)

model3Af = lm(SWE ~ Slope + Solar + Elevation1m, data=SWEdataA)
summary(model3Af)
AIC(model3Af)
vif(model3Af)

model3Ag = lm(SWE ~ WEI + Northness + Elevation, data=SWEdataA)
summary(model3Ag)
AIC(model3Ag)
vif(model3Ag)

model3Ah = lm(SWE ~ Elevation + Solar + Eastness, data=SWEdataA)
summary(model3Ah)
```

```
AIC(model3Ah)
vif(model3Ah)

model3Ai = lm(SWE ~ WEI + Northness + Eastness, data=SWEdataA)
summary(model3Ai)
AIC(model3Ai)
vif(model3Ai)

model3Aj = lm(SWE ~ WEI + Eastness + Slope, data=SWEdataA)
summary(model3Aj)
AIC(model3Aj)
vif(model3Aj)

model3Ak = lm(SWE ~ Elevation1m + Solar + Slope, data=SWEdataA)
summary(model3Ak)
AIC(model3Ak)

model3Al = lm(SWE ~ Solar + Slope + Eastness, data=SWEdataA)
summary(model3Al)
AIC(model3Al)

model3Am = lm(SWE ~ WEI + Slope + Elevation, data=SWEdataA)
summary(model3Am)
AIC(model3Am)
vif(model3Am)

model3An = lm(SWE ~ WEI + Eastness + Elevation, data=SWEdataA)
summary(model3An)
AIC(model3An)
vif(model3Am)
```

4 Variables

```
model4Aa = lm(SWE ~ Eastness + Slope + WEI + Northness, data=SWEdataA)
summary(model4Aa)
AIC(model4Aa)
vif(model4Aa)


model4Ab = lm(SWE ~ Elevation + Northness + WEI + Eastness, data=SWEdataA)
summary(model4Ab)
AIC(model4Ab)
```

```
vif(model4Ab)

model4Ac = lm(SWE ~ Northness + Slope + WEI + Elevation, data=SWEdataA)
summary(model4Ac)
AIC(model4Ac)
vif(model4Ac)

model4Ad = lm(SWE ~ WEI + Eastness + Slope + Elevation, data=SWEdataA)
summary(model4Ad)
AIC(model4Ad)
vif(model4Ad)

model4Ae = lm(SWE ~ Solar + Eastness + Slope + Elevation, data=SWEdataA)
summary(model4Ae)
AIC(model4Ae)
vif(model4Ae)
```

5 Variables

```
model5Aa = lm(SWE ~ Elevation + Solar + Northness + Eastness + WEI,
data=SWEdataA)
summary(model5Aa)
AIC(model5Aa)

model5Ab = lm(SWE ~ Elevation + Northness + Slope + Eastness + WEI,
data=SWEdataA)
summary(model5Ab)
AIC(model5Ab)
vif(model5Ab)

model5Ac = lm(SWE ~ Slope + Elevation + Solar + Eastness + WEI, data=SWEdataA)
summary(model5Ac)
AIC(model5Ac)
```

6 Variables

```
model6A = lm(SWE ~ Elevation + Slope + Northness + Solar + Eastness + WEI,
data=SWEdataA)
summary(model6A)
AIC(model6A)

step(AIC)
```

```
fit<-lm(SWE ~ Elevation1m + Slope + Northness + Eastness + SolClass + WEI10m +
AvyZone, data=SWEdataA)
step<-stepAIC(fit, direction="both")
```

<u>Basin B</u>

1 Variable

```
model1Ba = lm(SWE ~ Elevation, data=SWEdataB)
summary(model1Ba)
AIC(model1Ba, k=2)

model1Bb = lm(SWE ~ Slope, data=SWEdataB)
summary(model1Bb)
AIC(model1Bb, k=2)

model1Bc = lm(SWE ~ Northness, data=SWEdataB)
summary(model1Bc)
AIC(model1Bc, k=2)

model1Bd = lm(SWE ~ Solar, data=SWEdataB)
summary(model1Bd)
AIC(model1Bd, k=2)

model1Be = lm(SWE ~ Eastness, data=SWEdataB)
summary(model1Be)
AIC(model1Be, k=2)

model1Bf = lm(SWE ~ WEI, data=SWEdataB)
summary(model1Bf)
AIC(model1Bf, k=2)

model1Bg = lm(SWE ~ WEI, data=SWEdataB)
summary(model1Bg)
AIC(model1Bg, k=2)
```

2 Variables

```
model2Ba = lm(SWE ~ Northness + Slope, data=SWEdataB)
summary(model2Ba)
AIC(model2Ba)
vif(model2Ba)
```

```
model2Bb = lm(SWE ~ Solar + Eastness, data=SWEdataB)
summary(model2Bb)
AIC(model2Bb)

model2Bc = lm(SWE ~ Elevation + Eastness, data=SWEdataB)
summary(model2Bc)
AIC(model2Bc)
vif(model2Bc)

model2Bd = lm(SWE ~ Slope + Eastness, data=SWEdataB)
summary(model2Bd)
AIC(model2Bd)
vif(model2Bd)

model2Be = lm(SWE ~ WEI + Slope, data=SWEdataB)
summary(model2Be)
AIC(model2Be)
vif(model2Be)

model2Bf = lm(SWE ~ Eastness + Solar, data=SWEdataB)
summary(model2Bf)
AIC(model2Bf)
vif(model2Bf)

model2Bg = lm(SWE ~ WEI + Elevation, data=SWEdataB)
summary(model2Bg)
AIC(model2Bg)
vif(model2Bg)


model2Bh = lm(SWE ~ WEI + Eastness, data=SWEdataB)
summary(model2Bh)
AIC(model2Bh)
vif(model2Bh)

model2Bi = lm(SWE ~ WEI + Northness, data=SWEdataB)
summary(model2Bi)
AIC(model2Bi)
vif(model2Bi)
```

3 Variables

```
model3Ba = lm(SWE ~ WEI + Slope + Eastness, data=SWEdataB)
summary(model3Ba)
AIC(model3Ba)
vif(model3Ba)

model3Bb = lm(SWE ~ Slope + Northness + Eastness, data=SWEdataB)
summary(model3Bb)
AIC(model3Bb)
vif(model3Bb)

model3Bc = lm(SWE ~ WEI + Northness + Slope, data=SWEdataB)
summary(model3Bc)
AIC(model3Bc)
vif(model3Bc)

model3Bd = lm(SWE ~ Solar + Slope + Eastness, data=SWEdataB)
summary(model3Bd)
AIC(model3Bd)
vif(model3Bd)

model3Be = lm(SWE ~ Elevation + Slope + WEI, data=SWEdataB)
summary(model3Be)
AIC(model3Be)
vif(model3Be)

model3Bh = lm(SWE ~ Northness + WEI + Eastness, data=SWEdataB)
summary(model3Bh)
AIC(model3Bh)
vif(model3Bh)

model3Bi = lm(SWE ~ AvyZone + SolClass + Elevation, data=SWEdataB)
summary(model3Bi)
AIC(model3Bi)

model3Bf = lm(SWE ~ Elevation + Solar + Eastness, data=SWEdataB)
summary(model3Bf)
AIC(model3Bf)
vif(model3Bf)

model3Bg = lm(SWE ~ Elevation + WEI + Eastness, data=SWEdataB)
summary(model3Bg)
AIC(model3Bg)
vif(model3Bg)
```

```
model3Bh = lm(SWE ~ Elevation + Slope + Eastness, data=SWEdataB)
summary(model3Bh)
AIC(model3Bh)
vif(model3Bh)

model4Ba = lm(SWE ~ Slope + Elevation + WEI + Eastness, data=SWEdataB)
summary(model4Ba)
AIC(model4Ba)
vif(model4Ba)

model4Bb = lm(SWE ~ Slope + Eastness + WEI + Northness, data=SWEdataB)
summary(model4Bb)
AIC(model4Bb)
vif(model4Bb)

model4Bc = lm(SWE ~ Solar + Slope + Elevation + Eastness, data=SWEdataB)
summary(model4Bc)
AIC(model4Bc)
vif(model4Bc)

model4Bd = lm(SWE ~ Elevation + WEI + Slope + Northness, data=SWEdataB)
summary(model4Bd)
AIC(model4Bd)
vif(model4Bd)


model5Ba = lm(SWE ~ Northness + Slope + Solar + Eastness + Elevation,
data=SWEdataB)
summary(model5Ba)
AIC(model5Ba)

model5Bb = lm(SWE ~ WEI + Northness + Elevation + Eastness + Slope,
data=SWEdataB)
summary(model5Bb)
AIC(model5Bb)
vif(model5Bb)

model5Bc = lm(SWE ~ WEI + Slope + Solar + Eastness + Elevation, data=SWEdataB)
summary(model5Bc)
AIC(model5Bc)

model6B = lm(SWE ~ WEI + Elevation + Slope + Northness + Eastness + Solar,
data=SWEdataB)
```

```
summary(model6B)
AIC(model6B)
```

APPENDIX E

BINARY REGRESSION TREE *R* CODE

Basin A

```
library(rpart)

BRTbsA <- rpart(SWE ~ Elevation + Slope + Northness + Eastness + Solar + WEI,
cp=0, method="anova", data=SWEdataA)
printcp(BRTbsA)
plotcp(BRTbsA)
summary(BRTbsA)
par(mfrow=c(1,2))
rsq.rpart(BRTbsA)
plot(BRTbsA, uniform=TRUE, main="Basin A Ablation Period: Regression Tree for
SWE")
text(BRTbsA, use.n=TRUE, cex=.8)
```

Prune

```
pBRTbsA<- prune(BRTbsA, cp=
BRTbsA$cptable[which.min(BRTbsA$cptable[,"xerror"]),"CP"])
plot(pBRTbsA, uniform=TRUE, main="Basin A Ablation Period: Pruned Regression
Tree for SWE")
text(pBRTbsA, use.n=TRUE, all=TRUE, cex=.8)
```

Derive R-squared

Code 1

```
par(mfrow=c(1,2))
rsq.rpart(BRTbsA)
tmp <- printcp(BRTbsA)
rsq.val <- 1-tmp[,c(3,4)]
rsq.val[nrow(rsq.val),]

par(mfrow=c(1,2))
rsq.rpart(pBRTbsA)
tmp <- printcp(pBRTbsA)
rsq.val <- 1-tmp[,c(3,4)]
rsq.val[nrow(rsq.val),]
```

Code 2

```
printcp(pBRTbsA)
plotcp(pBRTbsA)
summary(pBRTbsA)
par(mfrow=c(1,2))
rsq.rpart(pBRTbsA)
```

Trial BRT to Derive R-squared

```
fit1<- rpart(SWE ~ Solar + WEI, method="anova", data=SWEdataA)
plot(fit1)
text(fit1,use.n=T)
rsq.rpart(fit1)
```

Regression Tree: Basin B

```
BRTbsB <- rpart(SWE ~ Elevation + Slope + Northness + Eastness + Solar + WEI, cp=0,
method="anova", data=SWEdataB)
plotcp(BRTbsB)
plot(BRTbsB, uniform=TRUE, main="Basin B Ablation Period: Regression Tree for
SWE")
text(BRTbsB, use.n=TRUE, cex=.8)


BRTbsB <- rpart(SWE ~ Elevation + Slope + Northness + Eastness + Solar + WEI,
method="anova", data=SWEdataB)
printcp(BRTbsB)
plotcp(BRTbsB)
summary(BRTbsB)
par(mfrow=c(1,2))
rsq.rpart(BRTbsB)
plot(BRTbsB, uniform=TRUE, main="Basin B Ablation Period: Regression Tree for
SWE")
text(BRTbsB, use.n=TRUE, cex=.8)
post(BRTbsB, file =
"C:/Users/jason.welz/Documents/Thesis/Data_analysis/Rcode/RegTreeSWEB.ps", title =
"Basin B: Regression Tree for SWE")
```

Prune

```
pBRTbsB<- prune(BRTbsB, cp=
BRTbsB$cptable[which.min(BRTbsB$cptable[,"xerror"]),"CP"])
printcp(pBRTbsB)
plotcp(pBRTbsB)
summary(pBRTbsB)
par(mfrow=c(1,2))
rsq.rpart(pBRTbsB)
pBRTbsB<- prune(BRTbsB, cp=
BRTbsB$cptable[which.min(BRTbsB$cptable[,"xerror"]),"CP"])
plot(pBRTbsB, uniform=TRUE, main="Basin B Peak SWE Period: Pruned Regression
Tree for SWE")
text(pBRTbsB, use.n=TRUE, all=TRUE, cex=.8)
```

```
post(pBRTbsB, file =
"C:/Users/jason.welz/Documents/Thesis/Data_analysis/Rcode/PrunedRegTreeSWEB.ps"
, title = "Basin B: Pruned Regression Tree for SWE")
```

Derive R-squared

Code 1

```
par(mfrow=c(1,2))
rsq.rpart(BRTbsB)
tmp <- printcp(BRTbsB)
rsq.val <- 1-tmp[,c(3,4)]
rsq.val[nrow(rsq.val),]

par(mfrow=c(1,2))
rsq.rpart(pBRTbsB)
tmp <- printcp(pBRTbsB)
rsq.val <- 1-tmp[,c(3,4)]
rsq.val[nrow(rsq.val),]
```

Code 2

```
printcp(pBRTbsA)
plotcp(pBRTbsA)
summary(pBRTbsA)
par(mfrow=c(1,2))
rsq.rpart(pBRTbsA)

rsq.rpart
rsq.val <- 1tmp[,c(3,4)]
rsq.val[nrow(rsq.val),]
rpartPred <- predict(pBRTbsB,Eastness, type = "class")
confusionMatrix(pBRTbsB, testing$anova)
```

Boxplots: Observed vs Modeled Accumulation Period

```
par(mfrow=c(1,2))
SWEdataA <-
read.table("J:/Desktop_Files/Snow_Transect_Data/Master_spreadsheet_new/UTM_data/
Snow_Data_10mUTM_R_Acc_BasinA.csv", header=TRUE, sep=",")
boxplot(SWEdataA$SWE,SWEdataA$MLRSWE,SWEdataA$BRTSWE, main="Basin
A",ylab="SWE (mm)", beside=T, names=c("Observed", "MLR", "BRT"))
SWEdataB <-
read.table("J:/Desktop_Files/Snow_Transect_Data/Master_spreadsheet_new/UTM_data/
Snow_Data_10mUTM_R_Acc_BasinB.csv", header=TRUE, sep=",")
```

```
boxplot(SWEdataB$SWE,SWEdataB$MLRSWE,SWEdataB$BRTSWE, main="Basin
B",ylab="SWE (mm)", beside=T, names=c("Observed", "MLR", "BRT"))

quantile(SWEdataA$BRTSWE, probs=c(0,0.25,0.5,0.75,1), na.rm=TRUE)

favstats(SWE, data=SWEdataA)
favstats(MLRSWE, data=SWEdataA)
favstats(BRTSWE, data=SWEdataA)

favstats(SWE, data=SWEdataB)
favstats(MLRSWE, data=SWEdataB)
favstats(BRTSWE, data=SWEdataB)
```

Boxplots: Observed vs Modeled Peak SWE Period

```
par(mfrow=c(1,2))
SWEdataA <-
read.table("J:/Desktop_Files/Snow_Transect_Data/Master_spreadsheet_new/UTM_data/
Snow_Data_10mUTM_R_pkSWE_BasinA.csv", header=TRUE, sep=",")
boxplot(SWEdataA$SWE,SWEdataA$MLRSWE,SWEdataA$BRTSWE, main="Basin
A",ylab="SWE (mm)", beside=T, names=c("Observed", "MLR", "BRT"))
SWEdataB <-
read.table("J:/Desktop_Files/Snow_Transect_Data/Master_spreadsheet_new/UTM_data/
Snow_Data_10mUTM_R_pkSWE_BasinB.csv", header=TRUE, sep=",")
boxplot(SWEdataB$SWE,SWEdataB$MLRSWE,SWEdataB$BRTSWE, main="Basin
B",ylab="SWE (mm)", beside=T, names=c("Observed", "MLR", "BRT"))
```

Boxplots: Observed vs Modeled Ablation Period

```
par(mfrow=c(1,2))
SWEdataA <-
read.table("J:/Desktop_Files/Snow_Transect_Data/Master_spreadsheet_new/UTM_data/
Snow_Data_10mUTM_R_Abl_BasinA.csv", header=TRUE, sep=",")
boxplot(SWEdataA$SWE,SWEdataA$MLRSWE,SWEdataA$BRTSWE, main="Basin
A",ylab="SWE (mm)", beside=T, names=c("Observed", "MLR", "BRT"))
SWEdataB <-
read.table("J:/Desktop_Files/Snow_Transect_Data/Master_spreadsheet_new/UTM_data/
Snow_Data_10mUTM_R_Abl_BasinB.csv", header=TRUE, sep=",")
boxplot(SWEdataB$SWE,SWEdataB$MLRSWE,SWEdataB$BRTSWE, main="Basin
B",ylab="SWE (mm)", beside=T, names=c("Observed", "MLR", "BRT"))
```

T-test: MLR vs BRT Basins A and B Peak SWE Period

```
t.test(x=SWEdataAB$MLRSWE, y=SWEdataAB$BRTSWE)
alternative=c("two-sided", data=SWEdataAB, var.equal=T)
```

T-test: Obs SWE vs MLR SWE Basin A Peak SWE Period

```
t.test(x=SWEdataA$MLRSWE, y=SWEdataA$SWE)
alternative=c("two-sided", data=SWEdataA, var.equal=T)
```

T-test: Obs SWE vs BRT SWE Basin A Peak SWE Period

```
t.test(x=SWEdataA$BRTSWE, y=SWEdataA$SWE)
alternative=c("two-sided", data=SWEdataA, var.equal=T)

t.test(SWEdataA$SWE~SWEdataA$BRTSWE,
alternative="greater",mu=0,conf.level=0.95,data=SWEdataA,var.equal=F)
```

T-test: Obs SWE vs MLR SWE Basin B Peak SWE Period

```
t.test(x=SWEdataB$MLRSWE, y=SWEdataB$SWE)
alternative=c("two-sided", data=SWEdataB, var.equal=T)
```

T-test: Obs SWE vs BRT SWE Basin B Peak SWE Period

```
t.test(x=SWEdataB$BRTSWE, y=SWEdataB$SWE)
alternative=c("two-sided", data=SWEdataB, var.equal=T)
```

T-test: MLR vs BRT Basins A Peak SWE Period

```
t.test(x=SWEdataA$MLRSWE, y=SWEdataA$BRTSWE)
alternative=c("two-sided", data=SWEdataA, var.equal=T)
```

T-test: MLR vs BRT Basins B Peak SWE Period

```
t.test(x=SWEdataB$MLRSWE, y=SWEdataB$BRTSWE)
alternative=c("two-sided", data=SWEdataB, var.equal=T)
```

APPENDIX F

BRT MODEL CODES FOR RASTER CALCULATOR IN ARCGIS

Basin A: Accumulation
=Con("sol_a_10mutm">=453300, 191, Con("wei_a_10mutm">=-0.522, 454, 621))

Basin B: Accumulation
=Con("East_B_10mUTM"<0.879, 259, 645)

Basin A: Peak SWE
=Con(“sol_a_10mutm”>=363100, Con("wei_a_10mutm" >=0.855,
Con("wei_a_10mutm" >=2.29, 204, 375), Con("wei_a_10mutm" <0.855,
Con("slop_a_10mutm" >=13.59, 479, 632))), Con("sol_a_10mutm"<363100,
Con("slop_a_10mutm" <35.29, 767, 1199)))

Basin B: Peak SWE
Con("WEI_B_10mUTM" >= -1.173, Con("East_B_10mUTM" < 0.991,
Con("WEI_B_10mUTM">=1.339, 243, Con("Elev_B_10mUTM"<2911, 377, 664),
773)), Con("Slop_B_10mUTM" < 20.53, 587, 1084)))

Basin A: Ablation
Con("wei_a_10mutm" >= -4.931, Con("nor_a_10mutm" < 0.032, 48,
Con("nor_a_10mutm" >= 0.032, Con("slop_a_10mutm" < 35.55, 173, 466))), 804)
Con("sol_a_10mutm" >= 363100, Con("wei_a_10mutm" >= 0.855,
Con("wei_a_10mutm" >= 2.29, 204, 375), Con("wei_a_10mutm" < 0.855,
Con("slop_a_10mutm" >= 13.59, 479, 632))), Con("sol_a_10mutm" < 363100,
Con("slop_a_10mutm" < 35.29, 767, 1199)))

Basin B: Ablation
Con("East_B_10mUTM" < 0.886,35, Con("East_B_10mUTM" >= 0.886,
Con("Sol_B_10mUTM" >= 350600, Con("Elev_B_10mUTM" < 2926, 65,
Con("Elev_B_10mUTM" >= 2926, Con("WEI_B_10mUTM" >= -0.378, 239, 1117))),
1606)))